

The Effective Theory of Inflation in the Standard Model of the Universe and the CMB+LSS data analysis

D. Boyanovsky ^{(a,b,c),*} C. Destri ^{(d,c),†} H. J. de Vega ^{(b,c),‡} and N. G. Sanchez ^{(c)§}

^(a) *Department of Physics and Astronomy,
University of Pittsburgh, Pittsburgh,
Pennsylvania 15260, USA.*

^(b) *LPTHE, Laboratoire Associé au CNRS UMR 7589,
Université Pierre et Marie Curie (Paris VI) et Denis Diderot (Paris VII),
Tour 24, 5^{ème}. étage, 4, Place Jussieu,
75252 Paris, Cedex 05, France.*

^(c) *Observatoire de Paris, LERMA,
Laboratoire Associé au CNRS UMR 8112,
61, Avenue de l'Observatoire, 75014 Paris, France.*

^(d) *Dipartimento di Fisica G. Occhialini,
Università Milano-Bicocca and INFN,
sezione di Milano-Bicocca,
Piazza della Scienza 3, 20126 Milano, Italia*

(Dated: December 9, 2019)

Inflation is today a part of the Standard Model of the Universe supported by the cosmic microwave background (CMB) and large scale structure (LSS) datasets. Inflation solves the horizon and flatness problems and naturally generates density fluctuations that seed LSS and CMB anisotropies, and tensor perturbations (primordial gravitational waves). Inflation theory is based on a scalar field φ (the inflaton) whose potential is fairly flat leading to a slow-roll evolution. This review focuses on the following new aspects of inflation. We present the effective theory of inflation à la Ginsburg-Landau in which the inflaton potential is a polynomial in the field φ and has the universal form $V(\varphi) = N M^4 w(\varphi/[\sqrt{N} M_{Pl}])$, where $w = \mathcal{O}(1)$, $M \ll M_{Pl}$ is the scale of inflation and $N \sim 60$ is the number of efolds since the cosmologically relevant modes exit the horizon till inflation ends. The slow-roll expansion becomes a systematic $1/N$ expansion and the inflaton couplings become **naturally small** as powers of the ratio $(M/M_{Pl})^2$. The spectral index and the ratio of tensor/scalar fluctuations are $n_s - 1 = \mathcal{O}(1/N)$, $r = \mathcal{O}(1/N)$ while the running index turns to be $dn_s/d\ln k = \mathcal{O}(1/N^2)$ and therefore can be neglected. The energy scale of inflation $M \sim 0.7 \times 10^{16}$ GeV is completely determined by the amplitude of the scalar adiabatic fluctuations. A complete analytic study plus the Monte Carlo Markov Chains (MCMC) analysis of the available CMB+LSS data (including WMAP5) with fourth degree trinomial potentials showed: (a) the **spontaneous breaking** of the $\varphi \rightarrow -\varphi$ symmetry of the inflaton potential. (b) a **lower bound** for r in new inflation: $r > 0.023$ (95% CL) and $r > 0.046$ (68% CL). (c) The preferred inflation potential is a **double well**, even function of the field with a moderate quartic coupling yielding as most probable values: $n_s \simeq 0.964$, $r \simeq 0.051$. This value for r is within reach of forthcoming CMB observations. The present data in the effective theory of inflation clearly **prefer new inflation**. Study of higher degree inflaton potentials show that terms of degree higher than four do not affect the fit in a significant way. In addition, horizon exit happens for $\varphi/[\sqrt{N} M_{Pl}] \sim 0.9$ making higher order terms in the potential w negligible. We summarize the physical effects of **generic** initial conditions (different from Bunch-Davies) on the scalar and tensor perturbations during slow-roll and introduce the transfer function $D(k)$ which encodes the observable initial conditions effects on the power spectra. These effects are more prominent in the *low* CMB multipoles: a change in the initial conditions during slow roll can account for the observed CMB quadrupole suppression. Slow-roll inflation is generically preceded by a short **fast-roll** stage. Bunch-Davies initial conditions are the natural initial conditions for the fast-roll perturbations. During fast-roll, the potential in the wave equations of curvature and tensor perturbations is purely attractive and leads to a suppression of the curvature and tensor CMB quadrupoles. A MCMC analysis of the WMAP+SDSS data including fast-roll shows that the quadrupole mode exits the horizon about 0.2 efold before fast-roll ends and its amplitude gets suppressed. In addition, fast-roll fixes the initial inflation redshift to be $z_{init} = 0.9 \times 10^{56}$ and the **total number** of efolds of inflation to be $N_{tot} \simeq 64$. Fast-roll fits the TT, the TE and the EE modes well reproducing the quadrupole suppression. A thorough study of the quantum loop corrections reveals that they are very small and controlled by powers of $(H/M_{Pl})^2 \sim 10^{-9}$, a conclusion that validates the reliability of the effective theory of inflation. The present review shows how powerful is the Ginsburg-Landau effective theory of inflation in predicting observables that are being or will soon be contrasted to observations.

Contents

I. Introduction to the Effective Theory of Inflation	3
A. Overview and present status of inflation	3
B. The Standard Cosmological Model	9
C. The Horizon and Flatness problems in non-inflationary cosmology and their inflationary resolution.	12
1. The horizon problem	12
2. The flatness problem	14
3. The solution to the horizon problem in inflation	14
4. The solution to the flatness problem in inflation	15
5. The Entropy of the Universe	16
6. The Age of the Universe	17
D. Inflationary Dynamics in the Effective Theory of Inflation	18
1. Inflation and Inflaton field dynamics	22
2. Slow-roll, the Universal Form of the Inflaton Potential and the Energy Scale of Inflation	25
3. Inflationary Dynamics: Homogeneous Inflaton	28
4. Fixing the Total Number of Inflation e-folds from Fast-Roll and the CMB Quadrupole suppression	32
E. Gauge invariant Scalar and Tensor Fluctuations	33
1. Scalar Curvature Perturbations	34
2. Tensor Perturbations	36
3. Initial conditions	37
4. The power spectrum of adiabatic scalar and tensor perturbations	38
5. The energy scale of inflation and the quasi-scale invariance during inflation.	40
 II. Theoretical predictions, MCMC data analysis, early fast-roll stage and CMB quadrupole suppression.	 41
A. Ginsburg-Landau polynomial realizations of the Inflaton Potential	41
1. Binomial inflaton potentials for chaotic inflation	43
2. Binomial inflaton potentials for new inflation	44
3. Contrasting the results of new and chaotic binomial inflation.	46
B. Trinomial Chaotic Inflation: Spectral index, amplitude ratio, running index and limiting cases	48
1. The small asymmetry regime: $-1 < h \leq 0$.	49
2. The flat potential limit $h \rightarrow -1^+$	50
3. The singular limit $z = 1$ and then $h \rightarrow -1^+$ yields the Harrison-Zeldovich spectrum	51
4. The high asymmetry $h < -1$ regime.	52
C. Trinomial New Inflation: Spectral index, amplitude ratio, running index and limiting cases	53
1. The weak coupling limit $y \rightarrow 0$	56
2. The strong coupling limit $y \rightarrow \infty$	56
3. The extremely asymmetric limit $ h \rightarrow \infty$	57
4. Regions of n_s and r covered by New Inflation and by Chaotic Inflation.	57
D. The Monte Carlo Markov Chain Method of Data Analysis	58
1. CMB, LSS and Inflation within a MCMC analysis.	60
2. MCMC results for Trinomial New Inflation.	63
3. MCMC results for Chaotic Trinomial Inflation.	66
E. Higher degree terms in inflaton potentials	69
1. Family of models	70
2. Broken Symmetry models.	71
3. Field reconstruction for new inflation	73
4. Chaotic inflation models.	74
5. Field reconstruction for chaotic inflation	75
6. Conclusions	77

*Electronic address: boyan@pitt.edu

†Electronic address: Claudio.Destri@mib.infn.it

‡Electronic address: devega@lpthe.jussieu.fr

§Electronic address: Norma.Sanchez@obspm.fr

F. The initial conditions for the scalar and tensor quantum fluctuations.	77
1. Initial conditions and the energy momentum tensor of scalar and tensor perturbations.	78
2. Scalar perturbations	78
3. Tensor perturbations	80
4. The Transfer Function of Initial Conditions and its Asymptotic Behaviour	80
5. The effect of initial conditions on the low multipoles of the CMB	83
G. The early fast-roll inflationary stage and the CMB quadrupole suppression	84
1. The Effect of Fast-roll on the Inflationary Fluctuations.	85
2. MCMC analysis of CMB and LSS data including the early fast-roll inflationary stage	91
3. MCMC analysis with Binomial New Inflation without the fast-roll stage: $D_{\mathcal{R}}(k) = 0$.	91
4. MCMC analysis with Binomial New Inflation including the fast-roll stage: $D_{\mathcal{R}}(k) \neq 0$.	95
5. Real Space Two Point TT-Correlator	99
6. Conclusions	100
III. Quantum Loop Corrections	100
A. The domain of validity of the effective theory of inflation.	100
1. Large Inflaton Fields	100
2. Transplanckian and Resonant Fluctuation Modes.	102
B. Quantum Loop Corrections to the Inflaton Dynamics	102
1. Quantum Decay Rate	102
2. Particle decay in inflationary cosmology	105
3. Quantum corrections to the equations of motion for the inflaton	111
4. Quantum corrections to the Friedmann equation: the one loop effective potential	113
5. Quantum corrections to superhorizon modes and their scaling dimensions	115
6. Connection with non-gaussianity	118
C. Quantum Loop Corrections to the inflaton potential and the power spectra from superhorizon modes and trace anomalies	119
1. Statement of the problem	120
2. Light scalar field coupled to the inflaton	122
3. Heavy scalar field coupled to the inflaton	125
4. Scalar curvature perturbations	125
5. Tensor perturbations	127
6. Spinor fields	127
7. Quantum Corrections to the Scalar Curvature and Tensor power spectra	130
8. Conclusions and further questions	131
D. Outlook and future perspectives	132
Acknowledgments	132
References	132

I. INTRODUCTION TO THE EFFECTIVE THEORY OF INFLATION

A. Overview and present status of inflation

Inflation was introduced to solve several outstanding problems of the standard Big Bang model [1] and has now become an important part of the standard cosmology. It provides a natural mechanism for the generation of scalar density fluctuations that seed large scale structure, thus explaining the origin of the temperature anisotropies in the cosmic microwave background (CMB), and for the generation of tensor perturbations (primordial gravitational waves) [2, 3, 4, 5, 6].

A distinct aspect of inflationary perturbations is that they are generated by quantum fluctuations of the scalar field(s) that drive inflation. After their wavelength becomes larger than the Hubble radius, these fluctuations are amplified and grow, becoming classical and decoupling from causal microphysical processes. Upon re-entering the horizon, during the radiation and matter dominated eras, these classical perturbations seed the inhomogeneities which generate structure upon gravitational collapse [3, 5, 6]. A great diversity of inflationary models predict fairly generic features: a gaussian, nearly scale invariant spectrum of (mostly) adiabatic scalar and tensor primordial fluctuations, which provide an excellent fit to the highly precise wealth of data provided by the Wilkinson Microwave Anisotropy

Probe (WMAP)[8, 9, 10] making the inflationary paradigm fairly robust. Precision CMB data reveal peaks and valleys in the temperature fluctuations resulting from acoustic oscillations in the electron-photon fluid at recombination. These are depicted in fig. 1 where up to five peaks can be seen.

Baryon acoustic oscillations driven by primordial fluctuations produce a peak in the galaxy correlations at $\sim 109 h^{-1}$ Mpc (comoving sound horizon) [7]. This peak is the real-space version of the acoustic oscillations in momentum (or l) space and are confirmed by LSS data [7].

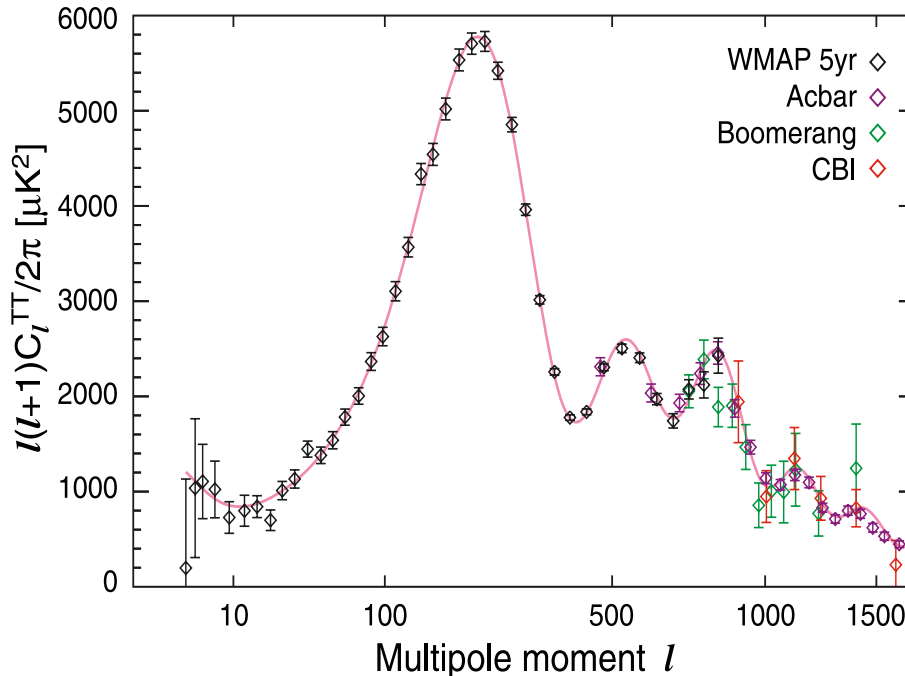


FIG. 1: Acoustic oscillations from WMAP 5 years data set plus other CMB data. Theory and observations nicely agree except for the lowest multipoles: the quadrupole CMB suppression. See sects. IIF and IIG for discussions on this.

Perhaps the most striking validation of inflation as a mechanism for generating *superhorizon* fluctuations is the anticorrelation peak in the temperature-polarization (TE) angular power spectrum at $l \sim 150$ corresponding to superhorizon scales [8] and depicted in fig. 2. The observed TE power spectrum can only be generated by fluctuations that exited the horizon during inflation and re-entered the horizon later, when the expansion of the universe decelerates.

The confirmation of many of the robust predictions of inflation by current high precision observations places inflationary cosmology on solid grounds.

Amongst the wide variety of inflationary scenarios, single field slow-roll models provide an appealing, simple and fairly generic description of inflation. Its simplest implementation is based on a scalar field (the inflaton) whose homogeneous expectation value drives the dynamics of the scale factor, plus small quantum fluctuations. The inflaton potential is fairly flat during inflation and it dominates the universe energy during inflation. This flatness not only leads to a slowly varying Hubble parameter, hence ensuring a sufficient number of e-folds of inflation, but also provides an explanation for the gaussianity of the fluctuations as well as for the (almost) scale invariance of their power spectrum. A flat potential precludes large non-linearities in the dynamics of the *fluctuations* of the scalar field.

The current WMAP data are validating the single field slow-roll scenario [8, 9, 10]. Furthermore, because the potential is flat the scalar field is almost **massless**, and modes cross the horizon with an amplitude proportional to the Hubble parameter. This fact combined with a slowly varying Hubble parameter yields an almost scale invariant primordial power spectrum. The slow-roll approximation has been recently cast as a systematic $1/N$ expansion [11], where $N \sim 60$ is the number of e-folds before the end of inflation when modes of cosmological relevance today first crossed the Hubble radius.

The observational progress begins to discriminate among different inflationary models, placing stringent constraints on them. The upper bound on the ratio r of tensor to scalar fluctuations obtained by WMAP convincingly excludes the massless monomial φ^4 potential [8, 9, 10] and hence **strongly suggests** the presence of a **mass term** in the single field inflaton potential [12, 13]. Therefore, as a minimal single field model, one should consider a sufficiently

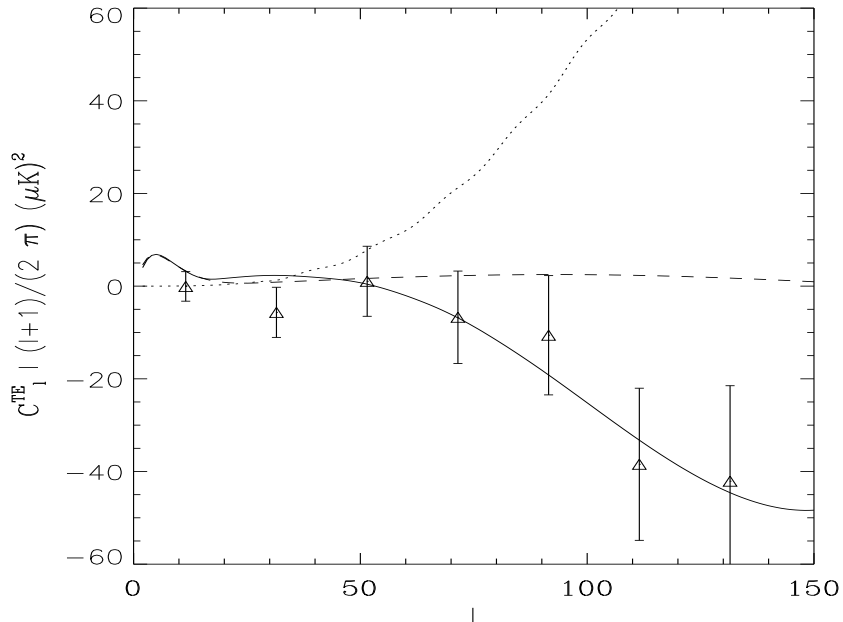


FIG. 2: Temperature-Polarization angular power spectrum. The large-angle TE power spectrum predicted in primordial adiabatic models (solid), primordial isocurvature models (dashed) and by defects such as cosmic strings (dotted). The WMAP TE data (Kogut et al. [8]) are shown for comparison, in bins of $\Delta l = 10$. Superhorizon adiabatic modes from inflation fit the data while subhorizon sources of TE power go in directions opposite to the data.

general polynomial, the simplest polynomial potential bounded from below being the fourth order trinomial potential [14].

The observed low value of the CMB quadrupole with respect to the Λ CDM theoretical value has been an intriguing feature on large angular scales since first observed by COBE/DMR [15], and confirmed by the WMAP data [9, 10]. In the best fit Λ CDM model, using the WMAP5 data we find that the probability that the quadrupole is as low or lower than the observed value is just 0.031. Even if one does not care about the specific multipole and looks for any multipole as low or lower than the observed quadrupole with respect to the Λ CDM model value, then the probability remains smaller than 5%. Therefore, it is relevant to find a cosmological explanation of the quadrupole suppression beyond the Λ CDM model. An early fast-roll stage can explain the CMB quadrupole suppression as we discuss below.

This review article focuses on the following new aspects of inflationary cosmology:

- An effective field theory description of slow-roll single field inflation à la Ginsburg-Landau. In the Ginsburg-Landau framework, the potential is a polynomial in the field starting by a constant term [16]. Linear terms can always be eliminated by a constant shift of the inflaton field. The quadratic term can have a positive or a negative sign associated to chaotic or new inflation, respectively. This effective Ginsburg-Landau field theory is characterized by only **two** energy scales: the scale of inflation M and the Planck scale $M_{Pl} = 2.43534 \cdot 10^{18}$ GeV $\gg M$. In this context we propose a **universal** form for the inflaton potential in slow-roll models [11]:

$$V(\varphi) = N M^4 w(\chi), \quad (1.1)$$

where $N \sim 60$ is the number of efolds since the cosmologically relevant modes exit the horizon till the end of inflation and χ is a dimensionless, slowly varying field

$$\chi = \frac{\varphi}{\sqrt{N} M_{Pl}}.$$

The slow-roll expansion becomes in this way a systematic $1/N$ expansion. The couplings in the inflaton Lagrangian become naturally small due to suppression factors arising from eq.(1.1) as the ratio of the two relevant energy scales here: M and M_{Pl} . The spectral index, the ratio of tensor/scalar fluctuations, the running index

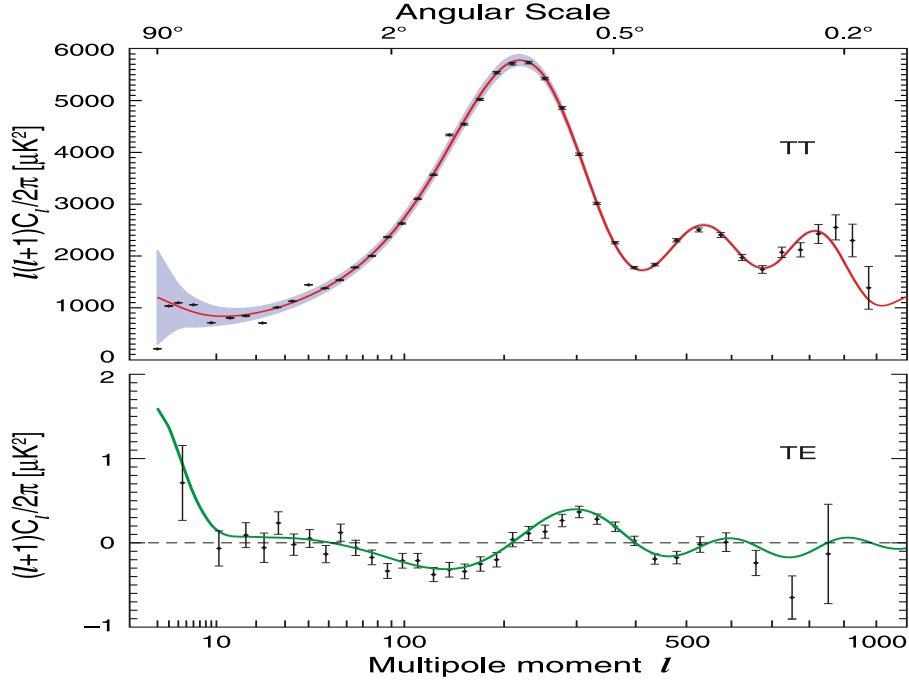


FIG. 3: The temperature (TT) and temperature-polarization correlation (TE) power spectra based on the 5 year WMAP data [10].

and the amplitude of the scalar adiabatic fluctuations are naturally

$$n_s - 1 = \mathcal{O}\left(\frac{1}{N}\right) \quad , \quad r = \mathcal{O}\left(\frac{1}{N}\right) \quad , \quad \frac{dn_s}{d\ln k} = \mathcal{O}\left(\frac{1}{N^2}\right) \quad , \quad |\Delta_{k\,ad}^{\mathcal{R}}| \sim N \left(\frac{M}{M_{Pl}}\right)^2 \quad , \quad (1.2)$$

for **all** inflaton potentials in the class of eq.(1.1). Hence, the energy scale of inflation M is completely determined by the amplitude of the scalar adiabatic fluctuations $|\Delta_{k\,ad}^{\mathcal{R}}|$ and using the WMAP5 results for it, we find $M \sim 10^{16}$ GeV. The running index results $dn_s/d\ln k \sim 10^{-4}$ and therefore can be neglected. Namely, within the class of models eq.(1.1) one does not need to measure the ratio r in order to learn about the scale of inflation. Moreover, we were able to provide **lower** bounds for r and **predict its value** in the effective theory of inflation using the CMB+LSS data and Monte Carlo Markov Chains (MCMC) simulations [14].

- Besides its simplicity, the trinomial potential (minimal single field model in the Ginsburg-Landau spirit) is rich enough to describe the physics of inflation and accurately reproduce the WMAP data [14]. It is well motivated within the Ginsburg-Landau approach as an effective field theory description (see ref.[16, 17]). We provide a complete analytic study complemented by a statistical analysis. The MCMC analysis of the available CMB+LSS data with the Ginsburg-Landau effective field theory of inflation showed [14]:

(i) The data strongly indicate the **breaking** (whether spontaneous or explicit) of the $\varphi \rightarrow -\varphi$ symmetry of the inflaton potentials both for new and for chaotic inflation. (ii) Trinomial new inflation naturally satisfies this requirement and provides an excellent fit to the data. (iii) Trinomial chaotic inflation produces the best fit in a very narrow corner of the parameter space. (iv) The chaotic symmetric trinomial potential is almost certainly **ruled out** (at more than 95%CL). In trinomial chaotic inflation the MCMC runs go towards a potential in the *boundary* of the parameter space and which resembles a spontaneously symmetry broken potential of new inflation. (v) The above results and further physical analysis here lead us to conclude that **new inflation** gives the best description of the data. (vi) We find a **lower bound** for r within trinomial new inflation potentials: $r > 0.023$ (95% CL) and $r > 0.046$ (68% CL). (vii) The preferred new inflation potential is a double well, even function of the field with a moderate quartic coupling $y \sim 1$,

$$w(\chi) = \frac{y}{32} \left(\chi^2 - \frac{8}{y} \right)^2 = -\frac{1}{2} \chi^2 + \frac{y}{32} \chi^4 + \frac{2}{y} \quad . \quad (1.3)$$

[see eq.(1.1)]. This new inflation model yields as most probable values: $n_s \simeq 0.964$, $r \simeq 0.051$. This value for r is within reach of forthcoming CMB observations [14]. For the best fit value $y \simeq 1.26$, the inflaton field

exits the horizon in the negative concavity region $w''(\chi) < 0$ intrinsic to new inflation. We find for the best fit, $M = 0.543 \times 10^{16}$ GeV for the scale of inflation and $m = 1.21 \times 10^{13}$ GeV for the inflaton mass. We derived explicit formulae and study in detail the spectral index n_s of the adiabatic fluctuations, the ratio r of tensor to scalar fluctuations and the running index $dn_s/d\ln k$ [14]. We use these analytic formulas as hard constraints on n_s and r in the MCMC analysis. Our analysis differs in this **crucial** aspect from previous MCMC studies in the literature involving the CMB data.

- The dependence of the observables (n_s , r and $dn_s/d\ln k$) on the degree of the inflaton potential $2n$ is studied and confronted to the WMAP and large scale structure data [18]. This shows that higher degree terms ($n > 2$) in the inflaton potential do not affect the fit in a significant way in new inflation. The window of consistency with the WMAP and LSS data **narrows** for growing n in chaotic inflation. New inflation yields a good fit to the r and n_s data in a wide range of field and parameter space. Small field inflation yields $r < 0.16$ while large field inflation yields $r > 0.16$ (for $N = 50$). All members of the new inflation family predict a small but negative running $-4(n+1) \times 10^{-4} \leq dn_s/d\ln k \leq -2 \times 10^{-4}$. (The values of r , n_s , $dn_s/d\ln k$ for arbitrary N follow by a simple rescaling from the $N = 50$ values). The reconstruction program carried out in ref.[18] suggests quite generally that for n_s consistent with the WMAP and LSS data and $r < 0.1$ the **symmetry breaking scale** for new inflation is $|\varphi_{min}| \sim 20 M_{Pl}$ while the **field scale** at Hubble crossing is $|\varphi_{exit}| \sim 7 M_{Pl}$. This corresponds to $\chi_{exit} \sim 0.9$ which can make negligible the higher order terms in $w(\chi_{exit})$ for new inflation. The family of chaotic models feature $r \geq 0.16$ (for $N = 50$) and only a *restricted subset* of chaotic models are consistent with the combined WMAP bounds on r , n_s , $dn_s/d\ln k$ with a narrow window in field amplitude around $|\varphi_{exit}| \sim 15 M_{Pl}$. We conclude that a measurement of $r < 0.16$ (for $N = 50$) distinctly rules out a large class of chaotic scenarios and favors small field new inflationary models. As a general consequence, **new inflation** emerges clearly more favoured than chaotic inflation.
- The dynamics of inflation is usually described by the classical evolution of a scalar field (the inflaton). The use of classical dynamics is justified by the enormous stretching of physical lengths during inflation. When the physical wavelength of the fluctuations become larger than the Hubble radius, these fluctuations effectively become classical. This is probably the only case where the time evolution itself leads to the classicalization of fluctuations and microscopic scales near the Planck scale 10^{-32} cm $\lesssim \lambda = 2\pi/k \lesssim 10^{-28}$ cm become macroscopic today in the range $1 \text{ Mpc} \lesssim \lambda_{today} \lesssim 10^4 \text{ Mpc}$. This happens thanks to a redshift by $\sim 10^{56}$ since the beginning of inflation for a total number of inflation e-folds $N_{tot} \sim 64$.

We discuss the validity of the effective theory of inflation. It is valid generically as long as the energy density is $\ll M_{Pl}^4$. This is true thanks to eq.(1.1) even when the inflaton field φ takes values equal to many times M_{Pl} .

We summarize the quantum loop corrections to inflationary dynamics (see [19, 20]). Novel phenomena emerges at the quantum level as a consequence of the lack of kinematic thresholds, among them the phenomenon of inflaton decay into its own quanta. A thorough study of the effect of quantum fluctuations reveals that these loop corrections are suppressed by powers of $(H/M_{Pl})^2$ where H is the Hubble parameter during inflation [19, 20]. The amplitude of temperature fluctuations constrains the scale of inflation with the result that $(H/M_{Pl})^2 \sim 10^{-9}$. Therefore, quantum loop corrections are very small and controlled by the ratio $(H/M_{Pl})^2$, a conclusion that validates the reliability of the classical approximation and the effective field theory approach to inflationary dynamics. The quantum corrections to the power spectrum are computed and expressed in terms of n_s , r and $dn_s/d\ln k$. Trace anomalies dominate the quantum corrections to the primordial power spectrum (see sec. III C).

- Scalar (curvature) and tensor (gravitational wave) perturbations originate in quantum fluctuations during inflation. These are usually studied within the slow-roll approximation and with Bunch-Davies initial conditions. We summarize the physical effects on the power spectrum of generic initial conditions with particular attention to back-reaction effects [21, 22]. We introduce a *transfer function* $D(k)$ which encodes the effect of generic initial conditions on the power spectra. The constraint from renormalizability and small back reaction entails that $D(k) \lesssim \mu^2/k^2$ for large k where μ characterizes the asymptotic decay of the occupation number. This implies that observable effects from initial conditions are more prominent in the *low* CMB multipoles. The effects on high l -multipoles are suppressed by a factor $\sim 1/l^2$ due to the large k fall off of $D(k)$. Hence, a change from the Bunch-Davies initial conditions for the fluctuations can naturally account for the low observed value of the CMB quadrupole [21, 22].
- Slow-roll inflation is generically preceded by a short fast-roll stage during which the kinetic and the potential energy of the inflaton field are of the same order. This fast-roll stage is followed by the usual slow-roll regime during which the kinetic energy is much smaller than the potential energy. The fast-roll stage leads to a purely attractive potential in the wave equations of curvature and tensor perturbations. This in turn leads

to a suppression of the quadrupole in curvature and tensor perturbations which exited the horizon during the fast-roll stage. Within the context of the effective field theory and for generic initial conditions on the inflaton field, it is shown that a quadrupole suppression consistent with observations is a natural consequence of the fast-roll stage [21, 22, 23]. A **new** parameter emerges in this way in the early universe model: the comoving wave number k_{tran} characteristic scale of this attractive potential. This mode k_{tran} happens to exit the horizon precisely **at the transition** from the fast-roll to the slow-roll stage. The fast-roll stage dynamically modifies the initial power spectrum of perturbations by a transfer function $D(k)$. We perform a MCMC analysis of the WMAP and SDSS data combined with the most recent supernovae compilation [24] and including the fast-roll stage. We find the value $k_{tran} = 0.290 \text{ Gpc}^{-1}$ (today) and $k_{tran}^{init} = 1.69 \cdot 10^{14} \text{ GeV} = 14 \text{ } m$ at the beginning of inflation. These values fix the redshift since the beginning of inflation till today to $z_{init} = 0.915 \times 10^{56}$. From that we find the **total number of efolds** N_{tot} during inflation to be (see sec. ID 4)

$$N_{tot} \simeq 63 - \frac{1}{2} \log \left(\frac{H}{10^{-4} M_{Pl}} \right),$$

where H is the Hubble parameter at the beginning of inflation. The values of H and N_{tot} favoured by the current WMAP data within the effective theory of inflation and respecting the lower bound for N_{tot} that solves the horizon problem (see sec. IC 3) turn to be $H \simeq 0.4 \times 10^{14} \text{ GeV}$ and $N_{tot} \simeq 64$. That is, the MCMC analysis of the CMB+LSS data including the early fast-roll explanation of the CMB quadrupole suppression **imposes** $N_{tot} \simeq 64$. The quadrupole mode $k_Q = 0.238 \text{ Gpc}^{-1}$ exits the horizon earlier than k_{tran} , about 0.2 efolds before the end of fast-roll. Including the fast-roll stage improves the fits to the TT, the TE and the EE modes, well reproducing the quadrupole suppression.

As we discuss in sec. IIG, inflation generically starts by a fast-roll stage where the kinetic and potential energy of the inflaton are of the same order. This is followed by a slow-roll regime where the kinetic energy is much smaller than the potential energy. The slow-roll regime of inflation is an attractor of the dynamics during which the Universe is dominated by vacuum energy. Inflation ends when again the kinetic energy of the inflaton becomes large as the field is rolling near the minimum of the potential. Eventually, the energy stored in the homogeneous inflaton is transferred explosively into the production of particles via spinodal or parametric instabilities [25, 26, 27, 28]. More precisely, non-linear phenomena eventually **shut-off** the instabilities and **stop** inflation [25, 29, 30]. All these processes lead to the transition to a radiation dominated era. This is the standard picture of the transition from inflation to standard hot big bang cosmology.

We formulate here inflation as an effective field theory within the Ginsburg-Landau spirit [11, 16]. The theory of the second order phase transitions, the Ginsburg-Landau theory of superconductivity, the current-current Fermi theory of weak interactions, the sigma model of pions, nucleons (as skyrmions) and photons are all successful effective field theories. The present review shows how powerful is the effective theory of inflation **to predict observable quantities** that can be or will be soon contrasted with experiments. There are **two kind** of predictions in the effective theory of inflation: first, predictions on the order of magnitude of the CMB observables valid for all inflaton potentials in the class of eq.(1.1) [see eqs.(1.2)]; second, precise quantitative predictions as those presented in secs. IID-IIG.

The Ginsburg-Landau realization of the inflationary potential presented in this review fits the amplitude of the CMB anisotropy remarkably well and reveals that the Hubble parameter, the inflaton mass and non-linear couplings are see-saw-like, namely powers of the ratio $(M/M_{Pl})^2 \sim 10^{-9}$ multiplied by further powers of $1/N$. Therefore, the smallness of the couplings is not a result of fine tuning but a **natural** consequence of the form of the potential, of the validity of the effective field theory description and slow-roll. The quantum expansion in loops is therefore a double expansion on $(H/M_{Pl})^2$ and $1/N$. Notice that graviton corrections are also at least of order $(H/M_{Pl})^2$ because the amplitude of tensor modes is of order H/M_{Pl} . We show in sec. ID 2 that the form of the potential which fits the WMAP+LSS data and is consistent with slow-roll eqs.(1.1) implies the small values for the inflaton self-couplings [11].

The infrared (superhorizon) modes in the quantum loops produce large contributions of the order $\sim N$. However, as shown in sec. IIIC these large infrared contributions get multiplied by slow-roll factors of order $\sim 1/N$. As a result, the superhorizon contributions to physical magnitudes turn to be of order N^0 [19, 20] times factors of the order of $(H/M_{Pl})^2$.

We note that the effective theory of inflation describes an evolution spanning about 26 orders of magnitude in length scales from the beginning till the end of the inflationary era. This is the largest scale change described by a field theory so far.

It must be stressed that the energy scale of inflation, $M \sim 10^{16} \text{ GeV}$ is the energy scale of at least two other important physical situations: (a) the scale of Grand Unification of strong and electroweak interactions and (b) the

large energy scale in the see-saw formula for neutrino masses [see eq.(1.181)]. This coincidence suggests a physical link between the three areas.

Many deep problems remain to be solved in the early universe. One of them is the reheating problem. Namely, how the universe thermalizes after inflation and at what temperature. Baryogenesis provides a lower bound on the reheating temperature [2]. The mechanisms of thermalization uncovered in refs. [31] can provide a starting point to understand the reheating.

The units used in this review are such that $\hbar = c = 1$.

B. The Standard Cosmological Model

The history of the Universe is a history of expansion and cooling down.

On large scales the Universe is homogeneous and isotropic and its geometry is described by the Friedmann-Robertson-Walker (FRW) metric

$$ds^2 = dt^2 - a^2(t) \left[\frac{dr^2}{1 - k r^2} + r^2 (d\theta^2 + \sin^2 \theta d\phi^2) \right], \quad (1.4)$$

where r , θ and ϕ are comoving spherical coordinates, t is the cosmic time (the proper time of a comoving observer), $a(t)$ the scale factor, and $k = 0, \pm 1$ stands for the scalar curvature of three-dimensional spatial sections. $k = 0$, $k > 0$ and $k < 0$ describes flat, closed and open universe, respectively. The dynamics of the scale factor is completely determined by Einstein's equations and the equation of state. Overwhelming observational evidence indicates that the geometry of the Universe is spatially flat, namely $k = 0$. Thus the FRW metric simplifies to

$$ds^2 = dt^2 - a^2(t) d\vec{x}^2 \quad (1.5)$$

or in conformal time η

$$ds^2 = a^2(\eta) [d\eta^2 - (d\vec{x})^2]. \quad (1.6)$$

where $d\eta = dt/a(t)$. Notice that this cosmological expansion has no center: it happens everywhere at all spatial points \vec{x} and it is identical everywhere. The scale factor grows monotonically with time.

Physical scales are stretched by the scale factor $a(t)$ with respect to the time independent comoving scales

$$l_{phys}(t) = a(t) l_{com}. \quad (1.7)$$

A physical wavelength redshifts proportional to the scale factor [eq.(1.7)], therefore its time derivative obeys the Hubble law

$$\dot{l}_{phys}(t) = H(t) l_{phys}(t) = \frac{l_{phys}(t)}{d_H(t)}.$$

where $H(t) \equiv \dot{a}(t)/a(t)$ and $d_H(t)$ is the Hubble radius.

The redshift z at time t is defined as

$$z + 1 \equiv \frac{a_0}{a(t)} \quad (1.8)$$

where a_0 stands for the scale factor today and we choose $a_0 \equiv 1$. The farther back in time, the larger is the redshift and the smaller is $a(t)$.

The temperature decreases as the universe expands as

$$T(t) = \frac{T_0}{a(t)}. \quad (1.9)$$

Eq.(1.9) applies to all particles in thermal equilibrium as well as to massless decoupled particles (radiation). Since the temperature decreased with time, the Universe underwent a succession of phase transitions towards the less symmetric phases [36].

The combination of data from CMB and LSS, and numerical simulations lead to the Λ CDM or *concordance model* which has now become the standard cosmology. This impressive convergence of observational data and theoretical and numerical results describes a Universe that is composed of a cosmological constant, dark matter, baryonic (atoms) matter and radiation. This model provides the **only consistent** explanation of the broad set of precise and independent astronomical observations over a wide range of scales available today. Namely:

ρ_c	$(2.36 \text{ meV})^4$	h	0.705 ± 0.013
H_0	$h/[3 \text{ Gpc}] = h/[9.77813 \text{ Gyr}]$	Ω_Λ	0.726
M_{Pl}	$2.43534 \times 10^{18} \text{ GeV}$	Ω_M	0.274
M	$0.543 \times 10^{16} \text{ GeV}$	Ω_r	$8.49 \cdot 10^{-5}$
m	$1.21 \times 10^{13} \text{ GeV}$	n_s	0.960 ± 0.014

TABLE I: Selected Cosmological Parameters [10, 35]. m and M are given by eq.(2.24).

- WMAP data and previous CMB data.
- Light Elements Abundances.
- Large Scale Structures (LSS) Observations. Baryon acoustic oscillations (BAO).
- Acceleration of the Universe expansion: Supernova Luminosity/Distance (SN) and Radio Galaxies.
- Gravitational Lensing Observations.
- Lyman α Forest Observations.
- Hubble Constant (H_0) Measurements.
- Properties of Clusters of Galaxies.

In the homogeneous and isotropic FRW universe described by eq.(1.5), the matter distribution must be homogeneous and isotropic, with an energy momentum tensor having in spatial average the isotropic fluid form

$$\langle T_\nu^\mu \rangle = \text{diag}[\rho, -p, -p, -p], \quad (1.10)$$

where ρ , p are the energy density and pressure, respectively. In such space-time geometry the Einstein equations of general relativity reduce to the Friedmann equation, which determines the evolution of the scale factor from the energy density

$$\left[\frac{\dot{a}(t)}{a(t)} \right]^2 = H^2(t) = \frac{\rho}{3M_{Pl}^2}. \quad (1.11)$$

where $M_{Pl} = 1/\sqrt{8\pi G} = 2.43534 \times 10^{18} \text{ GeV} = 0.434 \times 10^{-5} \text{ g}$. The spatially flat Universe has today the critical density

$$\rho_c = 3 M_{Pl}^2 H_0^2 = 1.878 h^2 10^{-29} \text{ g/cm}^3 = 1.0537 10^{-5} h^2 \text{ GeV/cm}^3. \quad (1.12)$$

where $H_0 = 100 h \text{ km/sec/Mpc}$ is the Hubble constant today, $h = 0.705 \pm 0.013$ [10, 35] and then $H_0 = 1.5028 10^{-42} \text{ GeV}$. Notice that eq.(1.11) implies that $a(t)$ is a monotonic function of time.

The energy momentum tensor conservation reduces to the single conservation equation,

$$\dot{\rho} + 3 H(t) (\rho + p) = 0 \quad (1.13)$$

The two equations (1.11) and (1.13) can be combined to yield the acceleration of the scale factor,

$$\frac{\ddot{a}}{a} = -\frac{1}{6 M_{Pl}^2}(\rho + 3 p) \quad (1.14)$$

which will prove useful later. In order to provide a close set of equations we must append an equation of state $p = p(\rho)$ which is typically written in the form

$$p = w(\rho) \rho \quad (1.15)$$

The following are important cosmological solutions:

Cosmological Constant $\Rightarrow w = -1$: **AD** de Sitter expansion $\Rightarrow \rho = \text{constant}$; $a(t) = a(0) e^{Ht}$; $H = \sqrt{\rho/[3 M_{Pl}^2]}$

$$\text{Radiation} \Rightarrow w = 1/3 : \mathbf{RD} \text{ (Radiation domination)} \Rightarrow \rho(t) = \rho(t_r) a^{-4}(t) ; a(t) = a(t_r) \sqrt{t/t_r} \quad (1.16)$$

$$\text{Non-relativistic (cold) Matter} \Rightarrow w = 0 : \mathbf{MD} \text{ (Matter domination)} \Rightarrow \rho(t) = \rho(t_{eq}) a^{-3}(t) ; a(t) = a(t_{eq}) (t/t_{eq})^{2/3}$$

where t_r and t_{eq} are the values of cosmic time at which the Universe becomes radiation or matter dominated, respectively.

Notice from eqs.(1.14) and (1.16) that accelerated expansion ($\ddot{a}(t) > 0$) takes place if $w < -1/3$.

The universe started by a very short accelerated inflationary stage dominated by the vacuum energy, lasting $\sim 10^{-36}$ sec ending by redshift $z \sim 10^{29}$ and approximately described by the de Sitter metric. This inflationary stage was followed by decelerated expansion, first by the radiation dominated era and then by the matter dominated era. Finally, the universe entered again an accelerated phase dominated by the dark energy, described by a cosmological constant in the Standard Model of the Universe, at $z \simeq 0.5$.

Particle physics at energy scales below ~ 200 GeV is on solid experimental footing in the framework of the standard model of strong and electroweak interactions.

Current theoretical ideas supported by the renormalization group running of the couplings in the standard model of particle physics and its supersymmetric extensions show that the strong, weak and electromagnetic interactions are unified in a grand unified theory (GUT) at the scale $M_{GUT} \sim 10^{16}$ GeV. Furthermore, the characteristic scale at which gravity calls for a quantum description is the Planck scale $M_{Pl} = 1/\sqrt{8\pi G} = 2.43534 \cdot 10^{18}$ GeV $\gg M_{GUT}$.

The connection between the standard model of particle physics and early Universe cosmology is through the semiclassical Einstein equations that couple the space-time geometry to the matter-energy content. As argued above, gravity can be studied semi-classically at energy scales well below the Planck scale. The standard model of particle physics is a *quantum field theory*, thus the space-time is classical but with sources that are quantum fields. Semiclassical gravity is defined by the Einstein's equations with the expectation value of the quantum energy-momentum tensor $\hat{T}^{\mu\nu}$ as the source

$$G^{\mu\nu} = R^{\mu\nu} - \frac{1}{2} g^{\mu\nu} R = \frac{\langle \hat{T}^{\mu\nu} \rangle}{M_{Pl}^2}. \quad (1.17)$$

The expectation value of $\hat{T}^{\mu\nu}$ is taken in a given quantum state (or density matrix) compatible with homogeneity and isotropy which must be translational and rotational invariant. Such state yields an expectation value for the energy momentum tensor with the fluid form eq.(1.10), and the Einstein equations (1.17) reduce to the Friedmann equation (1.11).

All of the ingredients are now in place to understand the evolution of the early Universe. Einstein's equations determine the evolution of the scale factor, particle physics provides the energy momentum tensor and statistical mechanics provides the fundamental framework to describe the thermodynamics from the microscopic quantum field theory of the strong, electroweak interactions and beyond.

The sources for Einstein equations are dark energy, dark and ordinary matter and radiation. The standard model of particle physics describes ordinary matter and radiation.

Dark energy accounts **today** for $72 \pm 1.5\%$ of the energy of the Universe [10]. The current observed value is $\rho_\Lambda = \Omega_\Lambda \rho_c = (2.36 \text{ meV})^4$, $1 \text{ meV} = 10^{-3} \text{ eV}$ [10, 35]. The equation of state is $p_\Lambda = -\rho_\Lambda$ within observational errors corresponding to a cosmological constant.

The nature of the dark energy (today) is not yet understood. A plausible explanation of the dark energy may be the quantum zero point energy of a light matter field in the cosmological space-time. This has the equation of state of a cosmological constant. Notice that the renormalized value of the zero point energy in the cosmological space-time is finite and may be naturally of the order of the (mass)⁴ of the light field involved.

Matter accounts today for $28 \pm 1.5\%$ of the energy of the Universe [10]. 84% of the matter is **dark matter**. Therefore, dark matter is an essential constituent of the universe. The nature of dark matter is still unknown but is certainly beyond the Standard Model of strong and electroweak particle interactions [3, 36]. It is probably formed by particles in the keV mass scale [86].

Main events in the universe after inflation are (see fig. 4):

- Beging of the **RD** era and end of inflation: $z \sim 10^{29}$, $T_{reh} \sim 10^{16} \text{ GeV}$, $t \sim 10^{-36} \text{ sec}$.
- Electro-Weak phase transition: $z \sim 10^{15}$, $T_{EW} \sim 100 \text{ GeV}$, $t \sim 10^{-11} \text{ sec}$.
- QCD phase transition (confinement): $z \sim 10^{12}$, $T_{QCD} \sim 170 \text{ MeV}$, $t \sim 10^{-5} \text{ sec}$.
- Big bang nucleosynthesis (BBN): $z \sim 10^9$, $\ln(1+z) \sim 21$, $T \simeq 0.1 \text{ MeV}$, $t \sim 20 \text{ sec}$.
- Radiation-Matter equality: $z \simeq 3200$, $\ln(1+z) \simeq 8$, $T \simeq 0.7 \text{ eV}$, $t \sim 57000 \text{ yr}$.

- CMB last scattering: $z \simeq 1100$, $\ln(1+z) \simeq 7$, $T \simeq 0.25$ eV, $t \sim 370000$ yr.
- Matter-Dark Energy equality: $z \simeq 0.47$, $\ln(1+z) \simeq 0.38$, $T \simeq 0.345$ meV $t \sim 8.9$ Gyr.
- Today: $z = 0$, $\ln(1+z) = 0$, $T = 2.725$ K $= 0.2348$ meV, $t \equiv t_0 = 13.72$ Gyr.

In fig. 4 we plot ρ_Λ/ρ , ρ_{Matter}/ρ and $\rho_{radiation}/\rho$ as functions of $\log(1+z)$ where $\rho_\Lambda = \Lambda$, $\rho_{Matter} = \Omega_M/a^3$ and $\rho_{radiation} = \Omega_r/a^4$. Notice that $\rho_\Lambda + \rho_{Matter} + \rho_{radiation} = \rho$.

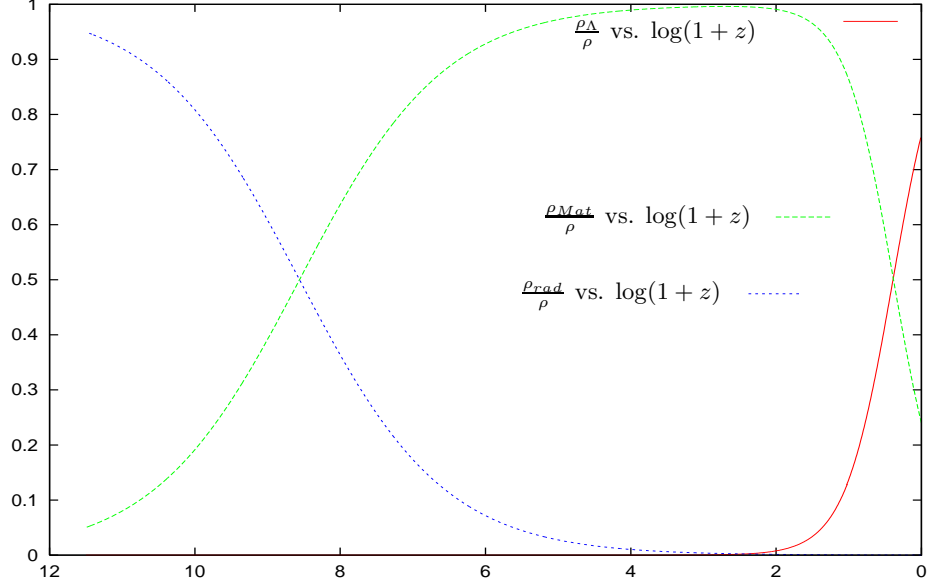


FIG. 4: $\frac{\rho_\Lambda}{\rho}$, $\frac{\rho_{Matter}}{\rho}$ and $\frac{\rho_{radiation}}{\rho}$ vs. $\log(1+z)$.

In summary, the Friedmann equation (1.11) can be written as

$$H^2(t) = H_0^2 \left[\Omega_\Lambda + \frac{\Omega_M}{a^3} + \frac{\Omega_r}{a^4} \right]. \quad (1.18)$$

The temperature of the universe in the post-inflation radiation dominated era (reheating temperature T_r) is bounded from below in order to explain the baryon asymmetry and the Big Bang Nucleosynthesis (BBN). This amounts to a further constraint on the inflationary model. The BBN constraint is the milder. If the observed baryon asymmetry is produced at the electroweak scale, the constraint on the reheating temperature is $\gtrsim 100$ GeV, however the origin of the baryon asymmetry may be at the GUT scale in which case the reheating temperature should be $T_r > 10^9$ GeV [2].

C. The Horizon and Flatness problems in non-inflationary cosmology and their inflationary resolution.

In this section we discuss the horizon and flatness problems that arise in cosmology when there is not an inflationary era before the RD and MD stages.

1. The horizon problem

The particle horizon is the size of the causally connected region at a given time t . It is given by,

$$d(t) = a(t) \int_{t_{min}}^t \frac{dt'}{a(t')}. \quad (1.19)$$

where t_{min} stands for the minimal time where the classical geometry (1.5) applies. The comoving size of the horizon

$$\eta \equiv \int_{t_{min}}^t \frac{dt'}{a(t')}, \quad (1.20)$$

is just the conformal time. η is the maximum comoving distance traveled by a photon since t_{min} . Objects separated by comoving distances larger than η were never in causal contact [3].

For a decelerated matter or radiation dominated geometry, it follows that

$$a(t) = a(t_s) \left(\frac{t}{t_s} \right)^b \quad \text{with} \quad b = \frac{1}{2} \quad \text{for RD} \quad \text{and} \quad b = \frac{2}{3} \quad \text{for MD}. \quad (1.21)$$

Here t_s stands for t_r or t_{eq} , the starting times of the RD or MD eras, respectively.

Inserting eq.(1.21) into eq.(1.19) yields,

$$d(t) = \frac{1}{1-b} \left[t - t_{min} \left(\frac{t}{t_{min}} \right)^b \right] \quad (1.22)$$

Therefore, since $0 < b < 1$ we can take the $t_{min} \rightarrow 0$ limit with the result

$$d(t) = \frac{t}{1-b} = \frac{b}{1-b} \frac{1}{H(t)} = \frac{1}{1-b} \left[\frac{a(t)}{a(t_s)} \right]^{\frac{1}{b}}. \quad (1.23)$$

Notice that $d(t) \rightarrow 0$ for $t \rightarrow 0$ implying that the regions in causal contact were smaller and smaller for $t \rightarrow 0$. This goes against an homogeneous and isotropic universe at early times.

On the contrary, for late times $d(t)$ grows **faster** in eq.(1.23) than the scale factor since $1/b > 1$.

At the time of matter-radiation equality $t \simeq 81300$ yr and $z \simeq 3200$. Therefore, d_0 , the particle horizon today is dominated by the matter dominated era ($b = 2/3$):

$$d_0 = \frac{2}{H_0} = 2 \times 13.9 \text{ Gyr} = 8.55 \text{ Gpc} \quad (1.24)$$

ignoring the present accelerated expansion of the universe.

The photons seen today as the CMB decoupled from matter at $z_d \simeq 1100$, that is $t_d \simeq 370000$ yr. A sphere with the size $d(t_d)$ of the particle horizon at decoupling is the last scattering surface of the photons. The expansion of the universe stretches this sphere and the angle subtended today by this particle horizon is

$$\theta_d = (z_d + 1) \frac{d(t_d)}{d_0} = \frac{1}{\sqrt{z_d + 1}} \simeq 0.03 = 1.7^\circ, \quad (1.25)$$

where we used eq.(1.23) with $b = 2/3$. Thus, the sky should split into

$$\frac{4\pi}{\theta_d^2} = 4\pi (z_d + 1) \simeq 13800 \quad (1.26)$$

patches which had never communicated before the CMB formed. Hence, one would expect a different CMB temperature at each patch. The **horizon problem** is that the CMB temperature in all these patches is the **same** up to fluctuations of order 0.01%, as we know from COBE and WMAP.

We have ignored in this subsection the presence of dark energy. Taking into account the cosmological constant as in sec. IC 6 slightly changes the coefficients in eqs.(1.25) and (1.26):

$$\theta_d = \frac{1.112}{\sqrt{z_d + 1}} \simeq 0.034 = 1.9^\circ, \quad \frac{4\pi}{\theta_d^2} \simeq 11170,$$

where we used eqs.(1.47) and (1.49). This analysis shows that the presence (or absence) of dark energy is irrelevant to the horizon problem since dark energy started to dominate the Universe expansion fairly recently at $z \simeq 0.5$.

2. The flatness problem

Present data [10, 35] supports the spatially flat FRW geometry eq.(1.5)

$$\Omega_0 \equiv \frac{\rho_0}{\rho_c} = 1.003 \pm 0.02 . \quad (1.27)$$

where $\Omega_0 \equiv \Omega(\text{today})$, $\rho_0 \equiv \rho(\text{today})$ and ρ_c is defined by eq.(1.12). However, one can consider the more general homogeneous and isotropic FRW metric eq.(1.4) in which case the Friedmann equation (1.11) takes now the form

$$H^2(t) = \frac{\rho}{3M_{Pl}^2} - \frac{k}{a^2} \quad (1.28)$$

Hence,

$$\Omega = \frac{\rho}{\rho_c} = 1 + \frac{k}{a^2 H^2} \quad (1.29)$$

For a decelerated universe eq.(1.21) we obtain

$$\Omega - 1 = \frac{k}{a^2(t_s) b^2} \left(\frac{t}{t_s} \right)^{2-2b} .$$

Since $2 - 2b > 0$ this quantity **grows** with time. Hence, in order to explain the flatness of the universe today [see eq.(1.27)], the universe must have been **even much flatter** in early times.

3. The solution to the horizon problem in inflation

The solution of the horizon problem provided by inflation can be understood within de Sitter inflation which is an approximation to slow-roll inflation.

The particle horizon during de Sitter inflation [see eq.(1.16)] is given by

$$d(t) = e^{Ht} \int_{t_{min}}^t dt' e^{-Ht'} = \frac{1}{H} \left[e^{H(t-t_{min})} - 1 \right] \simeq \frac{1}{H} \frac{a(t)}{a(t_{min})} \quad (1.30)$$

Here, the size of the causally connected regions grows **exactly** as the scale factor while in decelerated geometries the particle horizon grows **faster** than the scale factor [see eq.(1.23)]. In addition, for t_{min} deep in the past, $d(t) \rightarrow \infty$ since $a(t)/a(t_{min}) \rightarrow \infty$ for fixed t . This is consistent with an homogeneous and isotropic universe at early times since homogeneity and isotropy can establish in a bigger and bigger causally connected region.

The horizon problem arises when $d(t_d) \ll d_0$ as shown by eq.(1.25). Now, since the contribution to $d(t_d)$ from the inflationary epoch [see eq.(1.30)] can be **very large** if $a(t_{end}) \gg a(t_{min})$, where t_{end} stands for the end of inflation, inflation **can solve** the horizon problem. We derive now a lower bound for the ratio

$$e^{N_{tot}} \equiv \frac{a(t_{end})}{a(t_{min})} . \quad (1.31)$$

N_{tot} is the total number of e-folds during inflation.

In order to explain the smallness of the CMB anisotropy today, the particle horizon taken at the end of inflation and then red-shifted today must be at least of the size of the particle horizon today [eq.(1.24)]. That is, the visible universe today was contained inside the horizon during inflation,

$$\frac{1}{H} \frac{a_0}{a(t_{min})} \simeq \frac{1}{H} \frac{a(t_{end})}{a(t_{min})} \left(\frac{a_{eq}}{a_r} \right)_{RD} \left(\frac{a_0}{a_{eq}} \right)_{MD} \geq \frac{3.362 \dots}{H_0} \quad (1.32)$$

where a_r and a_{eq} stand for the scale factor at the beginning and at the end of the RD era, respectively and we used the particle horizon today given by eq.(1.49) which takes into account the present accelerated phase of the universe. We assume for simplicity a sudden transition from the inflationary to the RD era, namely $a(t_{end}) = a(t_r)$. In reality there must be an intermediate reheating stage after inflation where radiation is abundantly created becoming the dominant component in the Universe and establishing the onset of the RD era.

We now insert in eq.(1.32) the following relations obtained from eqs.(1.8) and (1.16),

$$a_{eq} = \frac{a_0}{1 + z_{eq}} \quad , \quad \frac{a_{eq}}{a_r} = \sqrt{\frac{t_{eq}}{t_r}} = \sqrt{\frac{H_r}{H_{eq}}} . \quad (1.33)$$

Notice that the Hubble parameter at the end of inflation and the beginning of the radiation era H_r is smaller than the Hubble parameter at the beginning of inflation H . As we show in sec. 1D3, $H_r \simeq H/\sqrt{N}$ where $N \sim 60$ is the number of efolds since the cosmologically relevant modes exit the horizon till the end of inflation. For simplicity, we used in eq.(1.30) the Hubble parameter H at the beginning of inflation. Replacing the above results, eqs.(1.32) and (1.33), into eq.(1.31) yields

$$e^{N_{tot}} \geq \frac{3.362 \dots}{H_0} \sqrt{H_{eq} H} \frac{N^{\frac{1}{4}}}{1 + z_{eq}} \quad (1.34)$$

Let us consider the Friedmann equation at the transition from RD to MD (at matter-radiation equality)

$$H_{eq}^2 = \frac{2 \rho_m(t_{eq})}{3 M_{Pl}^2} .$$

where $\rho_m(t_{eq}) = \rho_r(t_{eq})$ stand for the matter and radiation densities at matter-radiation equality. Since,

$$\frac{\rho_m(t_{eq})}{\rho_m(t_0)} = \left(\frac{a_0}{a_{eq}} \right)^3 \quad \text{and} \quad \rho_m(t_0) = \Omega_M \rho_c ,$$

we find using also eq.(1.12)

$$H_{eq} = \sqrt{2 \Omega_M} \left(\frac{a_0}{a_{eq}} \right)^{\frac{3}{2}} H_0 = \sqrt{2 \Omega_M} (1 + z_{eq})^{\frac{3}{2}} H_0 . \quad (1.35)$$

Inserting eq.(1.35) into eq.(1.34) yields

$$e^{N_{tot}} \geq 3.362 \dots \sqrt{\frac{H}{H_0}} \left(\frac{2 \Omega_M N}{1 + z_{eq}} \right)^{\frac{1}{4}} . \quad (1.36)$$

and

$$a_r = 100 \beta \left(\frac{2 \Omega_M N}{1 + z_{eq}} \right)^{\frac{1}{4}} \sqrt{\frac{H_0}{M_{Pl}}} , \quad (1.37)$$

where

$$\beta \equiv \sqrt{\frac{10^{-4} M_{Pl}}{H}} . \quad (1.38)$$

Introducing in eqs.(1.36)-(1.38) the explicit values $1 + z_{eq} = 3200$, $N \simeq 60$ and those from table I yields,

$$N_{tot} \geq 64.8 - \log \beta \quad , \quad e^{N_{tot}} \geq \frac{1.39}{\beta} 10^{28} \quad , \quad a_r \simeq 2.5 \beta 10^{-29} . \quad (1.39)$$

As we shall see below [see eq.(1.178)], $\beta \gtrsim 1$ for generic slow-roll inflationary models reproducing the CMB data.

We conclude that an inflationary stage before the RD era **solves** the horizon problem provided inflation lasts **at least sixty-four efolds**.

4. The solution to the flatness problem in inflation

The total density today Ω_0 can be related to the total density at the beginning of inflation following eq.(1.29):

$$\sqrt{|\Omega_0 - 1|} = \sqrt{|\Omega(t_{min}) - 1|} \frac{a(t_{min}) H(t_{min})}{a_0 H_0} .$$

Now, eq.(1.32) precisely ensures that

$$\frac{a(t_{min})}{a_0} \frac{H(t_{min})}{H_0} \leq 1. \quad (1.40)$$

Therefore, having at least sixty-two e-folds of inflation guarantees that $\sqrt{|\Omega_0 - 1|} \leq \sqrt{|\Omega(t_{min}) - 1|}$. There is no need to fine-tune $\Omega(t_{min})$ to unity as it was the case in absence of inflation. The observed value of Ω_0 eq.(1.27) can be explained as the result of a value for $\Omega(t_{min}) \sim \Omega_0$ provided eq.(1.40) is valid which is guaranteed by $N_{tot} \gtrsim 64$.

5. The Entropy of the Universe

The entropy of the universe today is dominated by the photons (the CMB) and takes the value

$$S \sim d_0^3 s_\gamma = 0.66 \times 10^{89}$$

where d_0 is the particle horizon today [eq.(1.24)], s_γ the entropy per unit comoving volume of the photon gas

$$s_\gamma = \frac{2\pi^2}{45} g T^3,$$

$g = 2$ counts the photon polarizations and $T = 2.725$ K is the CMB temperature.

An important problem in cosmology has been to explain such huge value for the entropy today [2, 4].

Let us show that the entropy is constant from the microscopic evolution equation (1.13). Let us consider the energy $E(t)$ inside a comoving volume V_c :

$$E(t) = \rho(t) a^3(t) V_c$$

while the physical volume grows as $V(t) = a^3(t) V_c$. Multiplying eq.(1.13) by $V(t)$ yields,

$$V_c a^3(t) [\dot{\rho} + 3 H(t) (\rho + p)] = \dot{E}(t) + p \dot{V}(t) = 0$$

Therefore, according to the first principle of thermodynamics

$$T dS = dE + p dV = 0$$

and entropy is conserved.

Eq.(1.13) is valid both in classical and quantum field theory as shown in [25, 29]. Namely, the entropy remains **constant** according to the **microscopic** evolution equations. Entropy grows upon coarse-graining of degrees of freedom when quantum decoherence happens as it is the case during inflation. Namely, inflation stretches the lengths by a enormous factor of at least $\sim e^{64} \sim 10^{28}$ making classical the quantum description of matter [29, 67].

More precisely, the huge number of ultrarelativistic particles created during the reheating phase between slow-roll quasi-de Sitter inflation and the RD era must be described by a **density matrix** (probably out of thermal equilibrium) and not by a pure quantum state by the end of reheating. Let us estimate the entropy during reheating.

The entropy by the end of reheating and the beginning of the RD era is dominated by ultrarelativistic particles within a horizon size patch. The horizon size by the end of inflation follows from eqs.(1.30) and (1.31) to be $d(t_{end}) \sim e^{N_{tot}} / H$. Approximating the expansion during reheating by the RD scale factor, the horizon size patch gets redshifted by $\sqrt{H/H_{reh}}$, where H_{reh} stands for the Hubble parameter by the end of reheating and the patch size results

$$d_{reh} \sim \sqrt{\frac{H}{H_{reh}}} d(t_{end}) \sim \frac{e^{N_{tot}}}{\sqrt{H H_{reh}}}. \quad (1.41)$$

The reheating temperature T_{reh} is related to the Hubble parameter H_{reh} by the Friedmann equation:

$$H_{reh}^2 = \frac{\pi^2 g_{rh}}{90 M_{Pl}^2} T_{reh}^4, \quad (1.42)$$

where g_{rh} is the number of ultrarelativistic degrees of freedom by the end of reheating and we used $\rho_r = (\pi^2 g_{rh}/30) T_{reh}^4$ for the energy density of the ultrarelativistic particles. The entropy by the end of reheating is,

$$S_{rh} \sim \frac{2\pi^2 g_{rh}}{45} T_{reh}^3 d_{reh}^3. \quad (1.43)$$

Using eqs.(1.41)-(1.43) and imposing that this value accounts for the entropy today $\sim 10^{89}$ yields

$$S_{rh} \sim 2^{\frac{3}{2}} \left(\frac{2 \pi^2 g_{rh}}{45} \right)^{\frac{1}{4}} e^{3 N_{tot}} \left(\frac{M_{Pl}}{H} \right)^{\frac{3}{2}} \geq 10^{89}$$

That is,

$$N_{tot} \geq 62.4 - \frac{1}{2} \log \beta - \frac{1}{12} \log \frac{g_{rh}}{1000} . \quad (1.44)$$

We thus obtain a lower bound on N_{tot} similar to eq.(1.39) for the solution of the horizon problem.

In summary a number of efolds $N_{tot} \gtrsim 64$ during inflation reproduces the value of the entropy of the universe today and solves both the horizon and flatness problems.

6. The Age of the Universe

Usually, the age of the universe is computed in cosmic time. At the beginning of the matter dominated era the Universe was only $\sim 10^5$ yrs old. Hence, to compute the age of the universe today we can restrict ourselves to the matter and dark energy dominated eras. Therefore, neglecting radiation the Friedmann equation (1.11) in cosmic time takes the form

$$\frac{1}{a} \frac{da}{dt} = H_0 \sqrt{\Omega_\Lambda + \frac{1 - \Omega_\Lambda}{a^3}} ,$$

where $\Omega_\Lambda = \rho_\Lambda / \rho_c$ and then

$$H_0 t = \int_0^a \frac{da}{a \sqrt{\Omega_\Lambda + \frac{1 - \Omega_\Lambda}{a^3}}} = \frac{2}{3\sqrt{\Omega_\Lambda}} \text{Arg Sinh} \left[\sqrt{\frac{\Omega_\Lambda}{1 - \Omega_\Lambda}} a^{\frac{3}{2}} \right] \quad (1.45)$$

Therefore, the scale factor grows as

$$a(t) = \left(\frac{\Omega_\Lambda}{1 - \Omega_\Lambda} \right)^{\frac{1}{3}} \left[\sinh \left(\frac{3}{2} \sqrt{\Omega_\Lambda} H_0 t \right) \right]^{\frac{2}{3}} . \quad (1.46)$$

We have today $t = t_0$ and $a(t_0) = 1$. We thus obtain from eq.(1.45)

$$t_0 = \frac{2}{3 H_0 \sqrt{\Omega_\Lambda}} \text{Arg Sinh} \left[\sqrt{\frac{\Omega_\Lambda}{1 - \Omega_\Lambda}} \right]$$

Here, $\Omega_\Lambda = 0.726$ [10] yields for the age of the Universe in cosmic time

$$t_0 = \frac{0.9887}{H_0} = \frac{9.667}{h} \text{ Gyr} = 13.71 \text{ Gyr}$$

where we used $h = 0.705$ [10]. t_0 grows monotonically with Ω_Λ . In particular, $t_0 \xrightarrow{\Omega_\Lambda \rightarrow 0} 2/(3 H_0)$.

From eq.(1.46) we notice that $a(t)$ exhibits the matter dominated behaviour $\sim t^{\frac{2}{3}}$ for early times $t \ll t_0$ and the de Sitter behaviour $\sim e^{H_0 \Omega_\Lambda t}$ for late times $t \gtrsim t_0$.

For times $t \lesssim 1$ Gyr, $z \lesssim 4$, Ω_Λ can be neglected in eq.(1.18) and the cosmic time results

$$t = \frac{1}{H_0} \int_0^a \frac{a da}{\sqrt{\Omega_r + \Omega_M} a} = \frac{2 \sqrt{\Omega_r}}{3 H_0 \Omega_M} \left[\left(a - \frac{2 \Omega_r}{\Omega_M} \right) \sqrt{1 + \frac{\Omega_M}{\Omega_r} a} + \frac{2 \Omega_r}{\Omega_M} \right] .$$

The Friedmann equation (1.11) in conformal time eq.(1.20) takes the form

$$\frac{1}{a^2} \frac{da}{d\eta} = H_0 \sqrt{\Omega_\Lambda + \frac{1 - \Omega_\Lambda}{a^3}} .$$

Thus [90],

$$H_0 \eta = \int_0^a \frac{da}{a^2 \sqrt{\Omega_\Lambda + \frac{1-\Omega_\Lambda}{a^3}}} = \frac{1}{3^{\frac{1}{4}} \Omega_\Lambda^{\frac{1}{6}} (1-\Omega_\Lambda)^{\frac{1}{3}}} F(\phi, q) . \quad (1.47)$$

Here, $F(\phi, q)$ is the elliptic integral of first kind,

$$\cos \phi = \frac{(1-\sqrt{3})\Omega_\Lambda^{\frac{1}{3}} a + (1-\Omega_\Lambda)^{\frac{1}{3}}}{(1+\sqrt{3})\Omega_\Lambda^{\frac{1}{3}} a + (1-\Omega_\Lambda)^{\frac{1}{3}}} \quad \text{and} \quad q = \sin\left(\frac{5\pi}{12}\right) = \frac{1+\sqrt{3}}{2\sqrt{2}} . \quad (1.48)$$

The age of the universe in conformal time η_0 follows by setting $a = 1$ in eqs.(1.47)-(1.48),

$$\eta_0 = \frac{3.3623\dots}{H_0} = \frac{32.88\dots}{h} \text{ Gyr} = \frac{10.1\dots}{h} \text{ Gpc} = 47.6 \text{ Gyr} = 14.3 \text{ Gpc} , \quad (1.49)$$

where we used $\Omega_\Lambda = 0.726$ and $h = 0.705$ [10]. Notice that η_0 coincides with the particle horizon today eq.(1.19).

From eq.(1.47) we obtain the scale factor as function of the conformal time,

$$a(\eta) = \left(\frac{1-\Omega_\Lambda}{\Omega_\Lambda} \right)^{\frac{1}{3}} \frac{1 - \text{cn}(u, q)}{\sqrt{3} - 1 + (1 + \sqrt{3}) \text{cn}(u, q)} \quad (1.50)$$

where $u \equiv 3^{\frac{1}{4}} \Omega_\Lambda^{\frac{1}{6}} (1-\Omega_\Lambda)^{\frac{1}{3}} H_0 \eta$ and $\text{cn}(u, k)$ is the Jacobi cosinus function [88].

Since the integral in eq.(1.47) converges for $a = \infty$, the conformal time ranges in the finite interval:

$$0 \leq \eta \leq \eta_1 \equiv \frac{2.8044\dots}{\Omega_\Lambda^{\frac{1}{6}} (1-\Omega_\Lambda)^{\frac{1}{3}}} \frac{1}{H_0} = 4.554\dots \frac{1}{H_0} .$$

It follows from eqs.(1.47) and (1.50) that the scale factor behaves for early times as matter dominated,

$$a(\eta) \stackrel{\eta \rightarrow 0}{\simeq} \frac{1}{4} (1-\Omega_\Lambda) (H_0 \eta)^2 \rightarrow 0 ,$$

while for times η approaching η_1 , $a(\eta)$ exhibits a de Sitter behaviour,

$$a(\eta) \stackrel{\eta \rightarrow \eta_1}{\simeq} \frac{1}{\sqrt{\Omega_\Lambda} H_0 (\eta_1 - \eta)} \rightarrow \infty .$$

We see that the comoving particle horizon keeps growing, asymptotically reaching the limiting size $\eta_1 \simeq 63.2 \text{ Gyr} = 19.4 \text{ Gpc}$ for $a(\eta) \rightarrow \infty$.

D. Inflationary Dynamics in the Effective Theory of Inflation

As discussed in the previous section, inflation was originally proposed to solve the flatness, horizon and entropy problems [1] thus becoming an important paradigm in cosmology. At the same time, it provides a natural mechanism for the generation of scalar density fluctuations that seed large scale structure as well as that of tensor perturbations (primordial gravitational waves), thus explaining the origin of the temperature anisotropies in the cosmic microwave background (CMB). Inflation is the statement that the cosmological scale factor $a(t)$ has a *positive acceleration*, namely, $\ddot{a}(t)/a(t) > 0$. Hence, eq.(1.14) requires the equation of state $w = p/\rho < -1/3$.

Inflation gives rise to a remarkable phenomenon: physical wavelengths grow *faster* than the size of the Hubble radius

$$d_H = \frac{a(t)}{\dot{a}(t)} = \frac{1}{H(t)} ,$$

indeed,

$$\frac{\dot{\lambda}_{phys}}{\lambda_{phys}} = \frac{\dot{a}}{a} = H(t) = \frac{\dot{d}_H}{d_H} + d_H \frac{\ddot{a}}{a} , \quad (1.51)$$

Therefore, during inflation ($\ddot{a} > 0$), eq.(1.51) states that *physical wavelengths become larger than the Hubble radius*. Once a physical wavelength becomes larger than the Hubble radius, it is causally disconnected from physical processes. The inflationary era is followed by the radiation dominated and matter dominated stages where the acceleration of the scale factor becomes negative since $p/\rho = 1/3$ in a radiation dominated era and $p = 0$ in a matter dominated era [see eq.(1.14)]. With a negative acceleration of the scale factor, the Hubble radius grows **faster** than the scale factor, and wavelengths that were outside the Hubble radius, can now re-enter the Hubble radius. This is depicted in fig. 5. This

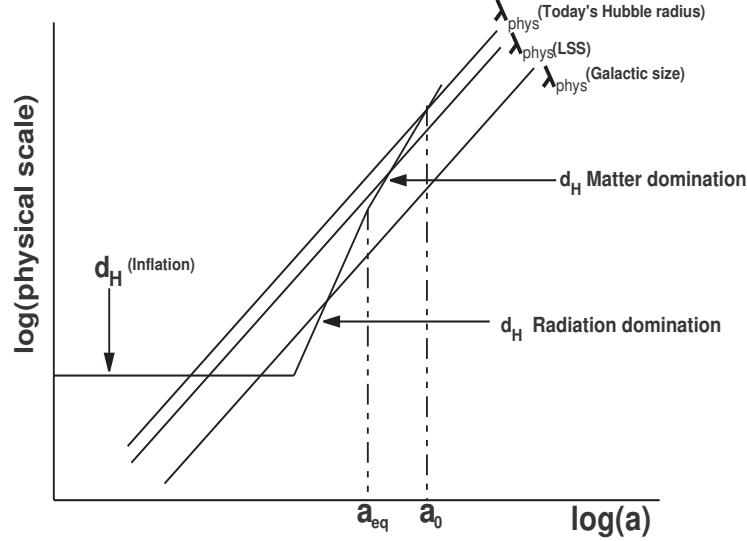


FIG. 5: Logarithm of physical scales vs. logarithm of the scale factor. The Hubble radius d_H is shown for the inflationary (De Sitter), radiation dominated and matter dominated stages. The physical wavelengths for today's Hubble radius $d_H(today)$, and a galactic scale λ_{gal} are shown. We see that modes that leave the horizon during inflation get back during the RD and MD eras with wavelengths today between the galactic sizes and today's Hubble radius.

is the main concept behind the inflationary paradigm for the generation of the CMB temperature fluctuations as well as for providing the seeds for large scale structure formation: quantum fluctuations generated early in the inflationary stage exit the Hubble radius during inflation, and eventually re-enter the horizon during the matter dominated era.

The basic mechanism for generation of temperature anisotropies and primordial gravitational waves through inflation is the following [2, 3, 4]: the energy momentum tensor is split into the classical fluid component $T_{fluid}^{\mu\nu}$ [eq.(1.10)] that drives the classical FRW metric plus small quantum fluctuations $\delta T^{\mu\nu}$, namely

$$T^{\mu\nu} = T_{fluid}^{\mu\nu} + \delta T^{\mu\nu}.$$

The quantum fluctuations of the matter fields induce quantum fluctuations in the metric (space-time geometry) $\delta G^{\mu\nu} = \delta T^{\mu\nu}/M_{Pl}^2$. In the linearized approximation, the different wavelengths of the perturbations evolve independently. After a given wavelength exits the Hubble radius, the corresponding perturbation becomes *causally disconnected* from microphysical processes. Perturbations that re-enter the horizon late in the RD era and during the MD era, induce small fluctuations in the space-time metric which generate fluctuations in the matter distribution driving acoustic oscillations in the photon-baryon fluid. At the last scattering surface, when photons decouple from the plasma these oscillations are imprinted in the power spectrum of the temperature anisotropies of the CMB and seed the inhomogeneities which generate structure upon gravitational collapse[3, 5].

The horizon problem, namely why the temperature of the CMB is nearly homogeneous and isotropic (to one part in 10^5) is solved by an inflationary epoch because the wavelengths corresponding to the Hubble radius at the time of recombination were *inside* the Hubble radius hence in causal contact during inflation (see sec. IC 3). This mechanism is depicted in fig. 5.

Slow-roll inflation leads to a gaussian and nearly scale invariant spectrum of adiabatic scalar (curvature) and tensor (gravitational waves) primordial fluctuations. These predictions of inflationary models make the inflationary paradigm robust and have been spectacularly confirmed by the WMAP data for curvature (temperature) fluctuations [8, 9, 10].

WMAP has also provided perhaps the most striking validation of inflation as a mechanism for generating *superhorizon* fluctuations, through the measurement of the anticorrelation peak in the temperature-polarization (TE) angular power spectrum at $l \sim 150$ corresponding to superhorizon scales [8, 9].

Let us now estimate the wavenumbers of the cosmologically relevant modes that reenter the horizon today. They have a wavelength at most of the order of the horizon today [eq.(1.49)]

$$\eta_0 = \frac{3.362 \dots}{H_0} \simeq \frac{10.1}{h} \text{ Gpc} \simeq 14.3 \text{ Gpc}$$

Notice that the conformal time eq.(1.20) coincides at any time with the comoving size of the horizon eq.(1.19).

Actually, a more precise calculation in eq.(1.68) yields for the CMB quadrupole modes (the longest observed wavelengths) [22, 23]

$$k_Q = \frac{3.342 \dots}{\eta_0 - \eta_{LSS}} = 1.014 \times H_0 = 0.238 \text{ Gpc}^{-1} = 1.52 \times 10^{-42} \text{ GeV} , \quad (1.52)$$

where LSS stands for last scattering surface. Notice that half the quadrupole wavelength today is very close to the horizon size today eq.(1.49).

According to eqs.(1.37)-(1.39) the physical wavenumber k of a mode today and its physical wavenumber k^{init} at the beginning of inflation are related by the redshift factor

$$k^{init} = \frac{e^{N_{tot}}}{a_r} k = 2.49 \cdot 10^{56} \beta^{-1} e^{N_{tot}-64} k . \quad (1.53)$$

The total number of efolds during inflation must be $N_{tot} \geq 64$ according to eq.(1.39). We choose $N_{tot} = 64$ as benchmark value since the detailed analysis of the fast-roll explanation of the quadrupole suppression (see secs. I D 4 and I I G) favours $N_{tot} = 64$ [23]. Another **hint** to choose $N_{tot} \simeq 64$ comes from the WMAP preferred value $n_s \simeq 0.96$ (see sec. I I G).

In particular, we find for the quadrupole mode from eqs.(1.52) and (1.53)

$$k_Q^{init} = 3.79 \beta^{-1} e^{N_{tot}-64} 10^{14} \text{ GeV} . \quad (1.54)$$

[Recall that $1 \text{ GeV} = 1.564 \times 10^{41} (\text{Gpc})^{-1}$].

CMB and LSS observations allow to detect the k -modes over four orders of magnitude, in a range going from $\sim 1 \text{ Mpc}$ to $\sim 10^4 \text{ Mpc}$: $k_Q < k < 10^4 k_Q$. At the beginning of inflation this corresponds to the physical wavenumbers

$$3.8 \cdot 10^{14} \text{ GeV} \beta^{-1} e^{N_{tot}-64} < k^{init} < 3.8 \cdot 10^{18} \text{ GeV} \beta^{-1} e^{N_{tot}-64} . \quad (1.55)$$

These energy values are to be compared with the inflaton mass scale [eq.(1.178)] $m \sim 10^{13} \text{ GeV}$. We see that the cosmologically relevant modes are in a range going from ~ 30 inflaton masses m till the Planck scale for typical values $N_{tot} \sim 64$ and $H \sim 10^{-4} M_{Pl}$. These Planck scale k -values are high energy modes within the effective theory of inflation since $k \gg M$ for them.

A k -mode crosses the horizon when $k \eta \sim 1$, η being the comoving horizon size eq.(1.20). Actually, it is convenient to redefine η after inflation as,

$$\eta \equiv \int_{t_{end}}^t \frac{dt'}{a(t')} = \int_{a_r}^a \frac{da}{a^2 H(a)} , \quad (1.56)$$

where $a_r \sim 10^{-29}$ eq.(1.39). Alternatively, the horizon crossing condition for a k -mode can be taken $k = H(t) a(t)$ as depicted in fig. 1. Using eqs.(1.18) and (1.56) we find

$$\eta(z) = \frac{I(z)}{H_0} \quad \text{where} \quad I(z) \equiv \int_{a_r}^{\frac{1}{z+1}} \frac{da}{\sqrt{\Omega_r + \Omega_M a + \Omega_\Lambda a^4}} \quad (1.57)$$

and the wavevector $k(z)$ that reenters the horizon at redshift z is given by

$$k(z) \sim \frac{H_0}{I(z)} . \quad (1.58)$$

We normalize $k(z)$ such that $k(z=0) = k_Q$ given by eq.(1.52) and we use that $I(0) = 3.3623$. This yields,

$$k(z) = 3.409 \frac{H_0}{I(z)} . \quad (1.59)$$

For $z \gtrsim 1$, Ω_Λ can be neglected in the integrand of $I(z)$ and we obtain

$$I(z) = \frac{2\sqrt{\Omega_r}}{\Omega_M} \left[\sqrt{1 + \frac{\Omega_M}{\Omega_r(z+1)}} - 1 \right] = 0.0659 \left[\sqrt{1 + \frac{3227}{z+1}} - 1 \right] . \quad (1.60)$$

The corresponding ℓ -multipole is given by the maximum of the spherical Bessel function [3] $j_\ell(x)$ where

$$x \equiv k (\eta_0 - \eta_{LSS}) \gg 1 , \quad (1.61)$$

and

$$\eta_0 - \eta_{LSS} = \frac{1}{H_0} \int_{\frac{1}{1+z_{LSS}}}^1 \frac{da}{\sqrt{\Omega_r + \Omega_M a + \Omega_\Lambda a^4}} , \quad (1.62)$$

is the comoving distance between today and the last scattering surface (LSS). We find using table I and $z_{LSS} = 1100$,

$$\eta_0 - \eta_{LSS} = \frac{3.296}{H_0} . \quad (1.63)$$

Hence, k^{init} (at the beginning of inflation) and x are related by

$$k^{init} = 1.135 \cdot 10^{14} \text{ GeV } e^{N_{tot}-64} \beta^{-1} x . \quad (1.64)$$

and we find for $x(z)$

$$x(z) = k(z) (\eta_0 - \eta_{LSS}) = \frac{11.24}{I(z)} . \quad (1.65)$$

where we used eqs.(1.53), (1.59), (1.61) and (1.63).

For large ℓ and x the maximum of $j_\ell(x)$ is at $\ell \sim x$ where Watson's formula applies [88]

$$j_\ell(x) \stackrel{\ell, x \gg 1}{\approx} \sqrt{\frac{\pi}{2x}} \left(\frac{3y}{\ell + \frac{1}{2}} \right)^{\frac{1}{3}} S(y) , \quad (1.66)$$

where,

$$y \equiv \frac{(x^2 - [l + 1/2]^2)^{3/2}}{3 [l + 1/2]^2} \quad \text{and} \quad S(y) \equiv J_{\frac{1}{3}}(y) + J_{-\frac{1}{3}}(y) .$$

Here $J_{\pm\frac{1}{3}}(y)$ are Bessel functions. The function $y^{\frac{1}{3}} S(y)$ has its maximum at $y = 0.685948\dots$ and hence eq.(1.66) gives the maximum of $j_\ell(x)$ at

$$\ell + \frac{1}{2} = x \left[1 - \frac{0.808617\dots}{x^{\frac{2}{3}}} + \mathcal{O}\left(x^{-\frac{4}{3}}\right) \right] , \quad x = \left(\ell + \frac{1}{2} \right) \left[1 + \frac{0.808617\dots}{\left(\ell + \frac{1}{2} \right)^{\frac{2}{3}}} + \mathcal{O}\left(\left[\ell + \frac{1}{2} \right]^{-\frac{4}{3}} \right) \right] , \quad x, \ell \gg 1 . \quad (1.67)$$

Therefore, $\ell + \frac{1}{2}$ is **smaller** than x at the maximum of $j_\ell(x)$ by an amount of the order $x^{\frac{1}{3}}$. In particular, at $\ell = 2$ eq.(1.67) yields $x = 3.597\dots$ for the position of the maximum which is only 8% larger than the exact result $x = 3.342\dots$. Namely, the physical quadrupole ($\ell = 2$) wavemodes today k_Q are related to the particle horizon by [3]

$$k_Q (\eta_0 - \eta_{LSS}) = 3.342\dots , \quad (1.68)$$

where the spherical Bessel function $j_2(k [\eta_0 - \eta_{LSS}])$ takes its maximum value, and $\eta_0 - \eta_{LSS}$ is given by eq.(1.63). Therefore, using the present value for H_0 [10] we obtain $k_Q = 0.238 \text{ (Gpc)}^{-1}$.

z	$k^{init} e^{64-N_{tot}} \beta$	ℓ
0	$3.7 \cdot 10^{14}$ GeV	2
1100	$1.9 \cdot 10^{16}$ GeV	161
1678	$2.6 \cdot 10^{16}$ GeV	220
3200	$4.5 \cdot 10^{16}$ GeV	385

TABLE II: The reentering redshift z , the initial wavenumber k and the corresponding CMB multipole ℓ .

The modes reentering during the MD and Λ D eras are in the range

$$0 \leq z \leq 3200 \quad , \quad 2 \leq \ell \leq 392 \quad , \quad k_Q^{init} \leq k^{init} \leq 4.44 \cdot 10^{16} \text{ GeV } e^{N_{tot}-64} \beta^{-1} .$$

where we used eqs.(1.60), (1.65) and (1.67). For example, $\ell(z = 1100) = 161$ and $\ell(z = 1678) = 220$ (first peak in fig. 1) reenter in the MD era. We display in Table II the reentering redshift z , the wavenumber k^{init} and the corresponding CMB multipole ℓ .

We have from eqs.(1.60) and (1.65) for $x \gtrsim 3$, $\ell \gtrsim 2$,

$$x(z) = 5.35 \sqrt{\Omega_r} (z+1) \left[1 + \sqrt{1 + \frac{\Omega_M}{\Omega_r (z+1)}} \right] = 0.0493 (z+1) \left[1 + \sqrt{1 + \frac{3227}{z+1}} \right] ,$$

$$z+1 = \frac{10.14 x^2}{x + 79.55} . \quad (1.69)$$

For example, we get $\ell \simeq x \simeq 10^4$ for $z \simeq 10^5$ which is well after BBN. For such modes $k^{init} \simeq \beta^{-1} 10^{18} e^{N_{tot}-64}$ GeV. We want to draw the attention on the fact that $k^{init} < M_{Pl}$ for $\ell < 2 \times 10^4 e^{N_{tot}-64} \beta^{-1}$ and $z < 2 \times 10^5 e^{N_{tot}-64} \beta^{-1}$ as follows from eqs.(1.64), (1.67) and (1.69). Namely, the range eq.(1.55) of CMB detectable modes **does not contain** trans-planckian wavenumbers for the value $N_{tot} \sim 64$ derived in sec. ID 4. Truly trans-Planckian modes $k \gg M_{Pl}$ are unobservable through the CMB-LSS data. Information about trans-Planckian modes could be obtained perhaps in the future through the 21cm H line [84]. The CMB multipoles $\ell < 200$ exhibiting features [8, 9, 10] are definitely **sub-Planckian** if $N_{tot} \sim 64$, since they have $k^{init} < 2 \beta^{-1} e^{N_{tot}-64} 10^{16}$ GeV according to eqs.(1.64) and (1.67).

1. Inflation and Inflaton field dynamics

A simple implementation of the inflationary scenario is based on a single scalar field, the *inflaton* with a Lagrangian density

$$\mathcal{L} = a^3(t) \left[\frac{\dot{\varphi}^2}{2} - \frac{(\nabla \varphi)^2}{2a^2(t)} - V(\varphi) \right] , \quad (1.70)$$

where $V(\varphi)$ the inflaton potential. Since the universe expands exponentially fast during inflation, gradient terms are exponentially suppressed and can be neglected. At the same time, the exponential stretching of spatial lengths classicalize the physics and permits a classical treatment. One can therefore consider an homogeneous and classical inflaton field $\varphi(t)$ which obeys the evolution equation

$$\ddot{\varphi} + 3 H(t) \dot{\varphi} + V'(\varphi) = 0 . \quad (1.71)$$

in the isotropic and homogeneous FRW metric eq.(1.5) which is sourced by the inflaton.

The energy density and the pressure for a spatially homogeneous inflaton are given by

$$\rho = \frac{\dot{\varphi}^2}{2} + V(\varphi) \quad , \quad p = \frac{\dot{\varphi}^2}{2} - V(\varphi) . \quad (1.72)$$

The scale factor $a(t)$ obeys the Friedmann equation eq.(1.11) which here takes the form

$$H^2(t) = \frac{1}{3M_{Pl}^2} \left[\frac{1}{2} \dot{\varphi}^2 + V(\varphi) \right] . \quad (1.73)$$

The time derivative of the Hubble parameter takes the form

$$\dot{H}(t) = -\frac{\dot{\varphi}^2}{2 M_{Pl}^2} \quad (1.74)$$

where we used eqs.(1.71) and (1.73). This shows that $H(t)$ **decreases monotonically** with time.

The inflaton fields starts at $t = 0$ with some chosen values of φ and $\dot{\varphi}$ and evolves together with the scale factor according to eqs.(1.71) and (1.73). The inflaton clearly rolls down the slope of the potential going towards a local minimum of $V(\varphi)$. The basic constraint on the inflationary potential is

$$V(\varphi_{min}) = V'(\varphi_{min}) = 0 . \quad (1.75)$$

That is, the inflaton potential **must vanish** at its minimum φ_{min} in order to have a finite number of efolds. The inflaton evolves from its initial value (which is model dependent) towards the minimum φ_{min} . If $V(\varphi_{min}) > 0$, we see from eq.(1.73) that inflation will be eternal. That is, a de Sitter phase will continue forever with the inflaton at the constant value φ_{min} .

There are two main classes of inflaton potentials leading to two main classes of inflation.

(a) In **small field inflation** the minimum of the potential is at a non-zero value $\varphi_{min} \neq 0$ and the inflaton field starts near (or at) $\varphi = 0$ evolving towards $\varphi = \varphi_{min}$. These are typically discrete symmetry ($\varphi \rightarrow -\varphi$) breaking potentials [32],

$$V(\varphi) = \frac{\lambda}{4} \left(\varphi^2 - \frac{m^2}{\lambda} \right)^2 = -\frac{m^2}{2} \varphi^2 + \frac{\lambda}{4} \varphi^4 + \frac{m^4}{4\lambda} \quad , \quad \text{new inflation} . \quad (1.76)$$

For historical reasons small field inflation is often called **new inflation**.

(b) In **large field inflation** the minimum of the potential is at $\varphi_{min} = 0$ and the inflaton field starts at $\varphi \gg M$ evolving towards $\varphi = 0$. These are typically unbroken symmetry potentials [33],

$$V(\varphi) = +\frac{m^2}{2} \varphi^2 + \frac{\lambda}{4} \varphi^4 \quad , \quad \text{chaotic inflation} . \quad (1.77)$$

For historical reasons large field inflation is often called **chaotic inflation**.

As we discussed in sec. IB, inflation should last at least $N_{tot} \gtrsim 64$ efolds in order to solve the entropy, horizon and flatness problems. Inflation can produce such large number of efolds provided it lasts enough time. This can be achieved if the inflaton evolves slowly (slow-roll), namely $\dot{\varphi}^2 \ll V(\varphi)$. This implies from eq.(1.72) that

$$\rho = -p \simeq V(\varphi) \simeq \text{constant},$$

as the equation of state leading to a de Sitter universe. Eq.(1.73) yields as scale factor

$$a(t) \simeq e^{H t} \quad , \quad H \simeq \sqrt{\frac{V(\varphi)}{3 M_{Pl}^2}} \quad (1.78)$$

[see eq.(1.16)]. However, eq.(1.78) is only an approximation to the slow-roll inflationary dynamics [see the discussion in sec. ID 3 and eqs.(1.102) and (1.105)].

While inflationary dynamics is typically studied in terms of a *classical* homogeneous inflaton field as explained above, such classical field must be understood as the expectation value of a *quantum field* in an isotropic and homogeneous quantum state. In ref.[25, 29, 30] the *quantum dynamics* of inflation was studied for inflaton potentials belonging to the two main classes small and large field inflation discussed above.

The initial quantum state was taken to be a gaussian wave function(al) with vanishing or non-vanishing expectation value of the field. This state evolves in time with the full inflationary potential which features an unstable (spinodal) region for $\varphi^2 < m^2/(3\lambda)$ where $V''(\varphi) < 0$ in the broken symmetric case eq.(1.76). Just as in the case of Minkowski space time, there is a band of spinodally or parametrically unstable wavevectors, in which the amplitude of the quantum fluctuations grows exponentially fast [25, 36]. Because of the cosmological expansion wave vectors are redshifted into the unstable band and when the wavelength of the unstable modes becomes larger than the Hubble radius these modes become *classical* with a large amplitude and a frozen phase. These long wavelength modes assemble into a classical coherent and homogeneous condensate, which obeys the equations of motion of the classical inflaton[25, 29, 30]. This phenomenon of classicalization and the formation of a homogeneous condensate takes place during the *first* 5–10 efolds after the beginning of the inflationary stage. The **non perturbative** quantum field theory treatment in refs.[25, 29, 30] shows that this rapid redshift and classicalization justifies the use of an homogeneous classical inflaton leading to the following robust conclusions [25, 29, 30]:

- The quantum fluctuations of the inflaton are of two different kinds:

(a) Large amplitude quantum inflaton fluctuations generated at the beginning of inflation through spinodal instabilities or parametric resonance depending on the inflationary scenario chosen. They have at the beginning of inflation physical wavenumbers in the range of (see [25, 29, 30])

$$k \lesssim 10 m, \quad (1.79)$$

and they become superhorizon a few efolds after the beginning of inflation. The phase of these long-wavelength inflaton fluctuations freeze out and their amplitude grows thereby effectively forming a homogeneous *classical* inflaton condensate. The study of more general initial quantum states featuring highly excited distribution of quanta lead to similar conclusions [30]: during the first few efolds of evolution the rapid redshift produces a classicalization of long-wavelength inflaton fluctuations and the emergence of a homogeneous coherent inflaton condensate obeying the *classical equations of motion* in terms of the inflaton potential.

(b) Cosmological scales relevant for the observations *today* between ~ 1 Mpc and the horizon today had first crossed (exited) the Hubble radius inside a window of about 10 e-folds from ~ 63 to ~ 53 efolds before the end of inflation [2]. These correspond to small fluctuations of high physical wavenumbers at the beginning of inflation in the range given by eq.(1.55). Since [eq.(1.178)] $m \sim 10^{13}$ GeV, we see that the large amplitude modes eq.(1.79) for typical values $N_{tot} \sim 64$ and $H \sim 10^{-4} M_{Pl}$ are **below** the wavenumbers k of the cosmologically relevant modes eq.(1.55).

- During the rest of the inflationary stage the dynamics is described by this classical homogeneous condensate that obeys the classical equations of motion with the inflaton potential. Thus, inflation even if triggered by an initial quantum state or density matrix of the quantum field, is effectively described in terms of a classical homogeneous scalar condensate.

The body of results emerging from these studies provide a justification for the description of inflationary dynamics in terms of a *classical* homogeneous scalar field. The conclusion is that after a few initial e-folds during which the unstable wavevectors are redshifted well beyond the Hubble radius, all what remains for the ensuing dynamics is a homogeneous classical condensate, plus small quantum fluctuations corresponding to the wave k -modes.

These **small** quantum fluctuations include scalar curvature and tensor gravitational fluctuations. They must be treated together with the inflaton fluctuations in the unified gauge invariant approach we present in sec. IE [5]. In the treatment of **large** amplitude quantum inflaton fluctuations, gravitational fluctuations can be safely neglected [25].

Inflation based on a scalar inflaton field should be considered as an **effective theory**, namely, not necessarily a fundamental theory but as a low energy limit of a microscopic fundamental theory. The inflaton may be a coarse-grained average of fundamental scalar fields, or a composite (bound state) of fields with higher spin, just as in superconductivity. Bosonic fields do not need to be fundamental fields, for example they may emerge as condensates of fermion-antifermion pairs $\langle \bar{\Psi}\Psi \rangle$ in a grand unified theory (GUT) in the cosmological background. In order to describe the cosmological evolution it is enough to consider the effective dynamics of such condensates. The relation between the low energy effective field theory of inflation and the microscopic fundamental theory is akin to the relation between the effective Ginsburg-Landau theory of superconductivity [16] and the microscopic BCS theory, or like the relation of the $O(4)$ sigma model, an effective low energy theory of pions, photons and nucleons (as skyrmions), with quantum chromodynamics (QCD) [17]. The guiding principle to construct the effective theory is to include the appropriate symmetries [17]. Contrary to the sigma model where the chiral symmetry strongly constraints the model [17], only general covariance can be imposed on the inflaton model.

In summary, the physics during inflation is characterized by:

- Out of equilibrium matter field evolution in a rapidly expanding space-time dominated by the vacuum energy. The scale factor is quasi-de Sitter: $a(t) \simeq e^{Ht}$.
- Extremely high energy density at the scale of $\lesssim 10^{16}$ GeV.
- Explosive particle production at the beginning of inflation due to spinodal or parametric **instabilities** for new and chaotic inflation, respectively [25, 29].
- The enormous redshift as a consequence of a large number of e-folds (~ 64) classicalizes the dynamics: an **assembly** of (superhorizon) fluctuations behave as the classical and homogeneous inflaton field. The inflaton which is a long-wavelength condensate slowly rolls down the potential hill towards its minimum [29].
- Quantum non-linear phenomena eventually **shut-off** the instabilities and **stop** inflation [25, 29, 30].

As indicated above eq.(1.55), the cosmologically relevant fluctuations have at the beginning of inflation physical wavelengths in a range reaching the Planck scale

$$3.3 \cdot 10^{-32} e^{64-N_{tot}} \beta \text{ cm} \lesssim \lambda^{init} = 2\pi/k^{init} \lesssim 3.3 \cdot 10^{-28} e^{64-N_{tot}} \beta \text{ cm} ,$$

These fluctuations become macroscopic through the huge redshift during inflation and the subsequent expansion of the universe with wavelengths today in the range $1 \text{ Mpc} \lesssim \lambda_{today} \lesssim 10^4 \text{ Mpc}$. Namely, a total redshift of 10^{56} . During this process these quantum fluctuations classicalize just due to the huge stretching of the lengths. A field theoretical treatment shows that the quantum density matrix of the inflaton becomes diagonal in the inflaton field representation as inflation ends [29, 67].

2. Slow-roll, the Universal Form of the Inflaton Potential and the Energy Scale of Inflation

The inflaton potential $V(\varphi)$ must be a slowly varying function of φ in order to permit a slow-roll solution for the inflaton field $\varphi(t)$ which guarantees a total number of efolds ~ 64 as discussed in secs. IC and ID. Slow-roll inflation corresponds to a fairly flat potential and the slow-roll approximation usually invokes a hierarchy of dimensionless ratios in terms of the derivatives of the potential [3, 5, 6, 8]. We recast here the slow-roll approximation as an expansion in $1/N$ where $N \sim 60$ is the number of efolds since the cosmologically relevant modes exit the horizon till the end of inflation [11].

We start by writing the inflaton potential in dimensionless variables as [12]

$$V(\varphi) = M^4 v \left(\frac{\varphi}{M_{Pl}} \right) , \quad (1.80)$$

where M is the energy scale of inflation and $v(\psi)$ a dimensionless function. The effective theory of inflation is consistent provided $M \ll M_{Pl}$ which is actually the case as shown by the WMAP data of the CMB anisotropy amplitude [see below, eqs.(1.175) and (1.177)]. The inflaton potential eq.(1.80) has the slow-roll property built-in since a change of φ of the order $\lesssim M$ leads to a small change on $V(\varphi)$ thanks to $M \ll M_{Pl}$.

In the slow-roll regime higher time derivatives can be neglected in the evolution eqs.(1.71) and (1.73) with the result

$$3 H(t) \dot{\varphi} + V'(\varphi) = 0 \quad , \quad H^2(t) = \frac{V(\varphi)}{3M_{Pl}^2} \quad (1.81)$$

These first order equations can be solved in closed form as

$$N[\varphi] = - \int_{\varphi/M_{Pl}}^{\varphi_{end}/M_{Pl}} v(\psi) \frac{d\psi}{d\varphi} d\psi . \quad (1.82)$$

where $\psi = \varphi/M_{Pl}$ and $N[\varphi]$ is the number of e-folds since the field φ exits the horizon till the end of inflation (where φ takes the value φ_{end}). This is in fact the slow roll solution of the evolution equations eqs.(1.71) and (1.73) in terms of quadratures.

Eq.(1.82) indicates that $N[\varphi]$ scales as ψ^2 and therefore the field $\varphi = \psi M_{Pl}$ is of the order $\sqrt{N} \sim \sqrt{60}$ for the cosmologically relevant modes. Therefore, we propose as universal form for the inflaton potential [11]

$$V(\varphi) = N M^4 w(\chi) , \quad (1.83)$$

where χ is a dimensionless, slowly varying field

$$\chi = \frac{\varphi}{\sqrt{N} M_{Pl}} , \quad (1.84)$$

More precisely, we choose $N \equiv N[\varphi]$ as the number of e-folds since a pivot mode k_0 exits the horizon till the end of inflation. Eq.(1.83) includes all well known slow-roll families of inflation models such as new inflation [32], chaotic inflation [33], natural inflation [48], etc.

The dynamics of the rescaled field χ exhibits the slow time evolution in terms of the *stretched* dimensionless cosmic time variable,

$$\tau = \frac{t M^2}{M_{Pl} \sqrt{N}} \quad , \quad \mathcal{H} \equiv \frac{H M_{Pl}}{\sqrt{N} M^2} = \mathcal{O}(1) . \quad (1.85)$$

The rescaled variables χ and τ change slowly with time. A large change in the field amplitude φ results in a small change in the χ amplitude, a change in $\varphi \sim M_{Pl}$ results in a χ change $\sim 1/\sqrt{N}$. The form of the potential, eq.(1.83), the rescaled dimensionless inflaton field eq.(1.84) and the time variable τ make **manifest** the slow-roll expansion as a consistent systematic expansion in powers of $1/N$ [11].

We can choose $|w''(0)| = 1$ without losing generality. Then, the inflaton mass scale around zero field is given by a see-saw formula

$$m^2 = |V''(\varphi = 0)| = \frac{M^4}{M_{Pl}^2} \quad , \quad m = \frac{M^2}{M_{Pl}} \quad . \quad (1.86)$$

The Hubble parameter when the cosmologically relevant modes exit the horizon is given by

$$H = \sqrt{N} \, m \, \mathcal{H} \sim 7 \, m \quad , \quad (1.87)$$

where we used that $\mathcal{H} \sim 1$. As a result, $m \ll M$ and $H \ll M_{Pl}$. The value of M is determined by the amplitude of the CMB fluctuations within the effective theory of inflation. We obtain in sec. 1D [see eqs.(1.177) and (1.178)]: $M \sim 0.70 \, 10^{16} \, \text{GeV}$, $m \sim 2.04 \, 10^{13} \, \text{GeV}$ and $H \sim 10^{14} \, \text{GeV}$ for generic slow-roll potentials eq.(1.83).

The energy density and the pressure [eq.(1.72)] in terms of the dimensionless rescaled field χ and the slow time variable τ take the form,

$$\frac{\rho}{N \, M^4} = \frac{1}{2 \, N} \left(\frac{d\chi}{d\tau} \right)^2 + w(\chi) \quad , \quad \frac{p}{N \, M^4} = \frac{1}{2 \, N} \left(\frac{d\chi}{d\tau} \right)^2 - w(\chi) \quad . \quad (1.88)$$

The equations of motion (1.71) and (1.73), in the same variables become

$$\begin{aligned} \mathcal{H}^2(\tau) &= \frac{\rho}{N \, M^4} = \frac{1}{3} \left[\frac{1}{2 \, N} \left(\frac{d\chi}{d\tau} \right)^2 + w(\chi) \right] \quad , \\ \frac{1}{N} \frac{d^2\chi}{d\tau^2} + 3 \, \mathcal{H} \frac{d\chi}{d\tau} + w'(\chi) &= 0 \quad . \end{aligned} \quad (1.89)$$

In addition, eqs.(1.89) imply for the derivative of the Hubble parameter

$$\frac{d\mathcal{H}}{d\tau} = -\frac{1}{2} \left(\frac{d\chi}{d\tau} \right)^2 \quad .$$

Notice that,

$$\frac{d}{d\tau} \ln a = N \, \mathcal{H} \quad .$$

The slow-roll approximation follows by neglecting the $1/N$ terms in eqs.(1.89). Both $w(\chi)$ and $\mathcal{H}(\tau)$ are of order N^0 for large N . Both equations make manifest the slow-roll expansion as an expansion in $1/N$.

Eq.(1.82) in terms of the field χ takes the form

$$- \int_{\chi_{exit}}^{\chi_{end}} \frac{w(\chi)}{w'(\chi)} d\chi = 1 \quad . \quad (1.90)$$

This gives $\chi = \chi_{exit}$ at horizon exit as a function of the couplings in the inflaton potential $w(\chi)$.

Inflation ends after a finite number of efolds provided [see eq.(1.75)]

$$w(\chi_{end}) = w'(\chi_{end}) = 0 \quad . \quad (1.91)$$

So, this condition is enforced in the inflationary potentials.

For the quartic degree potentials $V(\varphi)$ eqs.(1.76)-(1.77), the corresponding dimensionless potentials $w(\chi)$ take the form

$$w(\chi) = \frac{y}{32} \left(\chi^2 - \frac{8}{y} \right)^2 = -\frac{1}{2} \chi^2 + \frac{y}{32} \chi^4 + \frac{2}{y} \quad , \quad \text{BNI : binomial new inflation} \quad , \quad (1.92)$$

$$w(\chi) = \frac{1}{2} \chi^2 + \frac{y}{32} \chi^4 \quad , \quad \text{BCI : binomial chaotic inflation} \quad , \quad (1.93)$$

where the coupling y is of **order one** and

$$\lambda = \frac{y}{8N} \left(\frac{M}{M_{Pl}} \right)^4 \ll 1 \quad \text{since} \quad M \ll M_{Pl} \quad .$$

For a general potential $V(\varphi)$ we can always eliminate the linear term by a shift in the field φ without loosing generality,

$$V(\varphi) = V_0 \pm \frac{1}{2} m^2 \varphi^2 + \sum_{n=3}^{\infty} \frac{\lambda_n}{n} \varphi^n \quad , \quad (1.94)$$

and

$$w(\chi) = w_0 \pm \frac{1}{2} \chi^2 + \sum_{n=3}^{\infty} \frac{G_n}{n} \chi^n \quad , \quad (1.95)$$

where the dimensionless coefficients G_n are of order one. We find from eqs. (1.83) and (1.84),

$$V_0 = N M^4 w_0 \quad , \quad \lambda_n = \frac{G_n M^4}{N^{\frac{n}{2}-1} M_{Pl}^n} \quad , \quad (1.96)$$

In particular, we get comparing with eqs.(1.76), (1.77), (1.92) and (1.93),

$$\lambda_3 = \frac{G_3}{\sqrt{N}} \frac{M^4}{M_{Pl}^3} \quad , \quad \lambda = \lambda_4 = \frac{G_4}{N} \left(\frac{M}{M_{Pl}} \right)^4 \quad , \quad G_4 = \frac{y}{8} \quad . \quad (1.97)$$

We find the dimensionful couplings λ_n suppressed by the n th power of M_{Pl} as well as by the factor $N^{\frac{n}{2}-1}$. Notice that this suppression factors are natural and come from the ratio of the two relevant energy scales here: the Planck mass and the inflation scale M .

In new inflation with the potential of eq.(1.92), the inflaton starts near the local maximum $\chi = 0$ and keeps rolling down the potential hill till it reaches the absolute minimum $\chi = \sqrt{8/y}$. In chaotic inflation [eq.(1.93)] the inflaton starts at some significant value $\chi \gtrsim 3$ and rolls down the potential hill till it reaches the absolute minimum $\chi = 0$. The initial values of χ and $\dot{\chi}$ must be chosen to have a total of $\gtrsim 64$ efolds of inflation. In all cases $\chi(0)$ and $\dot{\chi}(0)$ turn to be of order one.

There are two *generic* inflationary regimes: slow-roll and fast-roll depending on whether

$$\begin{aligned} \frac{1}{2N} \left(\frac{d\chi}{d\tau} \right)^2 &\ll w(\chi) \quad : \quad \text{slow-roll regime} \\ \frac{1}{2N} \left(\frac{d\chi}{d\tau} \right)^2 &\sim w(\chi) \quad : \quad \text{fast-roll regime} \end{aligned} \quad (1.98)$$

Both regimes show up in **all** inflationary models in the class eq.(1.83). A fast-roll stage emerges from generic initial conditions for the inflaton field. This fast-roll stage is generally very short and is followed by the slow-roll stage (see sec. ID 3). The slow-roll regime is an attractor in this dynamical system.

The possibility of using $1/N$ as an expansion to study inflationary dynamics was advocated in ref.[60]. The analysis above confirms this early suggestion and establishes the slow-roll expansion as a systematic expansion in $1/N$ where N is the number of e-folds since the cosmologically relevant modes exited the horizon till the end of inflation [11].

The generalization of the universal form eq.(1.83) to inflationary models with more than one field is straightforward

$$V(\varphi_1, \varphi_2) = N M^4 w \left(\frac{\varphi_1}{\sqrt{N} M_{Pl}}, \frac{\varphi_2}{\sqrt{N} M_{Pl}} \right) \quad .$$

(See ref.[13] for hybrid inflation).

Eq.(1.83) for the inflaton potential resembles the moduli potential coming from supersymmetry breaking,

$$V_{susy}(\varphi) = m_{susy}^4 v \left(\frac{\varphi}{M_{Pl}} \right) \quad , \quad (1.99)$$

where m_{susy} stands for the supersymmetry breaking scale. Potentials with such form were used in the inflationary context in refs.[48, 58]. In our context, eq.(1.99) implies that $m_{susy} \sim 10^{16}$ Gev. That is, the supersymmetry breaking scale m_{susy} turns out to be at the GUT scale $m_{susy} \sim M_{GUT}$.

It must be stressed that the validity of the inflaton potential eq.(1.83) is independent of whether or not there is an underlying supersymmetry. In addition, the observational support on inflaton potentials like eq.(1.83) can be taken as a first signal of the presence of supersymmetry in a cosmological context. No experimental signals of supersymmetry are known so far despite the enormous theoretical work done on supersymmetry since 1971.

3. Inflationary Dynamics: Homogeneous Inflaton

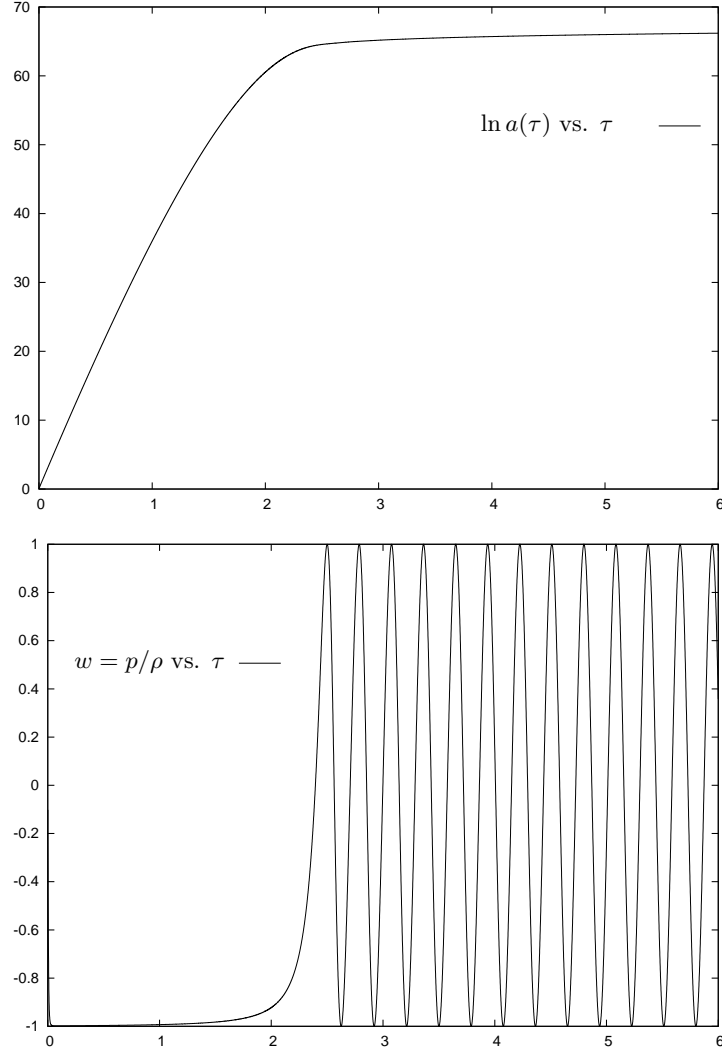


FIG. 6: Upper panel: $\ln a(\tau)$ which is the number of e-folds as a function of the stretched cosmic time eq.(1.85). We see that $a(\tau)$ grows exponentially with time (quasi-de Sitter inflation) for $\tau < \tau_{end} \simeq 2.39$. Lower panel: the equation of state $w = p/\rho$ vs. τ [eq.(1.15)]. We have $w \simeq -1$ after the fast-roll stage and before the end of inflation. That is, for $0.0247 \lesssim \tau < \tau_{end} \simeq 2.39$ w oscillates with zero average: $\langle w \rangle = 0$ during the subsequent matter dominated era. Both figures are for the inflaton potential eq.(1.92) with $y = 1.26$ and $N_{tot} = 64$ e-folds of inflation. $w = p/\rho$ is plotted for $0 < \tau < 0.0365$ allowing to see the fast-roll stage in fig. 26.

To leading order in the slow-roll approximation (neglecting $1/N$ corrections) the inflaton equations of motion (1.89)

are solvable in terms of quadratures

$$\tau = - \int_{\chi(0)}^{\chi} d\chi' \frac{\sqrt{3 w(\chi')}}{w'(\chi')} . \quad (1.100)$$

where we used that

$$\mathcal{H}(\tau) = \sqrt{\frac{w(\chi)}{3}} + \mathcal{O}\left(\frac{1}{N}\right) , \quad (1.101)$$

to leading order in $1/N$. We find for the new inflationary model (broken symmetric potential) eq.(1.92):

$$\chi(\tau) = \chi(0) e^{\sqrt{\frac{y}{6}} \tau} + \mathcal{O}\left(\frac{1}{N}\right) = \sqrt{\frac{8}{y}} e^{-\sqrt{\frac{y}{6}} (\tau_{end} - \tau)} + \mathcal{O}\left(\frac{1}{N}\right) , \quad (1.102)$$

$$\begin{aligned} \mathcal{H}(\tau) &= \sqrt{\frac{2}{3y}} \left[1 - e^{-\sqrt{\frac{2y}{3}} (\tau_{end} - \tau)} \right] + \mathcal{O}\left(\frac{1}{N}\right) , \\ w = \frac{p}{\rho} &= -1 + \frac{y}{6N} \frac{1}{\sinh^2 \left[\sqrt{\frac{y}{6}} (\tau_{end} - \tau) \right]} + \mathcal{O}\left(\frac{1}{N^2}\right) \end{aligned} \quad (1.103)$$

$$\text{for } 0 \leq \tau \leq \tau_{end} = \sqrt{\frac{3}{2y}} \ln \left[\frac{8}{\chi^2(0)y} \right] + \mathcal{O}\left(\frac{1}{\sqrt{N}}\right) . \quad (1.104)$$

where we used eqs.(1.72), (1.100) and (1.101). Inflation ends when the equation of state becomes $w \sim 0$. According to eq.(1.103), w vanishes when $\tau_{end} - \tau \sim \mathcal{O}(1/\sqrt{N})$. Therefore, expressions eqs.(1.102)-(1.103) are valid as long as

$$0 \leq \tau_{end} - \tau < \mathcal{O}\left(\frac{1}{\sqrt{N}}\right) .$$

That is, eqs.(1.102) hold while the inflaton is not very near the minimum of the potential $\chi_{end} = \sqrt{8/y}$.

We obtain for the scale factor $a(t)$ integrating the Hubble parameter $\mathcal{H}(\tau)$

$$\begin{aligned} \log \frac{a(t)}{a(0)} &= \sqrt{\frac{2}{3y}} N \tau - \frac{N}{8} \chi^2(0) \left[e^{\sqrt{\frac{2y}{3}} \tau} - 1 \right] = \\ &= \sqrt{\frac{2N}{3y}} m t - \frac{N}{8} \chi^2(0) \left[e^{\sqrt{\frac{2y}{3N}} m t} - 1 \right] , \end{aligned} \quad (1.105)$$

where we used eqs.(1.85) and (1.102). It must be noticed that $a(t)$ **is not** a de Sitter scale factor, even in the large N limit at fixed τ .

As a pedagogical example of inflationary dynamics we display the main features for the new inflationary model (broken symmetric potential) eq.(1.92) for $y = 1.26$. This value of y is favoured by the MCMC analysis of the CMB and LSS data (see secs. IID and IIG). We solved eqs.(1.89) numerically and plot the results in figs. 6, 7 and 8. We choose initial kinetic energy equal to the initial potential energy of the inflaton (and hence zero initial pressure),

$$\frac{1}{2N} \dot{\chi}^2(0) = w(\chi(0)) \quad (1.106)$$

(no slow-roll initially). We choose the initial value of the inflaton such that the total number of efolds during inflation is $N_{tot} \simeq 64$ full-filling the constraints of sec. IC. This is achieved for $\chi(0) = 0.740$, $\dot{\chi}(0) = 12.6$. Qualitatively similar results are obtained for any values for $\chi(0)$ and $\dot{\chi}(0)$ of order one.

The inflaton reaches very soon, by $\tau \simeq 0.0247$ and $\ln a = 1.0347$, a slow-roll stage as displayed in figs. 6, 7 and 8. This is a general property and implies that the slow-roll regime is an **attractor** for this dynamical system [41]. We see a de Sitter-like expansion during the slow-roll stage $0.0247 \lesssim \tau \lesssim 2.39$ during which the Hubble parameter decreases slowly and monotonically. Both $\chi(\tau)$ and $\dot{\chi}(\tau)$ grow at the same pace during slow-roll according to eq.(1.102) with

$$\dot{\chi}(\tau) \simeq \sqrt{\frac{y}{6}} \chi(\tau) .$$

[Compare with fig. 7 where $\sqrt{y/6} = 0.4583$].

Inflation ends at $\tau = \tau_{end} \simeq 2.39$ when the pressure becomes positive. This time corresponds to $t_{end} \simeq 0.901 \cdot 10^{-36}$ sec according to eqs.(1.85) and (2.24). The slow-roll analytic expression eq.(1.104) yields

$$\tau_{end}^{slow-roll} = \sqrt{\frac{3}{2y}} \ln \left[\frac{8}{\chi^2(0)y} \right] \simeq 2.67$$

which exceeds by 12 %, namely by $\mathcal{O}(1/\sqrt{N}) \simeq 0.13$ for $N = 60$, the exact numerical result $\tau_{end} \simeq 2.39$.

At the end of inflation the number of efolds is $\ln a \simeq 64$, the inflaton is near its minimum $\chi = \sqrt{8/y} \simeq 2.52$, $\dot{\chi}$ starts to oscillate around zero and $\mathcal{H}(\tau)$ begins a rapid decrease (see figs. 6, 7 and 8). At this time the inflaton field is no longer slowly coasting in the $w''(\chi) < 0$ region but rapidly approaching its equilibrium minimum. When inflation ends the inflaton is at its minimum up to corrections of order $1/\sqrt{N}$. Therefore, we see from the Friedmann eq.(1.89) and eqs.(1.102) that

$$\frac{1}{N} \left(\frac{d\chi}{d\tau} \right)^2 (\tau_{end}) = \mathcal{O} \left(\frac{1}{N} \right) \quad , \quad w(\chi(\tau_{end})) = \mathcal{O} \left(\frac{1}{N} \right) \quad \text{therefore,} \quad \mathcal{H}(\tau_{end}) = \mathcal{O} \left(\frac{1}{\sqrt{N}} \right) , \quad (1.107)$$

while $\mathcal{H}(0) = \mathcal{O}(1)$. Namely, the Hubble parameter decreases by a factor of the order $\sqrt{N} \sim 8$ during slow-roll inflation. We see in fig. 8 that the exact $\mathcal{H}(\tau)$ decreases by a factor six during slow-roll inflation, confirming the slow-roll analytic estimate.

We can compute the total number of inflation efolds N_{tot} to leading order in slow-roll inserting the analytic formula for τ_{end} eq.(1.104) in eq.(1.105) with the result,

$$N_{tot} = \frac{N}{y} \left[\ln \left(\frac{8}{\chi^2(0)y} \right) - 1 + \frac{1}{8} y \chi^2(0) \right] + \mathcal{O} \left(\frac{1}{\sqrt{N}} \right) . \quad (1.108)$$

In the case considered, $y = 1.26$ and $\chi(0) = 0.740$, eq.(1.108) yields $N_{tot} = 1.22 N$, about 14% in excess of the exact result $N_{tot} = 64$. We find here again an error $\mathcal{O}(1/\sqrt{N}) \simeq 0.13$ for $N = 60$.

In the upper panel of fig. 6 we depict $\ln a(\tau)$ vs. τ , that is the number of e-folds as a function of time [by definition $N_e(t) \equiv \ln a(\tau)$].

We have carried out analogous numerical studies in scenarios of chaotic inflation with similar results: if the initial kinetic energy of the inflaton is of the same order as the potential energy, a *fast-roll* stage is *always* present.

An initial state for the *inflaton* (inflaton classical dynamics) with approximate *equipartition* between kinetic and potential energies is a more *general* initialization of cosmological dynamics in the effective field theory than slow-roll which requires that the inflaton kinetic energy is much smaller than its potential energy. The most *generic* initialization of the inflaton dynamics in the effective field theory leads to a *fast-roll* stage followed by slow-roll inflation [22].

The equations of motion (1.89) can be linearized around the absolute minimum of the potential $\chi_{end} = \sqrt{8/y}$ with asymptotic solution

$$\begin{aligned} \chi(\tau) &\stackrel{\tau \gg 1}{\simeq} \sqrt{\frac{8}{y}} + \frac{2}{\sqrt{3} N \tau} \cos \left[\sqrt{2 N} (\tau - \tau_{end}) \right] \left[1 + \mathcal{O} \left(\frac{1}{\tau} \right) \right] \\ \mathcal{H}(\tau) &\stackrel{\tau \gg 1}{\simeq} \frac{2}{3 N \tau} \left[1 + \mathcal{O} \left(\frac{1}{\tau} \right) \right] . \end{aligned} \quad (1.109)$$

or, in dimensionful variables

$$\begin{aligned} \varphi(t) &\stackrel{m t \gg 1}{\simeq} \frac{m}{\sqrt{\lambda}} + \frac{2}{\sqrt{3}} \frac{M_{Pl}}{m t} \cos \left[\sqrt{2} m (t - t_{end}) \right] \left[1 + \mathcal{O} \left(\frac{1}{m t} \right) \right] \\ H(t) &\stackrel{m t \gg 1}{\simeq} \frac{2}{3 t} \left[1 + \mathcal{O} \left(\frac{1}{m t} \right) \right] . \end{aligned} \quad (1.110)$$

Notice that this asymptotic behaviour is independent of the coupling y and is in agreement with the numerical integration of eqs.(1.89) plotted in fig. 7.

The energy density and the pressure take in this regime the form

$$\frac{\rho}{N M^4} = \frac{4}{3 N^2 \tau^2} \quad , \quad w = \frac{p}{\rho} = -\sin \left[2 \sqrt{2 N} (\tau - \tau_{end}) \right] = -\sin \left[2 \sqrt{2} m (t - t_{end}) \right] ,$$

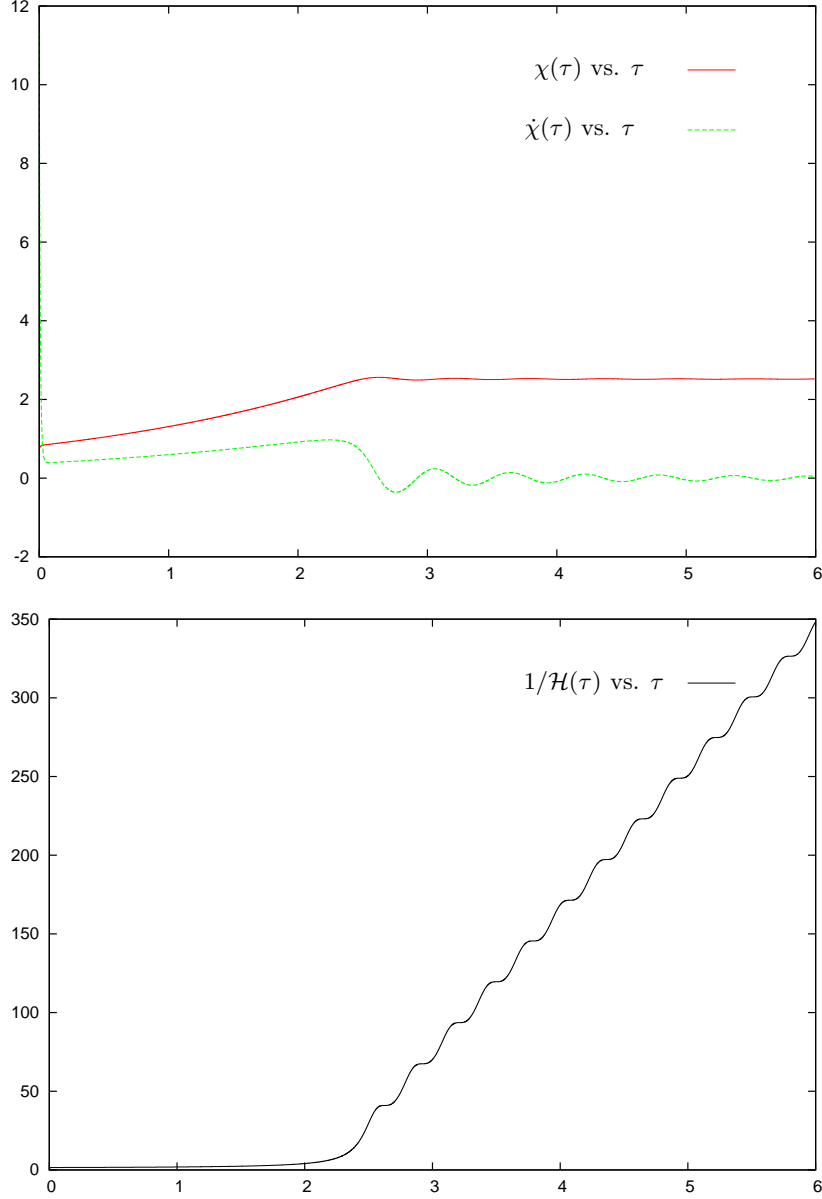


FIG. 7: Upper panel: $\chi(\tau)$ and $\dot{\chi}(\tau)$ as a function of the stretched cosmic time τ for $\chi(0) = 0.740$ and initial kinetic energy equal to the initial potential energy eq.(1.106) which implies $\dot{\chi}(0) = 12.6$. After a short fast-roll stage for $\tau \lesssim 0.0247$ the inflaton field slowly rolls toward its absolute minimum at $\chi = \sqrt{8/y} \simeq 2.52 \dots$, $\dot{\chi} = 0$. $\chi(\tau)$ and $\dot{\chi}(\tau)$ are plotted for $0 < \tau < 0.034$ allowing to see the fast-roll stage in fig. 26. Lower panel: $1/\mathcal{H}$ vs. τ . $1/\mathcal{H}$ grows slowly during inflation $\tau < \tau_{end} \simeq 2.39$ and grows as $1/\mathcal{H} \simeq \frac{3}{2} N (\tau - \tau_{end})$ in the subsequent matter dominated era.

where we used eqs.(1.88) and (1.109). [Compare with fig. 6 where the oscillation frequency of w takes the value $2\sqrt{2}N \simeq 21.91$.]

The inflationary stage is here followed by a matter dominated stage as we see from figs. 6 and 7. This is always the case when one considers an homogeneous inflaton field. In order to reach a radiation dominated era, inhomogeneous modes, namely k -modes with nonzero $k \gg m$, must be present and dominating the energy of the universe.

As discussed in section IC a successful inflationary scenario requires at least a total number of e-folds ~ 64 to solve the horizon and entropy problems.

Wavelengths of cosmological relevance today exited the Hubble radius about $N \sim 60$ e-folds before the *end* of inflation within a window of width $\Delta N \sim 10$. This window corresponds to a small interval $\Delta\tau \lesssim 0.5$. A scale k_0

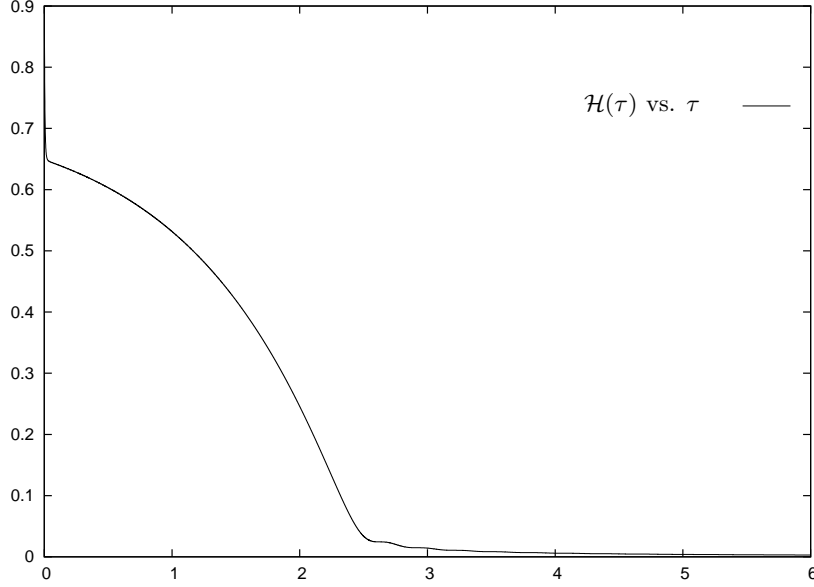


FIG. 8: $\mathcal{H}(\tau)$ as a function of the stretched cosmic time τ for the same inflaton potential, initial conditions and coupling y as in figs. 6 and 7. In fig. 26 $\mathcal{H}(\tau)$ is plotted for $0 < \tau < 0.034$ allowing to more clearly see the fast-roll stage.

which exits the horizon about 3 or 6 efolds after the beginning of inflation is chosen as pivot. We see from figs. 6 and 7 that this corresponds to $\tau \sim 0.076$ or 0.15 and $\chi_{exit} \sim 0.9$ in both cases. We have from eq.(1.84) in dimensionful variables,

$$\varphi_{exit} \sim 7 M_{Pl} . \quad (1.111)$$

The value of the inflaton field at horizon exit is $\chi_{exit} \sim 0.9$ **smaller** than one for new inflation and the coefficients G_n in the inflaton potential $w(\chi)$ [eq.(1.95)] are of order one. Therefore, higher order terms in $w(\chi)$ can be neglected. This is the basic reason why one can restrict to quartic potentials in new inflation (see discussion in sec. II E).

It is interesting to obtain the energy scale of the inflaton field at symmetry breaking and horizon crossing. For the broken-symmetry new inflation potential eq.(1.92), we have for the symmetry breaking scale $\chi_{min} = \sqrt{8/y}$ which corresponds to the dimensionful inflaton field [see eq.(1.84)] [18]:

$$\varphi_{min} = \sqrt{N} M_{Pl} \chi_{min} = \sqrt{\frac{8N}{y}} M_{Pl} \sim 20 M_{Pl} .$$

We want to draw attention to the fact that the energy density for such fields φ_{min} and φ_{exit} is of the order $N M^4 \ll M_{Pl}^4$ due to eq.(1.83). Therefore, the effective theory of inflation **does** apply for such fields φ_{exit} (see sec. III A).

We consider translationally and rotationally invariant cosmology where the only source of inhomogeneities are (small) quantum fluctuations. Indeed, inhomogeneities cannot be excluded at the beginning of inflation but the redshift of scales during inflation by at least a factor $e^{64} \sim 10^{28}$ effectively erases all eventual initial inhomogeneities. As a consequence of this, all structures and inhomogeneities in the present universe originated from the small quantum fluctuations during inflation (see sec. I E).

4. Fixing the Total Number of Inflation e-folds from Fast-Roll and the CMB Quadrupole suppression

We shall discuss in sec. II G how an early fast-roll stage of inflation can explain the CMB quadrupole suppression. Such analysis shows that in order to explain the CMB quadrupole suppression, the quadrupole mode must exit the horizon by the end of fast-roll.

The physical quadrupole ($l = 2$) wavemode today k_Q is given by eq.(1.52) $k_Q = 0.238 \text{ (Gpc)}^{-1}$, while at the beginning of inflation (see Table VII),

$$k_Q^{init} = 11.5 m = 1.39 \times 10^{14} \text{ GeV} . \quad (1.112)$$

The total number of inflation efolds N_{tot} equals N plus the number of efolds from the beginning of inflation till the pivot scale k_0 exits the horizon. According to Table VII,

$$N_{tot} \simeq N_{CosmoMC} + 6.2 = N_{WMAP} + 3, \quad (1.113)$$

where $N_{CosmoMC}$ and N_{WMAP} stand for the number of efolds since the respective pivot scale k_0 exits the horizon till the end of inflation.

Using eqs.(1.52) and (1.112) the redshift z_{init} at the begining of inflation takes the value,

$$\frac{1}{a_{init}} = 1 + z_{init} \equiv \frac{k_Q^{init}}{k_Q} = 0.915 \times 10^{56} \simeq e^{129}.$$

Equating this relation with the redshift at the begining of inflation eq.(1.53) yields

$$N_{tot} \simeq 63 + \ln \beta. \quad (1.114)$$

Therefore, the early fast-roll stage not only explains the CMB quadrupole supression but in addition **fixes the total** number of efolds during inflation. Combining this with the lower bound eq.(1.39) on N_{tot} that solves the horizon problem yields,

$$\ln \beta \geq 0.9 \quad , \quad \beta \geq 2.46 \quad \text{and} \quad N_{tot} \geq 63.9.$$

This bound for β is very close to the new inflation best fit eq.(2.24) $\beta \sim 2$. We conclude that the lower bound eq.(1.39) should be practically saturated and

$$N_{tot} \simeq 64 \quad , \quad \beta \simeq 2.5. \quad (1.115)$$

These values of N_{tot} and β a fortiori fufill also the lower bound eq.(1.44) from the entropy. Furthermore, our MCMC simulations give good fits for $N \sim 60$. $N_{tot} \sim 64$ corresponds to $N_{CosmoMC} \sim 57$ and $N_{WMAP} \sim 61$ according to eq.(1.113). These values are indistinguishable in practice from $N \sim 60$ in the slow-roll ($1/N$) expansion since $1/57 - 1/60 \simeq 0.0009$ and $1/61 - 1/60 \simeq 0.0003$.

Combining the lower bound for N_{tot} eq.(1.39) with eqs.(1.38) and (1.114) yields a lower bound for β and consequently an upper bound for H ,

$$\beta \geq 2.5 \quad , \quad H \leq 0.4 \times 10^{14} \text{GeV}.$$

This is compatible with the estimate eq.(1.178) and the best fit eq.(2.24) for H .

The value of $H_r \simeq H/\sqrt{N}$ [see eq.(1.107)] can be bounded from **below** in order to explain the baryon asymmetry and the BBN. The bound depends on the mechanism responsible of these phenomena. For example, if the baryon asymmetry follows from the out of equilibrium decay of GUT bosons we have $H_r > 10^9 \text{GeV}$ [2]. This implies $\beta < 180$ and the **lower** bound from eq.(1.114),

$$N_{tot} \simeq 63 + \ln \beta < 68.2, \quad (1.116)$$

which is respected by our best value $N_{tot} \simeq 64$ from eq.(1.115).

In summary, combining the value of the observed CMB anisotropy amplitude and the MCMC analysis of the CMB+LSS data including the early fast-roll stage leading to the CMB quadrupole suppression **fixes** $N_{tot} \simeq 64$.

The fact that several independent theoretical arguments and data (MCMC analysis of CMB+LSS data with BNI plus the fast-roll stage in secs. IID 2 and IIG 4, simple sharp transition from inflation to RD which entails eq.(1.53) and the a_r value eq.(1.39) derived in sec. IC 3) combine consistently yielding $N_{tot} \simeq 64$ is a **major success** of the effective theory of inflation.

E. Gauge invariant Scalar and Tensor Fluctuations

The effective field theory of slow-roll inflation has two main ingredients: the classical Friedmann equation in terms of a *classical* part of the energy momentum tensor described by a homogeneous and isotropic condensate, and a quantum part. The latter features scalar fluctuations determined by a gauge invariant combination of the inflaton field and metric fluctuations, and a tensor component, namely gravitational waves. A consistency condition for this description is that the contributions from the fluctuations to the energy momentum tensor be much smaller than those

from the homogeneous and isotropic condensate. The effective field theory must include renormalization counterterms so that it is insensitive to the possible ultraviolet singularities of the short wavelength fluctuations. Different initial conditions on the mode functions of the quantum fluctuations yield different values for their contribution to the energy momentum tensor.

Criteria for acceptable initial conditions must include the following: (i) back reaction effects from the quantum fluctuations should not modify the inflationary dynamics described by the inflaton, (ii) the ultraviolet counterterms that renormalize the energy momentum tensor should not depend on the particular choice of initial conditions, namely different initial conditions *should not* introduce new ultraviolet divergences: a single renormalization scheme, independent of initial conditions, should render the energy momentum tensor UV finite. This set of criteria imply that the ultraviolet allowed states have their large k behaviour constrained up to the fourth order in $1/k$ [37].

Notice that only gauge invariant fluctuations and the full gauge invariant energy-momentum tensor of scalar and tensor fluctuations are physically meaningful.

1. Scalar Curvature Perturbations

The gauge invariant curvature perturbation of the comoving hypersurfaces is given in terms of the Newtonian (Bardeen) potential ψ and inflaton fluctuation $\delta\varphi$ by [5]

$$\mathcal{R} = -\psi - \frac{H}{\dot{\varphi}} \delta\varphi . \quad (1.117)$$

where $\dot{\varphi}$ stands for the derivative of the inflaton field φ with respect to the cosmic time t .

In longitudinal gauge and in cosmic time the metric including the fluctuation takes the form

$$ds^2 = (1 + 2\phi) dt^2 - a^2(t) (1 - 2\psi) d\vec{x}^2 ,$$

where ϕ is the other Newtonian or Bardeen potential. In single-field inflation one can impose the condition $\phi = \psi$ [5].

It is convenient to introduce the gauge invariant potential [5],

$$u(\vec{x}, t) = -z \mathcal{R}(\vec{x}, t) , \quad (1.118)$$

where

$$z \equiv a(t) \frac{\dot{\varphi}(t)}{H(t)} . \quad (1.119)$$

The action for the gauge invariant curvature fluctuations field $u(\vec{x}, t)$ follows from the Einstein-Hilbert action for the gravitational field plus the action for the inflaton in the cosmological space-time. The quadratic part of the action takes in conformal time η [eq.(1.20)] the form [5],

$$S = \frac{1}{2} \int d\eta d^3x \left[(\partial_\eta u)^2 - (\nabla u)^2 + \frac{\partial_\eta^2 z}{z} u^2 \right] . \quad (1.120)$$

The gauge invariant field $u(\vec{x}, t)$ expanded in terms of conformal time mode functions and creation and annihilation operators takes the form [5]

$$u(\vec{x}, \eta) = \int \frac{d^3k}{(2\pi)^{\frac{3}{2}}} \left[\alpha_{\mathcal{R}}(\vec{k}) S_{\mathcal{R}}(k; \eta) e^{i\vec{k}\cdot\vec{x}} + \alpha_{\mathcal{R}}^\dagger(\vec{k}) S_{\mathcal{R}}^*(k; \eta) e^{-i\vec{k}\cdot\vec{x}} \right] , \quad (1.121)$$

where the operators obey canonical commutation relations

$$\left[\alpha_{\mathcal{R}}(\vec{k}), \alpha_{\mathcal{R}}^\dagger(\vec{k}') \right] = \delta(\vec{k} - \vec{k}') , \quad (1.122)$$

the vacuum state is annihilated by the operators $\alpha_{\mathcal{R}}(k)$ and the mode functions obey the equation that follows from eq.(1.120)

$$\left[\frac{d^2}{d\eta^2} + k^2 - \frac{1}{z} \frac{d^2 z}{d\eta^2} \right] S_{\mathcal{R}}(k; \eta) = 0 . \quad (1.123)$$

Canonical commutation relations for the field $u(\vec{x}, t)$ entail that these solutions $S_{\mathcal{R}}(k; \eta)$ are normalized through their Wronskian as

$$W[S_{\mathcal{R}}(k; \eta), S_{\mathcal{R}}^*(k; \eta)] = S_{\mathcal{R}}(k; \eta) S_{\mathcal{R}}^{\prime*}(k; \eta) - S_{\mathcal{R}}^{\prime}(k; \eta) S_{\mathcal{R}}^*(k; \eta) = i. \quad (1.124)$$

(here prime stands for derivative with respect to the conformal time).

Eq.(1.123) is a Schrödinger-type differential equation in the variable η . The potential felt by the fluctuations

$$W_{\mathcal{R}}(\eta) \equiv \frac{1}{z} \frac{d^2 z}{d\eta^2} \quad (1.125)$$

can be expressed in terms of the inflaton potential and its derivatives. In order to achieve this, it is more convenient to pass to cosmic time, in terms of which,

$$\frac{d^2 z}{d\eta^2} = a^2 (\ddot{z} + H \dot{z}). \quad (1.126)$$

From eqs.(1.119) and (1.125) and using the inflation equations of motion (1.71)-(1.73), the potential $W_{\mathcal{R}}(\eta)$ can be written as [22]

$$W_{\mathcal{R}}(\eta) = a^2(\eta) H^2(\eta) \left[2 - 7\epsilon_v + 2\epsilon_v^2 - \frac{\sqrt{8\epsilon_v} V'}{M_{Pl} H^2} - \eta_v(3 - \epsilon_v) \right], \quad (1.127)$$

where we take for the sign of the square root $\sqrt{\epsilon_v}$ the sign of $\dot{\varphi}$ and

$$\epsilon_v \equiv \frac{1}{2 M_{Pl}^2} \frac{\dot{\varphi}^2}{H^2}, \quad (1.128)$$

$$\eta_v \equiv M_{Pl}^2 \frac{V''(\varphi)}{V(\varphi)}. \quad (1.129)$$

ϵ_v and η_v are the known slow-roll parameters [5]. Notice that eqs.(1.127)-(1.129) are **exact** (no slow-roll approximation).

In terms of the dimensionless variables eqs.(1.83)-(1.85) we obtain for the potential $W_{\mathcal{R}}(\eta)$,

$$W_{\mathcal{R}}(\eta) = a^2(\eta) \mathcal{H}^2(\eta) m^2 N \left[2 - 7\epsilon_v + 2\epsilon_v^2 - \sqrt{\frac{8\epsilon_v}{N}} \frac{w'}{\mathcal{H}^2} - \eta_v(3 - \epsilon_v) \right], \quad (1.130)$$

while the slow-roll parameters take the form

$$\epsilon_v = \frac{1}{2N} \frac{1}{\mathcal{H}^2} \left(\frac{d\chi}{d\tau} \right)^2, \quad \eta_v = \frac{1}{N} \frac{w''(\chi)}{w(\chi)}. \quad (1.131)$$

We explicitly see that the slow-roll parameters are suppressed by powers of $1/N$. This result is valid for **all** models in the class defined by eq.(1.83) regardless of the precise form of $w(\chi)$.

Another exact formula for ϵ_v is

$$\epsilon_v = -\frac{\dot{H}}{H^2} = \frac{1}{N} \frac{d}{d\tau} \frac{1}{\mathcal{H}}, \quad (1.132)$$

where we used eqs.(1.11), (1.14) and (1.128).

Using eqs.(1.89) and (1.131), we obtain to first order in $1/N$,

$$\epsilon_v = \frac{1}{2N} \left[\frac{w'(\chi)}{w(\chi)} \right]^2 + \mathcal{O}\left(\frac{1}{N^2}\right) \quad (1.133)$$

We can obtain the general expression of the conformal time integrating by parts in eq.(1.20),

$$\eta = \int \frac{dt}{a(t)} = \int \frac{da}{a^2 H} = -\frac{1}{a H} - \int \frac{\dot{H}}{a H^2} dt = -\frac{1}{a H} + \int \frac{\epsilon_v}{a^2 H} da$$

where we used eq.(1.132). In the slow-roll approximation we can consider ϵ_v constant and pull out it of the integral as follows

$$\int \frac{\epsilon_v}{a^2 H} da = \epsilon_v \int \frac{da}{a^2 H} \left[1 + \mathcal{O}\left(\frac{1}{N}\right) \right] = \epsilon_v \eta \left[1 + \mathcal{O}\left(\frac{1}{N}\right) \right] .$$

We thus get the result

$$\eta = -\frac{1}{a H \left[1 - \epsilon_v + \mathcal{O}\left(\frac{1}{N^2}\right) \right]} \quad \text{or} \quad a(\eta) = -\frac{1}{\eta H \left[1 - \epsilon_v + \mathcal{O}\left(\frac{1}{N^2}\right) \right]} . \quad (1.134)$$

We can now write the potential $W_{\mathcal{R}}(\eta)$ during slow-roll and to leading order in $1/N$

$$W_{\mathcal{R}}(\eta) = \frac{2}{\eta^2} \left[1 + \frac{3}{2} (3 \epsilon_v - \eta_v) \right] = \frac{\nu_{\mathcal{R}}^2 - \frac{1}{4}}{\eta^2} , \quad \nu_{\mathcal{R}} = \frac{3}{2} + 3 \epsilon_v - \eta_v + \mathcal{O}\left(\frac{1}{N^2}\right) . \quad (1.135)$$

where we used eqs.(1.101) and (1.130)-(1.134).

In the slow-roll regime we can consider ϵ_v and η_v constants in time in eq.(1.135). The general solution of eqs.(1.123)-(1.125) is then given by

$$S_{\mathcal{R}}(k; \eta) = A_{\mathcal{R}}(k) g_{\nu_{\mathcal{R}}}(\eta) + B_{\mathcal{R}}(k) g_{\nu_{\mathcal{R}}}^*(\eta) , \quad (1.136)$$

where the function $g_{\nu}(\eta)$ is given by

$$g_{\nu}(k; \eta) = \frac{1}{2} i^{\nu+\frac{1}{2}} \sqrt{-\pi \eta} H_{\nu}^{(1)}(-k \eta) , \quad (1.137)$$

$A_{\mathcal{R}}(k)$, $B_{\mathcal{R}}(k)$ are constants determined by the initial conditions and $H_{\nu}^{(1)}(z)$ is a Hankel function.

For wavevectors deep inside the Hubble radius $|k \eta| \gg 1$ the mode functions have the asymptotic behavior

$$g_{\nu}(k; \eta) \stackrel{\eta \rightarrow -\infty}{\sim} \frac{1}{\sqrt{2k}} e^{-i k \eta} , \quad g_{\nu}^*(k; \eta) \stackrel{\eta \rightarrow -\infty}{\sim} \frac{1}{\sqrt{2k}} e^{i k \eta} , \quad (1.138)$$

and for $\eta \rightarrow 0^-$, the mode functions behave as:

$$g_{\nu}(k; \eta) \stackrel{\eta \rightarrow 0^-}{\sim} \frac{\Gamma(\nu)}{\sqrt{2\pi k}} \left(\frac{2}{i k \eta} \right)^{\nu-\frac{1}{2}} . \quad (1.139)$$

The complex conjugate formula holds for $g_{\nu}^*(k; \eta)$.

In particular, in the scale invariant case $\nu = \frac{3}{2}$ which is the leading order in the slow-roll expansion, the mode functions eqs.(1.137) simplify to

$$g_{\frac{3}{2}}(k; \eta) = \frac{e^{-i k \eta}}{\sqrt{2k}} \left[1 - \frac{i}{k \eta} \right] . \quad (1.140)$$

2. Tensor Perturbations

Taking into account small fluctuations the FRW geometry eq.(1.5) becomes in conformal time

$$ds^2 = a^2(\eta) (d\eta^2 - d\vec{x}^2) + a^2(\eta) h_{\mu\nu} dx^{\mu} dx^{\nu} .$$

where $h_{\mu\nu} \ll 1$ stands for the metric perturbation with $h_{00} = h_i^i = 0$. In the transverse traceless gauge $h_{0i} = \partial^i h_{ij} = 0$ and there are two independent polarization states. These are usually denoted by $\lambda = \times$ and $+$. The quantum modes associated with these two states are called gravitons. The action for the metric fluctuations follows by expanding the Einstein-Hilbert action to quadratic order in $h_{\mu\nu}$ and it takes the form [5]

$$S = \frac{1}{2} \left(\frac{M_{Pl}}{2} \right)^2 \int d\eta d^3x a^2(\eta) \partial_{\mu} h_j^i \partial^{\mu} h_i^j . \quad (1.141)$$

Tensor perturbations correspond to minimally coupled massless fields with two physical polarizations. Tensor perturbations (gravitational waves) are gauge invariant. The quantum fields (gravitons) are written as

$$h_j^i(\vec{x}, \eta) = \frac{2}{a(\eta) M_{Pl}} \sum_{\lambda=\times,+} \int \frac{d^3k}{(2\pi)^{\frac{3}{2}}} \epsilon_j^i(\lambda, \vec{k}) \left[e^{i\vec{k}\cdot\vec{x}} \alpha_{T,\lambda}(\vec{k}) S_T(k, \eta) + e^{-i\vec{k}\cdot\vec{x}} \alpha_{T,\lambda}^\dagger(\vec{k}) S_T^*(k, \eta) \right], \quad (1.142)$$

where λ labels the two standard transverse and traceless polarizations \times and $+$. The operators $\alpha_{T,\lambda}(\vec{k})$, $\alpha_{T,\lambda}^\dagger(\vec{k})$ obey canonical commutation relations eq.(1.122), and $\epsilon_{ij}(\lambda, \vec{k})$ are the two independent symmetric and traceless-transverse tensors constructed from the two independent polarization vectors transverse to $\hat{\mathbf{k}}$, chosen to be real and normalized such that $\epsilon_j^i(\lambda, \vec{k}) \epsilon_k^j(\lambda', \vec{k}) = \delta_k^i \delta_{\lambda,\lambda'}$.

It follows from eq.(1.141) that the mode functions $S_T(k; \eta)$ obey the differential equation,

$$S_T''(k; \eta) + \left[k^2 - \frac{a''(\eta)}{a(\eta)} \right] S_T(k; \eta) = 0. \quad (1.143)$$

In the slow-roll regime we find from eq.(1.134),

$$\frac{a''(\eta)}{a(\eta)} = \frac{\nu_T^2 - \frac{1}{4}}{\eta^2}, \quad \nu_T = \frac{3}{2} + \epsilon_v + \mathcal{O}\left(\frac{1}{N^2}\right). \quad (1.144)$$

and the general solution of eq.(1.143) is then given by

$$S_T(k; \eta) = A_T(k) g_{\nu_T}(\eta) + B_T(k) g_{\nu_T}^*(\eta), \quad (1.145)$$

where the function $g_\nu(\eta)$ is given by eq.(1.137) and $A_T(k)$, $B_T(k)$ are constants determined by the initial conditions.

We see that both scalar curvature and tensor perturbations obey in conformal time Schrödinger-type differential equations (1.123) and (1.143) with potentials:

$$W_{\mathcal{R}}(\eta) = \frac{1}{z} \frac{d^2 z}{d\eta^2}, \quad W_T(\eta) = \frac{a''(\eta)}{a(\eta)}, \quad (1.146)$$

respectively.

3. Initial conditions

We treat both scalar and tensor perturbations on the same footing by focusing on mode functions solutions of the general equation

$$\left[\frac{d^2}{d\eta^2} + k^2 - \frac{\nu^2 - \frac{1}{4}}{\eta^2} \right] S(k, \eta) = 0. \quad (1.147)$$

where ν can be considered time independent during the slow-roll regime. For general initial conditions we write

$$S(k; \eta) = A(k) g_\nu(k; \eta) + B(k) g_\nu^*(k; \eta). \quad (1.148)$$

where the solution $g_\nu(k; \eta)$ is given by eq.(1.137). For the specific cases of scalar curvature or tensor perturbations, the mode functions and coefficients $A(k)$, $B(k)$ will feature a subscript index \mathcal{R} and T , respectively.

The coefficients $A(k)$, $B(k)$ for the general solution eq.(1.148) are determined by an initial condition on the mode functions $S(k; \eta)$ at a given initial conformal time $\bar{\eta}$, namely

$$B(k) = -i[g_\nu(k; \bar{\eta}) S'(k; \bar{\eta}) - g_\nu'(k; \bar{\eta}) S(k; \bar{\eta})], \quad A(k) = -i[g_\nu^{*'}(k; \bar{\eta}) S(k; \bar{\eta}) - g_\nu^*(k; \bar{\eta}) S'(k; \bar{\eta})]. \quad (1.149)$$

The constancy of the Wronskian eq.(1.124) and eq.(1.148) imply the constraint,

$$|A(k)|^2 - |B(k)|^2 = 1. \quad (1.150)$$

The S-vacuum state $|0\rangle_S$ is annihilated by the operators $\alpha_{\vec{k}}$ associated with the modes $S(k; \eta)$. A different choice of the coefficients $A(k)$; $B(k)$ determines different choices of vacua, the Bunch-Davies vacuum corresponds to $A(k) =$

1, $B(k) = 0$. An illuminating representation of these coefficients can be gleaned by computing the expectation value of the number operator in the Bunch-Davies vacuum. Consider the expansion of the fluctuation field both in terms of Bunch-Davies modes $g_\nu(k; \eta)$ and in terms of the general modes $S(k; \eta)$, for example for the scalar curvature \mathcal{R} (similarly for tensor fields with a subscript T and corresponding normalization)

$$u(\vec{k}, \eta) = a_{\vec{k}} g_{\nu_{\mathcal{R}}}(k; \eta) + a_{-\vec{k}}^\dagger g_{\nu_{\mathcal{R}}}^*(k; \eta) \equiv \alpha_{\mathcal{R}}(\vec{k}) S_{\mathcal{R}}(k; \eta) + \alpha_{\mathcal{R}}^\dagger(\vec{k}) S_{\mathcal{R}}^*(k; \eta) , \quad (1.151)$$

the creation and annihilation operators are related by a Bogoliubov transformation

$$\alpha_{\mathcal{R}}^\dagger(\vec{k}) = A_{\mathcal{R}}(k) a_{\vec{k}}^\dagger - B_{\mathcal{R}}(k) a_{-\vec{k}} \quad , \quad \alpha_{\mathcal{R}}(\vec{k}) = A_{\mathcal{R}}^*(k) a_{\vec{k}} - B_{\mathcal{R}}^*(k) a_{-\vec{k}}^\dagger . \quad (1.152)$$

The Bunch-Davis vacuum $|0\rangle_{BD}$ is annihilated by $a_{\vec{k}}$, hence we find the expectation value

$${}_{BD}\langle 0 | \alpha_{\mathcal{R}}^\dagger(\vec{k}) \alpha_{\mathcal{R}}(\vec{k}) | 0 \rangle_{BD} = |B_{\mathcal{R}}(k)|^2 = N_{\mathcal{R}}(k) . \quad (1.153)$$

Where $N_{\mathcal{R}}(k)$ is interpreted as the number of S-vacuum particles in the Bunch-Davis vacuum. In combination with the constraint eq.(1.150) the above result suggests the following representation for the coefficients $A(k)$; $B(k)$

$$A_{\mathcal{R}}(k) = \sqrt{1 + N_{\mathcal{R}}(k)} e^{i\theta_A(k)} \quad ; \quad B_{\mathcal{R}}(k) = \sqrt{N_{\mathcal{R}}(k)} e^{i\theta_B(k)} , \quad (1.154)$$

where $N_{\mathcal{R}}(k)$, $\theta_{A,B}(k)$ are real. The only relevant phase is the difference

$$\theta_k = \theta_B(k) - \theta_A(k) . \quad (1.155)$$

Notice that we provide the initial conditions at a given conformal time $\bar{\eta}$ which is obviously the same for all k -modes. This is the consistent manner to define the initial value problem (or Cauchy problem) for the fluctuations. This is different from what is often done in the literature when an ad-hoc dependence on k is given to $\bar{\eta}$ [50].

4. The power spectrum of adiabatic scalar and tensor perturbations

The power spectrum of curvature perturbations \mathcal{R} in the state with general initial conditions follows from eq.(1.118) and (1.121),

$$P_{\mathcal{R}}(k) \stackrel{\eta \rightarrow 0^-}{=} \frac{k^3}{2 \pi^2} \left| \frac{S_{\mathcal{R}}(k; \eta)}{z(\eta)} \right|^2 . \quad (1.156)$$

where the prefactor makes $P_{\mathcal{R}}(k)$ dimensionless and is chosen to follow the usual conventions [5].

From eq.(1.125) and (1.135) we see that in the slow-roll regime $z(\eta)$ behaves as

$$z(\eta) = \frac{z_0}{(-k_0 \eta)^{\nu_R - \frac{1}{2}}} , \quad (1.157)$$

where z_0 is the value of z when the pivot scale k_0 exits the horizon, that is at $\eta = \eta_0 = -1/k_0$. Combining this result with the small η limit eq.(1.139) we find from eqs.(1.156) and (1.157),

$$P_{\mathcal{R}}(k) = P_{\mathcal{R}}^{BD}(k) \left[1 + D_{\mathcal{R}}(k) \right] , \quad (1.158)$$

where we introduced the transfer function for the initial conditions of curvature perturbations:

$$\begin{aligned} D_{\mathcal{R}}(k) &= 2 |B_{\mathcal{R}}(k)|^2 - 2 \operatorname{Re} [A_{\mathcal{R}}(k) B_{\mathcal{R}}^*(k) i^{2\nu_R - 3}] = \\ &= 2 N_{\mathcal{R}}(k) - 2 \sqrt{N_{\mathcal{R}}(k) [1 + N_{\mathcal{R}}(k)]} \cos \left[\theta_k - \pi \left(\nu_R - \frac{3}{2} \right) \right] \end{aligned} \quad (1.159)$$

and

$$P_{\mathcal{R}}^{BD}(k) = \left(\frac{k}{2 k_0} \right)^{3 - 2 \nu_R} \frac{\Gamma^2(\nu_R)}{\pi^3} \left(\frac{k H}{a(t) \dot{\varphi}} \right)_{exit}^2 . \quad (1.160)$$

The index $_{exit}$ refers to the time where the pivot scale k_0 exits the horizon. In terms of the slow-roll parameter ϵ_v , using eq.(1.128) and $k = a_{exit} H$, expression (1.160) takes the form

$$P_{\mathcal{R}}^{BD}(k) = \left(\frac{k}{2k_0}\right)^{n_s-1} \frac{\Gamma^2(\nu_{\mathcal{R}})}{\pi^3} \frac{H^2}{2\epsilon_v M_{Pl}^2} \equiv |\Delta_{k\,ad}^{\mathcal{R}}|^2 \left(\frac{k}{k_0}\right)^{n_s-1}, \quad (1.161)$$

where in the slow-roll regime the amplitude $|\Delta_{k\,ad}^{\mathcal{R}}|^2$ is given by

$$|\Delta_{k\,ad}^{\mathcal{R}}|^2 = \frac{1}{8\pi^2\epsilon_v} \left(\frac{H}{M_{Pl}}\right)^2 \left\{ 1 + (3\epsilon_v - \eta_v) \left[\ln 4 + \psi\left(\frac{3}{2}\right) \right] + \mathcal{O}\left(\frac{1}{N^2}\right) \right\}, \quad (1.162)$$

and n_s stands for the spectral index

$$n_s - 1 = 3 - 2\nu_{\mathcal{R}} = 2\eta_v - 6\epsilon_v, \quad (1.163)$$

$\psi(z)$ is the digamma function and $\psi\left(\frac{3}{2}\right) = -1.463510026\dots$.

To leading order in $1/N$ and in terms of the dimensionless variables eqs.(1.83)-(1.85), the amplitude $|\Delta_{k\,ad}^{\mathcal{R}}|^2$ eq.(1.162) takes the form

$$|\Delta_{k\,ad}^{\mathcal{R}}|^2 = \frac{N^2}{12\pi^2} \left(\frac{M}{M_{Pl}}\right)^4 \frac{w^3(\chi)}{w'^2(\chi)}. \quad (1.164)$$

where $\chi \equiv \chi_{exit}$ stands for the inflaton field at horizon exit.

The power spectrum of tensor perturbations in the state with general initial conditions follows from eq.(1.142)

$$P_T(k) \stackrel{\eta \rightarrow 0^-}{=} \frac{4k^3}{M_{Pl}^2\pi^2} \left| \frac{S_T(k;\eta)}{a(\eta)} \right|^2 = P_T^{BD}(k) [1 + D_T(k)]. \quad (1.165)$$

The different prefactor in the scalar [eq.(1.156)] and tensor [eq.(1.165)] power spectra comes from the extra factor $M_{Pl}^2/2$ in front of the graviton action eq.(1.141) and the fact that the graviton has two independent polarizations.

We find in the Bunch-Davis initial state using eqs.(1.134) and (1.139) to leading order in $1/N$,

$$P_T^{BD}(k) = \frac{8}{\pi^3} \frac{H^2}{M_{Pl}^2} \Gamma^2(\nu_T) \left(\frac{k}{2}\right)^{3-2\nu_T} = |\Delta_k^T|^2 \left(\frac{k}{k_0}\right)^{n_T} \quad (1.166)$$

where

$$|\Delta_k^T|^2 = \frac{2}{\pi^2} \frac{H^2}{M_{Pl}^2} \left[1 + \mathcal{O}\left(\frac{1}{N}\right) \right] \quad \text{and} \quad n_T = 3 - 2\nu_T = -2\epsilon_v. \quad (1.167)$$

The transfer function $D_T(k)$ in eq.(1.165) for the initial conditions of tensor perturbations is given by

$$D_T(k) = 2|B_T(k)|^2 - 2\text{Re}[A_T(k)B_T^*(k)i^{2\nu_T-3}] = 2N_T(k) - 2\sqrt{N_T(k)[1+N_T(k)]} \cos\left[\theta_k - \pi(\nu_T - \frac{3}{2})\right] \quad (1.168)$$

The ratio of tensor to scalar fluctuations thus follows from eqs.(1.162) and (1.167)

$$r \equiv \frac{|\Delta_k^T|^2}{|\Delta_{k\,ad}^{\mathcal{R}}|^2} = 16\epsilon_v + \mathcal{O}\left(\frac{1}{N^2}\right). \quad (1.169)$$

We thus obtain for the spectral index n_s and the ratio r to leading order in $1/N$ using eqs.(1.128), (1.129), (1.163) and (1.133),

$$\begin{aligned} n_s - 1 &= -\frac{3}{N} \left[\frac{w'(\chi)}{w(\chi)} \right]^2 + \frac{2}{N} \frac{w''(\chi)}{w(\chi)} + \mathcal{O}\left(\frac{1}{N^2}\right), \\ r &= \frac{8}{N} \left[\frac{w'(\chi)}{w(\chi)} \right]^2 + \mathcal{O}\left(\frac{1}{N^2}\right). \end{aligned} \quad (1.170)$$

In eqs.(1.170) the value of χ is evaluated at horizon exiting setting $N[\chi] = N = 60$.

Since n_s and r are computed when the mode $k = k_0$ exits the horizon they are both k -dependent. However, their k -dependence is subleading in $1/N$. It can be shown that the running of n_s is of the order $1/N^2$ [5, 11],

$$\frac{dn_s}{d \ln k} = -\frac{2}{N^2} \frac{w'(\chi) w'''(\chi)}{w^2(\chi)} - \frac{6}{N^2} \frac{[w'(\chi)]^4}{w^4(\chi)} + \frac{8}{N^2} \frac{[w'(\chi)]^2 w''(\chi)}{w^3(\chi)} . \quad (1.171)$$

Therefore, the running is negligible $\sim 2 \times 10^{-4}$ for $N \sim 60$.

The higher order slow-roll parameters ξ_v and σ_v [5] turn to be of the order N^{-2} and N^{-3} , respectively:

$$\xi_v = M_{Pl}^4 \frac{V'(\varphi) V'''(\varphi)}{V^2(\varphi)} = \frac{1}{N^2} \frac{w'(\chi) w'''(\chi)}{w^2(\chi)} , \quad (1.172)$$

$$\sigma_v = M_{Pl}^6 \frac{[V'(\varphi)]^2 V^{(IV)}(\varphi)}{V^3(\varphi)} = \frac{1}{N^3} \frac{[w'(\chi)]^2 w''''(\chi)}{w^3(\chi)} . \quad (1.173)$$

Notice that the concavity $w''(\chi)$ of the inflaton potential at horizon exit can be expressed in terms of the observables n_s and r from eqs.(1.170) as

$$n_s - 1 + \frac{3}{8} r = \frac{2}{N} \frac{w''(\chi)}{w(\chi)} . \quad (1.174)$$

Hence, knowing the observed values of n_s and r determines whether the inflaton potential is convex or concave at horizon exit. A negative value of $w''(\chi)$ will rule out binomial chaotic inflation eq.(1.93).

5. The energy scale of inflation and the quasi-scale invariance during inflation.

Since, $w(\chi)$ and $w'(\chi)$ are of order one, we find from eq.(1.164)

$$\left(\frac{M}{M_{Pl}} \right)^2 \sim \frac{2\sqrt{3}\pi}{N} |\Delta_{k\,ad}^{\mathcal{R}}| \simeq 0.897 \times 10^{-5} . \quad (1.175)$$

where we used $N \simeq 60$, set $k = k_0$ with $k_0 = 0.002 \text{ (Mpc)}^{-1}$ the WMAP pivot scale and ref.[10]

$$|\Delta_{k\,ad}^{\mathcal{R}}| = (4.94 \pm 0.1) \times 10^{-5} . \quad (1.176)$$

This fixes the scale of inflation to be

$$M \sim 2.99 \times 10^{-3} M_{Pl} \sim 0.73 \times 10^{16} \text{ GeV} . \quad (1.177)$$

This value *pinpoints the scale of the potential* during inflation to be at the GUT scale suggesting a deep connection between inflation and the physics at the GUT scale in cosmological space-time.

As a consequence we get for the inflaton mass and the Hubble parameter during inflation from eq.(1.86)-(1.87),

$$m = \frac{M^2}{M_{Pl}} \sim 2.18 \times 10^{13} \text{ GeV} , \quad H \sim 10^{14} \text{ GeV} \quad (1.178)$$

Notice that these values for the inflation scale M and the inflaton mass are **model independent** within the class of models eq.(1.83). In addition, we see that

$$m \simeq 0.003 M .$$

Namely, the inflaton is a **very light** field in this context. We can therefore expect infrared and scale invariant phenomena here.

Since $M/M_{Pl} \sim 3 \times 10^{-3}$ [eq.(1.177)], we **naturally** find from eq.(1.97) the order of magnitude of the cubic and quartic couplings,

$$\lambda_3 \sim 10^{-6} m , \quad \lambda = \lambda_4 \sim 10^{-12} . \quad (1.179)$$

These relations are a **natural** consequence of the validity of the effective field theory and of slow-roll and relieve the **fine tuning problem**. We emphasize that the ‘see-saw-like’ form of the couplings is a consequence of the form of the

potential eq.(1.83) and is valid for all inflationary models within the class defined by eq.(1.83). This analysis reveals that small couplings are naturally explained in terms of powers of the ratio between the inflationary and Planck scales *and* integer powers of $1/\sqrt{N}$ [11].

Eqs.(1.177)-(1.179) apply in order of magnitude to all inflationary potentials within the universal slow-roll class eq.(1.83). We provide in eq.(2.24) the values for M , m and the coupling valid for the inflaton potential giving the best MCMC fit to the present CMB and LSS data. These values are consistent with the estimates eqs.(1.177)-(1.179), as it must be.

We see that $|n_s - 1|$ as well as the ratio r turn out to be of order $1/N$ for generic inflationary models. The case $n_s = 1$ and $r = 0$ corresponds to the Harrison-Zeldovich spectrum which is exactly scale invariant [see eq.(1.161)]. This nearly scale invariance is a natural property of inflation which is described by a quasi-de Sitter space-time geometry. This can be understood intuitively as follows: the geometry of the universe is scale invariant during de Sitter stage since the metric takes in conformal time the form

$$ds^2 = \frac{1}{(H \eta)^2} [(d\eta)^2 - (d\vec{x})^2] . \quad (1.180)$$

Therefore, the primordial power generated is scale invariant except for the fact that inflation is not eternal and lasts for N e-folds. Hence, the primordial spectrum is scale invariant up to $1/N$ corrections. The Harrison-Zeldovich (HZ) values $n_s = 1$, $r = 0$ correspond to a critical point as discussed in ref.[11]. This gaussian fixed point is **not** the inflationary model that reproduces the data but the inflation model hovers around it in the renormalization group sense with an almost scale invariant spectrum of scalar fluctuations during the slow-roll stage.

The HZ point $n_s = 1$, $r = 0$ follows in the $N \rightarrow \infty$ limit, that is, for eternal inflation the scale invariant de Sitter metric eq.(1.180). The HZ point is ruled out by CMB+LSS data. It must be noticed that the HZ point is theoretically excluded in new inflation as shown in figs. 10, 14 and 31. Chaotic inflation admits the HZ point but in a highly unphysical and unrealistic singular limit in which the inflaton potential identically vanishes as shown in sec. II B 3, eqs.(2.41) and (2.42).

The fact that $r \sim 1/N$ [eq.(1.170)] shows that the tensor fluctuations are suppressed by a factor $N \sim 60$ compared with the curvature scalar fluctuations. This suppression can be explained as follows: the scalar curvature fluctuations are quantum fluctuations around the classical inflaton while the tensor fluctuations are just quantum zero-point fluctuations. The inflaton is present through the quantity $z(t) = a(t) \dot{\varphi}(t)/H(t)$ [eq.(1.119)] both in the scalar curvature fluctuations equation (1.123) and in the scalar power spectrum eqs.(1.156) and (1.160), while solely the scalar factor $a(t)$ appears in the tensor fluctuations eq.(1.143) and in the tensor power spectrum eq.(1.165). Since the matter distribution is homogeneous and isotropic, it can only source scalar fluctuations in the geometry.

The observation of a nonzero r will have **twofold** relevance. First, it would be the **first** detection of (linearized) gravitational waves as predicted by Einstein's General Relativity. Second, $r > 0$ indicates the presence of gravitons, namely, **quantized** gravitational waves at tree level.

Neutrino oscillations and neutrino masses m_ν are currently explained in the see-saw mechanism as follows [61],

$$\Delta m_\nu \sim \frac{M_{Fermi}^2}{M_R} \quad (1.181)$$

where $M_{Fermi} \sim 250$ GeV is the Fermi mass scale, $M_R \gg M_{Fermi}$ is a large energy scale and Δm_ν is the difference between the neutrino masses for different flavors. The observed values for $\Delta m_\nu \sim 0.009 - 0.05$ eV naturally call for a mass scale $M \sim 10^{15-16}$ GeV close to the GUT scale[61].

We see thus, that the energy scale $\sim 10^{16}$ GeV appears in fundamental physics in at least three independent ways: grand unification scale, inflation scale and the scale M_R in the neutrino mass formula.

II. THEORETICAL PREDICTIONS, MCMC DATA ANALYSIS, EARLY FAST-ROLL STAGE AND CMB QUADRUPOLE SUPPRESSION.

A. Ginsburg-Landau polynomial realizations of the Inflaton Potential

In the Ginsburg-Landau spirit the potential is a polynomial in the field starting by a constant term [16]. Linear terms can always be eliminated by a constant shift of the inflaton field. The quadratic term can have a positive or a negative sign. In the first case the symmetry $\varphi \rightarrow -\varphi$ is unbroken (unless the potential contains terms odd in φ), in the latter case the symmetry $\varphi \rightarrow -\varphi$ is spontaneously broken since the minimum of the potential is at $\varphi \neq 0$.

Inflaton potentials with $w''(0) > 0$ lead to chaotic (large field) inflation while inflaton potentials with $w''(0) < 0$ lead to new (small field) inflation.

The inflaton potential must be bounded from below, therefore the next potential beyond the quadratic potential is the quartic one with a positive quartic coefficient.

The request of renormalizability restricts the degree of the inflaton potential to four. However, since the theory of inflation is an effective theory, potentials of degrees higher than four are acceptable.

In the context of an effective theory or Ginsburg-Landau model it is highly unnatural to set $m = 0$ [16]. This corresponds to be exactly at the critical point of the model where the mass vanishes, that is, in the statistical mechanical context the correlation length is infinite. In fact, the WMAP result unfavouring the $m = 0$ choice (purely φ^4 potential, see [8, 9, 10] and section IID) supports this purely theoretical argument against the φ^4 monomial potential. We want to stress that excluding the quadratic mass term in the potential $V(\varphi)$ implies to fine tune to zero the mass term which is only justified at isolated points (critical points in the statistical mechanical sense). Therefore, from a physical point of view, the pure quartic potential is a weird choice implying to fine tune to zero the coefficient of the mass term. In other words, one would be considering a field with self-interaction but lacking of the mass term.

Dropping the cubic term implies that $\varphi \rightarrow -\varphi$ is a symmetry of the inflaton potential. As stated in [12], we do not see reasons based on fundamental physics to choose a zero or a nonzero cubic term. Only the phenomenology, that is the fit to CMB data, can decide for the moment on the value of the cubic term. The MCMC analysis of the WMAP plus LSS data shows that the cubic term can be ignored for new inflation (see section IID and [14]).

A model with only one field is clearly unrealistic since the inflaton would then describe a stable and ultra-heavy ($\sim 10^{13}\text{GeV}$) particle. It is necessary to couple the inflaton with lighter particles, in which case the inflaton can decay into them. There are many available scenarios for inflation. Most of them add other fields coupled to the inflaton. This variety of inflationary scenarios may seem confusing since several of them are compatible with the observational data [8, 9, 10]. Indeed, future observations should constraint the models more tightly excluding some families of them. The hybrid inflationary [45] models are amongst those strongly disfavoured by the WMAP data since they give $n_s > 1$ in most of their parameter space contrary to the WMAP results [9, 10]. The regions of parameter space where hybrid inflation yields $n_s < 1$ are equivalently covered by one-field chaotic inflation [13].

The variety of inflationary models shows the **power** of the inflationary paradigm. Whatever the correct microscopic model for the early universe would be, it should include inflation with the generic features we know today. Many inflatons can be considered (multi-field inflation), but such family of models introduce extra features as non-adiabatic (isocurvature) density fluctuations, which in turn become strongly constrained by the WMAP data [8, 9, 10].

Our approach is different to the inflationary flow equations [54] where the inflaton potential **changes** (that is, **the model changes**) along the flow. We work with a **given** potential within the Ginsburg-Landau (GL) framework, that is the trinomial potential. We investigate the physics of this potential in the parameter space driven by the data through the Monte Carlo Markov Chains. In our work, n_s and r are computed analytically to order $1/N$.

Following the spirit of the Ginsburg-Landau theory of phase transitions [16], the simplest choice for the inflaton potential is a quartic trinomial for the inflaton potential [11, 12]:

$$w(\chi) = w_0 \pm \frac{1}{2} \chi^2 + \frac{h}{3} \sqrt{\frac{y}{2}} \chi^3 + \frac{y}{32} \chi^4. \quad (2.1)$$

where the coefficients w_0 , h and y are dimensionless and of order one and the signs \pm correspond to large and small field inflation, respectively (chaotic and new inflation, respectively).

We find from eqs.(1.95) and (2.1) that

$$2h = \frac{G_3}{\sqrt{G_4}},$$

and since the strength of the couplings are usually as $G_4 \sim G_3^2$, we conclude that the parameter h measures the **asymmetry** of the inflaton potential.

Inserting eq.(2.1) in eq.(1.83) yields,

$$V(\varphi) = V_0 \pm \frac{m^2}{2} \varphi^2 + \frac{m}{3} g \varphi^3 + \frac{\lambda}{4} \varphi^4. \quad (2.2)$$

where the mass $m^2 > 0$ and the couplings g and λ are given by the following see-saw-like relations,

$$m = \frac{M^2}{M_{Pl}} \quad , \quad g = h \sqrt{\frac{y}{2N}} \left(\frac{M}{M_{Pl}} \right)^2 \quad , \quad \lambda = \frac{y}{8N} \left(\frac{M}{M_{Pl}} \right)^4 \quad , \quad V_0 = N M^4 w_0. \quad (2.3)$$

Notice that $y \sim \mathcal{O}(1) \sim h$ guarantee that $g \sim \mathcal{O}(10^{-6})$ and $\lambda \sim \mathcal{O}(10^{-12})$ without any fine tuning as stressed before in eq.(1.179) [11]. Namely, the smallness of the couplings directly follow from the form of the inflaton potential eq.(1.83) and the amplitude of the scalar fluctuations that fixes $M \ll M_{Pl}$ in eqs.(1.175) and (1.177).

We now study in secs. II A 1-II A 3 binomial inflaton potentials. That is, we start by setting for simplicity the cubic coupling to zero in eq.(2.1). Trinomial inflaton potentials are investigated in secs. II B and II C.

1. Binomial inflaton potentials for chaotic inflation

Let us consider chaotic inflation with the binomial potential eq.(1.93)

$$w(\chi) = \frac{1}{2} \chi^2 + \frac{y}{32} \chi^4 \quad , \quad \text{chaotic inflation} \quad , \quad (2.4)$$

Chaotic inflation is obtained by choosing the initial field χ in the interval $(0, +\infty)$. The inflaton χ slowly rolls down the slope of the potential from its initial value till the absolute minimum of the potential at the origin.

It is convenient to define the field variable z by:

$$z \equiv \frac{y}{8} \chi^2 \quad . \quad (2.5)$$

In terms of z the chaotic trinomial potential takes the form

$$w(\chi) = \frac{2z}{y} (2+z) \quad .$$

When $z \lesssim 1$ we are in the quadratic regime where $w(\chi)$ is approximated by the χ^2 term. For $z \gtrsim 1$ we go to the non-linear regime in z and both terms in $w(\chi)$ are of the same order of magnitude.

Eq.(1.90) defines the field χ or equivalently z , in terms of the coupling y . We insert there eq.(2.4) for $w(\chi)$ and obtain

$$y = z + \log(1+z) \quad (2.6)$$

We see that z results to be a monotonically increasing function of the coupling y for $0 < y$, $z < +\infty$ and $2 < \chi < 2\sqrt{2}$. Recall that χ and z correspond to the time of horizon exit.

We obtain from eqs.(1.164), (1.170), (1.171), and (2.4) the spectral index, its running, the ratio r and the amplitude of adiabatic perturbations for binomial chaotic inflation,

$$n_s = 1 - \frac{y}{Nz} \frac{3z^2 + 5z + 4}{(z+2)^2} \quad , \quad (2.7)$$

$$\frac{dn_s}{d \ln k} = \frac{y^2}{z^2 N^2} \left[-3 \frac{z(z+1)}{(z+2)^2} - 24 \frac{(z+1)^4}{(z+2)^4} + 8 \frac{(3z+1)(z+1)^2}{(z+2)^3} \right] \quad , \quad (2.8)$$

$$r = \frac{16y}{Nz} \frac{(z+1)^2}{(z+2)^2} \quad , \quad |\Delta_{k ad}^{\mathcal{R}}|^2 = \frac{N^2}{12\pi^2} \left(\frac{M}{M_{Pl}} \right)^4 \frac{z^2 (2+z)^3}{y^2 (1+z)^2} \quad . \quad (2.9)$$

In chaotic binomial inflation, the limit $z \rightarrow 0^+$ implies weak coupling $y \rightarrow 0^+$, with

$$y \stackrel{z \rightarrow 0^+}{\simeq} 2z + \mathcal{O}(z^{\frac{3}{2}}) \quad , \quad \chi \stackrel{z \rightarrow 0^+}{\simeq} 2 + \mathcal{O}(z) \quad .$$

That is the quadratic potential and we find,

$$\begin{aligned} n_s &\stackrel{y \rightarrow 0^+}{\simeq} 1 - \frac{2}{N} \quad , \quad \frac{dn_s}{d \ln k} \stackrel{y \rightarrow 0}{\simeq} -\frac{2}{N^2} \\ r &\stackrel{y \rightarrow 0^+}{\simeq} \frac{8}{N} \quad , \quad |\Delta_{k ad}^{\mathcal{R}}|^2 \stackrel{y \rightarrow 0^+}{\simeq} \frac{N^2}{6\pi^2} \left(\frac{M}{M_{Pl}} \right)^4 \quad . \end{aligned} \quad (2.10)$$

The results in the $y \rightarrow 0^+$ coincide with those for the purely quadratic monomial potential $\frac{1}{2} \chi^2$.

In the limit $z \rightarrow +\infty$ which implies $y \rightarrow +\infty$ (strong coupling), we have

$$\begin{aligned}
y &\stackrel{z \rightarrow +\infty}{=} z + \log z + \mathcal{O}(1) \quad , \quad \chi \stackrel{z \rightarrow +\infty}{=} 2\sqrt{2} + \mathcal{O}\left(\frac{\log z}{z}\right) \quad , \\
n_s &\stackrel{y \rightarrow +\infty}{=} 1 - \frac{3}{N} \left[1 + \frac{\log z}{z} + \mathcal{O}\left(\frac{1}{z}\right) \right] \quad , \\
r &\stackrel{y \rightarrow +\infty}{=} \frac{16}{N} \left[1 + \frac{\log z}{z} + \mathcal{O}\left(\frac{1}{z}\right) \right] \quad . \\
|\Delta_{kad}^{\mathcal{R}}|^2 &\stackrel{y \rightarrow +\infty}{=} \frac{N^2}{12\pi^2} \left(\frac{M}{M_{Pl}} \right)^4 \frac{z}{\left[1 + \frac{\log z}{z} + \mathcal{O}\left(\frac{1}{z}\right) \right]^2} \quad .
\end{aligned} \tag{2.11}$$

Hence, χ , n_s and r in the limit $y \rightarrow +\infty$ coincide with those of the purely quartic monomial potential χ^4 :

$$\chi = 2\sqrt{2} \quad , \quad n_s = 1 - \frac{3}{N} \quad , \quad \frac{dn_s}{d \ln k} = -\frac{3}{N^2} \quad , \quad r = \frac{16}{N} \quad . \tag{2.12}$$

We have for $N = 60$,

$$n_s = 0.95 \quad , \quad \frac{dn_s}{d \ln k} = -0.00083 \quad , \quad r = 0.27 \quad .$$

This value for r is in tension with the WMAP+SDSS data which indicate $r < 0.22$ (95%CL). Therefore, the purely quartic monomial potential is excluded at more than 95% CL [8, 9, 10].

2. Binomial inflaton potentials for new inflation

Let us now consider new inflation with the binomial potential eq.(1.92),

$$w(\chi) = \frac{y}{32} \left(\chi^2 - \frac{8}{y} \right)^2 = -\frac{1}{2} \chi^2 + \frac{y}{32} \chi^4 + \frac{2}{y} \quad , \quad \text{new inflation} \quad . \tag{2.13}$$

New inflation is obtained by choosing the initial field χ in the interval $(0, +\sqrt{8/y})$. The inflaton χ slowly rolls down the slope of the potential from its initial value till the absolute minimum of the potential $\sqrt{8/y}$.

In terms of z the new trinomial potential takes the form.

$$w(\chi) = \frac{2}{y} (1 - z)^2 \quad .$$

Inserting eq.(2.13) into eq.(1.90) for the number of e-folds, we find the field χ at horizon crossing related to the coupling y ,

$$y = z - 1 - \log z \tag{2.14}$$

where $0 \leq z \leq 1$ since $0 \leq \chi \leq \sqrt{8/y}$ and eq.(2.5). z turns to be a monotonically decreasing function of y : z decreases from $z = 1$ till $z = 0$ when y increases from $y = 0$ till $y = \infty$. When $z \rightarrow 1$, y vanishes quadratically as,

$$y \stackrel{z \rightarrow 1}{=} \frac{1}{2} (1 - z)^2 \quad .$$

It is interesting to study the concavity of the potential eq.(2.13) for the inflaton field at horizon crossing. We find from eq.(2.13)

$$w''(\chi) = \frac{3}{8} y \chi^2 - 1 = 3z - 1 \quad .$$

We see that $w''(\chi)$ vanishes at $z = \frac{1}{3}$, that is at $y = \ln 3 - 2/3 = 0.431946 \dots$ [This is usually called the spinodal point]. Therefore,

$$w''(\chi) > 0 \quad \text{for} \quad y < 0.431946 \dots \quad \text{and} \quad w''(\chi) < 0 \quad \text{for} \quad y > 0.431946 \dots \quad . \tag{2.15}$$

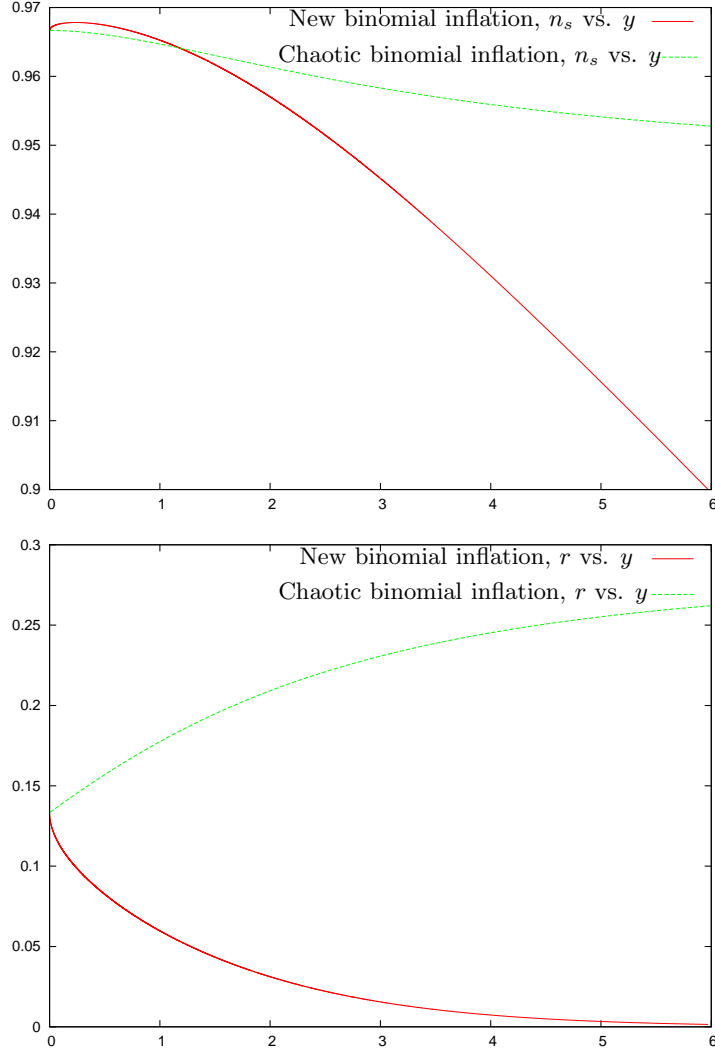


FIG. 9: Binomial Inflation. Upper panel: n_s vs. the quartic coupling y for new binomial and chaotic binomial inflation. There are maximum values for n_s : $n_s \leq 0.9678\dots$ and $n_s \leq 1 - 2/N = 0.9666\dots$, respectively. Lower panel: r vs. the quartic coupling y for new binomial and chaotic binomial inflation. The range of r in new binomial inflation is exactly **below** its range in chaotic binomial inflation. The ranges of n_s have an overlap.

Notice that for chaotic inflation eq.(2.4) we always have $w''(\chi) > 0$. The negative concavity case $w''(\chi) < 0$ for $y > 0.431946\dots$ is **specific** to new inflation eq.(2.13). Moreover $w''(\chi)$ can be expressed as a linear combination of the observables n_s and r as shown in eq.(1.174).

We obtain from eqs.(1.164), (1.170), (1.171) and (2.14) the spectral index, its running, the ratio r and the amplitude of adiabatic perturbations for binomial new inflation,

$$\begin{aligned} n_s &= 1 - \frac{y}{N} \frac{3z+1}{(1-z)^2} \quad , \quad \frac{dn_s}{d \ln k} = \frac{y^2 z}{N^2 (1-z)^4} (24z^2 - 35z + 3) \quad , \\ r &= \frac{16y}{N} \frac{z}{(1-z)^2} \quad , \quad |\Delta_{k ad}^{\mathcal{R}}|^2 = \frac{N^2}{12\pi^2} \left(\frac{M}{M_{Pl}} \right)^4 \frac{(1-z)^4}{y^2 z} \quad . \end{aligned} \quad (2.16)$$

In new binomial inflation the limit $z \rightarrow 1^-$ implies weak coupling $y \rightarrow 0^+$, that is, the potential is quadratic around the absolute minimum $\chi = \sqrt{8/y}$ and we find,

$$n_s \stackrel{y \rightarrow 0}{=} 1 - \frac{2}{N} \quad , \quad r \stackrel{y \rightarrow 0}{=} \frac{8}{N} \quad , \quad \chi \stackrel{y \rightarrow 0}{=} \sqrt{\frac{8}{y}} \rightarrow \infty \quad , \quad (2.17)$$

$$\frac{dn_s}{d \ln k} \stackrel{y \rightarrow 0}{=} -\frac{2}{N^2} \quad , \quad |\Delta_{k \text{ ad}}^{\mathcal{R}}|^2 \stackrel{y \rightarrow 0}{=} \frac{N^2}{3 \pi^2} \left(\frac{M}{M_{Pl}} \right)^4 \quad , \quad (2.18)$$

which coincide with n_s , $dn_s/d \ln k$ and r for the monomial quadratic potential in chaotic inflation eq.(2.10). There is an extra factor two in $|\Delta_{k \text{ ad}}^{\mathcal{R}}|^2$ for new inflation and $y \rightarrow 0^+$ due to the fact that $w''(\sqrt{8/y}) = 2$ at the absolute minimum of the potential eq.(2.13) while $w''(0) = 1$ at the absolute minimum of the potential eq.(2.4).

In the limit $z \rightarrow 0^+$ which implies $y \rightarrow +\infty$ (strong coupling), we have

$$z \stackrel{y \rightarrow +\infty}{=} e^{-y-1} \rightarrow 0^+$$

and

$$\begin{aligned} n_s &\stackrel{y \gg 1}{=} 1 - \frac{y}{N} \quad , \quad r \stackrel{y \gg 1}{=} \frac{16 y}{N} e^{-y-1} \quad , \quad \chi \stackrel{y \gg 1}{=} \sqrt{\frac{8}{y}} e^{-(y+1)/2} \rightarrow 0 \quad , \\ \frac{dn_s}{d \ln k} &\stackrel{y \gg 1}{=} -\frac{3 y^2 e^{-(y+1)}}{N^2} \quad , \quad |\Delta_{k \text{ ad}}^{\mathcal{R}}|^2 \stackrel{y \gg 1}{=} \frac{N^2}{12 \pi^2} \left(\frac{M}{M_{Pl}} \right)^4 \frac{e^{y+1}}{y^2} \quad . \end{aligned} \quad (2.19)$$

Notice that the slow-roll approximation is no longer valid when the coefficient of $1/N$ becomes much larger than unity. Hence, the results in eq.(2.19) are valid for $y \lesssim N$. We see that in this strong coupling regime r becomes very small and n_s becomes well below unity. The WMAP+LSS results exclude $n_s \lesssim 0.9$ [8, 9, 10]. Therefore, this strong coupling limit $y \gg 1$ is ruled out.

3. Contrasting the results of new and chaotic binomial inflation.

We plot in figs. 9 n_s and r vs. the coupling y , respectively. The curves are restricted to the region $0 < r < 0.3$ and $n_s > 0.9$ compatible with the WMAP data [9, 10].

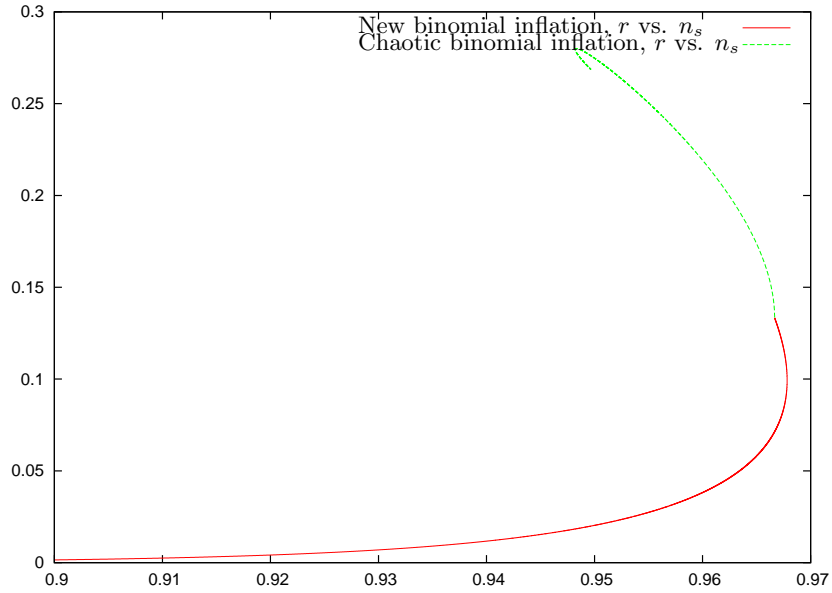


FIG. 10: r vs. n_s for new binomial and chaotic binomial inflation. We set here $N = 60$ and restrict the plot to the region $n_s > 0.9$. r in new binomial inflation is exactly **below** its range in chaotic binomial inflation.

We find from sec. II A 1 that in binomial chaotic inflation n_s and r cover the following range of values for $N = 60$:

$$\begin{aligned} 0.94821 \dots &= 1 - \frac{3.1072 \dots}{N} \leq n_s \leq 1 - \frac{2}{N} = 0.9666 \dots \quad , \\ 0.1333 \dots &= \frac{8}{N} \leq r \leq \frac{16.802 \dots}{N} = 0.2800 \dots \quad \text{binomial chaotic inflation} \quad . \end{aligned} \quad (2.20)$$

We find from sec. II A 2 that in binomial new inflation the following range of values for n_s and r are covered:

$$n_s \leq 1 - \frac{1.93051 \dots}{N} = 0.96782 \dots, \quad 0 < r \leq \frac{8}{N} = 0.1333 \dots \quad \text{binomial new inflation} . \quad (2.21)$$

The maximum value for n_s corresponds to $z = 0.4582 \dots$, $y = 0.2387 \dots$, $r = 0.1192 \dots$. We see that the range of r in new binomial inflation is exactly **below** its range in chaotic binomial inflation [see eqs.(2.20) and (2.21)] while the ranges of n_s have an overlap.

It must be noticed that there are maximum values for n_s **both** in new and chaotic binomial inflation: $n_s \leq 0.9678 \dots$ and $n_s \leq 0.97$ in new and chaotic binomial inflation, respectively. An observed value of n_s above any of these bounds would rule out the corresponding model.

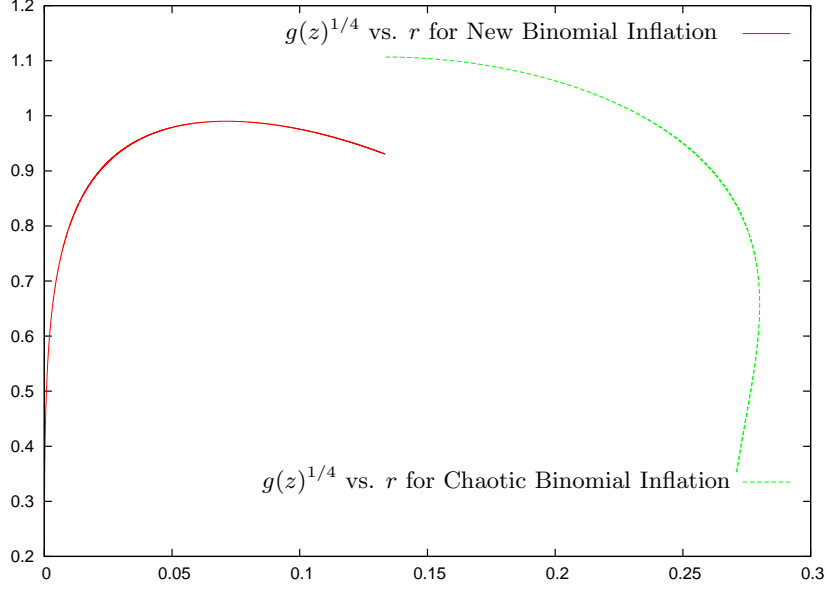


FIG. 11: $g^{\frac{1}{4}}(z)$ vs. r for new binomial and chaotic binomial inflation. We consider the domain $0 < r < 0.3$, $n_s > 0.9$ allowed by the WMAP data. The endpoints of the new and chaotic inflation curves at $r = 8/N = 0.1333 \dots$ correspond to $(3/4)^{\frac{1}{4}} = 0.930604 \dots$ and $(3/2)^{\frac{1}{4}} = 1.106682 \dots$, respectively. The endpoints do not coincide because the second derivatives of the binomial potential at the minimum differ by a factor two in new and chaotic inflation [see explanation below eq.(2.18)].

We plot in fig. 10 r vs. n_s for new binomial and chaotic binomial inflation. Notice that the two curves join at the quadratic monomial point $n_s = 1 - 2/N = 0.966 \dots$, $r = 8/N = 0.133 \dots$.

Notice that in new inflation, $n_s > 0.92$ **necessarily implies** $r > 0.042$ (see fig. 10). That is, within new binomial inflation, a lower bound for n_s as provided by WMAP data implies a lower bound for r . We will see this property generalized to trinomial new inflation in sec. IIC [13, 14].

The observed values of n_s and r therefore determine the value of the **couplings** (for the binomial potential only one coupling y). Once y is known, the **energy scale** of inflation M is determined by the observed value of the scalar fluctuations amplitude combined with eq.(1.164). We find

$$\begin{aligned} \frac{M}{M_{Pl}} &= \sqrt{\frac{2 \pi \Delta_{kad}^{\mathcal{R}}}{N}} g^{\frac{1}{4}}(z) = 2.27 \cdot 10^{-3} \times g^{\frac{1}{4}}(z) , \\ M &= 0.554 \cdot 10^{16} \text{ GeV} \times g^{\frac{1}{4}}(z) , \end{aligned} \quad (2.22)$$

where we set $N = 60$, used the WMAP value for $\Delta_{kad}^{\mathcal{R}}$ eq.(1.176) and we called:

$$\begin{aligned} g(z) &\equiv \frac{3 y^2 (z+1)^2}{z^2 (z+2)^3} \quad \text{binomial chaotic inflation} , \\ g(z) &\equiv \frac{3 z y^2}{(1-z)^4} \quad \text{binomial new inflation} . \end{aligned} \quad (2.23)$$

Notice that for $0 \leq y \leq \infty$,

$$\frac{3}{2} \geq g(z) \geq 0 \quad \text{binomial chaotic inflation} \quad , \quad 0.96099 \dots \geq g(z) \geq 0 \quad \text{binomial new inflation} \quad .$$

We plot in fig. 11 $g^{\frac{1}{4}}(z)$ vs. r for new binomial and chaotic binomial inflation. Notice that $g^{\frac{1}{4}}(z) = \mathcal{O}(1)$ in the domain of values $0 < r < 0.3$ and $n_s > 0.9$ compatible with the WMAP data [9, 10]. We thus see from eq.(2.22) and fig. 11 that the value of the inflation **energy scale** is in the GUT range for all values of n_s and r allowed by the observations.

We obtain from eq.(2.22) at the coupling value $y = 1.26$ that best fit the WMAP5+SDSS+SN data (new inflation, see Table VI),

$$M = 0.543 \times 10^{16} \text{ GeV} \quad , \quad m = 1.21 \times 10^{13} \text{ GeV} \quad \text{and} \quad H \simeq 6 \times 10^{13} \text{ GeV} \quad \text{for} \quad y = 1.26 \quad . \quad (2.24)$$

Notice that these values **agree** with the generic estimates eq.(1.177)-(1.178).

B. Trinomial Chaotic Inflation: Spectral index, amplitude ratio, running index and limiting cases

We consider now the trinomial potential with unbroken symmetry investigated in ref.[12, 14, 49]:

$$V(\varphi) = \frac{m^2}{2} \varphi^2 + \frac{m g}{3} \varphi^3 + \frac{\lambda}{4} \varphi^4 \quad , \quad (2.25)$$

where $m^2 > 0$ and g and λ are dimensionless couplings.

The corresponding dimensionless potential $w(\chi)$ eqs.(1.83)-(1.84) takes the form

$$w(\chi) = \frac{1}{2} \chi^2 + \frac{h}{3} \sqrt{\frac{y}{2}} \chi^3 + \frac{y}{32} \chi^4 \quad , \quad (2.26)$$

where the quartic coupling y is dimensionless as well as the asymmetry parameter h . The couplings in eq.(2.25) and eq.(2.26) are related by eq.(2.3).

Chaotic inflation is obtained by choosing the initial field χ in the interval $(0, +\infty)$. The inflaton χ slowly rolls down the slope of the potential from its initial value till the absolute minimum of the potential at the origin.

Computing the number of efolds from eq.(1.90), we find the field χ at horizon crossing related to the couplings y and h . Without loss of generality, we choose $h < 0$ and work with positive fields χ .

The potential eq.(2.26) has extrema at $\chi = 0$ and χ_{\pm} given by,

$$\chi_{\pm} = \sqrt{\frac{8}{y}} [-h \pm i \Delta] \quad , \quad \Delta \equiv \sqrt{1 - h^2} \quad . \quad (2.27)$$

That is, for $|h| < 1$, $w(\chi)$ has only one real extremum at $\chi = 0$ while for $|h| \geq 1$, $w(\chi)$ has three real extrema. There is always a minimum at $\chi = 0$ since $w''(0) = 1$. At the non-zero extrema we have

$$w''(\chi_{\pm}) = -2 \Delta (\Delta \pm i h) \quad .$$

We have for $|h| > 1$,

$$\chi_{\pm} = \sqrt{\frac{8}{y}} [-h \pm \sqrt{h^2 - 1}] \quad , \quad \text{and} \quad w''(\chi_{\pm}) = 2 \sqrt{h^2 - 1} (\sqrt{h^2 - 1} \mp h) \quad .$$

Hence, for any $h < -1$, we have $w''(\chi_+) > 0$ while $w''(\chi_-) < 0$. Notice that $\chi_{\pm} > 0$ for $h < -1$.

Therefore, we have chaotic inflation for positive field χ in the regime $|h| < 1$ using the inflaton potential eq.(2.26).

We can also have chaotic inflation with the potential eq.(2.26) for negative field if $h > 3/\sqrt{8}$, but for $|h| > 3/\sqrt{8}$ the absolute minimum is no more at $\chi = 0$ but at χ_+ . Since $w(\chi_+) < 0$ for $|h| > 3/\sqrt{8}$ we have to subtract in this case the value $w(\chi_+)$ from $w(\chi)$ in order to enforce eq.(1.91).

We consider in subsections IIB 1, IIB 2 and IIB 3 the regime $-1 < h \leq 0$, $\chi \geq 0$. The case $h < -1$ is analyzed in subsection IIB 4.

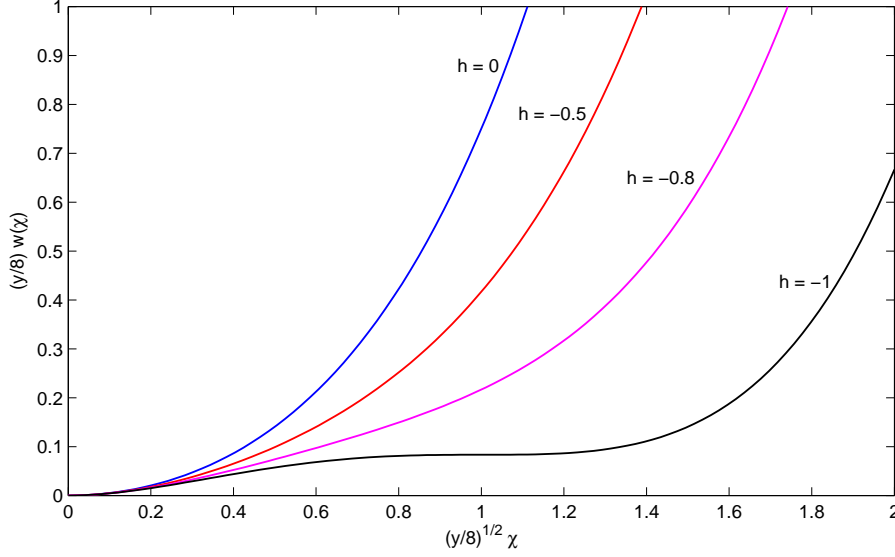


FIG. 12: Trinomial Chaotic Inflation. We plot here the chaotic inflation trinomial potential $\frac{y}{8} w(\chi)$ [eq.(2.26) with positive quadratic term] vs. the field variable $\sqrt{z} = \sqrt{y/8} \chi$ for different values of the asymmetry parameter h , namely, $h = 0, -0.5, -0.8$ and -1 . Notice the inflection point at $\sqrt{z} = 1$ when $h = -1$.

1. *The small asymmetry regime: $-1 < h \leq 0$.*

In chaotic inflation the inflaton field slowly rolls down the slope of the potential from its initial value till the absolute minimum of the potential at $\chi = 0$.

It is convenient to use the field variable z defined by eq.(2.5). $z = y \chi^2/8$. In terms of z the chaotic trinomial potential takes the form

$$w(\chi) = \frac{4}{y} z \left(1 + \frac{4}{3} h \sqrt{z} + \frac{1}{2} z \right).$$

When $z \lesssim 1$ we are in the quadratic regime where $w(\chi)$ is approximated by the χ^2 term. For $z \gtrsim 1$ we go to the non-linear regime in z and all three terms in $w(\chi)$ are of the same order of magnitude.

In fig. 12, we plot $y w(\chi)/8$ as a function of \sqrt{z} for several values of $h \geq -1$. We see that the potential becomes flatter as h decreases. For $h = -1$, both $w'(\chi)$ and $w''(\chi)$ vanish at $\sqrt{z} = 1$. The case $h = -1$ is singular since the inflaton gets stuck an infinite amount of time at the point $\sqrt{z} = 1$, $\chi = \sqrt{8/y}$.

By inserting eq.(2.26) for $w(\chi)$ into eq.(1.90) for $N[\chi]$ and setting $N[\chi] = N$ we obtain the field χ or equivalently z , at horizon exit, in terms of the coupling y and the asymmetry parameter h ,

$$y = z + \frac{4}{3} h \sqrt{z} + \left(1 - \frac{4}{3} h^2 \right) \log(1 + 2h \sqrt{z} + z) - \frac{4h}{3\Delta} \left(\frac{5}{2} - 2h^2 \right) \left[\arctan\left(\frac{h + \sqrt{z}}{\Delta}\right) - \arctan\left(\frac{h}{\Delta}\right) \right] \quad (2.28)$$

This defines the field z as a monotonically increasing function of the coupling y for $0 < y$, $z < +\infty$. Recall that χ and z corresponds to the time of horizon exit.

We obtain from eqs.(1.164), (1.170), (1.171), and (2.26) the spectral index, its running, the ratio r and the amplitude of adiabatic perturbations,

$$n_s = 1 - \frac{y}{2Nz} \left[\frac{3(1 + 2h\sqrt{z} + z)^2}{(1 + \frac{4}{3}h\sqrt{z} + \frac{1}{2}z)^2} - \frac{1 + 4h\sqrt{z} + 3z}{1 + \frac{4}{3}h\sqrt{z} + \frac{1}{2}z} \right], \quad (2.29)$$

$$\frac{dn_s}{d \ln k} = \frac{y^2}{2z^2 N^2} \left[-\frac{(1 + 2h\sqrt{z} + z)(h\sqrt{z} + \frac{3}{2}z)}{(1 + \frac{4}{3}h\sqrt{z} + \frac{1}{2}z)^2} - \frac{3(1 + 2h\sqrt{z} + z)^4}{(1 + \frac{4}{3}h\sqrt{z} + \frac{1}{2}z)^4} + \right]$$

$$+ 2 \frac{(1 + 2h\sqrt{z} + z)^2 (1 + 4h\sqrt{z} + 3z)}{(1 + \frac{4}{3}h\sqrt{z} + \frac{1}{2}z)^3} \Big], \quad (2.30)$$

$$r = \frac{4y}{Nz} \frac{(1 + 2h\sqrt{z} + z)^2}{(1 + \frac{4}{3}h\sqrt{z} + \frac{1}{2}z)^2}, \quad (2.31)$$

$$|\Delta_{kad}^{\mathcal{R}}|^2 = \frac{2N^2}{3\pi^2} \left(\frac{M}{M_{Pl}} \right)^4 \frac{z^2 (1 + \frac{4}{3}h\sqrt{z} + \frac{1}{2}z)^3}{y^2 (1 + 2h\sqrt{z} + z)^2}. \quad (2.32)$$

In chaotic inflation, the limit $z \rightarrow 0^+$ implies $y \rightarrow 0^+$ (shallow limit), we have in this limit:

$$\begin{aligned} y &\stackrel{z \rightarrow 0^+}{=} 2z + \mathcal{O}(z^{\frac{3}{2}}) \quad , \quad \chi &\stackrel{y \rightarrow 0^+}{=} 2 + \mathcal{O}(y) \quad , \quad n_s &\stackrel{y \rightarrow 0^+}{=} 1 - \frac{2}{N} \quad , \\ r &\stackrel{y \rightarrow 0^+}{=} \frac{8}{N} \quad , \quad |\Delta_{kad}^{\mathcal{R}}|^2 &\stackrel{y \rightarrow 0^+}{=} \frac{N^2}{6\pi^2} \left(\frac{M}{M_{Pl}} \right)^4. \end{aligned} \quad (2.33)$$

The results in the $y \rightarrow 0^+$ limit are **independent** of the asymmetry h and coincide with those for the purely quadratic monomial potential $\chi^2/2$.

In the limit $z \rightarrow +\infty$ which implies $y \rightarrow +\infty$ (strong coupling), we have for fixed $h > -1$,

$$\begin{aligned} y &\stackrel{z \rightarrow +\infty}{=} z + \frac{4}{3}h\sqrt{z} + \left(1 - \frac{4}{3}h^2\right) \log z + \mathcal{O}(1) \quad , \quad \chi &\stackrel{y \rightarrow +\infty}{=} 2\sqrt{2} + \mathcal{O}\left(\frac{1}{\sqrt{z}}\right) \quad , \\ n_s &\stackrel{y \rightarrow +\infty}{=} 1 - \frac{3}{N} \left[1 + \frac{4}{3} \frac{h}{\sqrt{z}} + \left(1 - \frac{4}{3}h^2\right) \frac{\log z}{z} + \mathcal{O}\left(\frac{1}{z}\right) \right] \quad , \\ r &\stackrel{y \rightarrow +\infty}{=} \frac{16}{N} \left[1 + \frac{4}{3} \frac{h}{\sqrt{z}} + \left(1 - \frac{4}{3}h^2\right) \frac{\log z}{z} + \mathcal{O}\left(\frac{1}{z}\right) \right] \quad , \\ |\Delta_{kad}^{\mathcal{R}}|^2 &\stackrel{y \rightarrow +\infty}{=} \frac{N^2}{12\pi^2} \left(\frac{M}{M_{Pl}} \right)^4 \frac{z}{\left[1 + \frac{4}{3} \frac{h}{\sqrt{z}} + \left(1 - \frac{4}{3}h^2\right) \frac{\log z}{z} + \mathcal{O}\left(\frac{1}{z}\right) \right]^2}. \end{aligned} \quad (2.34)$$

For $h = 0$, n_s and r in the limit $y \rightarrow +\infty$ coincide with those of the purely quartic monomial potential χ^4 given by eq.(2.12).

2. The flat potential limit $h \rightarrow -1^+$

We consider chaotic inflation in the regime $-1 < h \leq 0$, $\chi \geq 0$.

At $h = -1$ the potential eq.(2.26) exhibits an inflexion point at $\chi_0 \equiv \sqrt{8/y}$. Namely, $w'(\chi_0) = w''(\chi_0) = 0$ while $w(\chi_0) = 2/(3y) > 0$. That is, this happens at $z_0 = y\chi_0^2/8 = 1$.

Therefore, for $h > -1$ but very close to $h = -1$, the field evolution strongly slows down near the point $\chi = \chi_0$. This strong slow down shows up in the calculation of observables when the field χ at horizon crossing is $\chi > \chi_0$, namely, for $z > z_0 = 1$. For $\chi < \chi_0$, that is $z < 1$, the slow down of the field evolution will only appear if $z \simeq 1$. Therefore, the limit $h = -1$ is singular since the inflaton field gets trapped at the point $z = 1$.

Let us derive the $h \rightarrow -1^+$ limit of y , n_s and r from eqs.(2.28)-(2.32) in the regimes $z < 1$ and $z > 1$, respectively.

When $h \rightarrow -1^+$ we see from eq.(2.27) that $\Delta \rightarrow 0$ and the arguments of the two arctan in eq.(2.28) diverge. Hence, the arctan tends to $+\pi/2$ or $-\pi/2$. Depending on whether $z < 1$ or $z > 1$, the $\pi/2$'s terms cancel out or add, respectively. The special case $z = 1$ is investigated in the next subsection IIB3.

In the case $z < 1$ we get:

$$y = z - \frac{4}{3}\sqrt{z} - \frac{2}{3} \log(1 - \sqrt{z}) + \frac{2}{3} \frac{\sqrt{z}}{1 - \sqrt{z}} \quad , \quad h \rightarrow -1^+ \quad , \quad z < 1 \quad , \quad (2.35)$$

$$n_s = 1 - \frac{y}{2Nz} \left[3 \frac{(1-\sqrt{z})^4}{\left(1 - \frac{4}{3}\sqrt{z} + \frac{1}{2}z\right)^2} - \frac{(1-\sqrt{z})(1-3\sqrt{z})}{1 - \frac{4}{3}\sqrt{z} + \frac{1}{2}z} \right] , \quad h \rightarrow -1^+ , \quad z < 1 , \quad (2.36)$$

$$r = \frac{4y}{Nz} \frac{(1-\sqrt{z})^4}{\left(1 - \frac{4}{3}\sqrt{z} + \frac{1}{2}z\right)^2} , \quad h \rightarrow -1^+ , \quad z < 1 ,$$

$$|\Delta_{kad}^{\mathcal{R}}|^2 = \frac{2N^2}{3\pi^2} \left(\frac{M}{M_{Pl}} \right)^4 \frac{z^2 \left(1 - \frac{4}{3}\sqrt{z} + \frac{1}{2}z\right)^3}{y^2 (1-\sqrt{z})^4} . \quad (2.37)$$

In particular, in the regime $z \rightarrow 1^-$ we find,

$$n_s \stackrel{z \rightarrow 1^-}{\simeq} 1 - \frac{4}{N} , \quad r \stackrel{z \rightarrow 1^-}{\simeq} \frac{96}{N} (1-\sqrt{z})^3 \rightarrow 0 , \quad h \rightarrow -1^+ ,$$

$$y \stackrel{z \rightarrow 1^-}{\simeq} \frac{2}{3} \frac{1}{1-\sqrt{z}} \rightarrow \infty , \quad \chi \stackrel{z \rightarrow 1^-}{\simeq} 4\sqrt{3} \sqrt{1-\sqrt{z}} \rightarrow 0 , \quad |\Delta_{kad}^{\mathcal{R}}|^2 \stackrel{z \rightarrow 1^-}{\simeq} \left(\frac{N}{8\pi} \frac{M^2}{M_{Pl}^2} y \right)^2 . \quad (2.38)$$

That is, in the limit $h \rightarrow -1^+$, $z \rightarrow 1^-$ the ratio r becomes **very small** while the spectral index takes the value $n_s = 0.92$. The ratio r tends to zero in the regime $z \rightarrow 1^-$, $\chi \rightarrow \chi_0 = \sqrt{8/y}$ because $w'(\chi_0) = 0$ and r is proportional to $w'^2(\chi)$ according to eq.(1.170).

The $z \rightarrow 1^-$ regime for $h \rightarrow -1^+$ is a strong coupling limit since $y \rightarrow +\infty$ as shown by eq.(2.38). In addition, eq.(2.38) shows that for large y one must keep the product $y M^2$ fixed since it is determined by the amplitude of the adiabatic perturbations. We see from eq.(2.38) that $\tilde{M} \equiv \sqrt{y} M$ becomes the energy scale of inflation in the $y \rightarrow \infty$ limit: from eq.(1.177), $\tilde{M} \sim 10^{16} \text{GeV}$ according to the observed value of $|\Delta_{kad}^{\mathcal{R}}|/N$ displayed in eq.(1.175), while M and m vanish in the $y \rightarrow \infty$ limit

$$M = \frac{\tilde{M}}{\sqrt{y}} \stackrel{y \rightarrow \infty}{\simeq} 0 , \quad m = \frac{M^2}{M_{Pl}} = \frac{\tilde{M}^2}{y M_{Pl}} \stackrel{y \rightarrow \infty}{\simeq} 0 .$$

In fig. 14 we display r vs. n_s for fixed values of the asymmetry parameter h and the coupling y varying along the curves. The red curves correspond to chaotic inflation. In the bottom of fig. 14 we can see the curve for $h = -0.999$. The limiting curve for $h = -1$ (not drawn) will reach the point $n_s = 0.92$ and the bottom line $r = 0$ as described by eq.(2.38).

In the case $z > 1$, we get from eqs.(2.28)-(2.32),

$$y \stackrel{h \rightarrow -1^+}{\simeq} \frac{\pi}{3} \sqrt{\frac{2}{h+1}} + \mathcal{O}([h+1]^0) \rightarrow +\infty , \quad \chi \stackrel{h \rightarrow -1^+}{\simeq} 2 \sqrt{\frac{3z}{\pi}} [2(h+1)]^{\frac{1}{4}} \rightarrow 0 , \quad z > 1 ,$$

$$n_s \stackrel{h \rightarrow -1^+}{\simeq} 1 - \frac{\pi}{3\sqrt{2}Nz} \frac{1}{\sqrt{h+1}} \left[3 \frac{(1-\sqrt{z})^4}{\left(1 - \frac{4}{3}\sqrt{z} + \frac{1}{2}z\right)^2} - \frac{(1-\sqrt{z})(1-3\sqrt{z})}{1 - \frac{4}{3}\sqrt{z} + \frac{1}{2}z} \right] + \mathcal{O}([h+1]^0) , \quad z > 1 ,$$

$$r \stackrel{h \rightarrow -1^+}{\simeq} \frac{8\pi}{3\sqrt{2}Nz} \frac{1}{\sqrt{h+1}} \frac{(1-\sqrt{z})^4}{\left(1 - \frac{4}{3}\sqrt{z} + \frac{1}{2}z\right)^2} + \mathcal{O}([h+1]^0) , \quad z > 1 . \quad (2.39)$$

In this strong coupling regime the indices become **very large** and hence in contradiction with the data. In addition, the slow-roll expansion cannot be trusted when the coefficients of $1/N$ become large compared with unit. In conclusion, for $h \rightarrow -1^+$, the case of large field $z > 1$ is excluded by the data.

3. The singular limit $z = 1$ and then $h \rightarrow -1^+$ yields the Harrison-Zeldovich spectrum

We study in this section the case $z = 1$ in trinomial chaotic inflation. We obtain from eq.(2.28)

$$y \stackrel{z=1}{\simeq} 1 + \frac{4}{3}h + \left(1 - \frac{4}{3}h^2\right) \log[2(1+h)] - \frac{4h}{3\Delta} \left(\frac{5}{2} - 2h^2\right) \left[\arctan\left(\frac{h+1}{\Delta}\right) - \arctan\left(\frac{h}{\Delta}\right) \right] . \quad (2.40)$$

For $z = 1$, we find from eqs.(2.29)-(2.32) and (2.40) in the limit $h \rightarrow -1^+$,

$$y \stackrel{z=1, h \rightarrow -1^+}{\simeq} \frac{\pi}{3} \sqrt{\frac{1}{2(h+1)}} - \frac{1}{3} \log(h+1) + \mathcal{O}([h+1]^0) ,$$

$$\begin{aligned}
n_s &\stackrel{z=1, h \rightarrow -1^+}{=} 1 + \frac{2\pi}{N} \sqrt{2(h+1)} [1 + \mathcal{O}(h+1)] , \\
r &\stackrel{z=1, h \rightarrow -1^+}{=} \frac{16\pi}{N} \sqrt{2} (h+1)^{\frac{3}{2}} [1 + \mathcal{O}(h+1)] , \\
|\Delta_{kad}^{\mathcal{R}}|^2 &\stackrel{z=1, h \rightarrow -1^+}{=} \frac{N^2}{36} \left[\frac{M}{\pi M_{Pl} (h+1)^{\frac{1}{4}}} \right]^4 .
\end{aligned} \tag{2.41}$$

Therefore, we reach the Harrison-Zeldovich spectrum $n_s = 1$, $r = 0$ as a limiting value. This is a strong coupling regime $y \rightarrow \infty$ where in addition we must keep the ratio $M/(h+1)^{\frac{1}{4}}$ fixed for $h \rightarrow -1^+$ since it is determined by the amplitude of the adiabatic perturbations. That is, we must keep

$$\bar{M} \equiv \frac{M}{(h+1)^{\frac{1}{4}}} \quad \text{fixed as } h \rightarrow -1^+ ,$$

while M as well as m go to zero. Actually, the **whole** potential $V(\varphi)$ eq.(2.25) **vanishes** in this limit since,

$$\begin{aligned}
m &= \frac{M^2}{M_{Pl}} \stackrel{z=1, h \rightarrow -1^+}{=} \frac{\bar{M}^2}{M_{Pl}} \sqrt{h+1} \rightarrow 0 , \\
g &= h \sqrt{\frac{y}{2N}} \left(\frac{M}{M_{Pl}} \right)^2 \stackrel{z=1, h \rightarrow -1^+}{=} -\sqrt{\frac{\pi}{6N}} \left(\frac{\bar{M}}{M_{Pl}} \right)^2 \left(\frac{1+h}{2} \right)^{\frac{1}{4}} \rightarrow 0 , \\
\lambda &= \frac{y}{8N} \left(\frac{M}{M_{Pl}} \right)^4 \stackrel{z=1, h \rightarrow -1^+}{=} \sqrt{\frac{\pi}{24N}} \left(\frac{\bar{M}}{M_{Pl}} \right)^4 \sqrt{\frac{1+h}{2}} \rightarrow 0
\end{aligned} \tag{2.42}$$

The inflaton field is therefore a **massless** free field at $z = 1$ and $h \rightarrow -1^+$. This explains why the corresponding spectrum is the scale invariant Harrison-Zeldovich one. This is clearly a singular limit since one cannot obtain any inflation from an identically zero potential. Namely, taking the flat limit $h \rightarrow -1^+$ in the spectrum computed for $z = 1$, $h > -1$ with a fixed number of efolds N , yields the scale invariant Harrison-Zeldovich spectrum.

Notice that here we keep the number of efolds N *fixed* which makes the potential to vanish since otherwise the field will be stuck at the point $z = 1$ when $h = -1$ leading to eternal inflation ($N = \infty$).

In summary, this shows **theoretically** that the Harrison-Zeldovich spectrum which is a strong coupling limit $y \rightarrow \infty$, is *highly unplausible and unrealistic* since it appears only in the singular limit $z = 1$, $h \rightarrow -1^+$ where the inflaton potential identically vanishes. Recall that one can also get a Harrison-Zeldovich spectrum letting formally the number of efolds N to infinity in eqs.(1.170), that is letting inflation to last eternally.

Moreover, the Harrison-Zeldovich spectrum $n_s = 1$, $r = 0$ is excluded by the data [10].

4. The high asymmetry $h < -1$ regime.

In order to fulfill the finite number of efolds condition eq.(1.91) for $h < -1$ we have to add a constant term to the chaotic inflationary potential eq.(2.26). We therefore consider as inflaton potential in the $h < -1$ regime,

$$w(\chi) = \frac{1}{2} \chi^2 + \frac{h}{3} \sqrt{\frac{y}{2}} \chi^3 + \frac{y}{32} \chi^4 + \frac{2}{y} G(h) , \tag{2.43}$$

The absolute minimum of this potential is at

$$\chi_+ = \sqrt{\frac{8}{y}} [-h + D] \quad , \quad D \equiv \sqrt{h^2 - 1} \quad , \quad h < -1 . \tag{2.44}$$

and we have

$$G(h) \equiv \frac{8}{3} h^4 - 4 h^2 + 1 + \frac{8}{3} |h| D^3 \quad , \quad w''(\chi_+) = 2 \sqrt{h^2 - 1} \left(\sqrt{h^2 - 1} + |h| \right) > 0 . \tag{2.45}$$

That is, the inflaton mass squared in units of m^2 takes the value

$$2 D (D + |h|) .$$

Here, the inflaton field rolls down the slope of the potential from its initial value larger than χ_+ till the absolute minimum of the potential at $\chi = \chi_+$.

By inserting eq.(2.43) for $w(\chi)$ into eq.(1.90) for $N[\chi]$ and setting $N[\chi] \equiv N$ we obtain the field χ or equivalently $z = y \chi^2/8$, at horizon exit, in terms of the coupling y and the asymmetry parameter h :

$$y = z + \frac{4}{3} h \sqrt{z} + 1 + \frac{2}{3} h (D - h) + 2 G(h) \log \frac{\sqrt{z}}{D - h} + \frac{16}{3} h (h^2 - 1) (D - h) \log \left(\frac{\sqrt{z} + h + D}{2 D} \right). \quad (2.46)$$

This defines the field z as a monotonically increasing function of the coupling y for

$$0 < y < +\infty \quad , \quad z_+ = (D - h)^2 < z < +\infty .$$

Recall that χ and z corresponds to the time of horizon exit.

We obtain from eqs.(1.164), (1.170) and (2.43) the spectral index, the ratio r and the amplitude of adiabatic perturbations,

$$\begin{aligned} n_s &= 1 - \frac{y}{N} \frac{1}{(\sqrt{z} + h - D)^2} \left[\frac{6 z (\sqrt{z} + h + D)^2}{[z + 2(D + \frac{h}{3}) \sqrt{z} - \frac{2}{3} h (D - h) - 1]^2} - \frac{1 + 4 h \sqrt{z} + 3 z}{z + 2(D + \frac{h}{3}) \sqrt{z} - \frac{2}{3} h (D - h) - 1} \right], \\ r &= \frac{16 y}{N} \frac{z}{(\sqrt{z} + h - D)^2} \frac{(\sqrt{z} + h + D)^2}{[z + 2(D + \frac{h}{3}) \sqrt{z} - \frac{2}{3} h (D - h) - 1]^2}, \\ |\Delta_{k ad}^{\mathcal{R}}|^2 &= \frac{N^2}{12 \pi^2} \left(\frac{M}{M_{Pl}} \right)^4 \frac{[G(h) + 2 z + \frac{8}{3} h z^{3/2} + z^2] (\sqrt{z} + h - D)^2 [z + 2(D + \frac{h}{3}) \sqrt{z} - \frac{2}{3} h (D - h) - 1]^2}{y^2 z (\sqrt{z} + h + D)^2}. \end{aligned} \quad (2.47)$$

When $\sqrt{z} \rightarrow \sqrt{z_+}$, y vanishes quadratically and χ tends to infinity as

$$y \stackrel{z \rightarrow z_+}{\approx} 2 (\sqrt{z} - \sqrt{z_+})^2 + \mathcal{O}([\sqrt{z} - \sqrt{z_+}]^3) \quad , \quad \chi \stackrel{z \rightarrow z_+}{\approx} \frac{2 \sqrt{z_+}}{\sqrt{z} - \sqrt{z_+}} \rightarrow \infty .$$

In this limit the spectral index, the ratio r and the amplitude of adiabatic perturbations become,

$$n_s \stackrel{y \rightarrow 0}{\approx} 1 - \frac{2}{N} \quad , \quad r \stackrel{y \rightarrow 0}{\approx} \frac{8}{N} \quad , \quad |\Delta_{k ad}^{\mathcal{R}}|^2 \stackrel{y \rightarrow 0}{\approx} \frac{N^2}{6 \pi^2} \left(\frac{M}{M_{Pl}} \right)^4 .$$

These results are **independent** of the asymmetry h and coincide with those for the purely quadratic monomial potential $\frac{1}{2} \chi^2$.

We see here that

$$\frac{8}{N} < r < \frac{16}{N} \quad , \quad 1 - \frac{3}{N} < n_s < 1 - \frac{2}{N} \quad \text{for} \quad 0 < y < \infty . \quad (2.48)$$

Namely, the regime $h < -1$ of chaotic inflation covers values of r **larger** than the weak coupling limiting value $r = 8/N$ eq.(2.33) and **smaller** than the $y \rightarrow \infty$ pure quartic potential value $r = 16/N$ eq.(2.12).

C. Trinomial New Inflation: Spectral index, amplitude ratio, running index and limiting cases

We consider here new inflation described by the trinomial potential with broken symmetry investigated in ref.[12, 13, 14]

$$V(\varphi) = V_0 - \frac{m^2}{2} \varphi^2 + \frac{m g}{3} \varphi^3 + \frac{\lambda}{4} \varphi^4, \quad (2.49)$$

where $m^2 > 0$ and g and λ are dimensionless couplings. The corresponding dimensionless potential $w(\chi)$ takes the form

$$w(\chi) = -\frac{1}{2} \chi^2 + \frac{h}{3} \sqrt{\frac{y}{2}} \chi^3 + \frac{y}{32} \chi^4 + \frac{2}{y} F(h), \quad (2.50)$$

where the quartic coupling y is dimensionless as well as the asymmetry parameter h . The couplings in eq.(2.49) and eq.(2.50) are related by,

$$g = h \sqrt{\frac{y}{2N}} \left(\frac{M}{M_{Pl}} \right)^2, \quad \lambda = \frac{y}{8N} \left(\frac{M}{M_{Pl}} \right)^4, \quad (2.51)$$

and the constant w_0 [see eq.(2.1)] is related to V_0 in eq.(2.49) by

$$w_0 \equiv \frac{2}{y} F(h) = \frac{V_0}{N M^4}.$$

The constant $F(h)$ ensures that $w(\chi_+) = w'(\chi_+) = 0$ at the absolute minimum $\chi = \chi_+ = (\Delta + |h|) \sqrt{8/y}$ of the potential $w(\chi)$ according to eq.(1.91). Thus, inflation does not run eternally. $F(h)$ is given by

$$F(h) \equiv \frac{8}{3} h^4 + 4 h^2 + 1 + \frac{8}{3} |h| \Delta^3, \quad \Delta \equiv \sqrt{h^2 + 1}.$$

The parameter h reflects how asymmetric is the potential. Notice that $w(\chi)$ is invariant under the changes $\chi \rightarrow -\chi$, $h \rightarrow -h$. Hence, we can restrict ourselves to a given sign for h . Without loss of generality, we choose $h < 0$ and work with positive fields χ as in sec. II B..

We have near the absolute minimum $\chi = \chi_+$,

$$w(\chi) \stackrel{\chi \rightarrow \chi_+}{\approx} \Delta(\Delta + |h|) (\chi - \chi_+)^2 + \mathcal{O}(\sqrt{y}[\chi - \chi_+]^3), \quad (2.52)$$

That is, the inflaton mass squared in units of m^2 takes the value

$$2 \Delta(\Delta + |h|).$$

Notice that the inflaton mass squared takes the analogous value for chaotic inflation in the $h < -1$ regime changing $D \Rightarrow \Delta$ while $F(h)$ differs from $G(h)$ given by eq.(2.45) only by the sign of the $4 h^2$ term.

Recall that $y \sim \mathcal{O}(1) \sim h$ guarantees that $g \sim \mathcal{O}(10^{-6})$ and $\lambda \sim \mathcal{O}(10^{-12})$ *without* any fine tuning as stressed in sec. ID 2 [11].

In fig. 13, we plot

$$\frac{y}{8(h^2 + 1)^2} w(\chi) \quad \text{as a function of} \quad \frac{\sqrt{y}}{8} \frac{\chi}{\sqrt{h^2 + 1}}$$

for several values of $h < 0$. We see that the position of the minimum of the potential

$$\frac{\sqrt{y} \chi_+}{\sqrt{8} \sqrt{h^2 + 1}} = 1 + \frac{|h|}{\sqrt{h^2 + 1}}$$

grows as $|h|$ grows. Similarly, the maximum of the potential at the origin

$$\frac{y w(0)}{8(h^2 + 1)^2} = \frac{F(h)}{4(h^2 + 1)^2}$$

grows with $|h|$.

New inflation is obtained by choosing the initial field χ in the interval $(0, \chi_+)$. The inflaton χ slowly rolls down the slope of the potential from its initial value till the absolute minimum of the potential χ_+ .

Computing the number of efolds from eq.(1.90), we find the field χ at horizon crossing related to the coupling y and the asymmetry parameter h . We obtain by inserting eq.(2.50) for $w(\chi)$ into eq.(1.90) and setting $N[\chi] = N$,

$$y = z - 2 h^2 - 1 - 2 |h| \Delta + \frac{4}{3} |h| (|h| + \Delta - \sqrt{z}) + \frac{16}{3} |h| (\Delta + |h|) \Delta^2 \log \left[\frac{1}{2} \left(1 + \frac{\sqrt{z} - |h|}{\Delta} \right) \right] - 2 F(h) \log [\sqrt{z} (\Delta - |h|)] \quad , \quad z \equiv \frac{y}{8} \chi^2. \quad (2.53)$$

z turns to be a monotonically decreasing function of y . z decreases from

$$z = z_+ = (\Delta + |h|)^2 \quad (2.54)$$

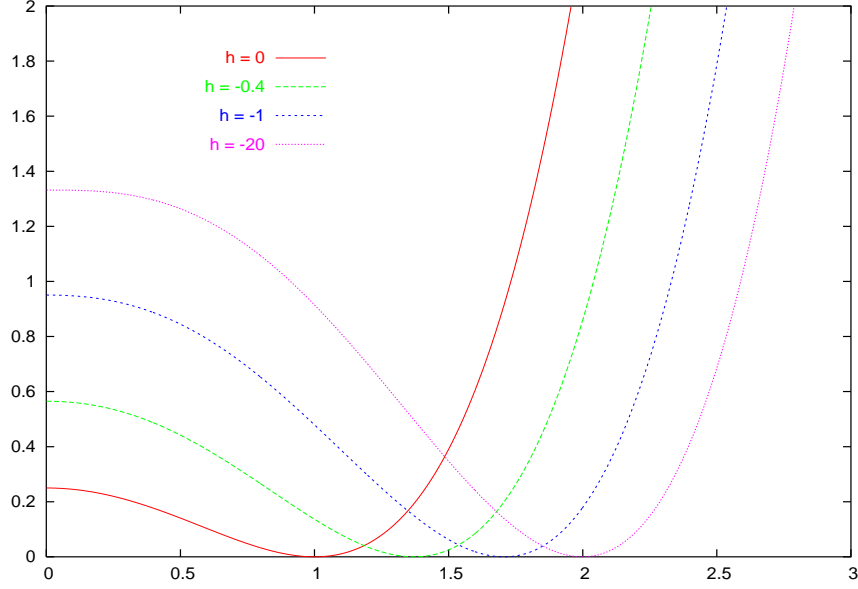


FIG. 13: Trinomial New Inflation. The new inflation trinomial potential $\frac{y w(\chi)}{8(h^2+1)^2}$ [eq.(2.50)] vs. the field variable $\frac{\sqrt{y} \chi}{\sqrt{8} \sqrt{h^2+1}}$ for $\chi \geq 0$ and different values of the asymmetry parameter $h = 0, -0.4, -1, -20$. We have normalized here the field variable and the potential by h -dependent factors in order to have a smooth $|h| \gg 1$ limit.

till $z = 0$ when y increases from $y = 0$ till $y = \infty$ while χ decreases from $\chi = \infty$ till $\chi = 0$. When $\sqrt{z} \rightarrow \sqrt{z_+}$, y vanishes quadratically as,

$$y \stackrel{z \rightarrow z_+}{\sim} 2 (\sqrt{z} - \sqrt{z_+})^2 + \mathcal{O} \left([\sqrt{z} - \sqrt{z_+}]^3 \right) \quad , \quad \chi \stackrel{z \rightarrow z_+}{\sim} \frac{2 \sqrt{z_+}}{\sqrt{z} - \sqrt{z_+}} \rightarrow \infty .$$

We obtain in analogous way from eqs.(1.164), (1.170), (1.171) and (2.50) the spectral index, its running, the ratio r and the amplitude of adiabatic perturbations,

$$n_s = 1 - 6 \frac{y}{N} \frac{z(z + 2h\sqrt{z} - 1)^2}{[F(h) - 2z + \frac{8}{3}h z^{3/2} + z^2]^2} + \frac{y}{N} \frac{3z + 4h\sqrt{z} - 1}{F(h) - 2z + \frac{8}{3}h z^{3/2} + z^2} \quad , \quad (2.55)$$

$$\begin{aligned} \frac{dn_s}{d \ln k} = & -\frac{2}{N^2} \sqrt{z} y^2 \frac{(z + 2h\sqrt{z} - 1)(h + \frac{3}{2}\sqrt{z})}{[F(h) - 2z + \frac{8}{3}h z^{3/2} + z^2]^2} - \frac{24}{N^2} y^2 z^2 \frac{(z + 2h\sqrt{z} - 1)^4}{[F(h) - 2z + \frac{8}{3}h z^{3/2} + z^2]^4} \\ & + \frac{8}{N^2} y^2 z \frac{(3z + 4h\sqrt{z} - 1)(z + 2h\sqrt{z} - 1)^2}{[F(h) - 2z + \frac{8}{3}h z^{3/2} + z^2]^3} \quad , \end{aligned} \quad (2.56)$$

$$r = 16 \frac{y}{N} \frac{z(z + 2h\sqrt{z} - 1)^2}{[F(h) - 2z + \frac{8}{3}h z^{3/2} + z^2]^2} \quad , \quad (2.57)$$

$$|\Delta_{k ad}^{\mathcal{R}}|^2 = \frac{N^2}{12 \pi^2} \left(\frac{M}{M_{Pl}} \right)^4 \frac{[F(h) - 2z + \frac{8}{3}h z^{3/2} + z^2]^3}{y^2 z (z + 2h\sqrt{z} - 1)^2} . \quad (2.58)$$

1. The weak coupling limit $y \rightarrow 0$

From eq.(2.53) we see that in the shallow limit $y \rightarrow 0$, z tends to $z_+ = (\Delta + |h|)^2$. $y(z)$ has its minimum $y = 0$ at $z = z_+$. We find from eqs.(2.53)-(2.58),

$$\chi \stackrel{y \rightarrow 0}{=} 2\sqrt{2}(\Delta + |h|)y^{-\frac{1}{2}} \rightarrow \infty, \quad n_s \stackrel{y \rightarrow 0}{=} 1 - \frac{2}{N} \simeq 0.967, \quad r \stackrel{y \rightarrow 0}{=} \frac{8}{N} \simeq 0.133, \quad (2.59)$$

$$\frac{dn_s}{d \ln k} \stackrel{y \rightarrow 0}{=} -\frac{2}{N^2} \simeq -0.000556, \quad |\Delta_{k ad}^{\mathcal{R}}|^2 \stackrel{y \rightarrow 0}{=} \frac{N^2}{3\pi^2} \left(\frac{M}{M_{Pl}}\right)^4 \Delta(\Delta + |h|), \quad (2.60)$$

which coincide with n_s , $dn_s/d \ln k$ and r for the monomial quadratic potential. That is, the $y \rightarrow 0$ limit is h -independent except for $|\Delta_{k ad}^{\mathcal{R}}|$. For fixed h and $y \rightarrow 0$ the inflaton potential eq.(2.50) becomes purely quadratic as we see from eq.(2.52):

$$w(\chi) \stackrel{y \rightarrow 0}{=} \Delta(\Delta + |h|)(\chi - \chi_+)^2 + \mathcal{O}(\sqrt{y}). \quad (2.61)$$

Notice that the amplitude of scalar adiabatic fluctuations eq.(2.59) turns out to be proportional to the square mass of the inflaton in this regime. We read this mass squared from eq.(2.61): $2\Delta(\Delta + |h|)$ in units of m^2 . The shift of the inflaton field by χ_+ has no observable consequences. For $h = 0$ we recover the results of the monomial quadratic potential eq.(2.10).

2. The strong coupling limit $y \rightarrow \infty$

In the steep limit $y \rightarrow \infty$, z tends to zero for new inflation. We find from eq.(2.53)

$$y \stackrel{z \rightarrow 0}{=} -F(h) \log z - q(h) - 1 + \mathcal{O}(\sqrt{z}) \rightarrow \infty, \quad \chi \stackrel{y \rightarrow \infty}{=} \sqrt{\frac{8}{y}} e^{-\frac{y+1+q(h)}{2F(h)}} \rightarrow 0, \quad (2.62)$$

where

$$q(h) \equiv 2F(h) \log(\Delta - |h|) - \frac{2}{3}(h^2 + |h|\Delta) \left\{ 8\Delta^2 \log \left[\frac{1}{2} \left(1 - \frac{|h|}{\Delta} \right) \right] - 1 \right\},$$

$q(h)$ is a monotonically increasing function of the asymmetry $|h|$: $0 \leq q(h) < \infty$ for $0 < |h| < \infty$.

Then, eqs.(2.55)-(2.56) yield,

$$\begin{aligned} n_s &\stackrel{y \gg 1}{=} 1 - \frac{y}{N F(h)}, \quad r \stackrel{y \gg 1}{=} \frac{16y}{N F^2(h)} e^{-\frac{y+1+q(h)}{F(h)}}, \\ \frac{dn_s}{d \ln k} &\stackrel{y \gg 1}{=} -\frac{2y^2|h|}{N^2 F^2(h)} e^{-\frac{y+1+q(h)}{2F(h)}}, \\ |\Delta_{k ad}^{\mathcal{R}}|^2 &\stackrel{y \gg 1}{=} \frac{N^2}{12\pi^2} \left(\frac{M}{M_{Pl}}\right)^4 \frac{F^3(h)}{y^2} e^{\frac{y+1+q(h)}{F(h)}}. \end{aligned} \quad (2.63)$$

In the case $h = 0$ we recover from the steep limit eqs.(2.62)-(2.63) the results for new inflation in the large y regime: we have $F(0) = 1$ and $q(0) = 0$ and eq.(2.63) becomes,

$$n_s \stackrel{y \gg 1, h \rightarrow 0}{=} 1 - \frac{y}{N}, \quad r \stackrel{y \gg 1, h \rightarrow 0}{=} \frac{16y}{N} e^{-y-1}, \quad (2.64)$$

$$\frac{dn_s}{d \ln k} \stackrel{y \gg 1, h \rightarrow 0}{=} -\frac{2y^2|h|}{N^2} e^{-y-1}, \quad |\Delta_{k ad}^{\mathcal{R}}|^2 \stackrel{y \gg 1, h \rightarrow 0}{=} \frac{N^2}{12\pi^2} \left(\frac{M}{M_{Pl}}\right)^4 \frac{e^{y+1}}{y^2}. \quad (2.65)$$

Only the behaviour of the running is non-uniform in h for $y \rightarrow \infty$ as we see comparing with eq.(2.19).

Notice that the slow-roll approximation is valid only when the coefficient of $1/N$ is smaller than N , and so for $y \lesssim N$. For $y \rightarrow \infty$, n_s is well below one and r is very small. This strong coupling limit is excluded since the WMAP+LSS data rule out $n_s \lesssim 0.9$.

3. The extremely asymmetric limit $|h| \rightarrow \infty$

Eqs.(2.53)-(2.58) have a finite limit for $|h| \rightarrow \infty$ with y and z scaling as h^2 . Define,

$$Z \equiv \frac{z}{h^2} \quad , \quad Y \equiv \frac{y}{h^2} \quad .$$

We have $0 \leq Z \leq 4$ for $+\infty \geq Y \geq 0$. Then, we find for $|h| \rightarrow \infty$ from eqs.(2.53)-(2.58) keeping Z and Y fixed,

$$Y = Z - \frac{4}{3} \sqrt{Z} - 4 - \frac{4}{3} \log \frac{Z}{4} + \frac{16}{3 \sqrt{Z}} \quad ,$$

$$n_s = 1 - 6 \frac{Y}{N} \frac{Z^2 (\sqrt{Z} - 2)^2}{[\frac{16}{3} - \frac{8}{3} Z^{\frac{3}{2}} + Z^2]^2} + \frac{Y}{N} \frac{3 Z - 4 \sqrt{Z}}{\frac{16}{3} - \frac{8}{3} Z^{\frac{3}{2}} + Z^2} \quad , \quad (2.66)$$

$$\frac{dn_s}{d \ln k} = - \frac{2}{N^2} Y^2 Z \frac{(\sqrt{Z} - 2)(\frac{3}{2} \sqrt{Z} - 1)}{[\frac{16}{3} - \frac{8}{3} Z^{3/2} + Z^2]^2}$$

$$- \frac{24}{N^2} Y^2 Z^4 \frac{(\sqrt{Z} - 2)^4}{[\frac{16}{3} - \frac{8}{3} Z^{3/2} + Z^2]^4} + \frac{8}{N^2} Y^2 Z^{\frac{5}{2}} \frac{(3 \sqrt{Z} - 4)(\sqrt{Z} - 2)^2}{[\frac{16}{3} - \frac{8}{3} Z^{3/2} + Z^2]^3} \quad , \quad (2.67)$$

$$r = 16 \frac{Y}{N} \frac{Z^2 (\sqrt{Z} - 2)^2}{[\frac{16}{3} - \frac{8}{3} Z^{\frac{3}{2}} + Z^2]^2} \quad , \quad |\Delta_{k ad}^{\mathcal{R}}|^2 = \frac{N^2 h^2}{12 \pi^2} \left(\frac{M}{M_{Pl}} \right)^4 \frac{[\frac{16}{3} - \frac{8}{3} Z^{\frac{3}{2}} + Z^2]^2}{Y^2 Z^2 (\sqrt{Z} - 2)^2} \quad . \quad (2.68)$$

In the $|h| \rightarrow \infty$ limit, the inflaton potential takes the form

$$W(\chi) \equiv \lim_{|h| \rightarrow \infty} \frac{w(\chi)}{h^2} = \frac{32}{3 Y} - \frac{1}{3} \sqrt{\frac{Y}{2}} \chi^3 + \frac{Y}{32} \chi^4 \quad .$$

This is an asymmetric potential without quadratic term. Notice that the cubic coupling has dimension of a mass in eq.(2.49) and hence this is **not** a massless potential contrary to the quartic monomial χ^4 .

In addition, eq.(2.68) shows that for large $|h|$ one must keep the product $|h| M^2$ fixed since this is determined by the amplitude of the adiabatic perturbations. We see from eq.(2.68) that in the $|h| \rightarrow \infty$ limit, $\tilde{M} \equiv \sqrt{|h|} M$ becomes the energy scale of inflation. $\tilde{M} \sim 10^{16} \text{GeV}$ [eq.(1.177)] according to the observed value of $|\Delta_{k ad}^{\mathcal{R}}|/N$ displayed in eq.(1.175), while M and m vanish as $|h| \rightarrow \infty$,

$$M = \frac{\tilde{M}}{\sqrt{|h|}} \xrightarrow{|h| \rightarrow \infty} 0 \quad , \quad m = \frac{M^2}{M_{Pl}} = \frac{\tilde{M}^2}{|h| M_{Pl}} \xrightarrow{|h| \rightarrow \infty} 0 \quad .$$

The MCMC analysis of the CMB+LSS data (see sec. IID 2) excludes large $|h|$ in new inflation as shown in fig. 17.

4. Regions of n_s and r covered by New Inflation and by Chaotic Inflation.

It follows from eqs.(2.56), (2.59) and (2.63) that new inflation for $h \leq 0$ covers the narrow **banana-shaped** sector between the black lines in the (n_s, r) plane depicted in fig. 14. We have in this region:

$$0 < r < \frac{8}{N} \quad , \quad n_s < 1 - \frac{1.9236 \dots}{N} \quad \text{for} \quad \infty > y > 0 \quad . \quad (2.69)$$

Chaotic inflation in the $h < -1$ region covers the even narrower **complementary** strip eq.(2.48) for $8/N < r < 16/N$. The zero coupling point $y \rightarrow 0$, $r = 8/N$, $n_s = 1 - 2/N$ being the border between the two regimes.

In summary, we see from fig. 14 that the regions of the trinomial new inflation and chaotic inflation are **complementary** in the (n_s, r) plane. New inflation describes the region of the (n_s, r) plane between the two black lines while chaotic inflation describes the whole plane to the right of the rightmost black line.

As we show in sec. IID below, chaotic inflation for $-1 < h \leq 0$ covers a wide region depicted by the red lines in the (n_s, r) plane (see fig. 14). However, as shown by fig. 21, this wide area is only a small corner of the field z - asymmetry h plane. Since new inflation covers the banana-shaped region between the black curves, we see from fig. 14 that the most probable values of r are **definitely non-zero** within trinomial new inflation. Precise lower bounds for r are derived from MCMC in sec. IID below.

D. The Monte Carlo Markov Chain Method of Data Analysis

Given a sufficiently rich set of empirical data and a theoretical model with several free parameters that should describe these data, one faces the problem of how to efficiently determine reliable bounds for those free parameters. More precisely, one needs to reconstruct the experimental probability distribution for the actual values of those parameters by means of (some form of) statistical inference.

The Monte Carlo Markov Chain (MCMC) method is a very efficient stochastic numerical method to carry out such a reconstruction, which could be quite difficult when the number of free parameters is not very small and the probability distribution to be reconstructed has a complicated profile.

In the case under consideration, the theoretical model is the standard cosmological model as presented in the previous sections, while the set of empirical data is that listed in the introduction [sec. IB]. Among these, the CMB and LSS observations play a distinguished rôle for their richness and precision.

A key step in any inference approach is the determination of the probability that a certain model, given certain values of its free parameters, will predict specific observational data. This requires some type of assumptions on the experimental uncertainties. Namely, after having assessed as much as possible the systematic errors, one needs to adopt a model for the statistical errors. This is especially important in the case of CMB anisotropies which are seeded by primordial classicalized quantum fluctuations which are intrinsically stochastic. In sec. IE these have been described as free-field gaussian fluctuations, as a direct consequence of the linearized approach. Primordial non-gaussianities and/or non-gaussianities induced by the evolution from decoupling till now are of course allowed in principle but not testable by present experimental accuracy, furthermore their discussion and treatment is beyond the scope of this review article.

The primordial fluctuations, even if assumed gaussian, are nonetheless quite different from statistical experimental errors, which are also usually assumed to be a normally-distributed noise. In fact, the latter may in principle be reduced (or better, the statistical estimator may be improved) by increasing the number of observations. On the contrary, there is only one realization for primordial fluctuations which corresponds to our observable universe. This is the source of the so-called cosmic variance.

To be specific, let us consider an ideal experiment capable of providing a complete and noiseless sky map of the CMB temperature anisotropies. Any such map is a function $t = t(\mathbf{n})$ yielding the temperature fluctuation in the direction \mathbf{n} with respect to the full sky mean value. According to the above assumption of gaussianity, these maps form a normal ensemble with zero average and rotational-invariant covariance $\langle t(\mathbf{n})t(\mathbf{n}') \rangle$, that is

$$\langle t(\mathbf{n}) \rangle = 0 \quad , \quad \langle t(\mathbf{n})t(\mathbf{n}') \rangle = C(\mathbf{n} \cdot \mathbf{n}') .$$

In a spherical harmonic decomposition we can then write (notice that the monopole term $\ell = 0$ vanishes by definition)

$$t(\mathbf{n}) = \sum_{\ell=1}^{\infty} \sum_{m=-\ell}^{m=\ell} a_{\ell m} Y_{\ell m}(\mathbf{n}) ,$$

with

$$\langle a_{\ell m} \rangle = \langle a_{\ell m}^* \rangle = 0 \quad , \quad \langle a_{\ell m} a_{\ell' m'}^* \rangle = \delta_{\ell \ell'} \delta_{m m'} C_{\ell}$$

and

$$C(\mathbf{n} \cdot \mathbf{n}') = \frac{1}{4\pi} \sum_{\ell} (2\ell + 1) C_{\ell} P_{\ell}(\mathbf{n} \cdot \mathbf{n}') .$$

Thus, the multipoles C_{ℓ} forming the so-called angular power spectrum, fully characterize the statistical properties of any map $t(\mathbf{n})$. It turns out that the C_{ℓ} are computable from the primordial gaussian fluctuations through their cosmological evolution from decoupling till the present age. Hence, they depend on the collection of cosmological parameters $\lambda = \{\lambda_1, \lambda_2, \dots, \lambda_n\}$, that is the free parameters in the cosmological model of choice.

We considered in this example the best measured Temperature–Temperature (TT) correlation. The same analysis can be repeated also for the other correlations, such as the Temperature–E_modes (TE), the E_modes–E_modes (EE) and the B_modes–B_modes (BB) correlation multipoles (E_modes and B_modes are special modes of the CMB polarization).

Apart from experimental errors, here and now in our universe we only observe one specific map $\bar{t}(\mathbf{n})$, so that we can

only try and infer the value of the parameters λ . Bayesian inference is based on the notion of conditional probability¹. The likelihood L of λ , given the experimental data $\bar{t}(\mathbf{n})$, is related to the probability of $\bar{t}(\mathbf{n})$ given certain value of the parameters λ in the following way:

$$L(\lambda | \bar{t}) \propto \Pr(\bar{t} | C(\lambda)) p(\lambda) \quad (2.70)$$

where

$$\Pr(t | C) = [\text{Det}(2\pi C)]^{-1/2} \exp \left[-\frac{1}{2} \int d^2 n \int d^2 n' t(\mathbf{n}) (C^{-1})(\mathbf{n} \cdot \mathbf{n}') t(\mathbf{n}') \right] \quad (2.71)$$

is the Gaussian distribution for all possible maps for a given covariance $C(\mathbf{n} \cdot \mathbf{n}')$ and $p(\lambda)$ is the prior probability on the parameters, which collects any a priori bias on their actual values. In terms of the spherical amplitudes $\bar{a}_{\ell m}$ corresponding to the observed map $\bar{t}(\mathbf{n})$ and of the multipoles C_ℓ we have

$$\Pr(\bar{t} | C) = \exp \left\{ -\frac{1}{2} \sum_{\ell m} \left[\frac{|\bar{a}_{\ell m}|^2}{C_\ell} + \log(2\pi C_\ell) \right] \right\} = \prod_{\ell} \left[(2\pi C_\ell)^{-1/2} \exp \left(-\frac{\bar{C}_\ell}{2 C_\ell} \right) \right]^{(2\ell+1)}$$

where

$$\bar{C}_\ell = \frac{1}{2\ell+1} \sum_{m=-\ell}^{m=\ell} |\bar{a}_{\ell m}|^2$$

is the most likely value of C_ℓ (that is, the value at which $\Pr(\bar{t} | C)$ takes its maximum value as a function of the C_ℓ 's). Notice that in this ideal example $\Pr(\bar{t} | C)$ assigns independent weights to the multipoles C_ℓ ; that is, the C_ℓ 's are correlated only by their dependence on the cosmological parameters.

Finally, properly normalizing $L(\lambda | \bar{t})$ with respect to λ yields the so-called posterior probability, which is just the sought experimental probability for the value λ .

The MCMC method reconstructs the profile of $L(\lambda | \bar{t})$ through the ergodic properties of sequences $\{\lambda^{(0)}, \lambda^{(1)}, \dots, \lambda^{(k)}, \dots\}$ (the chains), that start from points extracted with the prior probability and evolve through a suitable acceptance/rejection one-step algorithm such as the Metropolis rule:

$$W(\lambda^{(k+1)}, \lambda^{(k)}) = g(\lambda^{(k+1)}, \lambda^{(k)}) \min \left\{ 1, \frac{L(\lambda^{(k+1)} | \bar{t}) g(\lambda^{(k)}, \lambda^{(k+1)})}{L(\lambda^{(k)} | \bar{t}) g(\lambda^{(k+1)}, \lambda^{(k)})} \right\}$$

Here $W(\lambda, \lambda')$ is the actual one-step transition probability, while $g(\lambda, \lambda')$ is an implementation-dependent proposal probability. The ergodic (for good proposal probabilities) and detailed balance properties of this $W(\lambda, \lambda')$ guarantee that very long chains will contain λ values distributed according to the posterior probability. In this case, the specific choice of $g(\lambda, \lambda')$ will only affect the convergence rate of the process.

Of course, in a true experiment, such as WMAP, the observed sky map $\bar{t}(\mathbf{n})$ suffers from several errors and approximations, such as those introduced by the experimental noise, by the necessary map discretization (or *pixelization*) due to the finite resolving power or by the effects of removing various types of contamination sources in the sky. This complicates considerably any reliable calculation of that part of the likelihood (the Gaussian $\Pr(\bar{t} | C)$ in the ideal example above) which depends on λ only through the C_ℓ multipoles. Moreover, the experimental likelihood weakly correlates the C_ℓ 's. At any rate no substantial change is implied in the MCMC application, since the experimental likelihood of the C_ℓ has no relation at all with their dependence on the cosmological parameters. In practice, a MCMC determination of the posterior probability for λ uses a likelihood code for the C_ℓ multipoles provided by the experiment itself, such as WMAP, and some numerical program such as CMBFAST or CAMB to compute the theoretical $C_\ell(\lambda)$ within a given cosmological model as a function of λ . The publicly available open-source CosmoMC program [43] is a very useful and widely used package that integrates all the necessary aspects of MCMC data analysis for cosmology.

¹ In abstract terms, if A and B are two possible events and with $A \cap B$ we denote the joint event, then

$$\Pr(A \cap B) = \Pr(B \cap A) = \Pr(A|B) \Pr(B) = \Pr(B|A) \Pr(A)$$

defines $\Pr(A|B)$ and $\Pr(B|A)$. Thus, since by definition $\Pr(B) = \sum_A \Pr(A \cap B)$ if $\{A\}$ is a complete set of mutually exclusive events, we obtain Bayes' formula

$$\Pr(A|B) = \frac{L(A|B)}{\sum_{A'} L(A'|B)}$$

where $L(A|B) \equiv \Pr(B|A) \Pr(A)$ is the *likelihood* of A given the observation of B .

1. CMB, LSS and Inflation within a MCMC analysis.

Let us describe now the results of an accurate MCMC analysis of CMB and LSS data with the CosmoMC programme in which we have included the Trinomial New Inflation (TNI) and Trinomial Chaotic Inflation (TCI) models [14].

The experimental data were those of CMB and LSS. In ref. [14] the CMB data were the three years WMAP data, which contain also polarization maps and provide the dominating contribution, and also the small scale data (ACBAR, CBI2, BOOMERANG03). For LSS the SDSS data (release 4) were considered. In this MCMC analysis we neither marginalized over the the Sunayev-Zel'dovich amplitude nor included non-linear effects in the evolution of the matter spectrum. In any case, the relative corrections are not significant [9], especially in the present context. While ref.[14] was in the publication stage the five years WMAP data were released [10]. Also a new comprehensive compilation of supernovae observations was published [24]. We shall verify below that these new data do not change in any relevant way the overall picture drawn in ref. [14].

As discussed above, in a MCMC analysis one must also choose the prior probability for the cosmological parameters. This implies restricting the search to a subset of the full parameter space by imposing so-called hard constraints, whose number and type depend on previously acquired information both experimental and theoretical. Since the central cosmological parameters in this analysis are the spectral index n_s of the adiabatic fluctuations and the ratio r of tensor to scalar fluctuations, we impose as hard constraint that n_s and r are restricted to the theoretical regions in the (n_s, r) plane described by TNI and TCI, respectively, as discussed in subsection II C 4. Our analysis differs in this **crucial** aspect from previous MCMC studies involving the WMAP3 data [50]. As natural within slow-roll inflation, we also include the inflationary consistency relation $n_T = -r/8$ on the tensor spectral index. This constraint is in any case practically negligible.

Altogether we allow seven cosmological parameters to vary in our MCMC runs: the baryonic matter fraction ω_b , the dark matter fraction ω_c , the optical depth τ , the ratio of the (approximate) sound horizon to the angular diameter distance θ , the primordial superhorizon power in the curvature perturbation at 0.05 Mpc^{-1} , A_s , the scalar spectral index n_s and the tensor-scalar ratio r . The last three of these parameters characterize the primordial power spectrum, while the first four affect the formation, evolution and propagation of the CMB after the reentering of superhorizon fluctuations. The inflationary cosmological models thus defined can be briefly identified as $\Lambda\text{CDM}+\text{TNI}$ model and $\Lambda\text{CDM}+\text{TCI}$ model, according to the TNI potential eq. (2.49) and the TCI potential eq. (2.25), respectively.

For comparison, we report also the results of a MCMC study within the standard ΛCDM model augmented by the tensor-scalar ratio r (the $\Lambda\text{CDM}+r$ model). That is, in this case we treated n_s and r as unconstrained Monte Carlo parameters, using standard priors. The analysis with the $\Lambda\text{CDM}+r$ model is indeed by now quite standard and good priors are available already in CosmoMC.

In the case of TNI, since the characteristic banana-shaped allowed region in the (n_s, r) plane is quite narrow and non-trivial, it is convenient to use as MC parameters the two independent variables z and h of the trinomial inflationary setup. That is, n_s and r are parametrized in terms of z and h by the analytic expressions at order $1/N$, eqs.(2.55) and (2.57). To be more precise, rather than z we use the appropriate normalized variable

$$z_1 = 1 - \frac{z}{z_+} = 1 - \frac{z}{(\sqrt{h^2 + 1} + |h|)^2} \quad (2.72)$$

We recall that z contains the field at horizon crossing and the coupling y . z_+ stands for z at the absolute minimum of the potential. The variable z_1 grows monotonically from 0 to 1 as the coupling y grows from 0 to ∞ [see eq. (2.53) and (2.54)].

Concerning priors, we keep the same, standard ones, of the $\Lambda\text{CDM}+r$ model for the first five parameters (ω_b , ω_c , τ , θ and A_s), while we consider all the possibilities for z_1 and h , that is $0 < z_1 < 1$, $0 < |h| < \infty$. Moreover, in order to correctly compare the results with those of the $\Lambda\text{CDM}+r$ model, in which a flat prior distribution on r is indeed assumed, we reweight the statistics to convert to a flat prior distribution on r (this is feasible since the relation between r and z_1 is monotonic for any h).

In the case of the $\Lambda\text{CDM}+\text{TCI}$ model, it is more convenient to keep n_s and r as MC parameters and impose as hard priors that they lay in the region described by TCI (see fig. 14). This is because this region covers the major part of the probability support of n_s and r in the $\Lambda\text{CDM}+r$ model and the parametrization eqs.(2.29)-(2.31) in terms of the coupling parameters z and h becomes quite singular in the limit $h \rightarrow -1$. This is indeed the limit which allows to cover the region of highest likelihood.

The distributions for the field variable z and the asymmetry parameter h are then recovered from the (n_s, r) distribution by a numerical change of variables, starting from an uniform two dimensional grid in the $z - h$ plane and using eqs.(2.29) and (2.31). This requires a rather accurate determination of the (n_s, r) distribution, which is obtained by running very long parallel chains (with a total number of samples close to five million for the results

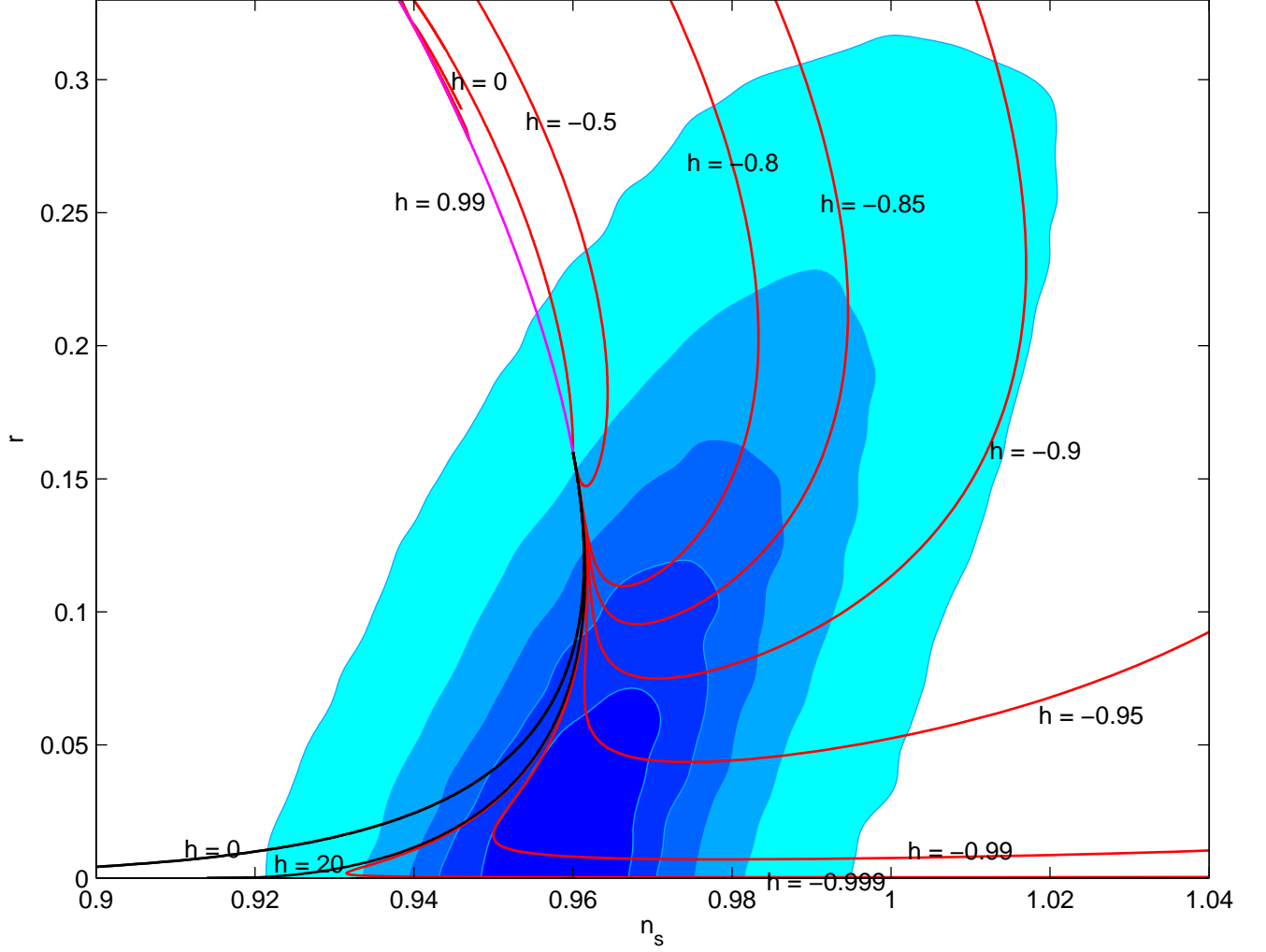


FIG. 14: Trinomial Inflation. We plot r vs. n_s for fixed values of the asymmetry parameter h and the field z varying along the curves. The red curves are those of chaotic inflation with $h \leq 0$ (only the short magenta curve has positive h), while the black curves are for new inflation. The color-filled areas correspond to 12%, 27%, 45%, 68% and 95% confidence levels according to the WMAP3 and Sloan data. Red and black curves are drawn for $N = 50$. A slightly better agreement with the data arises for $N = 60$. The color of the areas goes from the darker to the lighter for increasing CL. New inflation only covers a narrow area between the black lines while chaotic inflation covers a much wider area but, as shown by fig. 21, this wide area is only a small corner of the field z - asymmetry h plane. Since new inflation covers the banana-shaped region between the black curves, we see from this figure that the most probable values of r are **definitely non-zero** within trinomial new inflation. Precise lower bounds for r are derived from MCMC in eq.(2.73).

presented below). Quite naturally in this approach for TCI, the most likely values of the cosmological parameters and the corresponding maximum of the likelihood coincide to those of the Λ CDM+ r model.

In all our MCMC runs we kept fixed the number of efolds N since the horizon exit of the pivot scale k_0 till the end of inflation. The reason is that the main physics that determines the value of N is **not** contained in the available data but involves the reheating era. Therefore, although technically possible, it is not reliable to fit N with the CMB+LSS data solely within a pure, near scale-invariant slow roll scenario. Anyway, the precise value of N is certainly near $N = 60$ [2, 3, 4].

In this section we report the results of ref.[14] where the value $N = 50$ was chosen as a reference baseline value for numerical analysis. Anyway, from eqs.(1.170) and (2.75) we see that both $n_s - 1$ and r scale as $1/N$.

Therefore, decreasing or increasing N produces a scale transformation in the $(n_s - 1, r)$ plane, thus displacing the black and red curves in fig. 14 towards up and left or towards down and right. This produces, however, small

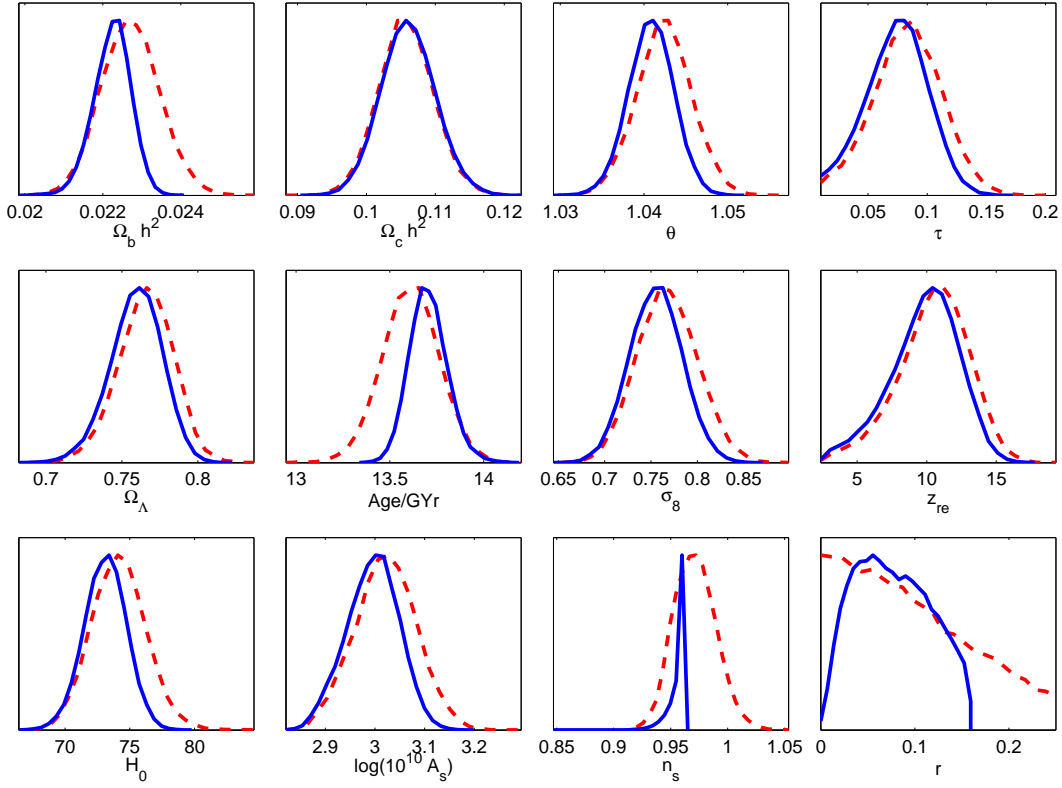


FIG. 15: Comparison of the marginalized probability distributions (normalized to have maximum equal to one) of the most relevant cosmological parameters (both primary and derived) between the model Λ CDM+TNI (Trinomial New Inflation, solid blue curves) and the Λ CDM+ r model (dashed red curves). Here $N = 50$ and WMAP3, small-scale CMB and SDSS data were used.

quantitative changes in our bounds for r as well as in the most probable values for r and n_s . We explicitly verified this statement by performing also a MCMC analysis using the last WMAP5 release and setting $N = 60$. The corresponding results are reported here for the first time. In summary, varying N from 50 to 60 has only minor, practically irrelevant effects in the MCMC fits we present in this review. This is partially due to the fact that in the theoretical formulas for n_s and r , eqs.(2.29), (2.85), (2.55) and (2.56), a change on N can be partially compensated by a change on y . The detailed analysis with variable N is at any rate beyond the scope of the present review.

Another **hint** to increase N above 50 comes from the WMAP5 data that gives a slightly larger n_s value and using the theoretical upper limit for n_s eq.(2.69), which gives $n_s < 0.9679 \dots$ for $N = 60$. This bound on n_s is compatible with the n_s value from WMAP5+BAO+SN and no running [10].

In addition, the early fast-roll stage explanation of the quadrupole suppression (see sec. II G and refs. [21, 22, 23]) allows to set an absolute wavelength scale for the primordial power which fixes the total number of efolds of inflation so we checked the consistency of our assumptions about N .

We have not introduced the running of the spectral index $dn_s/d\ln k$ in our MCMC fits since the running [eq.(1.171)] must be very small of the order $\mathcal{O}(N^{-2}) \sim 0.001$ in slow-roll and for generic potentials [11]. Indeed we found that adding $dn_s/d\ln k$, as given by eq. (2.30) or eq. (2.56), to the MCMC analysis yields insignificant changes on the fit of n_s and r . On the contrary, when the running is introduced as a free parameter, then the fit of n_s and r gets worse and values for the running much larger than $\mathcal{O}(N^{-2}) \sim 0.001$ follow [9, 10, 50]. We think that the present data are **not** yet precise enough to allow a determination of $dn_s/d\ln k$. That is, adding further parameters to the fit (like the running) does not improve the fit and does not teach anything new.

We provide in sec. II G 3 the MCMC analysis of the Binomial New Inflation model (BNI) described in sec. II A 2 [23], using the most recent CMB data (WMAP5 [10] and ACBAR08 [44]) and setting $N = 60$. The results obtained are consistent with and complementary to the analysis of the Λ CDM+TNI model presented in the next subsection.

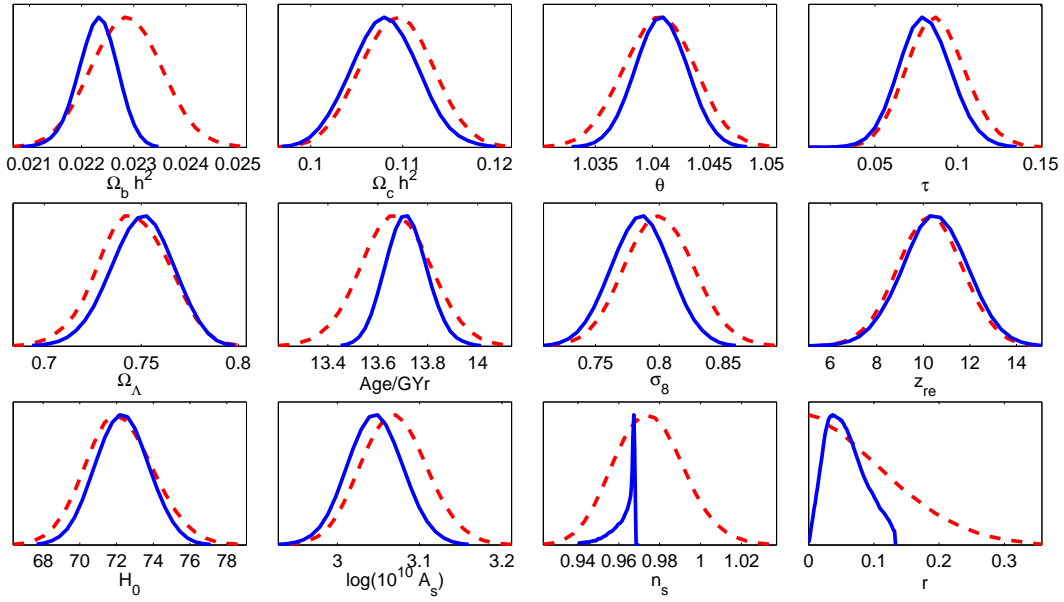


FIG. 16: Comparison of the marginalized probability distributions (normalized to have maximum equal to one) of the most relevant cosmological parameters (both primary and derived) between Λ CDM+TNI (solid blue curves) and the Λ CDM+ r model (dashed red curves). Here $N = 60$ and WMAP5, SN and SDSS data were used.

2. MCMC results for Trinomial New Inflation.

Our MCMC results for the Λ CDM+TNI model are summarized in figs. 15–19.

In fig. 15 we plot the marginalized probability distributions (normalized to have maximum equal to one) of the most relevant cosmological parameters, which are the primary ones allowed to vary independently in the MCMC runs plus some derived ones. The solid blue curves refer to the runs with the hard priors specific to TNI, with the statistics reweighted to correspond to a flat prior distribution on r . The dashed red curves are those of the Λ CDM+ r model. As should have been expected from fig. 14, the really significant changes are restricted solely to n_s and r . To provide further evidence of this, we compare in fig. 19 the joint probability distributions (τ, n_s) and (τ, r) of the Λ CDM+TNI model with those of the Λ CDM+ r model. We recall that the optical depth parameter τ is strongly correlated with n_s .

For the sake of comparison, we provide in fig. 16 the same probability distributions obtained with MCMC runs where $N = 60$ and WMAP5 data are used together with SDSS data and the most recent SN compiled observations. As anticipated earlier and as will be confirmed later on, no really significant changes can be appreciated apart from a slightly tighter determination for r .

In the lower panels of figs. 17 and 18 we provide an enlarged version of the marginalized probability distributions for n_s and r , together with their mean likelihoods, for both sets of data WMAP3+small-scale CMB+SDSS and WMAP5+SN+SDSS. In the upper panels we plot the marginalized probabilities and the mean likelihoods for the normalized coupling at horizon exit z_1 and for the asymmetry h , that are the two free parameters of the trinomial potential of new inflation. In this case the prior probability is flat over the full allowed range of z_1 . Again no significant differences can be observed, apart from those expected from the change from $N = 50$ to $N = 60$ which affects the theoretical bounds on n_s and r .

In figs. 17 and 18 one can observe a significant difference between probability distributions and mean likelihood distributions for n_s and r . Probability and mean likelihood depend quite differently on the shapes and parametrizations of the allowed (n_s, r) regions; if observational data were well concentrated within the allowed (n_s, r) regions, both types of distributions would have a gaussian-like shape over much narrower intervals and the difference would be much smaller. With the current data, the joint probability distributions over the parameters of the trinomial potential are very far from gaussian, as can be appreciated from fig. 21.

The theoretical constraints narrow the allowed region of parameters in a very nontrivial way. Otherwise, the parameters could cover a much wider region. Hence, the theoretically constrained distributions can hardly be gaussian and in fact they are not. In the case of trinomial new inflation, the narrow banana-shaped region depicted in fig. 14

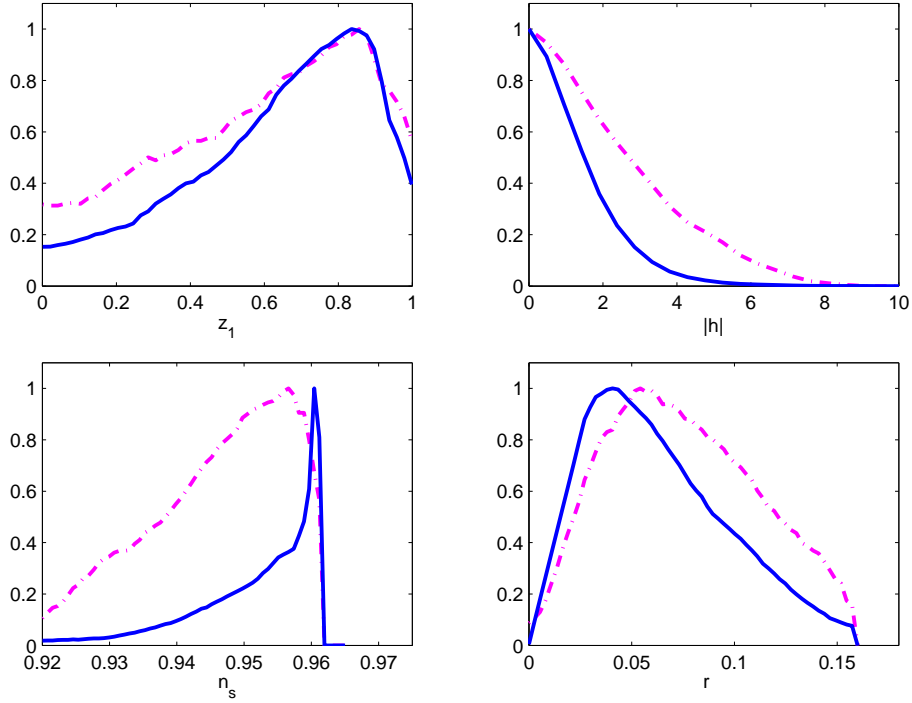


FIG. 17: Λ CDM+TNI for $N = 50$ with WMAP3, small-scale CMB and SDSS data. Upper panels: probability distributions (solid blue curves) and mean likelihoods (dot-dashed magenta curves), all normalized to have maximum equal to one, for the values of the normalized coupling at horizon exit z_1 and of the modulus $|h|$ of the asymmetry of the potential. Lower panels: probabilities and mean likelihoods for the values of n_s and r . Notice that $n_s < 0.9615\dots$ and $r \leq 0.16$ since these are the theoretical upper bounds for n_s and r in trinomial new inflation with $N = 50$. There appears a **lower bound** for the tensor–scalar ratio: $r > 0.016$ (95% CL), $r > 0.049$ (68% CL).

	WMAP3 + small scale CMB+SDSS		WMAP5+SN+SDSS	
parameter	Λ CDM+ r	Λ CDM+TNI	Λ CDM+ r	Λ CDM+TNI
$100\Omega_b h^2$	2.224	2.219	2.250	2.237
$\Omega_c h^2$	0.107	0.106	0.107	0.108
θ	1.043	1.041	1.038	1.041
100τ	8.313	8.468	8.824	7.885
H_0	73.3	72.85	72.20	72.24
σ_8	0.773	0.766	0.784	0.786
z_{re}	10.72	10.92	9.69	10.38
$\log[10^{10} A_s]$	3.022	3.019	3.060	3.045
n_s	0.960	0.956	0.962	0.963
r	0.009	0.055	0.009	0.043
$\Delta\chi^2$	0	+0.15	0	+0.08

TABLE III: Comparison of best fits between Λ CDM+ r and Λ CDM+TNI with the two data sets indicated on top. Also the negligible variation of $\chi^2 \equiv -2\log(\text{likelihood})$ is reported

is responsible for the marked difference between marginalized probability distribution and mean likelihood for n_s , as shown in fig. 17. Besides, the banana–shape of trinomial new inflation in the $n_s - r$ plane, produces a spike in the left lower panel of fig. 17. The sharp cut on the right is due to the theoretical upper bound on n_s given by eq. (2.69), the sharp rise on the left of the maximum is due to the marginalization over r .

Concerning most likely values (*i.e.* best fits), our results are summarized in table III. The increase in χ^2 from Λ CDM+ r to Λ CDM+TNI is roughly twice the standard deviation of χ^2 over ten parallel chains with a given model

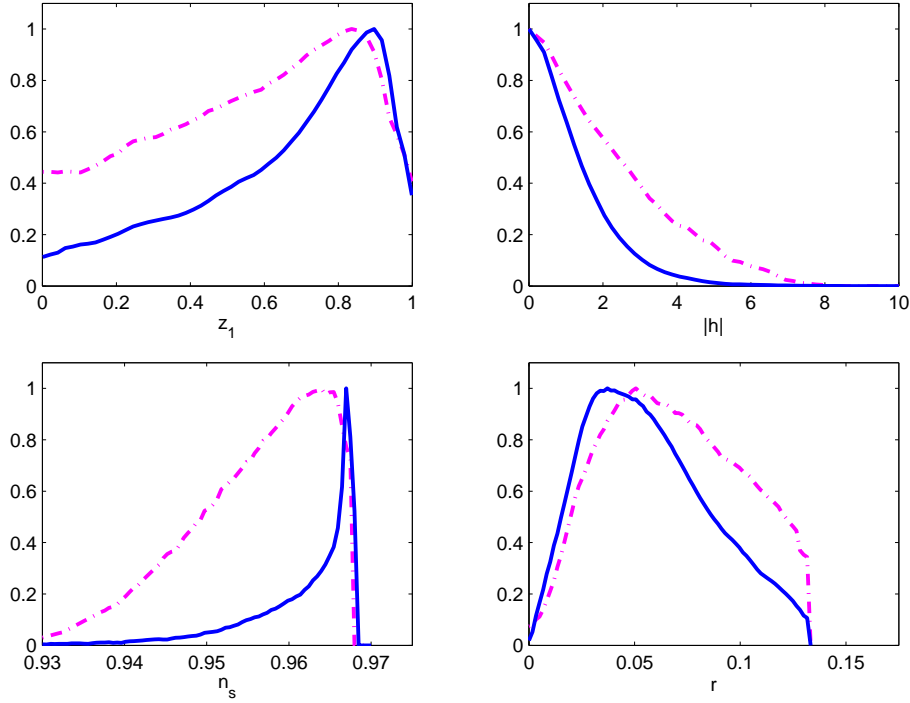


FIG. 18: Λ CDM+TNI for $N = 60$ and with WMAP5, SN and SDSS data. Upper panels: probability distributions (solid blue curves) and mean likelihoods (dot-dashed magenta curves), all normalized to have maximum equal to one, for the values of the normalized coupling at horizon exit z_1 and of the modulus $|h|$ of the asymmetry of the potential. Lower panels: probabilities and mean likelihoods for the values of n_s and r . Notice that here $n_s < 0.9678\dots$ and $r \leq 0.13$ since these are the theoretical upper bounds for n_s and r in trinomial new inflation with $N = 60$. There appears a **lower bound** for the tensor-scalar ratio: $r > 0.017$ (95% CL), $r > 0.046$ (68% CL).

and is therefore not significant.

Most importantly, as expected from fig. 14 and quite evident from figs. 15 and 16, we find a **lower bound** on r for Λ CDM+TNI:

$$\begin{aligned} r > 0.016 \quad (95\% \text{ CL}) \quad , \quad r > 0.049 \quad (68\% \text{ CL}) \quad (\text{WMAP3} + \text{smallscale CMB} + \text{SDSS}) \\ r > 0.017 \quad (95\% \text{ CL}) \quad , \quad r > 0.046 \quad (68\% \text{ CL}) \quad (\text{WMAP5} + \text{SN} + \text{SDSS}) . \end{aligned} \quad (2.73)$$

Let us now consider the MCMC results for the two parameters of the TNI potential, z_1 and h (see the upper panels of figs. 17 and 18 for the marginalized probabilities and the mean likelihoods obtained with flat priors on z_1 and h themselves). The asymmetry h turns out to have very little relevance, since its distribution is highly peaked near zero and we find that

$$|h| < 2.5 \quad \text{with 95\% CL} .$$

In fact, we could set it to a value of order 1 without a real loss of generality. Then the symmetric choice $h = 0$ would be the most natural, reducing the Λ CDM+TNI model to the Λ CDM+BNI treated in more detail in sec. II G 3 where also the MCMC results for the quadrupole suppression are presented.

The z_1 distribution exhibits a rather broad peak over most of its allowed values (recall that $0 < z_1 < 1$ by construction); still the peak is sufficiently well defined to sensibly consider the best fits

$$z_1 \simeq \begin{cases} 0.886 & (\text{WMAP3} + \text{smallscaleCMB} + \text{SDSS}) \\ 0.867 & (\text{WMAP5} + \text{SN} + \text{SDSS}) . \end{cases}$$

In particular for both dataset we find

$$z_1 < 0.95 \quad \text{with 95\% CL} .$$

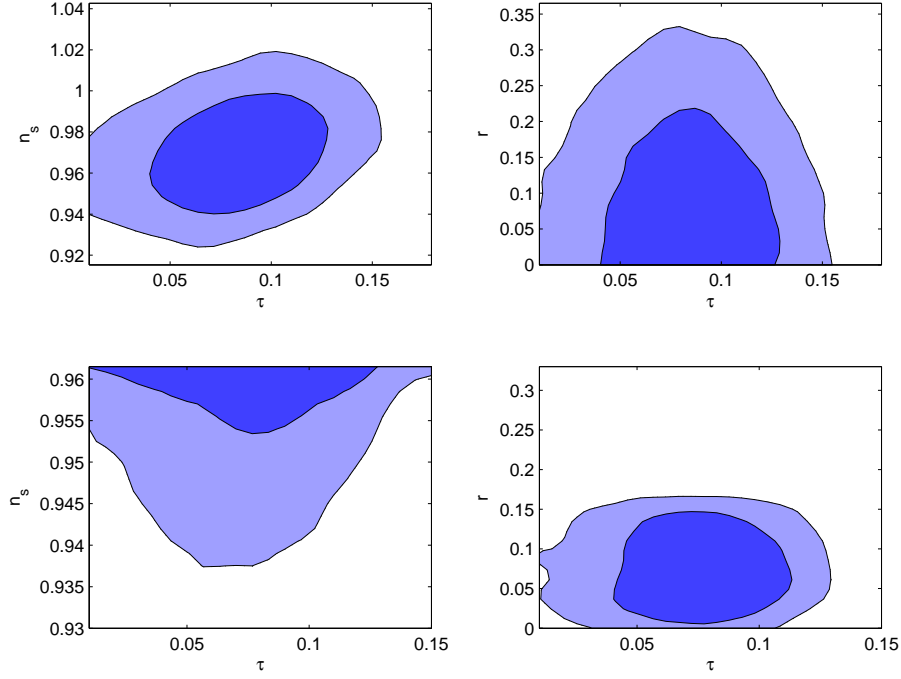


FIG. 19: Upper panels: 95% and 68% contour plots of joint probability (τ, n_s) distribution (left) and (τ, r) distribution (right) in the Λ CDM+ r model. Lower panels: the two joint distributions in the Λ CDM+TNI model. Recall that in this case there is the theoretical bound eq.(2.69) which gives $n_s < 0.9615 \dots$ for $N = 50$ and $n_s < 0.9679 \dots$ for $N = 60$.

thus excluding the $y \gg 1$ strong coupling region in which $z_1 \rightarrow 1$. This result can be read off directly from eq.(2.64) and fig. 14, since $y \gg 1$ implies a too small spectral index n_s . In the opposite limit $z_1 \rightarrow 0$ (that is, where one approaches the quadratic monomial potential at $y = 0$) the likelihood decreases because one gets a too large value for r with respect to the experimental data.

At $h = 0$ one can easily convert the results for z_1 into results for the coupling y of the TNI dimensionless potential eq.(2.50); we find the best fits

$$y \simeq \begin{cases} 1.28 & (\text{WMAP3} + \text{smallscaleCMB} + \text{SDSS}) \\ 1.15 & (\text{WMAP5} + \text{SN} + \text{SDSS}) . \end{cases} \quad (2.74)$$

and the bound (valid for both datasets)

$$y < 2.93 \quad \text{with 95\% CL}$$

after conversion to a flat prior distribution over y .

In conclusion, the most likely trinomial potentials for new inflation are almost symmetric (i. e. $h = 0$) and have moderate nonlinearity with the quartic coupling y of order 1 [eq.(2.74)]. Thus, we can take as inflaton potential the binomial eq.(2.13). The $\chi \rightarrow -\chi$ symmetry is here spontaneously broken since the absolute minimum of the potential is at $\chi \neq 0$.

3. MCMC results for Chaotic Trinomial Inflation.

Our results for the trinomial potential of chaotic inflation, eq.(2.26), are summarized in figs. 20, 21 and 22. In this case we report only MCMC results with the datasets WMAP3+small scale CMB+SDSS. The arguments we shall present below are actually not sensitive to the small changes in the likelihoods over the $n_s - r$ plane induced by the inclusion of more recent experimental data.

In fig. 20 we plot the marginalized probability distributions (normalized to have maximum equal to one) of the usual cosmological parameters as in fig. 15. Again, solid blue curves refer to the runs with the hard priors of chaotic

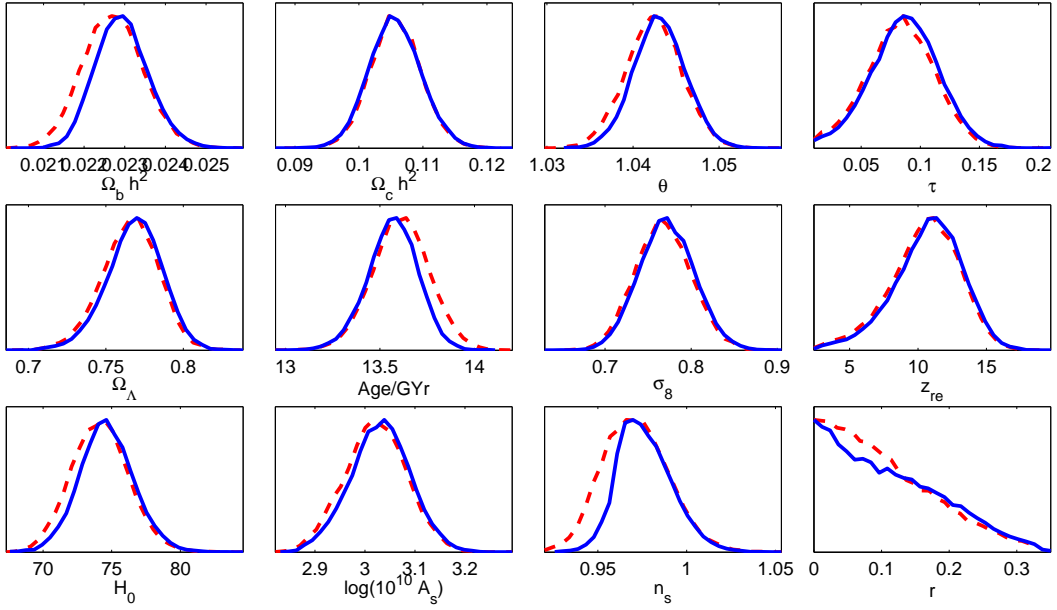


FIG. 20: Comparison of the marginalized probability distributions (normalized to have maximum equal to one) of the most relevant cosmological parameters (both primary and derived) between Λ CDM+TCI (Trinomial Chaotic Inflation, solid blue curves) and the Λ CDM+ r model (dashed red curves).

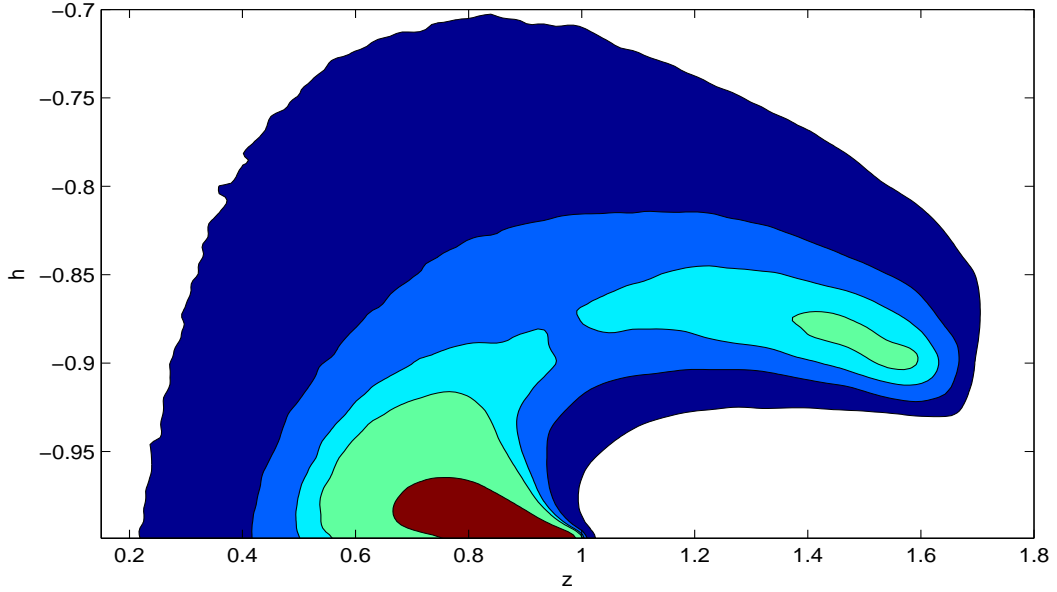


FIG. 21: Trinomial Chaotic Inflation. 12%, 27%, 45%, 68% and 95% confidence levels of the probability distribution in the field z - asymmetry h plane. The color of the areas goes from brown to dark blue for increasing CL. We see a strong preference of the data for a very asymmetric potential with $h < -0.95$ and a significant nonlinearity $0.7 < z < 1$ in chaotic inflation.

inflation, while the dashed red curves are those of the Λ CDM+ r model. As should have been expected from fig. 14, there are no really significant changes in any parameter.

In the upper panels of fig. 22 we plot the marginalized probabilities and the mean likelihoods for the parameters of the trinomial potential of chaotic inflation, the normalized coupling at horizon exit z , the quartic coupling y and the asymmetry h . These are numerically calculated from those of n_s and r (which are also reported in the lower panels of fig. 22), by means of eqs.(2.29), (2.31) and (2.46). The strong non-linearities of these relations are responsible for the peculiar shapes of the probabilities and mean likelihoods, and their marked relative differences, of the variables

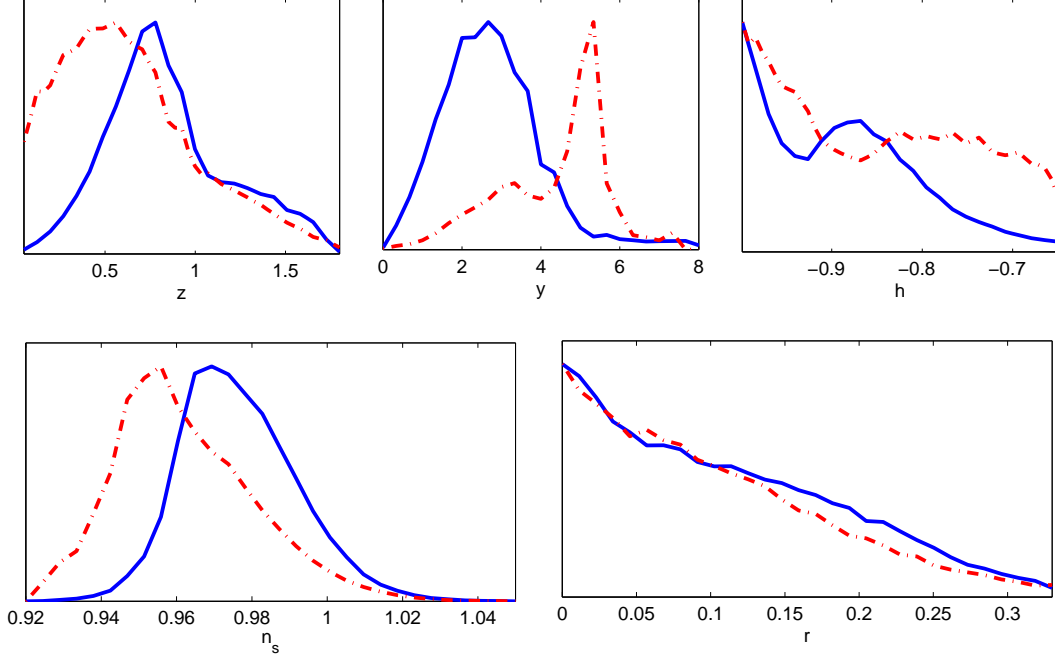


FIG. 22: Trinomial Chaotic Inflation. Upper panels: probability distributions (solid blue curves) and mean likelihoods (dot-dashed red curves), all normalized to have maximum equal to one, for the values of the normalized coupling at horizon exit z , of the quartic coupling y and of the asymmetry h of the potential. Lower panels: probabilities and mean likelihoods for the values of n_s and r . The data request a strongly asymmetric potential in chaotic inflation. That is, a strong breakdown of the $\chi \rightarrow -\chi$ symmetry.

in the upper panels.

Finally, in fig. 21 we depict the confidence levels at 12%, 27%, 45%, 68% and 95% in the (z, h) plane. The chaotic symmetric trinomial potential $h = 0$ is almost certainly **ruled out** since $h < -0.7$ at 95 % confidence level.

We see that the maximum probability is for strong asymmetry $h \lesssim -0.9$ and significant nonlinearity $0.5 \lesssim z \lesssim 1$ and $2.5 \lesssim y \lesssim 5$. That is, *all three* terms in the trinomial potential $w(\chi)$ *do contribute to the same order*.

Notice that the range $0.5 < z < 1$ corresponds for $h \rightarrow -1^+$ to the region where the quartic coupling is quite significant: $4.207 \dots < y < +\infty$ according to eq.(2.35).

Moreover, for these values of y and z , we have $\chi_{exit} \simeq 1.3$, $\varphi_{exit} \sim 10 M_{Pl}$ according to eq.(2.5). The coefficients G_n in the general inflaton potential $w(\chi)$ [eq.(1.95)] are of order unit and $\chi_{exit} \simeq 1.3$ is **larger** than unit for chaotic inflation. Therefore, higher order terms in $w(\chi)$ may affect the couplings obtained with quartic potentials in chaotic inflation.

The probability is maximum on a highly special and narrow corner in the (z, h) parameter space. This suggests:

- (i) the data force both the asymmetry as well as the coupling to be **large**.
- (ii) the fact that $z \sim 1$ implies large y means that we are in the nonlinear regime in z , that is $\chi_{exit} \simeq 1.3$ larger than unit. This suggests that higher order terms in χ may be added to $w(\chi)$ and will be relevant.
- (iii) If the preferred values are near the boundary of the parameter space, it could be that the true potential is **beyond** that boundary. The region of parameter space in which trinomial chaotic inflation yields $r \ll 1$ is very narrow and highly non-generic and corresponds to an inflaton potential contrary to the Landau-Ginsburg spirit [16] since adding higher degree terms in the field to the trinomial potential can produce relevant changes. This means that the fit for chaotic inflation can be unstable. The fit for new inflation is stable since for new inflation the maximum probability happens for a moderate nonlinearity and therefore will not be much affected by higher degree terms. Finally, the $r \rightarrow 0$ regime is obtained near the singular point $z = 1$, $h = -1$ where the inflaton potential vanishes for chaotic inflation.
- (iv) The MCMC runs appear to go towards the $h = -1$ limiting chaotic potential exhibiting an inflexion point (see fig. 12) which is at the boundary of the space of parameters. This may indicate that the true potential is **not** within the class of chaotic potentials. Since the runs go towards the maximal value of the asymmetry parameter

h where the inflaton potential exhibits an inflexion point, this supports the idea that the true potential **must** definitely break the $\chi \rightarrow -\chi$ symmetry, as new inflaton potentials do spontaneously. This **favours again** new inflation since the best fit to the trinomial new inflation potential corresponds to small or zero asymmetry parameter h . The spontaneous breakdown of the $\chi \rightarrow -\chi$ symmetry seems sufficient to obtain the best fit to the data without the presence of any explicit symmetry breaking term $\frac{h}{3} \sqrt{\frac{2}{3}} \chi^3$ [see eq.(2.50)].

E. Higher degree terms in inflaton potentials

In this section we study the dependence of the observables (n_s , r and $dn_s/d \ln k$) on the degree of the inflaton potential ($2n$) for new and chaotic inflation and confront them to the WMAP data [18]. This study shows in general that fourth degree potentials ($n = 2$) provide the best fit to the data [18]. We find that new inflation fits the data on an appreciable wider range of the parameters while chaotic inflation does this in a much narrow range. Therefore, amongst the families of inflationary models studied, new inflation emerges again as a leading contender in comparison with chaotic inflation. This analysis confirms the statement that within the framework of effective field theories with polynomial potentials, new inflation is a preferred model reproducing the present data [12, 13, 14].

The main results presented in this section are [18]:

- The region in inflaton field space which is consistent with the marginalized WMAP3 data can be explored in an expansion in $n_s - 1 + 2/N$.
- We find that the point $n_s = 1 - 2/N = 0.96$, $r = 8/N = 0.16$ which is in the region allowed by the WMAP3 analysis belongs both to new inflation models as a limiting point and to the simple chaotic inflation monomial, $m^2 \varphi^2/2$. This point describes a region in field and parameter space that separates small fields from large fields, and is a degeneracy point for the family of models describing both chaotic and new inflation.
- For all members $n = 2, 3, 4, \dots$ of the new inflation family, the small field region yields $r < 0.16$ while the large field region yields $r > 0.16$. All members of the new inflation family predict a small but negative running:

$$-4(n+1) \times 10^{-4} \leq dn_s/d \ln k \leq -2 \times 10^{-4}.$$

This new inflation family features a *large window* of consistency with the WMAP and LSS data for $n = 2$ that narrows for growing n . If forthcoming data on tensor modes pinpoints the tensor to scalar ratio to be $r < 0.1$, we predict that the *symmetry breaking scale* for these models is $\varphi_{min} \sim 20 M_{Pl}$ and that the scale of the field at which modes of cosmological relevance today cross the Hubble radius is $\varphi_{exit} \sim 6 M_{Pl}$.

- Chaotic inflationary models all yield a tensor to scalar ratio $r \geq 0.16$, where the minimum value $r = 0.16$ corresponds to small amplitude of the inflaton and coincides with the value obtained from the monomial $m^2 \varphi^2/2$. The combined marginalized data from WMAP3 yields a very small window of field amplitude, around $|\varphi_{exit}| \sim 15 M_{Pl}$ within which chaotic models are allowed by the data. These regions become progressively smaller for larger n . Some small regions in field space feature peaks in the running of the scalar index but in most of the region consistent with the WMAP3 data the running is again negligible ($\sim 10^{-3}$). If future observations determine a tensor to scalar ratio $r < 0.16$, this by itself will **rule out** a large family of chaotic inflationary models.

The precise value of N is certainly near $N = 60$ as discussed in sec. ID4. We will take in this section the value $N = 50$ as a reference baseline value for numerical analysis, but from the explicit expressions given below, it becomes a simple rescaling to obtain results for arbitrary values of N [see eq.(2.75) below]. That is, we use the leading value in the $1/N$ expansion eqs.(1.163), (1.169) and (1.171) to obtain their values for arbitrary N , namely

$$r[N] = r[50] \frac{50}{N}, \quad n_s[N] = n_s[50] + (1 - n_s[50]) \frac{N - 50}{N}, \quad \frac{dn_s}{d \ln k}[N] = \frac{dn_s}{d \ln k}[50] \left(\frac{50}{N} \right)^2. \quad (2.75)$$

The combination of WMAP and SDSS (LRG) data yields [9]

$$n_s = 0.958 \pm 0.016 \quad (\text{assuming } r = 0 \text{ with no running}) \quad (2.76)$$

$$r < 0.28 \text{ (95\% CL) no running}, \quad r < 0.67 \text{ (95\% CL) with running}. \quad (2.77)$$

The running must be very small and of the order $\mathcal{O}(1/N^2) \sim 10^{-3}$ according to eq.(1.171). Therefore, we can safely consider $dn_s/d \ln k = 0$ in our analysis. Figure 14 in the first reference under [9] and figure 14 here show that the

preferred value of n_s slowly grows with the preferred value of r for $r > 0$. We find approximately that

$$\frac{\Delta n_s}{\Delta r} \simeq 0.12 \quad (2.78)$$

Therefore, for $r \sim 0.1$ the central value of n_s shifts from $n_s = 0.958$ ($r = 0$) to $n_s = 0.97$ ($r = 0.1$) as can be readily gleaned from both quoted figures.

As a simple example that provides a guide post for comparison let us consider first the monomial potential

$$V(\varphi) = \frac{\lambda}{2n} \varphi^{2n}. \quad (2.79)$$

The case $n = 1$ yields a satisfactory fit to the WMAP data [8, 9, 10]. For these potentials it follows that,

$$w(\chi) = \frac{\chi^{2n}}{2n} \quad ; \quad M^4 = \lambda N^{n-1} M_{Pl}^{2n} \quad (2.80)$$

Inflation ends at $\chi_{end} = 0$, and the value of the dimensionless field χ at N efolds before the end of inflation is

$$|\chi| = 2 \sqrt{n}. \quad (2.81)$$

These results lead to

$$n_s - 1 = -\frac{n+1}{N} \quad , \quad r = \frac{8n}{N} \quad , \quad \frac{dn_s}{d \ln k} = -\frac{n+1}{N^2}. \quad (2.82)$$

Taking $N = 50$ as a baseline, these yield

$$n_s - 1 = -2(n+1) \times 10^{-2} \left(\frac{50}{N}\right) \quad , \quad r = 0.16 n \left(\frac{50}{N}\right) \quad , \quad \frac{dn_s}{d \ln k} = -4(n+1) \times 10^{-4} \left(\frac{50}{N}\right)^2. \quad (2.83)$$

1. Family of models

We study now the CMB observables n_s , r , $dn_s/d \ln k$ for families of new inflation and chaotic models determined by the following inflationary potentials:

$$V(\varphi) = V_0 - \frac{1}{2} m^2 \varphi^2 + \frac{\lambda}{2n} \varphi^{2n} \quad , \quad \text{broken symmetry} \quad (2.84)$$

$$V(\varphi) = \frac{1}{2} m^2 \varphi^2 + \frac{\lambda}{2n} \varphi^{2n} \quad , \quad \text{unbroken symmetry} . \quad (2.85)$$

Upon introducing the rescaled field χ given by eq.(1.84), the family of rescaled potentials is

$$w(\chi) = w_0 - \frac{1}{2} \chi^2 + \frac{g}{2n} \chi^{2n} \quad , \quad \text{broken symmetry} \quad (2.86)$$

$$w(\chi) = \frac{1}{2} \chi^2 + \frac{g}{2n} \chi^{2n} \quad , \quad \text{unbroken symmetry} . \quad (2.87)$$

w_0 and g are dimensionless and related to V_0 and λ by [compare with eq.(1.96)],

$$V_0 = w_0 N M^4 \quad , \quad \lambda = \frac{M^4 g}{M_{Pl}^{2n} N^{n-1}} . \quad (2.88)$$

New inflation models described by the dimensionless potential given by eq.(2.86) feature a minimum at χ_{min} which must obey the conditions eq.(1.91). These conditions yield,

$$g = \chi_{min}^{2-2n} \quad , \quad w_0 = \frac{\chi_{min}^2}{2n} (n-1) , \quad (2.89)$$

χ_{min} determines the scale of symmetry breaking φ_{min} of the inflaton potential upon the rescaling eq.(1.84), namely $\varphi_{min} = \sqrt{N} M_{Pl} \chi_{min}$. It is convenient to introduce the dimensionless variable

$$x = \frac{\chi}{\chi_{min}} \quad (2.90)$$

Thus, the minimum of the potential is at $x = 1$ and the family of inflation models eq.(2.86)-(2.87) take the form

$$w(\chi) = \frac{\chi_{min}^2}{2n} [n(1 - x^2) + x^{2n} - 1] \quad , \quad \text{broken symmetry} \quad , \quad (2.91)$$

$$w(\chi) = \frac{\chi_{min}^2}{2n} [n x^2 + x^{2n}] \quad , \quad \text{unbroken symmetry} \quad . \quad (2.92)$$

In terms of the variable x , the small and large field regions for the potential eq.(2.91) correspond to $x < 1$ and $x > 1$, respectively.

2. Broken Symmetry models.

Inflation ends when the inflaton field arrives to the minimum of the potential. For the new inflation family of models eq.(2.91) inflation ends for

$$\chi_{end} = \chi_{min} \quad . \quad (2.93)$$

In terms of the dimensionless variable x , the condition eq.(1.90) becomes

$$\frac{2n}{\chi_{min}^2} = I_n(X) \quad , \quad X = \frac{\chi_{exit}}{\chi_{min}} \quad , \quad (2.94)$$

where χ_{exit} is the inflaton field at horizon exit and

$$I_n(X) \equiv \int_X^1 \frac{dx}{x} \frac{n(1 - x^2) + x^{2n} - 1}{1 - x^{2n-2}} = \int_X^1 \frac{n - \sum_{m=0}^{n-1} x^{2m}}{\sum_{m=0}^{n-2} x^{2m}} \frac{dx}{x} \quad . \quad (2.95)$$

This integral can be computed in closed form as a finite sum of elementary functions [90].

For a fixed given value of X , χ_{min} and therefore the dimensionless coupling g are determined by the equation (2.94). Once we obtain this value, the CMB observables eqs.(1.163), (1.169) and (1.171) are obtained by evaluating the derivatives of $w(\chi)$ at the value $\chi_{exit} = \chi_{min} X$ with the corresponding value of the coupling g . Thus, a study of the range of possible values for n_s , r , $dn_s/d \ln k$ is carried out by exploring the relationship between these spectral indices as a function of X . For this study we choose the baseline value $N = 50$ from which the indices can be obtained for arbitrary value of N by the relation (2.75).

While the dependence of χ_{min} and g upon the variable X must in general be studied numerically, their behavior in the relevant limits, $X \rightarrow (0, 1)$ for small field inflation and $X \gg 1$ for large field inflation can be derived from eqs.(2.94)-(2.95).

For small field inflation and $X \rightarrow 0$, the lower limit of the integral dominates leading to

$$\chi_{min}^2 \stackrel{X \rightarrow 0}{\simeq} \frac{2n}{n-1} \frac{1}{\log \frac{1}{X}} \quad , \quad g \stackrel{X \rightarrow 0}{\simeq} \left(\frac{n-1}{2n} \log \frac{1}{X} \right)^{n-1} \quad , \quad (2.96)$$

thus, as $X \rightarrow 0$ these are *strongly coupled* models. This result has a clear and simple interpretation: for $N = 50$ to be the number of efolds between $x = X$ and $x = 1$ the coupling g must be large and the potential must be steep, otherwise there would be many more efolds in such interval.

For small field inflation and $X \rightarrow 1^-$ the integral $I_n(X)$ obviously vanishes and

$$\chi_{min}^2 \stackrel{X \rightarrow 1^-}{\simeq} \left(\frac{2}{1-X} \right)^2 \left[1 + \frac{2n-1}{9} (X-1) + \mathcal{O}(X-1)^2 \right] \quad , \quad g \stackrel{X \rightarrow 1^-}{\simeq} \left[\frac{1}{2} (1-X) \right]^{2(n-1)} \rightarrow 0 \quad , \quad (2.97)$$

thus, as $X \rightarrow 1^-$, these are a *weakly coupled family of models*.

For large field inflation and $X \gg 1$, the integral $I_n(X)$ is dominated by the term with the highest power, namely x^{2n} , leading to the behavior

$$\chi_{min}^2 \stackrel{X \gg 1}{\simeq} \frac{4n}{X^2} \quad , \quad g \stackrel{X \gg 1}{\simeq} \left(\frac{X^2}{4n} \right)^{n-1} \quad , \quad (2.98)$$

which leads to a strongly coupled regime.

Interesting and relevant information can be extracted by focusing on the region $X \sim 1$ which as discussed above corresponds to a weakly coupled family for broken symmetry potentials. This is the region near the *minimum* of the potential and the integral $I_n(X)$ can be evaluated simply by expanding $w(\chi)$ and its derivative near the minimum. To leading order in $(X - 1)$ the condition eq.(2.94) leads to eq.(2.97) and

$$(\chi_c - \chi_{min})^2 = 4 \quad \text{or} \quad |\chi_c - \chi_{min}| = 2. \quad (2.99)$$

This is precisely eq.(2.81) for $n = 1$ upon the shift $\chi_c \rightarrow \chi_c - \chi_{min}$. Namely, eq.(2.99) is the condition eq.(2.81) for the quadratic monomial potential with minimum at $\chi = \chi_{min}$ instead of $\chi = 0$ as in eq.(2.80). This is clearly a consequence of the fact that near the minimum $X = 1$ the potential is quadratic, therefore for $X \sim 1$ the quadratic monomial is an excellent approximation to the family of higher degree potentials and more so because $g \sim 0$. For $X \sim 1$ we find to leading order in $(X - 1)$ the values:

$$n_s = 0.96 + 0.04 \left(\frac{N - 50}{N} \right), \quad r = 0.16 \left(\frac{50}{N} \right), \quad \frac{dn_s}{d \ln k} = -0.0008 \left(\frac{50}{N} \right)^2. \quad (2.100)$$

The fact that the potential eq.(2.91) is quadratic around the minimum $X = 1$ explains why we have in this limit identical results for new inflation with the potential eq.(2.91) and chaotic inflation with the monomial potential $m^2 \phi^2/2$.

The values eq.(2.100) of r , n_s for $N \sim 50$ yield a good fit to the available CMB data.

The value $X \sim 0.2$ determines the *minimum value* of X for which n_s is consistent with the WMAP data for $r = 0$ (see figs. 23 and 24). For large values of X , n_s approaches asymptotically the values for the monomial potentials ϕ^{2n} given by eq.(2.83). For the larger degrees n , the asymptotic behavior of n_s and r settles at larger values of X , which is a consequence of the larger region in which the coupling is small for larger degrees n .

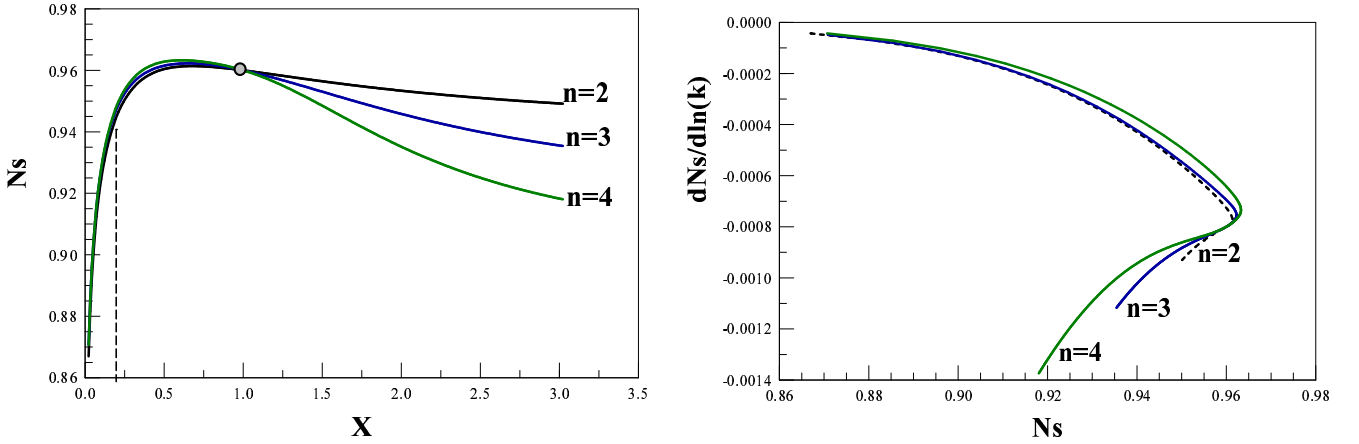


FIG. 23: Left panel: Scalar spectral index n_s for the degrees of the potential $n = 2, 3, 4$ for new inflation with $N = 50$. The vertical line delimits the smallest value of n_s (for $r = 0$) [9, 10]. The grey dot at $n_s = 0.96$, $X = 1$ corresponds to the value for the monomial potential $n = 1$, $m^2 \phi^2/2$. Notice that the small field behavior is n independent. For arbitrary N the result follows directly from the $N = 50$ value by using eq.(2.75). Right panel: Running of the scalar index $dn_s/d \ln k$ vs. n_s for degrees of the potential $n = 2, 3, 4$ respectively for new inflation with $N = 50$. The values for arbitrary N follow directly from the $N = 50$ value by using eq.(2.75).

Unlike the case of a pure monomial potential $\lambda \phi^{2n}$ with $n \geq 2$, there is a **large** region of field space within which the new inflation models given by eq.(2.84) are **consistent** with the bounds from marginalized WMAP3 data and the combined WMAP3 + LSS data [9].

Fig. 24 displays r vs n_s for the values $n = 2, 3, 4$ in new inflation and indicate the trend with n . While r is a monotonically increasing function of X , n_s features a *maximum* as a function of X , hence r becomes a **double-valued** function of n_s . The grey dot at $r = 0.16$, $n_s = 0.96$ corresponds to the monomial potential $m^2 \phi^2/2$ for $N = 50$. Values below the grey dot along the curve in fig. 24 correspond to small fields $X < 1$ while values above it correspond to large fields $X > 1$. We see that *large fields systematically lead to larger values of r* . Models that fit the WMAP data to 95% *CL* are within the tilted box in fig. 24. The tilt accounts for the growth of the preferred value of n_s with r [9] according to eq.(2.78).

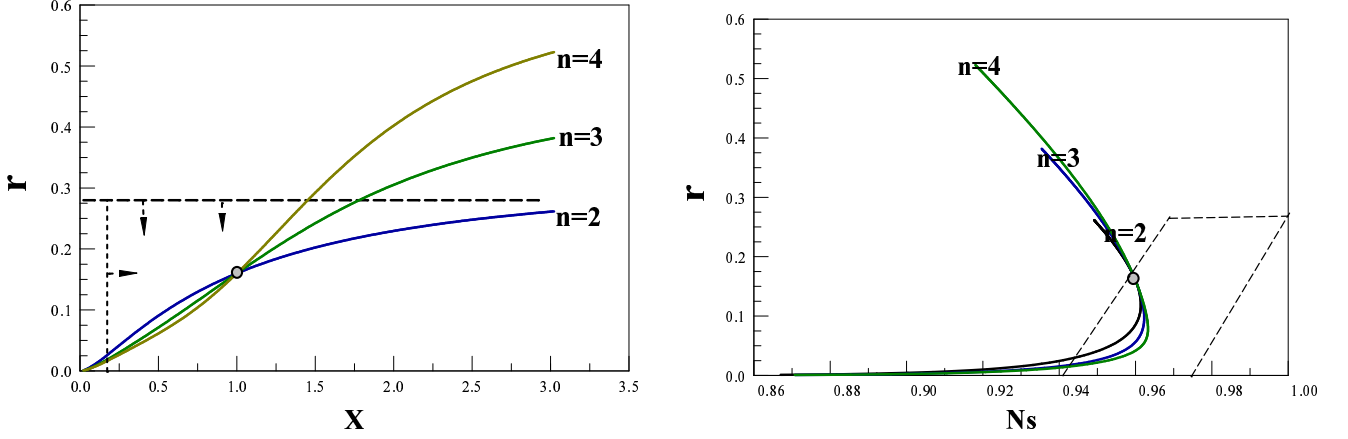


FIG. 24: Left panel: Tensor to scalar ratio r vs. X for the degrees of the potential $n = 2, 3, 4$ for new inflation with $N = 50$. The horizontal dashed line corresponds to the upper limit $r = 0.28$ (95%CL) from WMAP3 without running. The vertical dashed line determines the minimum value of X , $X \sim 0.2$, consistent with the WMAP limits for n_s as in fig. 23. The grey dot at $X = 1$, $r = 0.16$ corresponds to the value for the monomial potential $m^2 \phi^2/2$. The small field limit is nearly independent of n . For arbitrary N the result follows directly from the $N = 50$ value by using eq.(2.75). Right panel: Tensor to scalar ratio r vs. n_s for degrees of the potential $n = 2, 3, 4$ respectively for new inflation with $N = 50$. r turns to be a **double-valued** function of n_s exhibiting a maximum value for n_s . The values inside the box between the dashed lines correspond to the WMAP3 marginalized region of the (n_s, r) plane with (95%CL) : $r < 0.28$, $0.942 + 0.12 r \leq n_s \leq 0.974 + 0.12 r$, see eq.(2.78). The grey dot corresponds to the values for the monomial potential $m^2 \phi^2/2$ and the value $X = 1$: $r = 0.16$, $n_s = 0.96$.

Fig. 23 displays the running of the scalar index vs. n_s for the different members of the family of new inflation showing clearly that running is all but negligible in the entire range of values consistent with the WMAP data. This was expected since the running in slow-roll is of the order $\sim \frac{1}{N^2} \simeq 4 \times 10^{-4}$ [see eq.(1.171)] [11].

We note that $dn_s/d \ln k$ is a monotonically *decreasing* function of X approaching asymptotically the values for the monomials ϕ^{2n} given by eq.(2.83).

3. Field reconstruction for new inflation

The above analysis suggests to study the *inverse problem*, namely, for a given member of the family labeled by n , we may ask what is the value φ_{exit} of the field at Hubble crossing and what is the scale φ_0 of symmetry breaking of the potential which are consistent with the CMB+LSS data. This is tantamount to the program of reconstruction of the inflaton potential advocated in ref.[5] and is achieved as follows: eq.(2.94) yields $\chi_{min} = \chi_{min}[X]$ from which we obtain $\chi_{exit} = \chi_{min} X$. These results are then input into the expression for n_s by evaluating the potential $w(\chi)$ and its derivatives at the value of χ_{exit} . This yields $n_s = n_s[\chi_{exit}]$ which is then inverted to obtain $\chi_{exit} = \chi_{exit}[n_s]$ and thus φ_{exit} .

In the region $X \sim 1$ corresponding to the weakly coupled case, this reconstruction program can be carried out as a systematic series in

$$\Delta_X \equiv X - 1 = \frac{\chi_{exit}}{\chi_{min}} - 1, \quad (2.101)$$

by expanding the inflationary potential and its derivatives in a power series in x around $x = 1$ in the integrand of $I_n(X)$ [eq. (2.95)]. For $X = 1$ the value of the scalar index n_s is determined by the simple monomial $m^2 \phi^2/2$ from eq. (2.82) for $n = 1$ is given by $n_s - 1 = -2/N$. Therefore, in terms of n_s , the actual expansion parameter is $n_s - 1 + 2/N$.

We obtain n_s to first order in Δ_X from eqs.(1.163), (2.91), (2.97) and (2.101) with the result,

$$n_s - 1 = -\frac{2}{N} \left[1 + \frac{2n-1}{18} \Delta_X + \mathcal{O}(\Delta_X^2) \right]$$

then, by inverting this equation we find:

$$\Delta_X(n_s, n) = X - 1 = -\frac{9N}{2n-1} \left(n_s - 1 + \frac{2}{N} \right) + \mathcal{O} \left(\left[n_s - 1 + \frac{2}{N} \right]^2 \right), \quad (2.102)$$

and from eqs.(2.97) and (2.102) we find,

$$\chi_{min}(n_s, n) = \frac{2(2n-1)}{9N|n_s-1+\frac{2}{N}|} \left[1 - \frac{N}{2} \left(n_s - 1 + \frac{2}{N} \right) \right] + \mathcal{O} \left(\left[n_s - 1 + \frac{2}{N} \right] \right) \quad (2.103)$$

The leading order ($\propto 1/\Delta_X$) of this result for $\chi_{min}(n_s, n)$ can be simply cast as eq.(2.99): this is recognized as the condition to have 50 efolds for the quadratic monomial centered in the broken symmetry minimum [see discussion below eq.(2.99)].

Finally, the value of the (dimensionless) field χ_{exit} at Hubble crossing is determined from $\chi_{exit}(n_s, n) = \chi_{min} [1 + \Delta_X(n_s, n)]$ from which we obtain

$$\chi_{exit} = \frac{2(2n-1)}{9N|n_s-1+\frac{2}{N}|} \left[1 - \frac{(2n+17)N}{2(2n-1)} \left(n_s - 1 + \frac{2}{N} \right) \right] + \mathcal{O} \left(\left[n_s - 1 + \frac{2}{N} \right] \right). \quad (2.104)$$

The coupling constant g can be also expressed in terms of n_s in this regime with the result,

$$g = \left[\frac{9N|n_s-1+\frac{2}{N}|}{2(2n-1)} \right]^{2n-2} \rightarrow 0,$$

which exhibits the weak coupling character of this limit.

This analysis shows that the region in field space that corresponds to the region in n_s that *best fits the WMAP data* can be systematically reconstructed in an expansion in $n_s - 1 + 2/N$. This is yet another bonus of the $1/N$ expansion. Although the above analysis can be carried out to an arbitrary order in $n_s - 1 + 2/N$, it is more convenient to perform a numerical study of the region outside from $X \sim 1$ to find the values of χ_{exit} and χ_{min} as a function of n_s for fixed values of n , N .

Finally, the values for the dimensionful field φ are given by $\varphi_{exit} = \sqrt{N} M_{Pl} \chi_{exit}$, $\varphi_{min} = \sqrt{N} M_{Pl} \chi_{min}$. For the range of CMB parameters $r < 0.1$ and $n_s \leq 0.96$, the typical value of the *symmetry breaking scale* is $\varphi_{min} \sim 20 M_{Pl}$ and the value of the inflaton field at which cosmologically relevant wavelengths crossed the Hubble radius during new inflation is $\varphi_{exit} \sim 6 M_{Pl}$ with a weak dependence on n . For $0.1 < r < 0.16$ we have $|\varphi_{exit} - \varphi_{min}| \sim 15 M_{Pl}$.

We obtain for the coupling g in the $X \rightarrow 0$ limit which is a strong coupling regime [see eq.(2.96)] where $n_s \ll 1$,

$$g = \left[\frac{N}{4} \left(1 - \frac{1}{n} \right) (1 - n_s) \right]^{n-1}.$$

Finally, we have the $X \rightarrow \infty$ limit which is also a strong coupling limit [see eq.(2.98)] where $n_s \rightarrow 1 - (n+1)/N$ and we find,

$$\begin{aligned} \chi_{min}^2 &= (4n)^2 \left[\frac{N(1-n_s) - (n+1)}{4n(n-1) + 3 \left(1 + \frac{1}{n-2} \right)} \right]^{\frac{1}{n-1}} \rightarrow 0 \\ g &= \frac{4n(n-1) + 3 \left(1 + \frac{1}{n-2} \right)}{(4n)^{n-1} [N(1-n_s) - (n+1)]} \rightarrow \infty. \end{aligned} \quad (2.105)$$

4. Chaotic inflation models.

We now turn to the study of the family of chaotic inflationary potentials given by eq.(2.92). Taking that the end of inflation corresponds to $x = 0$, the condition eq.(1.90) now becomes

$$\frac{2n}{\chi_{min}^2} = J_n(X) = \int_0^X \frac{n + x^{2n-2}}{1 + x^{2n-2}} x \, dx. \quad (2.106)$$

Again, this integral can be computed in closed form as a sum of elementary functions [90]. For general values of X the integral will be studied numerically, but the small X region can be studied by expanding the integrand in powers of x^{2n-2} , with the result

$$1 = \frac{\chi_{min}^2 X^2}{4} \left[1 - \frac{n-1}{n^2} X^{2n-2} + \mathcal{O}(X^{4n-4}) \right]. \quad (2.107)$$

For small X and recalling that $X = \chi_{exit}/\chi_{min}$ this relation yields

$$|\chi_{exit}| = 2 \left[1 + \frac{n-1}{2n^2} X^{2n-2} + \mathcal{O}(X^{4n-4}) \right] \quad (2.108)$$

which is again, at dominant order the relation for the quadratic monomial potential eq.(2.81) for $n = 1$. This must be the case because the small field limit is dominated by the quadratic term in the potential. For small fields, $\chi_{min} \approx 2/X$ and the coupling g vanishes as,

$$g(X) \stackrel{X \rightarrow 0}{\rightarrow} \left(\frac{X}{2} \right)^{2n-2}. \quad (2.109)$$

The dependence of n_s and r in the full range of X for several representative values of n is studied numerically. In the small X regime, we obtain from eqs.(1.163), (1.169), (2.92) and (2.107) the expressions,

$$n_s - 1 = -\frac{2}{N} \left[1 - \frac{(2n-1)(n-1)(n-2)}{2n^2} X^{2n-2} + \mathcal{O}(X^{4n-4}) \right] \quad (2.110)$$

$$r = \frac{8}{N} \left[1 + \frac{(2n-1)(n-1)}{n^2} X^{2n-2} + \mathcal{O}(X^{4n-4}) \right] \quad (2.111)$$

As $X \rightarrow 0$, n_s and r tend to the result from the quadratic monomial potential, namely $n_s - 1 = -2/N$, $r = 8/N$ as must be the case because the quadratic term dominates the potential for $X \ll 1$.

For $X \rightarrow 0$ and $N = 50$, $n_s \rightarrow 0.96$ and $r \rightarrow 0.16$ which are the values from the quadratic monomial potential $m^2 \varphi^2/2$.

For $X \gg 1$, the values of n_s , r for the monomial potentials φ^{2n} are attained asymptotically, namely, (for $N = 50$): $n_s - 1 = -2(n+1) \times 10^{-2}$, $r = 0.16n$.

The range in which the chaotic family provides a good fit to the WMAP data is *very much smaller* than for new inflation. In chaotic inflation *only* for $n = 2$ the range of n_s is allowed by the WMAP data in a fairly extensive range of values of X , whereas for $n = 3, 4$ (and certainly larger), there is a *relatively small* window in field space for $X < 1$ which satisfies the data for n_s and r simultaneously.

The tensor to scalar ratio r in chaotic inflationary models is *larger* than 0.16 for all values of X , approaching asymptotically for large X the value $r = 0.16n$ associated to the monomial potentials φ^{2n} .

While the running $dn_s/d \ln k$ is again negligible, it is *strikingly different* from the new inflation case. *Again* this study, in combination with those for n_s and r as functions of X distinctly shows that **only** $n = 2$ in chaotic inflation is compatible with the bounds from the WMAP data, while for $n = 3, 4$ only a *small window* for $X < 1$ is allowed by the data. $dn_s/d \ln k$ takes negative as well as positive values for chaotic inflation, in contrast with new inflation where $dn_s/d \ln k$ is always < 0 .

The fact that the combined bounds on n_s , r and $dn_s/d \ln k$ from the WMAP3 data [9] provide much more stringent constraints on chaotic models is best captured by displaying r as a function of n_s in fig. 25. The region allowed by the WMAP data lies within the tilted box delimited by the vertical and horizontal dashed lines that represent the 95%CL band [9].

A complementary assessment of the allowed region for this family of effective field theories is shown in fig. 25 which distinctly shows that **only** the $n = 2$ case of chaotic inflation is allowed by the WMAP3 data.

5. Field reconstruction for chaotic inflation

The reconstruction program proceeds in the same manner as in the case of new inflation: the first step is to obtain $\chi_{min}(X)$ from eq.(2.106). Then ϵ_v and η_v are obtained as a function of X which yields $n_s(X)$. Inverting this relation we find $X = X(n_s)$ and finally $\chi_{exit}(n_s) = \chi_{min} X(n_s)$. While this program must be carried out numerically, we can gain important insight by focusing on the small X region and using eq.(2.107).

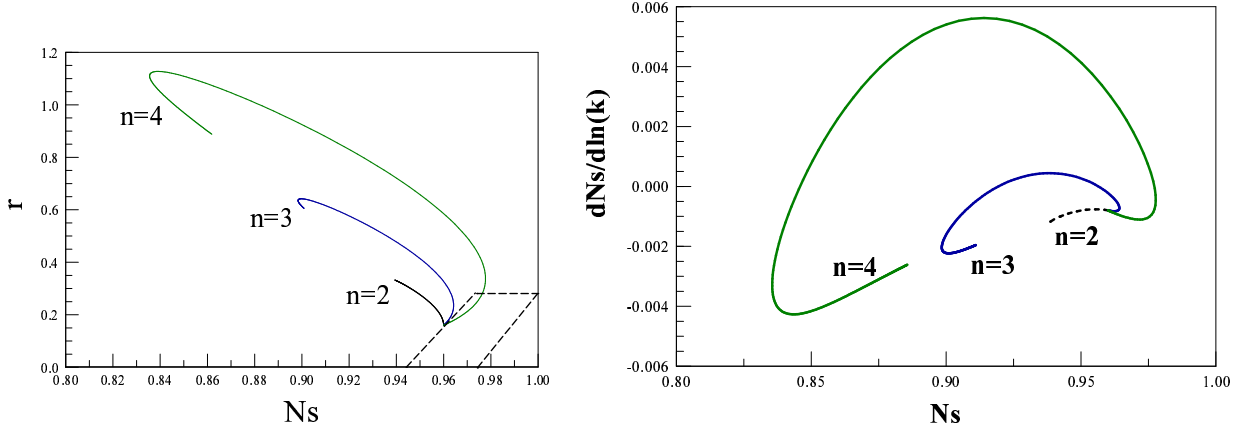


FIG. 25: Left panel: Tensor to scalar ratio r vs. n_s for degrees of the potential $n = 2, 3, 4$ respectively for chaotic inflation with $N = 50$. The range of 95% CL as determined by WMAP3 [9] is within the tilted box delimited by : $r < 0.28$, $0.942 + 0.12 r \leq n_s \leq 0.974 + 0.12 r$, see eq.(2.78). Right panel: Running of the scalar index $dn_s/d\ln k$ vs. n_s for degrees of the potential $n = 2, 3, 4$ respectively for chaotic inflation with $N = 50$.

From eqs.(1.163), (2.110) and (2.111) we find

$$n_s - 1 + \frac{2}{N} = X^{2n-2} \frac{(2n-1)(n-1)(n-2)}{n^2 N} + \mathcal{O}(X^{4n-4}) \quad (2.112)$$

As $X \rightarrow 0$ it follows that $n_s \rightarrow 1 - 2/N$ which is the value for the scalar index for the quadratic monomial potential $m^2\varphi^2/2$. However, for $n > 2$ this limit is approached from above, namely for $n > 2$ it follows that $n_s > 1 - 2/N$. The small X region corresponds to small departures of n_s from the value determined by the quadratic monomial $1 - 2/N$ but always larger than this value for $n > 2$. In the small field limit we reconstruct the value of χ_{exit} in an expansion in $n_s - 1 + 2/N$. The leading order in this expansion is obtained by combining eqs.(2.108) and (2.112), we obtain

$$|\chi_{exit}| = 2 \left[1 + \frac{(n_s - 1 + \frac{2}{N})N}{2(2n-1)(n-2)} \right] + \mathcal{O}([n_s - 1 + 2/N]^2) \quad (2.113)$$

Obviously, this leading order term is singular at $n = 2$, this is a consequence of the result eq.(2.112) which entails that for $n = 2$ the expansion must be pursued to higher order, up to X^{4n-4} .

We find from eqs.(1.163), (2.110) and (2.111) for $n = 2$,

$$n_s - 1 + \frac{2}{N} = -\frac{17}{24N} X^4 + \mathcal{O}(X^6) \quad , \quad n = 2 \quad , \quad (2.114)$$

therefore,

$$|\chi_{exit}| = 2 \left[1 + \sqrt{\frac{3N}{136} \left(1 - \frac{2}{N} - n_s \right)} \right] + \mathcal{O} \left(n_s - 1 + \frac{2}{N} \right) \quad , \quad n = 2 \quad . \quad (2.115)$$

We see that the derivative of χ_{exit} with respect to n_s is singular for $n = 2$ at $n_s = 1 - 2/N$. We note that for $n = 2$ there is a sign change with respect to the cases $n > 2$ and $n_s - 1 + 2/N \leq 0$ as determined by eq.(2.114).

It is clear that there is a small window in field space within which chaotic models provide a good fit to the WMAP3 data, for $N = 50$ we find:

$$\begin{aligned} n = 2 & : \quad 0.95 \lesssim n_s \leq 0.960 \quad , \quad 2.0 \leq |\chi_{exit}| \lesssim 2.25 \\ n = 3 & : \quad 0.96 \leq n_s \lesssim 0.965 \quad , \quad 2.0 \leq |\chi_{exit}| \lesssim 2.15 \\ n = 4 & : \quad 0.96 \leq n_s \leq 0.975 \quad , \quad 2.0 \leq |\chi_{exit}| \lesssim 2.10 \quad . \end{aligned} \quad (2.116)$$

Restoring the dimensions via eq.(1.84) these values translate into a narrow region of width $\Delta_X \varphi \lesssim 1.5 M_{Pl}$ around the scale $|\varphi_{exit}| \sim 15 M_{Pl}$.

Therefore, the joint analysis for n_s , r , $dn_s/d\ln k$ distinctly reveals that: (i) chaotic models favor *larger* values of r thus, larger tensor amplitudes, and (ii) chaotic models feature *smaller* regions in field space consistent with the CMB and large scale structure data. *Only* the case $n = 2$ features a larger region of consistency with the combined WMAP3 data.

6. Conclusions

We perform a systematic study of *families* of single field new and chaotic inflation slow-roll models characterized by effective field theories with potentials of the form [18]

$$V(\varphi) = V_0 - \frac{1}{2} m^2 \varphi^2 + \frac{\lambda}{2n} \varphi^{2n} \quad , \quad \text{broken symmetry} \quad (2.117)$$

$$V(\varphi) = \frac{1}{2} m^2 \varphi^2 + \frac{\lambda}{2n} \varphi^{2n} \quad , \quad \text{unbroken symmetry} \quad (2.118)$$

Unlike the approach followed in [8, 9] based on the inflationary flow equations [54], or more recent studies which focused on specific inflationary models [56], or on statistical analysis of models [54], we implement an expansion in $1/N$ where $N \sim 50$ is the number of efolds before the end of inflation when wavelengths of cosmological relevance today cross the Hubble radius during inflation. We provide in ref.[18] an analysis of the dependence of CMB observables (n_s , r and $dn_s/d\ln k$) with the degree n of the potential and establish the region in field space within which these families provide a good agreement with the WMAP3 data combined with large scale surveys.

For new inflation models with potentials eq.(2.117) there are two distinct regions corresponding to values of the inflaton field smaller (small field) or larger (large field) than the symmetry breaking scale. For this family we find a **wide range** in the (n_s, r) plane in which the different members $n = 2, 3, 4, \dots$ are allowed by the data both for small and large fields with negligible running of the scalar index [18]:

$$-4(n+1) \times 10^{-4} \leq dn_s/d\ln k \leq -2 \times 10^{-4} \quad .$$

For $N = 50$ the values $n_s = 0.96$, $r = 0.16$ which are those determined by the simple monomial potential $m^2 \varphi^2/2$ determine a divide and a degeneracy point in the field and parameter space. Small field regions yield $r < 0.16$ while large field regions correspond to $r > 0.16$.

The $1/N$ expansion also provides a powerful tool to implement a *reconstruction program* that allows to extract the value of the field N efolds before the end of inflation, and in the case of new inflationary models, the symmetry breaking scale.

We find that the region of field space favored by the WMAP3 data can be explored in a systematic expansion in $n_s - 1 + 2/N$ [18]. An analytic and numerical study of this region lead us to conclude that if forthcoming data on tensor modes favors $r < 0.16$ then new inflation **is favored**, and we **predict** for $r < 0.1$ that (i) the **symmetry breaking scale** is

$$\varphi_{min} \sim 20 M_{Pl} \quad ,$$

and (ii) the value of the field when cosmologically relevant wavelengths cross the Hubble radius is $|\varphi_{exit}| \sim 6 M_{Pl}$.

The family of chaotic inflationary models characterized by the potentials eq.(2.118) feature tensor to scalar ratios $r \geq 0.16$ (for $N = 50$), with the minimum, $r = 0.16$ obtained in the limit of small inflaton amplitude and corresponds to the monomial potential $m^2 \varphi^2/2$ which is again a degeneracy point for this family of models.

The combined marginalized data from WMAP3 [9] yields a very small window within which chaotic models are allowed by the data, the largest region of overlap with the (r, n_s) WMAP3 data corresponds to $n = 2$ and the width of the region decreases with larger n [18]. The typical scale of the field at Hubble crossing for these models is $|\varphi_{exit}| \sim 15 M_{Pl}$ (for $N = 50$). Some small regions in field space consistent with the WMAP3 data feature peaks in the running of the scalar index but in the region consistent with the WMAP3 data in chaotic inflation the running is again negligible. If future observations determine a tensor to scalar ratio $r < 0.16$, such bound will, all by itself, **rule out** the large family of chaotic inflationary models of the form (2.118) for any n [18].

F. The initial conditions for the scalar and tensor quantum fluctuations.

Scalar curvature and tensor (gravitational wave) quantum fluctuations generated during the inflationary stage determine the power spectrum of the anisotropies in the cosmic microwave background (CMB) providing the seeds

for large scale structure (LSS) formation. Curvature and tensor fluctuations obey the wave equation eq.(1.123) and (1.143), respectively, and the choice of a particular solution entails a choice of initial conditions [2, 3, 4]. The power spectra of these fluctuations depend in general on the initial conditions that define the particular solutions. These are usually chosen as Bunch-Davies [62] initial conditions, which select positive frequency modes asymptotically with respect to conformal time. The quantum states in the Fock representation associated with these initial conditions are known as Bunch-Davies states, the vacuum state being invariant under the maximal symmetry group $O(4, 1)$ of de Sitter space-time.

Alternative initial conditions were also considered [63]. The requirement that the energy momentum tensor be renormalizable constrains the UV asymptotic behaviour of the Bogoliubov coefficients that encode different initial conditions [37]. The availability of high precision cosmological data motivated a substantial effort to study the effect of different initial conditions upon the angular power spectrum of CMB anisotropies, focusing primarily in the high- ℓ region near the acoustic peaks [50]. However, the exhaustive analysis of the WMAP data [9, 10] render much less statistical significance to possible effects on small angular scales from alternative initial conditions (see also sec. III A 2).

1. Initial conditions and the energy momentum tensor of scalar and tensor perturbations.

The effective field theory of slow-roll inflation has two main ingredients: the classical Friedmann equations in terms of a *classical* part of the energy momentum tensor described by a homogeneous and isotropic condensate, and a quantum part. The latter features scalar fluctuations determined by a gauge invariant combination of the scalar field (inflaton) and metric fluctuations, a tensor component, gravitational waves plus contributions of further quantum fields (scalar, spinors, etc.) A consistency condition for this description is that the contributions from the fluctuations to the energy momentum tensor be much smaller than those from the homogeneous and isotropic condensate. The effective field theory must include renormalization counterterms so that it is insensitive to the ultraviolet singularities of the short wavelength fluctuations. Different initial conditions on the mode functions of the quantum fluctuations yield different values for their contribution to the energy momentum tensor. Different initial conditions on the mode functions of the quantum fluctuations yield different values for the energy momentum tensor.

Criteria for acceptable initial conditions must include the following: i) back reaction effects from the quantum fluctuations should not modify the inflationary dynamics described by the inflaton, ii) the ultraviolet counterterms that renormalize the energy momentum tensor should not depend on the particular choice of initial conditions, namely different initial conditions *should not* introduce new ultraviolet divergences: a single renormalization scheme, independent of initial conditions, should render the energy momentum tensor UV finite. This set of criteria imply that the ultraviolet allowed states have their large k behaviour constrained up to the fourth order in $1/k$ [37]. In ref. [37] only the energy momentum tensor of *inflaton* fluctuations was considered. However, the fluctuations of the inflaton field are *not* gauge invariant, and in order to establish a set of criteria for UV allowed initial states in a gauge invariant manner we studied the full gauge invariant energy momentum of scalar and tensor fluctuations [19, 20].

2. Scalar perturbations

The gauge invariant energy momentum tensor for quadratic scalar metric fluctuations has been obtained in ref.[20, 21, 77] where the reader is referred to for details. Its form simplifies in longitudinal gauge, and in cosmic time it is given by [20, 21, 77]

$$\langle T_{00} \rangle = M_{Pl}^2 \left[12 H \langle \psi \dot{\psi} \rangle - 3 \langle (\dot{\psi})^2 \rangle + \frac{9}{a^2(t)} \langle (\nabla \psi)^2 \rangle \right] + \frac{1}{2} \langle (\dot{\phi})^2 \rangle + \frac{\langle (\nabla \phi)^2 \rangle}{2 a^2(t)} + \frac{V''(\Phi)}{2} \langle \phi^2 \rangle + 2 V'(\Phi) \langle \psi \phi \rangle, \quad (2.119)$$

where $\Phi(t)$ stands for the zero mode of the inflaton field, $\phi(t, \vec{x})$ for the inflaton fluctuations around $\Phi(t)$, $\psi(t, \vec{x})$ is the longitudinal gauge form of the Bardeen potential and the dots stand for derivatives with respect to cosmic time. During inflation the Newtonian potential and the Bardeen potential are the same in the longitudinal gauge[5] and this property has been used in the above expression.

In longitudinal gauge, the equations of motion in cosmic time for the Fourier modes are[5]

$$\begin{aligned} \ddot{\psi}_{\vec{k}} + \left(H - 2 \frac{\ddot{\Phi}}{\dot{\Phi}} \right) \dot{\psi}_{\vec{k}} + \left[2 \left(\dot{H} - 2 H \frac{\ddot{\Phi}}{\dot{\Phi}} \right) + \frac{k^2}{a^2(t)} \right] \psi_{\vec{k}} &= 0, \\ \ddot{\phi}_{\vec{k}} + 3 H \dot{\phi}_{\vec{k}} + \left[V''[\Phi] + \frac{k^2}{a^2(t)} \right] \phi_{\vec{k}} + 2 V'[\Phi] \psi_{\vec{k}} - 4 \dot{\Phi} \dot{\psi}_{\vec{k}} &= 0, \end{aligned} \quad (2.120)$$

with the constraint equation

$$\dot{\psi}_{\vec{k}} + H \psi_{\vec{k}} = \frac{1}{2M_{Pl}^2} \phi_{\vec{k}} \dot{\Phi}. \quad (2.121)$$

Initial conditions on the mode functions of the quantum fluctuations correspond to an initial value problem at a fixed time hypersurface. For modes of cosmological relevance this time slice at which the initial conditions are established is such that these modes are *subhorizon*. Therefore, we must focus on the contribution to the energy momentum tensor from subhorizon fluctuations, and in particular in the large momentum region to assess the criteria for UV allowed states.

For subhorizon modes with wavevectors $k \gg a(t) H$, the solutions of the equation (2.120) are [5]

$$\psi_{\vec{k}}(t) \approx e^{\pm i k \eta} \Rightarrow \dot{\psi}_{\vec{k}}(t) \sim \frac{i k}{a(t)} \psi_{\vec{k}}(t). \quad (2.122)$$

For $k \gg a(t) H$ the constraint equation (2.121) entails that [20, 21, 77]

$$\psi_{\vec{k}}(t) \approx \frac{i a(t)}{2 M_{Pl}^2 k} \dot{\Phi} \phi_{\vec{k}}. \quad (2.123)$$

In slow-roll,

$$\dot{\Phi} = -\frac{V'(\Phi)}{3 H} \left[1 + \mathcal{O}\left(\frac{1}{N}\right) \right] = -H M_{Pl} \sqrt{2 \epsilon_v} \left[1 + \mathcal{O}\left(\frac{1}{N}\right) \right], \quad (2.124)$$

where the slow-roll parameters ϵ_v , η_v are of the order $1/N$ [11] and given by eqs.(1.131). Therefore, for subhorizon modes,

$$\psi_{\vec{k}}(t) \approx -i \sqrt{2 \epsilon_v} \left(\frac{H a(t)}{k} \right) \frac{\phi_{\vec{k}}}{2 M_{Pl}}. \quad (2.125)$$

These identities, valid in the limit $k \gg a(t) H$ allow to obtain an estimate for the different contributions to T_{00} . The first line of eq.(2.119), namely the contribution from the Newtonian potential mode with comoving wavevector k is

$$\langle T_{00}^{(\psi)} \rangle \approx 6 \epsilon_v H^2 \langle (\phi_{\vec{k}})^2 \rangle. \quad (2.126)$$

The first three terms in the second line of eq.(2.119) (the quadratic contribution from the scalar field fluctuations) is

$$\langle T_{00}^{\phi} \rangle \approx \left(\frac{k}{a(t)} \right)^2 \langle (\phi_{\vec{k}})^2 \rangle, \quad (2.127)$$

and the cross term is:

$$V'(\Phi) \langle \psi_{\vec{k}} \phi_{\vec{k}} \rangle \approx \epsilon_v H^2 \left(\frac{a(t) H}{k} \right) \langle (\phi_{\vec{k}})^2 \rangle, \quad (2.128)$$

Therefore, in slow-roll, ϵ_v , $\eta_v \ll 1$ and for subhorizon modes $k \gtrsim a(t) H$, the leading contribution to the energy momentum tensor for the scalar fluctuations is given by the contribution from the inflaton fluctuations, namely

$$\langle T_{00} \rangle \simeq \frac{1}{2} \langle (\dot{\phi})^2 \rangle + \frac{\langle (\nabla \phi)^2 \rangle}{2 a^2(t)} + \frac{V''(\Phi)}{2} \langle \phi^2 \rangle. \quad (2.129)$$

Furthermore, in terms of the slow-roll parameter η_v , $V'' = 3 \eta_v H^2$ and for subhorizon wavevectors with $k \gg a(t) H$ the last term in eq.(2.129) is subdominant and will be neglected. Hence, the contribution to the energy momentum tensor *from subhorizon fluctuations during the slow-roll stage* is determined by the subhorizon quantum fluctuations of the inflaton and given by

$$\langle T_{00} \rangle \simeq \frac{1}{2} \langle (\dot{\phi})^2 \rangle + \frac{\langle (\nabla \phi)^2 \rangle}{2 a^2(t)}. \quad (2.130)$$

This analysis allows us to connect with the the results in ref.[37] for inflaton fluctuations.

The inflaton fluctuation obeys the equation of motion

$$\ddot{\phi}_{\vec{k}} + 3 H \dot{\phi}_{\vec{k}} + \left[3 H^2 \eta_v + \frac{k^2}{a^2(t)} \right] \phi_{\vec{k}} = 0 . \quad (2.131)$$

In what follows it is convenient to pass to conformal time eq.(1.20) in terms of which, the FRW metric takes the form eq.(1.6) and the scalar factor is given in slow-roll by eq.(1.134).

In conformal time η the solution of eq.(2.131) is given by

$$\phi_{\vec{k}}(\eta) = \frac{1}{a(\eta)} \left[\alpha_{\vec{k}} S_{\phi}(k, \eta) + \alpha_{-\vec{k}}^{\dagger} S_{\phi}^*(k, \eta) \right] , \quad (2.132)$$

where the mode functions $S_{\phi}(k, \eta)$ are solutions of the wave equation

$$\left[\frac{d^2}{d\eta^2} + k^2 + M^2 a^2(\eta) - \frac{a''(\eta)}{a(\eta)} \right] S_{\phi}(k, \eta) = 0 , \quad (2.133)$$

here,

$$M^2 = V''(\Phi) = 3 H^2 \eta_v . \quad (2.134)$$

and prime stands for derivative with respect to the conformal time. Using eqs.(1.131) and (1.134), this equation simplifies during slow-roll to

$$\left[\frac{d^2}{d\eta^2} + k^2 - \frac{\nu_{\phi}^2 - \frac{1}{4}}{\eta^2} \right] S_{\phi}(k, \eta) = 0 , \quad (2.135)$$

where,

$$\nu_{\phi} = \frac{3}{2} + \epsilon_v - \eta_v + \mathcal{O}\left(\frac{1}{N^2}\right) . \quad (2.136)$$

The scalar fluctuations $\phi_{\vec{k}}$ therefore obey wave equations similar to the scalar curvature and tensor fluctuations as follows comparing eqs.(1.135), (1.144) and (2.135). These Hankel equations only differ on the value of the corresponding index ν .

The operators $\alpha_{\vec{k}}$, $\alpha_{\vec{k}}^{\dagger}$ in eq. (2.132) obey the usual canonical commutation relations eq.(1.122).

3. Tensor perturbations

The expectation value of the energy-momentum pseudo-tensor of tensor perturbations in a quantum state has been obtained in ref.[20, 21, 77] (see also ref.[39]) and is given by

$$\langle T_{00}^{(T)} \rangle = M_{Pl}^2 \left\{ H \langle \dot{h}_{kl} h_{kl} \rangle + \frac{1}{8} \left[\langle \dot{h}_{kl} \dot{h}_{kl} \rangle + \frac{1}{a^2(t)} \langle \nabla h_{kl} \nabla h_{kl} \rangle \right] \right\} , \quad (2.137)$$

where the dot stands for derivative with respect to cosmic time. Tensor perturbations (gravitational waves) are gauge invariant and were analyzed in sec. IE 2.

To leading order in slow-roll the mode functions for gravitational waves eqs.(1.143)-(1.144) obey the same equations of motion as for scalar fields but with vanishing mass, namely setting $\eta_v = 0$ in eqs.(2.135)-(2.136).

4. The Transfer Function of Initial Conditions and its Asymptotic Behaviour

For gauge invariant scalar perturbations, the analysis leading to eq.(2.130) indicates that in order to study the energy momentum tensor for general initial conditions it is enough to consider the leading order in the slow-roll expansion. Consistently with neglecting the contributions from the Newtonian potential as well as the term proportional to $V''[\Phi]$ for the inflaton fluctuations, we set $\nu = 3/2$ in the expression for the mode functions eq.(1.137). This simplification results in considering the scalar field fluctuations as massless and minimally coupled to gravity.

The energy density in the vacuum state defined by the new initial conditions is

$$\rho = {}_{\mathcal{S}}\langle 0|T_{00}|0\rangle_{\mathcal{S}} . \quad (2.138)$$

The renormalized energy density from the fluctuations of the inflaton field is found to be [19, 20, 21, 37]

$$\rho = \rho^{BD} + I_1 + I_2 , \quad (2.139)$$

where ρ^{BD} corresponds to the Bunch-Davies vacuum initial conditions $N_k = 0$ and

$$I_1 = \frac{1}{2\pi^2} \int_0^\infty dk k^2 \left\{ N_\phi(k) |\dot{F}(k, \eta)|^2 + \sqrt{N_\phi(k)[1 + N_\phi(k)]} \operatorname{Re} \left[e^{-i\theta_k} \left(\dot{F}(k, \eta) \right)^2 \right] \right\} \quad (2.140)$$

$$I_2 = \frac{1}{2\pi^2} \int_0^\infty dk k^2 \frac{k^2}{a^2} \left\{ N_\phi(k) |F(k, \eta)|^2 + \sqrt{N_\phi(k)[1 + N_\phi(k)]} \operatorname{Re} \left[e^{-i\theta_k} (F(k, \eta))^2 \right] \right\} \quad (2.141)$$

where $F(k, \eta)$ is given in terms of the Bunch-Davis mode function eq.(1.140) for $\nu = 3/2$ as

$$F(k, \eta) = (-H\eta) g_{\frac{3}{2}}(k, \eta) = \frac{H}{\sqrt{2} k^{\frac{3}{2}}} e^{-i k \eta} (i - k \eta) . \quad (2.142)$$

The power spectrum of the inflaton fluctuations is given by [5],

$$P_\phi(k, t) = {}_{\mathcal{S}}\langle 0|\phi_k(\eta)|^2|0\rangle_{\mathcal{S}} = P_\phi^{BD}(k, t) + \frac{k^3}{\pi^2} \left\{ N_\phi(k) |F(k, \eta)|^2 + \sqrt{N_\phi(k)[1 + N_\phi(k)]} \operatorname{Re} \left[e^{-i\theta_k} (F(k, \eta))^2 \right] \right\} , \quad (2.143)$$

where we used eq.(1.151) and

$$P_\phi^{BD}(k, t) = \frac{k^3}{2\pi^2} |F(k, \eta)|^2 . \quad (2.144)$$

We find,

$$I_1 = \frac{(H\eta)^4}{(2\pi)^2} \int_0^\infty dk k^3 \left\{ N_\phi(k) - \sqrt{N_\phi(k)[1 + N_\phi(k)]} \cos[2k\eta + \theta_k] \right\} \quad (2.145)$$

$$I_2 = \frac{(H^2\eta)^2}{(2\pi)^2} \int_0^\infty dk k \left\{ N_\phi(k) (1 + k^2 \eta^2) - \sqrt{N_\phi(k)[1 + N_\phi(k)]} [(1 - k^2 \eta^2) \cos[2k\eta + \theta_k] + 2k\eta \sin[2k\eta + \theta_k]] \right\} \quad (2.146)$$

$$P_\phi(k, t) = \left(\frac{H}{2\pi} \right)^2 \left\{ (1 + k^2 \eta^2)[1 + 2N_\phi(k)] - 2\sqrt{N_\phi(k)[1 + N_\phi(k)]} [(1 - k^2 \eta^2) \cos[2k\eta + \theta_k] + 2k\eta \sin[2k\eta + \theta_k]] \right\} .$$

Evaluating the power spectrum after horizon crossing $|k\eta| \ll 1$, yields

$$\left. \frac{P_\phi}{P_\phi^{BD}} \right|_{|k\eta| \ll 1} = 1 + D_\phi(k) , \quad (2.147)$$

where we have introduced the *transfer function for initial conditions*

$$D_\phi(k) = 2 |B_\phi(k)|^2 - 2 \operatorname{Re} [A_\phi(k) B_\phi^*(k)] = 2 N_\phi(k) - 2 \sqrt{N_\phi(k)[1 + N_\phi(k)]} \cos \theta_k . \quad (2.148)$$

The integrals $I_{1,2}$ are finite provided that asymptotically for $k \rightarrow \infty$ the occupation numbers behave as

$$N_\phi(k) = \mathcal{O} \left(\frac{1}{k^{4+\delta}} \right) , \quad (2.149)$$

with $\delta > 0$. Namely, the finiteness of the energy momentum tensor constrains the asymptotic behaviour of the occupation numbers to vanish faster than $1/k^4$ for $k \rightarrow \infty$ [37]. Of course, this asymptotic condition leaves a large freedom on the occupation numbers N_k .

We systematically impose the constraint eq.(2.149) which guarantees the finiteness of energy momentum tensor [19, 20, 21]. This is not always the case for initial conditions considered in the literature (see ref.[50]).

Let us establish a bound on the large momentum behavior of N_k inserting the asymptotic behavior

$$N_k = N_\mu \left(\frac{\mu}{k} \right)^{4+\delta}, \quad (2.150)$$

with $0 < \delta \ll 1$ in the integrals $I_{1,2}$. Namely, assuming that the integrals are dominated by the region of high momenta $k/H \gg 1$ and that the occupation number attains the largest possible values consistent with ultraviolet finiteness [eq.(2.149)]. We observe that $k|\eta| \gg 1$ in the early stages of inflation for large k , and that the maximum contribution from these integrals are at early time $\eta \sim -1/H$. Hence, the oscillatory terms in I_1, I_2 average out and we have from eqs.(2.145)-(2.146) [21],

$$I_1 \sim I_2 \sim \frac{N_\mu}{(2\pi)^2} \frac{\mu^4}{\delta}. \quad (2.151)$$

The contribution from the fluctuations to the energy momentum tensor does not lead to large back reaction effects affecting the inflationary dynamics provided that $I_1, I_2 \ll H^2 M_{Pl}^2$, which yields

$$N_\mu \ll 2\pi^2 \frac{H^2 M_{Pl}^2}{\mu^4} \delta. \quad (2.152)$$

Eq.(2.152) provides an occupation number distribution exhibiting the largest asymptotic value compatible with an UV finite energy momentum tensor. This maximal occupation number distribution falls off for $k \rightarrow \infty$ with the minimal acceptable power tail exponent $4 + \delta$ with $\delta \ll 1$ [21].

Gravitons are massless particles with two independent polarizations, therefore their energy momentum tensor is given by eq.(2.130) times a factor two. The first term in the energy momentum pseudotensor for gravitational waves eq.(2.137) features only one time derivative, which results in only one factor k for large momenta, whereas the terms with two time or spatial derivatives yield k^2 . Therefore, the first term is subdominant in the ultraviolet and the short wavelength contribution to the energy momentum (pseudo) tensor of gravitational waves is the same as that for a free massless scalar field, up to a factor 2 from the physical polarization states [20, 39]. Therefore, we can directly extend the results obtained above for scalar fluctuations to the case of tensor fluctuations.

Small backreaction effects from the fluctuations is a necessary consistency condition for the validity of the inflationary scenario. In addition, the condition that different initial states *should not affect* the renormalization aspects of the energy momentum tensor is a consistency condition on the renormalizability of the effective field theory of inflation: the theory should be insensitive to the short distance physics for *any* initial conditions. These criteria lead to the following important consequences [21]:

- If $\mu \sim M_{Pl}$ then $N_\mu \lesssim H^2/M_{Pl}^2 \ll 1$ because $H/M_{Pl} \ll 1$ in the effective field theory expansion and the effect of initial conditions becomes negligible.
- For $\mu \sim \sqrt{H M_{Pl}} \sim N^{\frac{1}{4}} M$, namely μ of the order of the scale of inflation during the slow-roll stage, then $N_\mu \lesssim 1$. For example for $\delta \sim 0.01$ one obtains $N_\mu \sim 0.1$. If $\mu \ll \sqrt{H M_{Pl}}$, for example $\mu \sim H$, the bound eq.(2.152) is rather loose allowing a wide range of N_μ with potentially appreciable effects.
- The condition that the occupation number falls off faster than $1/k^4$ for large wavevector, implies that the possible effects from different initial conditions are more prominent for the smaller wavevectors, those that exited the Hubble radius the *earliest*. For cosmologically relevant wavevectors, these are those that crossed about 60 e-folds before the end of inflation. Today those wavevectors correspond to the present Hubble scale, hence the low multipoles in the CMB.

We conclude that consistent with renormalizability and small back reaction there may be a substantial effect from the initial conditions when the characteristic scale is $\mu \leq \sqrt{H M_{Pl}}$. The rapid fall-off of the occupation numbers $N_\phi(k)$ for subhorizon wavelengths and the back-reaction constraint eq.(2.152) entails that for these modes the transfer function eq.(2.148) for initial conditions simplifies to

$$D_\phi(k) \stackrel{N_\phi(k) \ll 1}{\simeq} -2 \sqrt{N_\phi(k)} \cos \theta_k, \quad (2.153)$$

and that the *smaller values* of k yield the *larger corrections from initial conditions*. The result eq.(2.153) implies a **suppression** of the power spectrum for $\cos \theta_k > 0$. These observations will be crucial below when we study the effect of initial conditions on the multipoles of the CMB [21].

While this discussion focused on the fluctuations of the inflaton, they are directly applicable to the case of gauge invariant perturbations.

The contribution from gravitational waves to the energy momentum (pseudo) tensor is gauge invariant and up to a factor of two from the polarizations is exactly of the form eq.(2.130) with ϕ replaced by h [20]. Thus, the constraint on the occupation number eq.(2.150)-(2.152) from the analysis of the backreaction and renormalizability translate *directly* to the case of gravitational waves for the occupation number $N_T(k)$.

This implies that corrections to the power spectrum of tensor modes from initial conditions are substantial if μ , the asymptotic k scale of $N_T(k)$, is $\mu \leq \sqrt{H M_{Pl}} \sim N^{\frac{1}{4}} M$, [see discussion above for N_μ]. We get from eq.(1.168) for $N_T(k) \ll 1$ and to leading order in slow-roll,

$$D_T(k) \stackrel{N_T(k) \ll 1}{=} -2 \sqrt{N_T(k)} \cos \theta_k . \quad (2.154)$$

Again, for a positive $\cos \theta_k$, we have a **negative** $D_T(k)$. That is, the initial conditions **suppress** the tensor power spectrum in such case.

We have focused on the backreaction effects from initial conditions beginning with the gauge invariant energy momentum tensor for scalar and tensor perturbations. Since the fluctuation modes are initialized on a fixed time hypersurface while their wavelength are well inside the Hubble radius, we established a correspondence with ref.[37] which refer solely to the quantum fluctuations of the inflaton field. The effect of different initial conditions is encoded in the Bogoliubov coefficients, and in particular in the occupation numbers N_k and the phases θ_k . Ultraviolet allowed initial conditions require that N_k diminishes faster than $1/k^4$ for asymptotically large momenta. Small backreaction effects require in general that $N_k \ll 1$.

This analysis applies to UV allowed initial conditions on the quantum fluctuations associated with gauge invariant variables, both scalar and tensor perturbations, studied in sec. IE.

5. The effect of initial conditions on the low multipoles of the CMB

We have shown above that the fast fall off of the occupation number $N(k)$ (for the corresponding perturbation) entails that initial conditions can only provide substantial corrections for perturbation modes whose wavevectors crossed out of the Hubble radius *early* during inflation. In turn, today these wavevectors correspond to scales of the order of the Hubble radius, namely to the low multipoles in the CMB.

In the region of the Sachs-Wolfe plateau for $l \lesssim 30$, the matter-radiation transfer function can be set equal to unity and the C'_l s are given by [5, 38]

$$C_l = \frac{4\pi}{9} \int_0^\infty \frac{dk}{k} P_X(k) \{j_l[k(\eta_0 - \eta_{LSS})]\}^2 , \quad (2.155)$$

where P_X is the power spectrum of the corresponding perturbation, $X = \mathcal{R}$ for curvature perturbations and $X = T$ for tensor perturbations, $j_l(x)$ are spherical Bessel functions [89] and $\eta_0 - \eta_{LSS}$ is the comoving distance between today and the last scattering surface (LSS) given by eqs.(1.62) and (1.63).

Notice that $k/H_0 \sim d_H/\lambda_{phys}(t_0)$ is the ratio between today's Hubble radius and the physical wavelength. The power spectra for curvature (\mathcal{R}) or gravitational wave (T) perturbations are of the form given by eqs.(1.158), (1.161), (1.165), (1.166),

$$P_X = |\Delta_k^X|^2 \left(\frac{k}{k_0} \right)^{n_s-1} [1 + D_X(k)] , \quad (2.156)$$

with $n_s = n_{\mathcal{R}}$ for curvature perturbations, $n_s = 1 + n_T$ for tensor perturbations, and $k_0 \sim H_0$ is a pivot scale. Then, from eqs.(2.147) and (2.155), the relative change ΔC_l in the C'_l s due to the effect of generic initial conditions (generic vacua), is given by

$$C_l \equiv C_l^{BD} + \Delta C_l \quad , \quad \frac{\Delta C_l}{C_l} = \frac{\int_0^\infty D_X(\kappa x) f_l(x) dx}{\int_0^\infty f_l(x) dx} \quad (2.157)$$

where $x = k(\eta_0 - \eta_{LSS}) = k/\kappa$ and from eq.(1.63), $\kappa \equiv H_0/3.296\dots$. $D(\kappa x)$ is the transfer function of initial conditions for the corresponding perturbation and

$$f_l(x) = x^{n_s-2} [j_l(x)]^2 . \quad (2.158)$$

We now focus on curvature perturbations since these are directly related to the temperature fluctuations [8, 9, 10]. Since $n_s \sim 1$, the functions $f_l(x)$ are strongly peaked at $x \sim l$ as shown by eq.(1.67). Therefore, $\Delta C_l/C_l$ is dominated by wavenumbers $k \sim l \kappa$.

Low multipoles l correspond to wavelengths *today* of the order of the Hubble radius. These wavelengths crossed the Hubble radius about 60 efolds before the end of inflation. Therefore, since inflation lasted a total number of efolds $N_{tot} \gtrsim 64$, these wavevectors were subhorizon during the first few efolds, namely during the slow-roll stage $k \gg H$. As already discussed, let us take for these wavevectors the occupation number $N_k \ll 1$ as given by the asymptotic expression eq.(2.150) and assume that the angles θ_k are slowly varying functions of k in the region of k corresponding to *today's Hubble radius* so that $\cos \theta_k \approx \overline{\cos \theta}$. Then, we find that the fractional change in the coefficients C_l is given by [21]

$$\frac{\Delta C_l}{C_l} \approx -2 \sqrt{N_\mu} \left(\frac{3.3 \mu}{H_0} \right)^{2+\frac{\delta}{2}} \frac{1}{\overline{\cos \theta}} \frac{I_l(n_s - 2 - \frac{\delta}{2})}{I_l(n_s)} \quad (2.159)$$

where

$$I_l(n_s) = \frac{1}{2^{3-n_s}} \frac{\Gamma(3-n_s) \Gamma(\frac{1}{2}(2l+1-3+n_s+1))}{\Gamma^2(2-\frac{1}{2}n_s) \Gamma(\frac{1}{2}(2l+1+3-n_s+1))}. \quad (2.160)$$

To obtain an estimate of the corrections, we take the values $n_s = 1$, $\delta = 0$ and find

$$\frac{\Delta C_l}{C_l} \approx -\frac{4}{3} \sqrt{N_\mu} \left(\frac{3.3 \mu}{H_0} \right)^2 \frac{\overline{\cos \theta}}{(l-1)(l+2)}. \quad (2.161)$$

The $\sim 1/l^2$ behavior is a result of the $1/k^2$ fall off of $D(k)$, a consequence of the renormalizability condition on the occupation number.

When the scale μ in the asymptotic form of the occupation number eq.(2.150) is of the order of the largest scale of cosmological relevance *today*, one has $\mu \sim H_0$ and for example with $N_\mu \sim 0.1$ we find that the fractional change in the quadrupole is given by:

$$\frac{\Delta C_2}{C_2} \sim -\overline{\cos \theta}, \quad (2.162)$$

namely a *suppression* of the order of ~ 1 in the quadrupole provided that $\overline{\cos \theta} \sim 1$. This corresponds to μ of the order of the Hubble parameter during the slow-roll stage [21]. Namely, changing the initial conditions in such a way **can** explain the observed suppression of the CMB quadrupole [8, 9, 10, 15].

We emphasize that these are general arguments based on the criteria of renormalizability and small backreaction which initial conditions must fulfill [21].

In ref.[22] (see sec. II G) we showed that these initial conditions are effectively equivalent to the presence of a fast-roll stage before the slow-roll regime. We show in ref. [22] that a short stage just prior to the onset of slow-roll inflation and in which the inflaton field evolves *fast*, imprints by the beginning of slow-roll a behaviour on the curvature perturbations which is similar to the non-Bunch-Davis initial conditions considered above.

G. The early fast-roll inflationary stage and the CMB quadrupole suppression

Although there are no statistically significant departures from the slow-roll inflationary scenario at small angular scales ($l \gtrsim 100$), the WMAP data again confirm the surprisingly low quadrupoles C_2^{TT} and C_2^{TE} [9, 10] and suggest that it cannot be completely explained by galactic foreground contamination. The low value of the quadrupole has been an intriguing feature on large angular scales since first observed by COBE/DMR [15], and confirmed by the WMAP data [9, 10].

In order to asses the statistical relevance of the observed quadrupole suppression, we studied the best fit to the Λ CDM model using the WMAP5 data. We find that the probability that the quadrupole is as low or lower than the observed value is just 0.031. Even if one does not care about the specific multipole and looks for any multipole as low or lower than the observed quadrupole with respect to the Λ CDM model value, then the probability remains smaller than 5%. Therefore, it is relevant to find a cosmological explanation of the quadrupole suppression beyond the Λ CDM model.

Generically, the classical evolution of the inflaton has a brief **fast-roll stage** that precedes the slow-roll regime. The fast-roll stage leads to a purely attractive potential in the wave equations of curvature and tensor perturbations.

Such potential is a *generic* feature of this brief *fast-roll* stage that merges smoothly with slow-roll inflation. This stage is a consequence of generic initial conditions *for the classical inflaton dynamics* in which the kinetic and potential energy of the inflaton are of the same order, namely, the energy scale of slow-roll inflation. During the early fast-roll stage the inflaton evolves rapidly during a brief period, but slows down by the cosmological expansion settling in the slow-roll stage in which the kinetic energy of the inflaton is much smaller than its potential energy.

As shown in refs. [21, 22, 40] the attractive potential in the wave equations of curvature and tensor perturbations during the fast-roll stage leads to a **suppression** of the quadrupole moment for CMB and B-mode angular power spectra. Both scalar and tensor low multipoles are suppressed. However, the potential for tensor perturbations is about an order of magnitude smaller than the one for scalar fluctuations and hence the suppression of the low ℓ tensor perturbations is much less significant [21, 22].

The observation of a low quadrupole [9, 10, 15] and the surprising alignment of quadrupole and octupole [51, 52] sparked many different proposals for their explanation [53].

The fast-roll explanation of the quadrupole does not require to introduce new physics neither modifications of the inflationary potential. The only new feature is that the quadrupole mode should exit the horizon during the generic fast-roll stage that precedes slow-roll inflation.

A single **new** parameter emerges dynamically due to the fast-roll stage: the comoving wave number k_{tran} , characteristic scale of the attractive potential felt by the fluctuations during fast-roll. The fast-roll stage modifies the initial power spectrum by a transfer function $D(k)$ that we compute solving the classical inflaton evolution equations (see fig. 28). $D(k)$ effectively suppresses the primordial power for $k < k_{tran}$ and possesses the scaling property $D(k) = \Psi(k/k_{tran})$ where $\Psi(x)$ is an universal function. $D(k)$ has a main peak around $k_M \simeq 1.9 k_{tran}$ and oscillates around zero with decreasing amplitude as a function of k for $k > k_M$. $D(k)$ vanishes asymptotically for large k , as expected.

We reported in ref.[23] the results of a MCMC analysis of the WMAP-3, small-scale CMB and SDSS data including the fast-roll stage and find the value $k_{tran} = 0.290 \text{ Gpc}^{-1}$. This mode k_{tran} happens to exit the horizon precisely at the transition from the fast-roll to the slow-roll stage. The quadrupole mode $k_Q = 0.238 \text{ Gpc}^{-1}$ exits the horizon **during** the fast-roll stage approximately **0.2 efolds** earlier than k_{tran} . We compare in ref.[23] the fast-roll fit with a fit without fast-roll but including a sharp lower cutoff on the primordial power. That is, setting the the primordial power to zero for $k < k_{tran}$.

We analyze with MCMC and compare three classes of cosmological models:

- The usual slow-roll ΛCDM , the $\Lambda\text{CDM}+r$ and the $\Lambda\text{CDM}+r+\text{BNI}$ models. BNI stands for *Binomial New Inflation*. In this last model we **enforce** the theoretical functional relation between n_s and r valid in BNI.
- The slow-roll $\Lambda\text{CDM}+r+\text{BNI}$ model with a sharp cutoff for $k < k_{tran}$.
- The $\Lambda\text{CDM}+r+\text{BNI}$ model including both fast and slow-roll stages.

We observe that the oscillatory form of the fast-roll transfer function $D_{\mathcal{R}}(k)$, by **depressing as well as enhancing** the primordial power spectrum at long wavelengths (see fig. 28), leads also to new superimposed **oscillatory corrections** on the low multipoles. As far as fitting to current data is concerned, such corrections are more effective than the pure reduction caused by a sharp cutoff. The fast-roll oscillations yield better gains in likelihood than the sharp cutoff case [23].

The quadrupole suppression by the early fast-roll stage can be simply understood by causality in a qualitative way. During fast-roll inflation the Hubble parameter decreases fast (much faster than during slow-roll inflation) as shown in fig. 26. Therefore, the Hubble radius d_H grows with time and the d_H curve in fig. 5 is not horizontal but down bended during the fast-roll stage. Hence, the fluctuation modes cannot exit the horizon before slow-roll and therefore the primordial power gets suppressed for $k < k_{tran}$.

1. The Effect of Fast-roll on the Inflationary Fluctuations.

Both scalar curvature and tensor fluctuations obey the Schrödinger-type equation

$$\left[\frac{d^2}{d\eta^2} + k^2 - W(\eta) \right] S(k; \eta) = 0. \quad (2.163)$$

with η as the coordinate, k^2 as the energy and $W(\eta)$ the potential determined by the classical inflaton dynamics. $W_{\mathcal{R}}(\eta)$ and $W_T(\eta)$ are given by eqs.(1.130) and (1.146). The Schrödinger form of the mode equations (2.163) in one dimension suggests to consider them more generally as a *scattering problem* by a potential [21, 22].

During slow-roll both potentials $W_{\mathcal{R}}(\eta)$ and $W_T(\eta)$ are **repulsive** and have the shape of a centrifugal barrier:

$$W(\eta) \simeq \frac{\nu^2 - 1/4}{\eta^2} \quad \text{slow-roll},$$

where

$$\nu = \begin{cases} \nu_{\mathcal{R}} = \frac{3}{2} + 3\epsilon_v - \eta_v + \mathcal{O}\left(\frac{1}{N^2}\right) & \text{for curvature perturbations} \\ \nu_T = \frac{3}{2} + \epsilon_v + \mathcal{O}\left(\frac{1}{N^2}\right) & \text{for tensor perturbations.} \end{cases} \quad (2.164)$$

We choose as initial condition the Bunch-Davies asymptotic condition

$$S(k; \eta \rightarrow -\infty) = \frac{e^{-i k \eta}}{\sqrt{2k}}. \quad (2.165)$$

We formally consider here inflation and the conformal time starting at $\eta = -\infty$. However, it is natural to consider that the inflationary evolution of the universe starts at some negative value $\eta_i < \bar{\eta}$, where $\bar{\eta}$ is the conformal time when fast-roll ends and slow-roll begins.

It is convenient to explicitly separate the behavior of $W(\eta)$ during the slow-roll stage by writing

$$W(\eta) = \mathcal{V}(\eta) + \frac{\nu^2 - \frac{1}{4}}{\eta^2}, \quad (2.166)$$

The potential $\mathcal{V}(\eta)$ is localized in the fast-roll stage *prior* to slow-roll (during which cosmologically relevant modes cross out of the Hubble radius), $\mathcal{V}(\eta)$ vanishes during slow-roll. In terms of the potential $\mathcal{V}(\eta)$ the equations for the quantum fluctuations read,

$$\left[\frac{d^2}{d\eta^2} + k^2 - \frac{\nu^2 - \frac{1}{4}}{\eta^2} - \mathcal{V}(\eta) \right] S(k; \eta) = 0. \quad (2.167)$$

During the slow-roll stage, the fluctuations equations (2.163) can be solved in close form in terms of Bessel functions as discussed in secs. IE 1-IE 2. This does not apply during the fast-roll stage.

As discussed above, the potential $\mathcal{V}(\eta)$ describes the deviation from the slow-roll dynamics during the (brief) fast-roll stage prior to slow-roll and is vanishingly small for $\eta > \bar{\eta}$, where $\bar{\eta}$ denotes the beginning of the slow-roll stage during which modes of cosmological relevance today exit the Hubble radius.

The retarded Green's function $G_k(\eta, \eta')$ of eq.(2.167) for $\mathcal{V}(\eta) \equiv 0$ obeys

$$\left[\frac{d^2}{d\eta^2} + k^2 - \frac{\nu^2 - \frac{1}{4}}{\eta^2} \right] G_k(\eta, \eta') = \delta(\eta - \eta') \quad ; \quad G_k(\eta, \eta') = 0 \text{ for } \eta' > \eta, \quad (2.168)$$

it is given by

$$G_k(\eta, \eta') = i [g_\nu(k; \eta) g_\nu^*(k; \eta') - g_\nu(k; \eta') g_\nu^*(k; \eta)] \Theta(\eta - \eta'), \quad (2.169)$$

where $g_\nu(k; \eta)$ is given by eq.(1.137).

The solution of the mode equation (2.167) can be written as an integral equation using the Green's function eq.(2.169)

$$S(k; \eta) = g_\nu(k; \eta) + \int_{-\infty}^0 G_k(\eta, \eta') \mathcal{V}(\eta') S(k; \eta') d\eta'. \quad (2.170)$$

This is the Lippmann-Schwinger equation familiar in potential scattering theory. Inserting eq.(2.169) into eq.(2.170) yields,

$$S(k; \eta) = g_\nu(k; \eta) + i g_\nu(k; \eta) \int_{-\infty}^{\eta} g_\nu^*(k; \eta') \mathcal{V}(\eta') S(k; \eta') d\eta' - i g_\nu^*(k; \eta) \int_{-\infty}^{\eta} g_\nu(k; \eta') \mathcal{V}(\eta') S(k; \eta') d\eta'. \quad (2.171)$$

This solution has the Bunch-Davies asymptotic condition

$$S(k; \eta \rightarrow -\infty) = \frac{e^{-i k \eta}}{\sqrt{2k}}. \quad (2.172)$$

Since $\mathcal{V}(\eta)$ vanishes for $\eta > \bar{\eta}$, the mode functions $S(k; \eta)$ for $\eta > \bar{\eta}$ can be written as linear combinations of the mode functions $g_\nu(k; \eta)$ and $g_\nu^*(k; \eta)$,

$$S(k; \eta) = A(k) g_\nu(k; \eta) + B(k) g_\nu^*(k; \eta) \quad , \quad \eta > \bar{\eta} \quad , \quad (2.173)$$

where the coefficients $A(k)$ and $B(k)$ can be read from eq.(2.171),

$$\begin{aligned} A(k) &= 1 + i \int_{-\infty}^0 g_\nu^*(k; \eta) \mathcal{V}(\eta) S(k; \eta) d\eta \\ B(k) &= -i \int_{-\infty}^0 g_\nu(k; \eta) \mathcal{V}(\eta) S(k; \eta) d\eta . \end{aligned} \quad (2.174)$$

The coefficients $A(k)$ and $B(k)$ are therefore **calculated** from the **dynamics before** slow-roll, that is, during fast-roll. [recall that $\mathcal{V}(\eta) = 0$ for $\eta > \bar{\eta}$ during slow-roll.] $A(k)$ and $B(k)$ fulfil the constraint eq.(1.150) and can therefore be represented as in eq.(1.154).

Starting with Bunch-Davies initial conditions for $\eta \rightarrow -\infty$, the action of the fast-roll potential $\mathcal{V}(\eta)$ generates a mixture (Bogoliubov transformation) of the two linearly independent mode functions that result in the mode functions eq.(2.173) for $\eta > \bar{\eta}$ when the potential $\mathcal{V}(\eta)$ vanishes. This is clearly equivalent to starting the evolution of the fluctuations at the *beginning* of slow-roll $\eta = \bar{\eta}$ with initial conditions defined by the fast-roll Bogoliubov coefficients $A(k)$ and $B(k)$ given by eq.(2.174) as stressed in ref.[22]. Namely, one can obtain a similar suppression on the quadrupole either taking into account the fast-roll stage **or** changing the initial conditions of the mode functions at the beginning of slow-roll.

The integral equation (2.171) can be solved iteratively in a perturbative expansion if the potential $\mathcal{V}(\eta)$ is small when compared to

$$k^2 - \frac{\nu^2 - 1/4}{\eta^2} .$$

In such case, we can use for the coefficients $A(k)$, $B(k)$ the first approximation obtained by replacing $S(k; \eta')$ by $g_\nu(k; \eta')$ in the integrals eqs.(2.174)-(2.174). This is the Born approximation, in which

$$A(k) = 1 + i \int_{-\infty}^0 \mathcal{V}(\eta) |g_\nu(k; \eta)|^2 d\eta \quad , \quad B(k) = -i \int_{-\infty}^0 \mathcal{V}(\eta) g_\nu^2(k; \eta) d\eta . \quad (2.175)$$

That is, the standard slow-roll power spectrum $P^{sr}(k)$ results modified by the fast-roll stage as displayed in eqs.(1.156) and (1.158).

The simple expressions (2.175) are very illuminating. For asymptotically large k the form eq.(1.138) for the mode functions can be used, and if the potential $\mathcal{V}(\eta)$ is differentiable and of compact support, an integration by parts yields

$$B(k) \stackrel{k \rightarrow \infty}{\simeq} -\frac{1}{4k^2} \int_{-\infty}^0 e^{-2ik\eta} \mathcal{V}'(\eta) d\eta , \quad (2.176)$$

where the prime stands for derivative with respect to η . Therefore, according to the Riemann-Lebesgue lemma, $N_k = |B(k)|^2 \lesssim 1/k^4$ for large k and UV convergence in the integrals for the energy momentum tensor is guaranteed. Hence, an immediate consequence of the explanation of the initial conditions as a scattering problem with a localized potential is that these initial conditions are *automatically* ultraviolet allowed.

The transfer function of initial conditions given by eq.(1.159) can be computed in the Born approximation, which is indeed appropriate in this situation, using eqs.(2.175) for the Bogoliubov coefficients $A(k)$ and $B(k)$ to dominant order in $1/N$ [22]

$$D(k) = \frac{1}{k} \int_{-\infty}^0 d\eta \mathcal{V}(\eta) \left[\sin(2k\eta) \left(1 - \frac{1}{k^2 \eta^2} \right) + \frac{2}{k\eta} \cos(2k\eta) \right] . \quad (2.177)$$

The potential $\mathcal{V}(\eta)$ is obtained from eq.(2.166) as

$$\mathcal{V}(\eta) = W(\eta) - \frac{\nu^2 - 1/4}{\eta^2} .$$

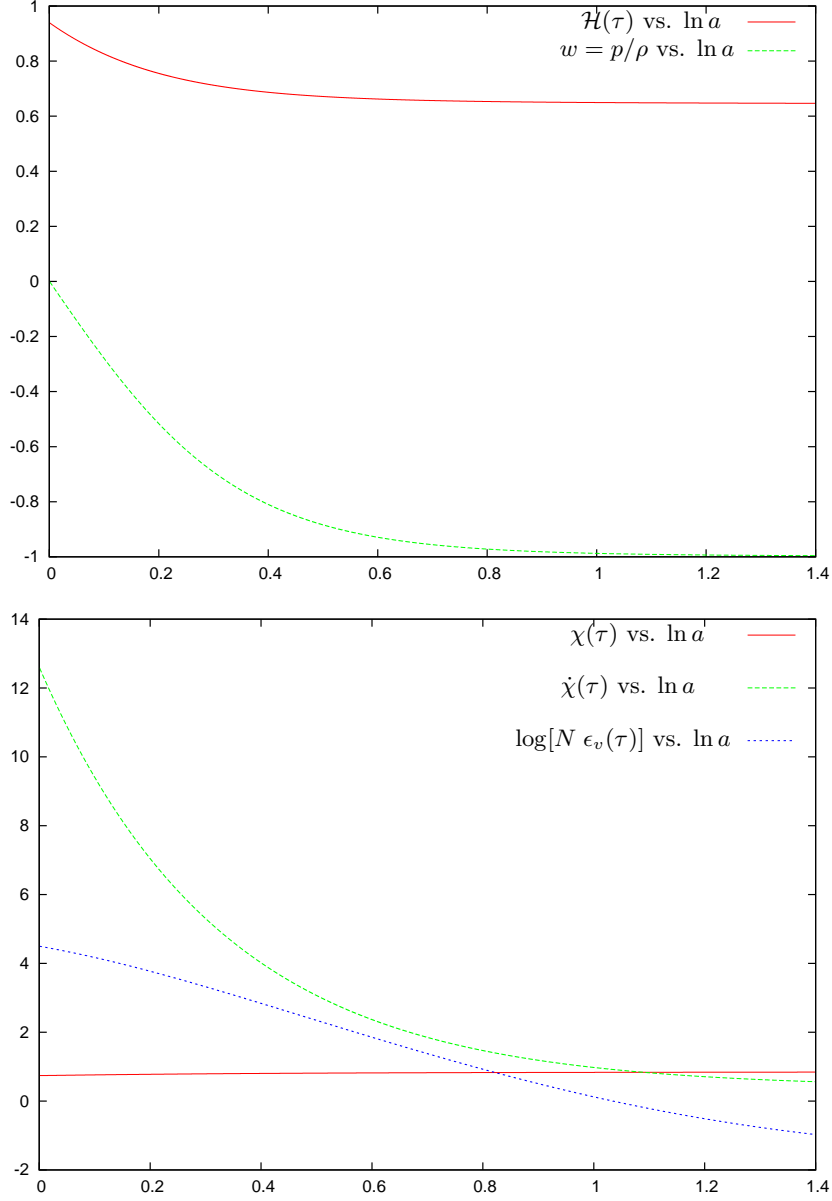


FIG. 26: Upper panel: the Hubble parameter $\mathcal{H}(\tau)$ and the equation of state $w = p/\rho$ as function of $\ln a$ during fast-roll inflation. Lower panel: the dimensionless fields $\chi(\tau)$, $\dot{\chi}(\tau)$ and the parameter $\log[\epsilon_v(\tau) N]$ as function of $\ln a$ during fast-roll. Notice that fast-roll ends when $\epsilon_v(\tau) \times N = 1$ at $\ln a(\tau) = 1.0347 \dots$. Both figures are for the inflaton potential eq.(1.92) with $y = 1.26$ and $N_{tot} \simeq 64$ e folds of inflation.

In the integral eq.(2.157) that yields the coefficients $\Delta C_l/C_l$, the transfer function $D(k)$ multiplies a function that is strongly peaked at $x \sim l$, namely, for momenta $k \sim l \kappa$. Therefore, if $k |\eta_0| \sim l \kappa |\eta_0| \gg 1$, the rapid oscillations in $D(k)$ average out in the integrand, resulting in a vanishing contribution to the $\Delta C_l/C_l$'s. Hence, there are significant contributions to $\Delta C_l/C_l$ only when $l \kappa |\eta_0| \sim 1$. For the quadrupole this corresponds to, $a_0 H_0 |\eta_0| \sim 1$.

Inserting the expression (2.177) for $D(k)$ into eq.(2.157) yields

$$\frac{\Delta C_\ell}{C_\ell} = \frac{1}{\kappa} \int_{-\infty}^0 d\eta \mathcal{V}(\eta) \Psi_\ell(\kappa \eta) \quad (2.178)$$

where

$$\Psi_\ell(x) \equiv 2 \ell(\ell + 1) \int_0^\infty \frac{dy}{y^4} [j_\ell(y)]^2 \left[\left(y^2 - \frac{1}{x^2} \right) \sin(2 y x) + \frac{2 y}{x} \cos(2 y x) \right] \quad (2.179)$$

$\Psi_\ell(x)$ is an odd function of x . $\Psi_2(x)$ turns to be **positive** for $x < 0$ as shown in ref.[22]. Since the potential $\mathcal{V}(\eta)$ turns to be an **attractive** potential $\mathcal{V}(\eta) < 0$, the correction $\Delta C_2/C_2$ given by eq.(2.178) in the Born approximation is **negative** clearly revealing a **suppression** in the CMB quadrupole.

The functions $\Psi_\ell(x)$ exhibit oscillations for $\ell > 2$ and take both positive as well as negative values for $x < 0$. Therefore, we see from eq.(2.178) that the $\ell > 2$ CMB multipoles can be suppressed as well as enhanced by the effect of fast-roll as explicitly shown in ref.[23].

The correction $\Delta C_l/C_l$ of higher multipoles is smaller, falling off as $1/l^2$ [22].

To explicitly compute $\mathcal{V}_\mathcal{R}(\eta)$ as a function of η for the curvature fluctuations we solve numerically the equations of motion (1.89) for new inflation [eq.(1.92)] and insert the solution for the inflaton $\chi(\eta)$ in eqs.(1.130)-(1.131). No large N approximation is used in this numerical calculation since we cover in the evolution the fast-roll region where slow-roll obviously does not apply [23].

It is illuminating to study $\chi(\tau)$, $\dot{\chi}(\tau)$, $\mathcal{H}(\tau)$, $p(\tau)/\rho(\tau)$ and $\log[N \epsilon_v(\tau)]$ [see eq.(1.131)] during the short fast-roll stage for new inflation [eq.(1.92)]. They are plotted in figs. 26 during the fast-roll stage (see figs. 6, 7 and 8 for the full inflationary stage). We choose the best fit coupling $y = 1.26$ [see table 6] and a total number of e-folds equal to 64. We choose the initial values of χ and $\dot{\chi}$ such that their initial kinetic and potential energies are equal [eq.(1.106)] and therefore $p/\rho = 0$, initially.

We see from figs. 26 that the equation of state $p/\rho(\tau)$ goes down from the initial value $p/\rho = 0$ to $p/\rho \simeq -1$ by the end of fast-roll. Both $\dot{\chi}(\tau)$ and $\epsilon_v(\tau)$ decrease very fast during fast-roll. We see that the fast-roll stage ends by $\tau \simeq 0.0247$ and $\log a(\tau) = 1.0347$ when $\epsilon_v(\tau) \times N = 1$. Notice that $\epsilon_v(0) = 1.5 \gg 1/N$ for the initial conditions eq.(1.106).

In fig. 27 we plot $\mathcal{V}_\mathcal{R}(\eta)$ vs. η for new inflation and the same initial conditions. We see that the potential $\mathcal{V}_\mathcal{R}(\eta)$ is **attractive** in the fast-roll stage and asymptotically vanishes by the end of fast-roll $\eta \sim -0.04$ [23].

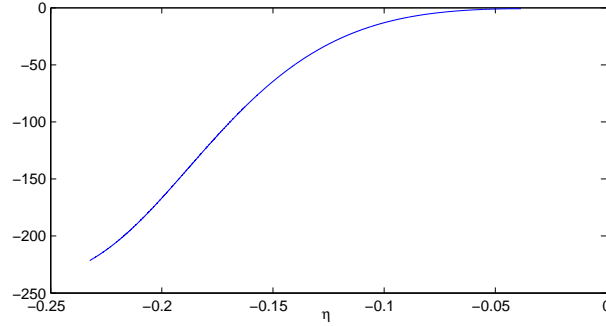


FIG. 27: The potential $\mathcal{V}_\mathcal{R}(\eta)$ felt by the fluctuations vs. η for new inflation with $y = 1.26$. $\mathcal{V}_\mathcal{R}(\eta)$ is **attractive** during fast-roll and vanishes by the end of fast-roll ($\eta \sim -0.04$).

We obtain the transfer function $D_\mathcal{R}(k)$ by inserting $\mathcal{V}_\mathcal{R}(\eta)$ into eq.(2.177) and computing the integral over η numerically. In fig. 28 we plot $D_\mathcal{R}(k)$ vs. k/m for new inflation [eq.(1.92)] and ten different couplings $0.00536 < y < 1.498$ with a total number of e-folds equal to 64. We see that $D_\mathcal{R}(k)$ oscillates around zero and therefore produces **suppressions as well as enhancements** in the low multipoles [see eq.(1.156)]. $D_\mathcal{R}(k)$ vanishes asymptotically for large k as expected.

The first peak in $D_\mathcal{R}(k)$ is clearly its dominant feature. The k of this peak corresponds to k -modes which are today horizon size and affect the lowest CMB multipoles (see below and table 2) [21, 22].

For small k the Born approximation to $D_\mathcal{R}(k)$ yields large negative values indicating that this approximation cannot be used in this particular small k regime. We introduce the scale k_{tran} by the condition $D_\mathcal{R}(k_{tran}) = -1$ and then just take $D_\mathcal{R}(k) = -1$ for $k \leq k_{tran}$. This corresponds to vanishing primordial power for the lowest values of k (see fig. 28).

From fig. 28 we also see that the plots of $D_\mathcal{R}(k)$ for different couplings follow from each other almost entirely by changing the scale in the variable k as summarized by eq.(2.180). Indeed, the characteristic scale k_{tran} plays here a further important role.

Analysing $\mathcal{V}_\mathcal{R}(\eta)$ and $D_\mathcal{R}(k)$ for different couplings y we find that they **scale** with k_{tran} . Namely,

$$\mathcal{V}_\mathcal{R}(\eta) = k_{tran}^2 Q(k_{tran} \eta) \quad , \quad D_\mathcal{R}(k) = \Psi\left(\frac{k}{k_{tran}}\right) \quad , \quad (2.180)$$

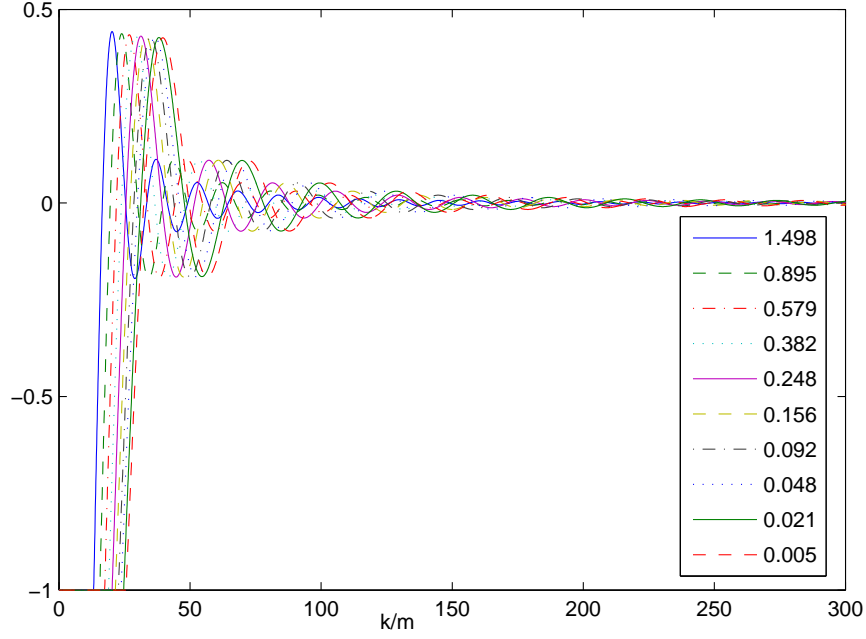


FIG. 28: The fast-roll transfer function $D_{\mathcal{R}}(k)$ vs. k/m for new inflation and ten different couplings $0.00536 < y < 1.498$. We see that the plots of $D_{\mathcal{R}}(k)$ for different couplings follow from each other by changing the scale in the variable k as summarized by eq.(2.180).

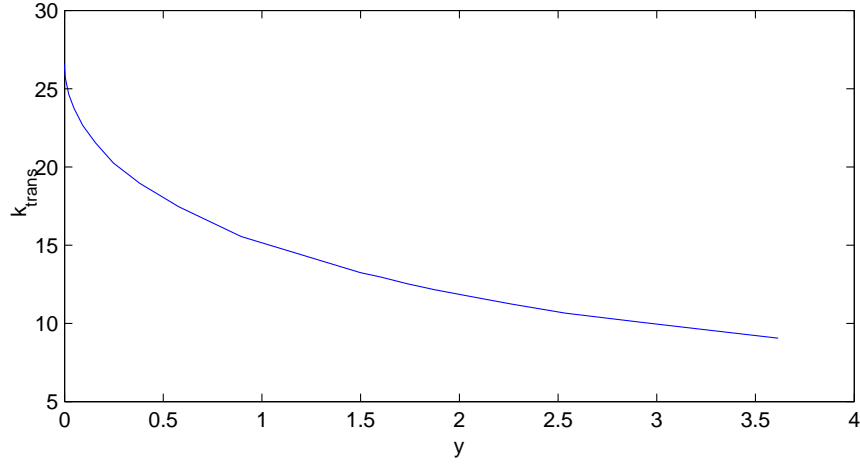


FIG. 29: k_{tran}/m vs. y for new inflation.

where $Q(x)$ and $\Psi(x)$ are universal functions. That is, $Q(x)$ and $\Psi(x)$ do not depend on the coupling y while k_{tran}/m is a function of y . We display k_{tran}/m vs. y in fig. 29. These scaling properties arise from the fact that the scale of the potential $\mathcal{V}_{\mathcal{R}}(\eta)$ in k^2 does determine the scale of variation of the transfer function $D_{\mathcal{R}}(k)$ with k .

We obtain the function $Q(x)$ from eq.(2.180) as,

$$Q(x) = \frac{1}{k_{tran}^2} \mathcal{V}_{\mathcal{R}} \left(\frac{x}{k_{tran}} \right) \quad (2.181)$$

We plot $Q(x)$ in fig. 30 as follows from the r. h. s. of eq.(2.181) for ten different values of y . We see that all the curves collapse on a common curve proving the validity of the quasi-scaling properties eq.(2.180).

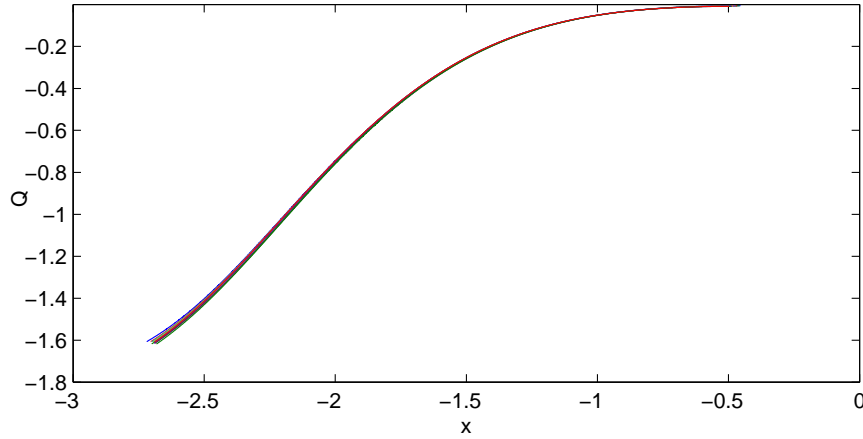


FIG. 30: $Q(x)$ for the ten values of y of fig. 28, according to eq.(2.181). All curves collapse to a common one proving the scaling properties eq.(2.180).

2. MCMC analysis of CMB and LSS data including the early fast-roll inflationary stage

In order to test the theoretical quadrupole suppression predicted by the fast-roll inflationary stage against the current experimental data we performed in ref. [23] a Monte Carlo Markov Chains (MCMC) analysis of the commonly available cosmological data using the *CosmoMC* program [43].

For LSS we considered SDSS (DR4). For CMB we first considered the three-years WMAP data (with the second release of WMAP likelihood code) and the small scale data (ACBAR-2003, CBI2, BOOMERANG03). While the work in ref. [23] was in progress, the five-years WMAP data were released, and we repeated our MCMC analysis almost completely with these new data, using also the newer 2007 ACBAR release (commonly denoted as ACBAR08) [44]. Actually WMAP3 or WMAP5 provide by far the dominant contribution and small scale experiments have very little relevance for the quadrupole suppression issue. In this review we only report MCMC results based on the WMAP5 data, in combination with the SDSS data and either ACBAR08 or the most recent supernovae compilation (SN for short) [24].

In our MCMC analysis we modified the *CosmoMC* code and introduced explicitly the transfer function $D_{\mathcal{R}}(k)$ in the primordial power spectrum according to eq. (1.156).

We ran *CosmoMC* on pc clusters with Message Passing Interface (MPI), producing from 10 to 24 parallel chains, with the ‘R-1’ stopping criterion set equal to 0.03 (this criterion looks at the fluctuations among parallel chains to decide when to stop the run). The statistical convergence was also verified a posteriori with the help of the *getdist* program of *CosmoMC*.

As discussed in section IID, the preferred reference model for slow-roll inflation cosmology is the Λ CDM+ r model, that is the standard six-parameters Λ CDM model augmented by the tensor-scalar ratio r . Indeed, the current experimental accuracy provides sensible bounds for the index n_s and the ratio r eqs.(1.163) and (1.169). Specific slow-roll scenarios, such as those based on new (small-field) or chaotic (large-field) inflation lead to specific theoretical constraints in the (n_s, r) plane presented in sec. IID [14].

We point out that we used the default *CosmoMC* pivot scale $k_0 = 0.05 \text{ Mpc}^{-1}$ rather than the customary WMAP choice of $k_0 = 0.002 \text{ Mpc}^{-1}$. As evident from eq. (1.161) this leads to a small difference with respect to the WMAP choice in the definition itself of the tensor to scalar ratio r . In particular, the *CosmoMC* r is roughly 10% larger than the WMAP one.

3. MCMC analysis with Binomial New Inflation without the fast-roll stage: $D_{\mathcal{R}}(k) = 0$.

Let us first present, to fix the reference, our MCMC analysis with the standard slow-roll primordial power eq.(1.161). That is, without including the early fast-roll stage and therefore with a vanishing transfer function $D_{\mathcal{R}}(k)$.

For instance, in the simplest binomial realization of new inflation described by the inflaton potential eq. (1.92), n_s and r are constrained to the curve C_{BNI} (BNI stands for *Binomial New Inflation*) parametrized by the quartic

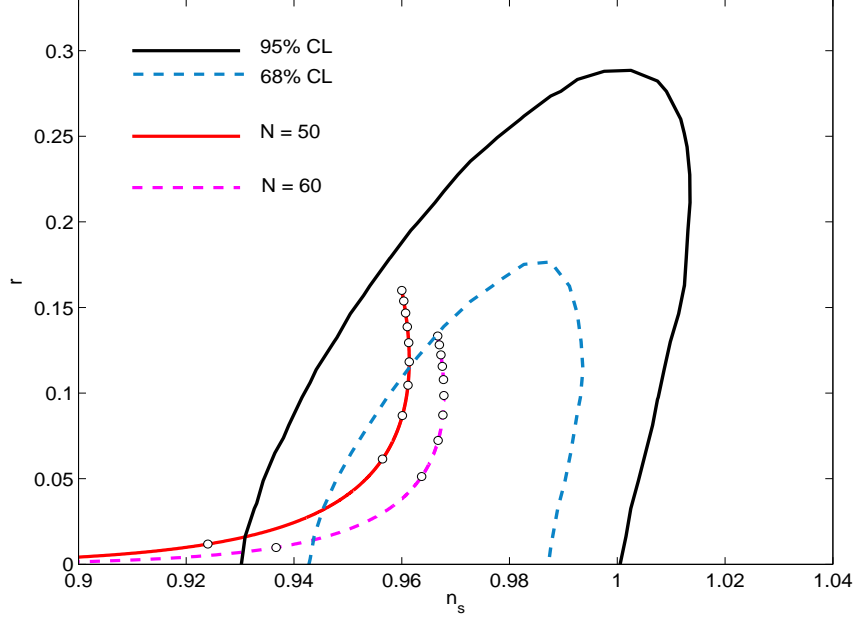


FIG. 31: Binomial New Inflation compared to $\Lambda\text{CDM}+r$ model in the (n_s, r) plane. The contour plots correspond to 68% and 95% confidence levels for $\Lambda\text{CDM}+r$ according to WMAP5, SN and SDSS data. C_{BNI} is the solid red curve for $N = 50$ or the dashed magenta curve for $N = 60$. The white dots correspond to the values $0.01 + 0.11 * n$, $n = 0, 1, \dots, 9$, of the variable z in eq. (2.182), starting from the leftmost ones. The quartic coupling y increases monotonically starting from the uppermost dots, corresponding to the free-field, purely quadratic inflaton potential $y = 0$, $z = 1$ till the strong coupling region $y \gg 1$, $z \ll 1$ in the lower part of the C_{BNI} curve. We see that very small values of r **are excluded** since they correspond to $n_s < 0.92$ outside the 95% confidence level contour. That is, we obtain a **lower bound** for r : $r > 0.027$ at 95% C. L.

coupling y as [see eq. (2.16)]:

$$n_s = 1 - \frac{y}{N} \frac{3z+1}{(1-z)^2}, \quad r = \frac{16y}{N} \frac{z}{(1-z)^2}, \quad y = z - 1 - \log z, \quad z = \frac{y}{8} \chi^2, \quad 0 < z < 1. \quad (2.182)$$

This situation is clearly displayed in fig. 31 in which the curve C_{BNI} , for the two choices $N = 50$ and $N = 60$, is drawn over the contour plots of the likelihood distribution for n_s and r in the $\Lambda\text{CDM}+r$ model obtained with CosmoMC, using the WMAP5, SN and SDSS data. Very similar contour plots apply when ACBAR08 is used in place of SN.

All the MCMC results reported below refer to the case $N = 60$.

The likelihood L , as function of the whole set of parameters, provides a quantitative measure of the power of a given model to fit the multipoles C_ℓ^γ . As customary, we set $-2 \log L = \chi_L^2$, although it is well known that, due particularly to cosmic variance, the shape of L as function of the C_ℓ^γ is not Gaussian especially for low ℓ .

Now, as evident from eq. (2.182) and fig. 31, one could expect from the ΛCDM model constrained to C_{BNI} a fit to the data not as good as in the $\Lambda\text{CDM}+r$ model since the current data seem to favor smaller values for r . However, we find very small increase of $\min \chi_L^2$ [23]

$$\min \chi_L^2(\Lambda\text{CDM}+r+\text{BNI}) - \min \chi_L^2(\Lambda\text{CDM}+r) \simeq 0.2. \quad (2.183)$$

This shows that the BNI constraint is naturally compatible with the data. This result was obtained for $N = 60$ by direct minimization of χ_L^2 in the neighbourhood of C_{BNI} , using the data of a large collection of long chain runs (with a grandtotal of more than one million steps) for the $\Lambda\text{CDM}+r$ model with the WMAP5, SN and SDSS data. The flat priors on the cosmological parameters were the standard ones of CosmoMC, that is

$$\begin{aligned} 0.005 < \omega_b < 0.1 \quad , \quad 0.01 < \omega_c < 0.99 \quad , \quad 0.5 < \theta < 10 \\ 0.01 < \tau < 0.8 \quad , \quad 2.7 < \log(10^{10} A_s) < 4 \quad , \quad 0.5 < n_s < 1.5 \end{aligned}$$

while for the tensor-scalar ratio we imposed as prior

$$0 < r < 0.35.$$

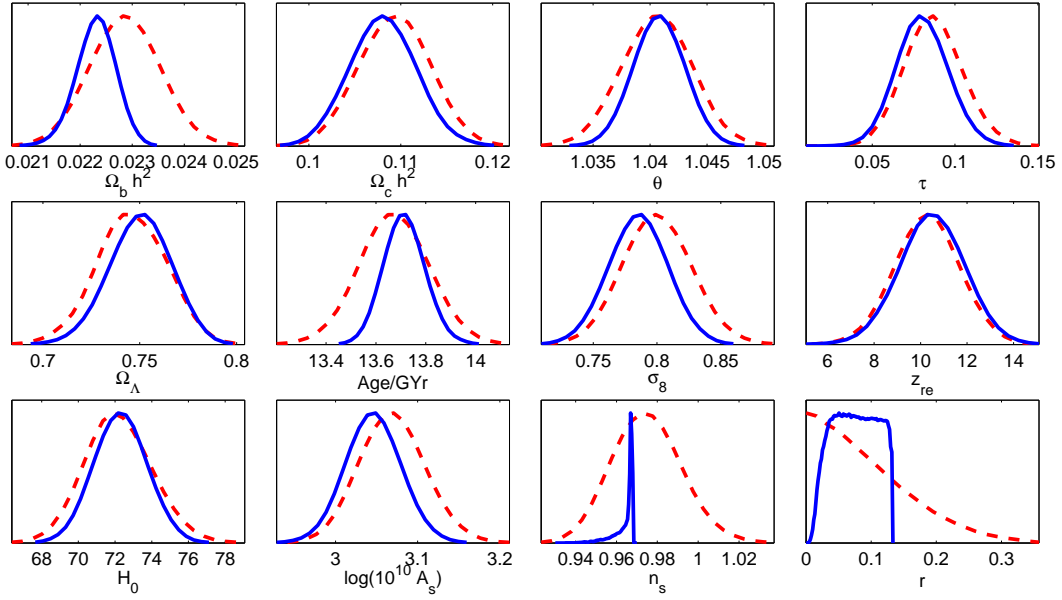


FIG. 32: The Λ CDM+BNI model (solid blue lines) compared to the Λ CDM+ r model (dashed red lines) in the probability distributions of relevant cosmological parameters, for $N = 60$ with WMAP5+SN+SDSS data.

	$10\omega_b$	ω_c	10θ	τ	$10^9 A_s$	n_s	r	$\Delta\chi_L^2/2$
Λ CDM	0.226	0.110	1.040	0.896	2.164	0.966	0	-0.2
Λ CDM+ r	0.225	0.110	1.039	0.785	2.108	0.962	0.010	—
Λ CDM+ r +BNI	0.225	0.110	1.040	0.807	2.115	0.964	0.052	+0.2
Λ CDM+BNI	0.226	0.111	1.040	0.867	2.159	0.965	0.057	-0.3

TABLE IV: Best fit values for the MCMC cosmological parameters without quadrupole suppression, using WMAP5, SN and SDDS. C_{BNI} means the curve on which n_s and r are constrained in Binomial New Inflation (BNI), eq. (2.182) with $N = 60$. Λ CDM+ r +BNI means the Λ CDM+ r model constrained on C_{BNI} using the constrained pair of variables (n_s, r) . Λ CDM+BNI denotes the Λ CDM model constrained on C_{BNI} using the single variable z eq. (2.182) as MCMC variable instead of the constrained pair (n_s, r) .

Another parametrization, that unlike the direct minimization of χ_L^2 over C_{BNI} , does take advantage of the explicit analytic parametrizations in eq. (2.182), is to use the single variable z as MCMC parameter, instead of the constrained pair (n_s, r) , with a flat prior over all the allowed range $0 < z < 1$. Let us call Λ CDM+BNI the 6-parameter model Λ CDM constrained on C_{BNI} using the variable z . Then, we find that taking into account the natural fluctuations due to the large number of data (which make the likelihood landscape over the MCMC parameters quite complex) and the various approximations and numerical errors in the theoretical calculation of the multipoles, the increasing in χ_L^2 due to the C_{BNI} constraint eq. (2.182) compared to the Λ CDM model essentially vanishes (see Table IV below).

For completeness and reference, we report in Table IV our best fit (or most likely) values for the MCMC cosmological parameters, as well as the variations in χ_L^2 with respect to the Λ CDM+ r model. The dataset includes WMAP5, SN and SDSS. We report in the first row of the table also our best fit for the standard Λ CDM model, which has six free parameters as the Λ CDM+BNI model since r is set to zero by fiat.

The slightly better performance of Λ CDM+BNI over Λ CDM+ r +BNI (and also over Λ CDM+ r itself) is not very relevant since is most likely due to the finer search possibility in a space with 6 parameters by compared to one in a space with 7 parameters. We want to draw the attention to the fact that including the constraint over C_{BNI} does not produce any statistically significant change on the most likely values of the cosmological parameters, except of course on n_s and r themselves. This shows how natural turns to be to constraint the CMB+LSS data by the BNI model. In particular, comparing the Λ CDM+BNI model with respect to the Λ CDM+ r model, the most likely value of n_s is practically unchanged, while that of r improves in Λ CDM+BNI: r changes from values of order 10^{-2} (or just 0) in Λ CDM to values such as 0.052 and 0.057 in Λ CDM+BNI.

Concerning marginalized distributions, we find no significant changes but for n_s and r . These results are very close to those in section IID, where TNI was considered, as can be appreciated from fig. 16 and 32. The only minor change

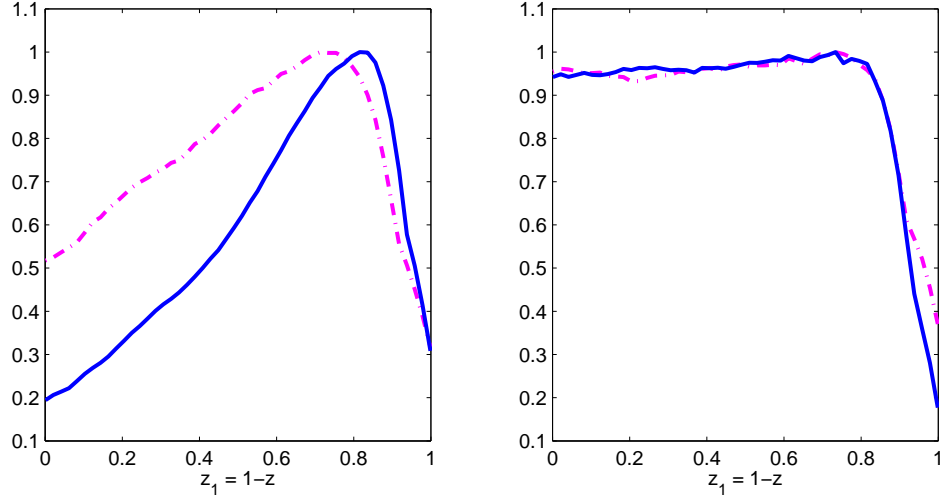


FIG. 33: Comparison of probability distributions (solid blue lines) and mean likelihoods (magenta dashed-dotted lines) in the Λ CDM+TNI model (left) and in the Λ CDM+BNI model (right). Here $N = 60$ and WMAP5, SN and SDSS data are used.

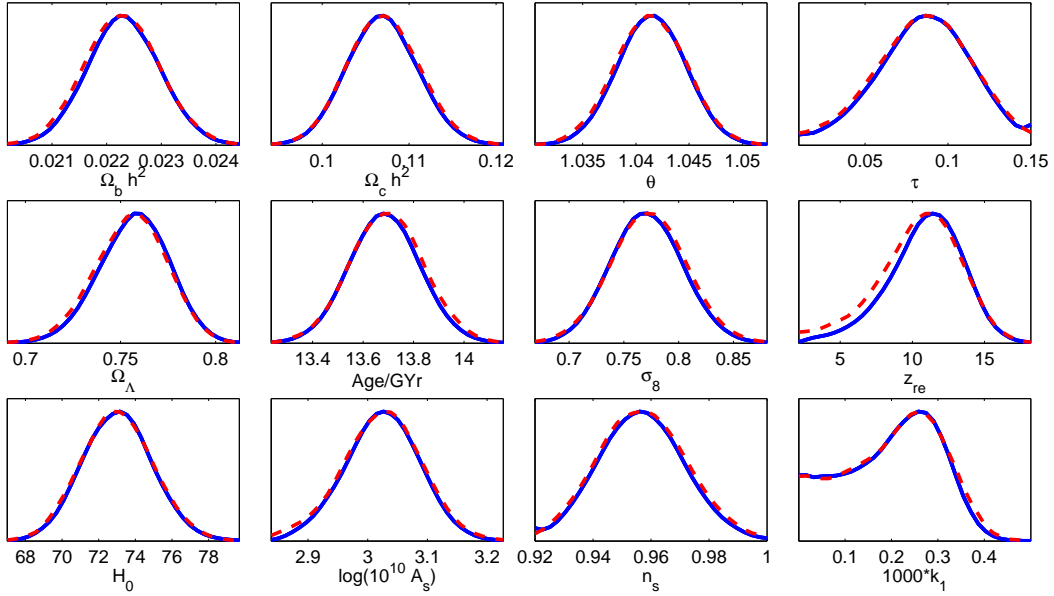


FIG. 34: Marginalized distributions (solid blue lines) and mean likelihoods (red dotted lines) for the parameters of the Λ CDM+sharp cutoff model, using the WMAP3+small scale_CMB+SDSS data. k_{tran} is in $(\text{Gpc})^{-1}$.

is in the broader shape of the peak in the marginalized distribution for r , which for BNI extends almost flatly up to the theoretical limit $r = 2/15 = 0.133\dots$. This is due to the absence in BNI of the asymmetry h which in the TNI case allows for the broadening of the allowed $n_s - r$ region as $z_1 \rightarrow 1$ (*i.e.* as $z = 1 - z_1 \rightarrow 0$, which is the strong coupling y regime). This effect may be directly observed in the probability distributions and mean likelihoods for z_1 , which we compare in fig. 33. As an obvious consequence, with respect to the TNI case, we obtain a higher bound on r in the Λ CDM+BNI model: $r > 0.027$ at 95% CL.

Our inflation-based 6-parameter Λ CDM+BNI model predicting a value of r well below 0.2 is **as likely** as the Λ CDM model itself. Recall that the current CMB+LSS data analysis, without any theoretical constraint, put only an upper bound on r (namely $r < 0.22$ with 95% C. L. in the most recent WMAP5 analysis [10]). This means that the theoretical grounds of a given model take a more important role in the analysis and interpretation of the CMB+LSS data. For instance, from an inflationary viewpoint, the choice that r exactly vanishes, appears **unlikely and unphysical**. Notice that $n_s - 1 = 0 = r$ corresponds to a singular limit and a critical (massless) point where

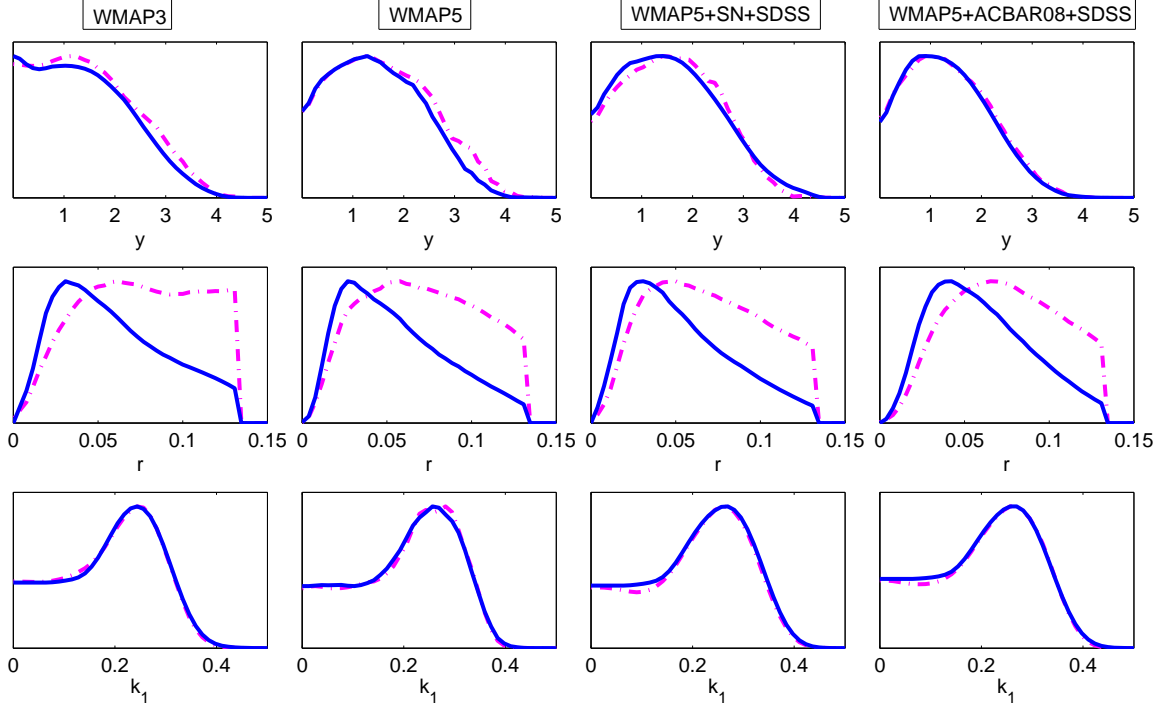


FIG. 35: Marginalized distributions (solid blue lines) and mean likelihoods (magenta dash-dotted lines) for the Λ CDM+fast-roll model, with flat prior on the coupling y and using the dataset shown on top of the columns. The slightly better fitting power of fast-roll over sharp-cut-off may be also seen from fig. 36 where the best fit for the C_ℓ^{TT} multipoles is compared to the experimental data at low ℓ .

the inflaton potential vanishes [14] while the CMB+LSS data analysis for both the Λ CDM+BNI and Λ CDM+TNI models yield **lower bounds** for r as discussed here and in sec. IID 2 [14, 23]. All together, our data analysis shows that the 6-parameter Λ CDM+BNI model is **better** than the standard 6-parameter Λ CDM model.

4. MCMC analysis with Binomial New Inflation including the fast-roll stage: $D_{\mathcal{R}}(k) \neq 0$.

Let us now further develop this argument by considering the quadrupole suppression, avoiding the a priori dismissal based on the simple invocation of cosmic variance or experimental inaccuracy. In the standard Λ CDM model the simplest, purely phenomenological way to decrease the low multipoles is to introduce a infrared sharp cutoff in the primordial power spectrum of the curvature fluctuations. That is, one assumes that $P_{\mathcal{R}}(k) = 0$ for $k < k_{\text{tran}}$ and treats k_{tran} as a new MCMC parameter to be fitted against the data. It is actually not necessary for the moment to include also a cut on the tensor power spectrum, since it would lead to changes certainly not appreciable within the current experimental accuracy.

With this procedure we obtained in ref.[23], using either the WMAP3 data alone or the WMAP3+small scale_CMB+SDSS data:

$$\min \chi_L^2(\Lambda\text{CDM} + \text{sharp cutoff}) - \min \chi_L^2(\Lambda\text{CDM}) \simeq -1.4$$

This result is slightly better than the one reported in ref.[9], but still the likelihood gain hardly compensates the price of a new parameter, especially because its nature appears quite *ad hoc*. Furthermore, the gain in likelihood is sizable smaller when WMAP5+SDSS+SN data are used:

$$\min \chi_L^2(\Lambda\text{CDM} + \text{sharp cutoff}) - \min \chi_L^2(\Lambda\text{CDM}) \simeq -0.9$$

In fig. 34 we plot the marginalized probabilities and mean likelihoods of the seven MCMC parameters plus other standard derived parameters in the WMAP3+small scale_CMB+SDSS case. If any other combination of more recent data such as WMAP5+SN are used, the plots are almost identical. The main point is that there are no significant

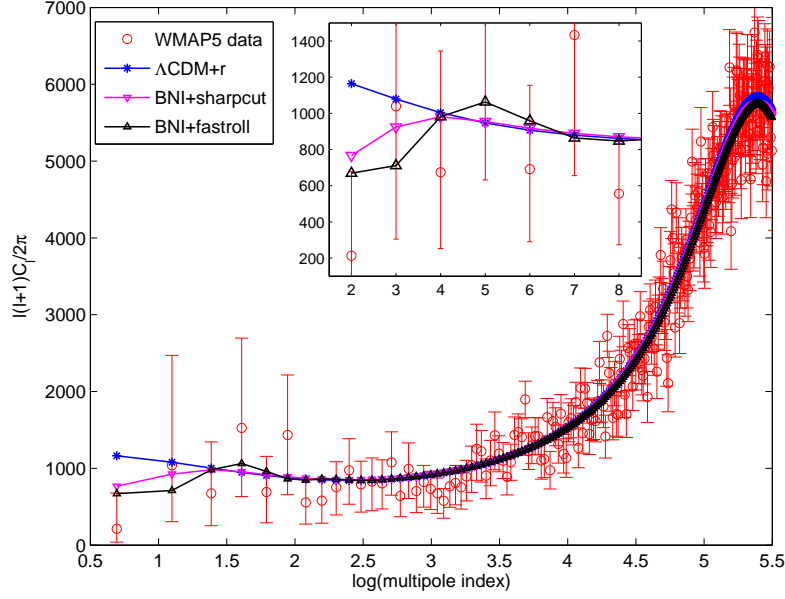


FIG. 36: Comparison, with the experimental WMAP5 data, of the theoretical C_ℓ^{TT} multipoles computed in the best fit point of the various models of the main text, using the WMAP5+SN+SDSS data. The insert contains an enlargement in linear scale of the first seven multipoles. The C_ℓ^{TT} units are $[\mu K^2]$. The error bars in the plotted range of ℓ are mostly due to cosmic variance. Error bars of the WMAP5 data are one-sigma (68%C.L.).

changes from ΛCDM to ΛCDM +sharp cutoff in their common parameters, in either most likely values or marginalized distributions. The distribution of the new cutoff parameter k_{tran} shows a well defined peak centered on its most likely value (ML), which corresponds to today's physical wavelength

$$(k_{\text{tran}})_{\text{ML}} = \begin{cases} 0.291 \text{ (Gpc)}^{-1} & (\text{WMAP3 only}) \\ 0.245 \text{ (Gpc)}^{-1} & (\text{WMAP5+ACBAR08+SDSS}) \\ 0.273 \text{ (Gpc)}^{-1} & (\text{WMAP5+SN+SDSS}) \end{cases} \quad (\Lambda\text{CDM} + \text{sharp cutoff}),$$

that is of the order of today's inverse Hubble radius, as expected.

Introducing the infrared sharp cutoff on $P_{\mathcal{R}}(k)$ in the ΛCDM +BNI model we find similar gains

$$\min \chi_L^2(\Lambda\text{CDM} + \text{BNI} + \text{sharp cutoff}) - \min \chi_L^2(\Lambda\text{CDM} + \text{BNI}) = \begin{cases} -1.4 & (\text{WMAP3}) \\ -1.1 & (\text{WMAP5}) \\ -1.0 & (\text{WMAP5+SN+SDSS}) \\ -0.7 & (\text{WMAP5+ACBAR08+SDSS}) \end{cases}$$

The differences in these gains are partly due to the tighter bound on r provided by the new WMAP5 data and by the SDSS data.

Let us now consider the fast-roll case, when the fast-roll transfer function $D_{\mathcal{R}}(k)$ eq.(2.177) and fig. 28 is used, treating the scale k_{tran} in eq.(2.180) as a MCMC parameter. That is, in the MCMC analysis we use the initial power spectrum eq.(1.156) modified by the fast-roll transfer function $D_{\mathcal{R}}(k)$. We computed once and forever $D_{\mathcal{R}}(k)$ from eq. (2.177) (see fig. 28). $D_{\mathcal{R}}(k)$ is a function of k and k_{tran} with the scaling form eq.(2.180), $\Psi(x)$ being an universal function.

We then find

$$\min \chi_L^2(\Lambda\text{CDM} + \text{BNI} + \text{fastroll}) - \min \chi_L^2(\Lambda\text{CDM} + \text{BNI}) = \begin{cases} -1.8 & (\text{WMAP3}) \\ -1.2 & (\text{WMAP5}) \\ -1.4 & (\text{WMAP5+SN+SDSS}) \\ -1.0 & (\text{WMAP5+ACBAR08+SDSS}) \end{cases}$$

We see that the gains in likelihood are *more significant in the fast-roll case* than in the sharp cutoff case [23]. Clearly, this fit improvement through power modification by fast-roll over power reduction by sharp cutoff is too small to

Λ CDM+BNI+sharp cutoff	k_{tran} (best fit)	n_s (best fit)	r (best fit)	r (95% CL)
WMAP3	0.275 Gpc $^{-1}$	0.960	0.150	> 0.028
WMAP5	0.257 Gpc $^{-1}$	0.961	0.040	> 0.025
WMAP5+SDSS+SN	0.245 Gpc $^{-1}$	0.963	0.048	> 0.022
WMAP5+SDSS+ACBAR08	0.260 Gpc $^{-1}$	0.965	0.060	> 0.029

TABLE V: The most likely values of k_{tran} , n_s , r and the lower bound on r in the Λ CDM+BNI+sharp cutoff model model. We used $N = 50$ in the run with the WMAP3 dataset, while we used $N = 60$ in the other three runs.

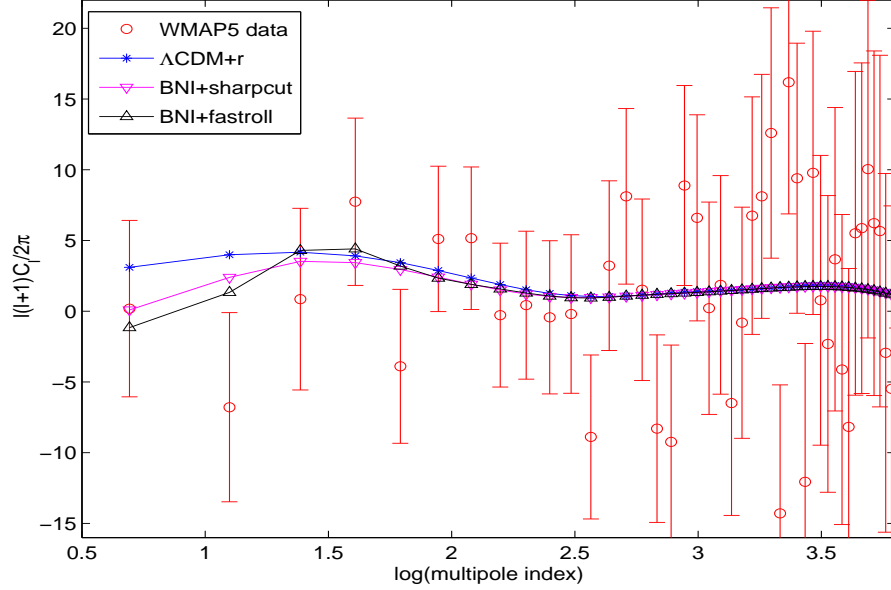


FIG. 37: Comparison, with the experimental WMAP5 data, of the theoretical C_ℓ^{TE} multipoles computed in the best fit point of the Λ CDM+ r model, fast-roll and sharp cutoff models. The C_ℓ^{TE} units are [μK^2]. Error bars of the WMAP5 data are one-sigma (68% c.l.).

constitute a real experimental evidence. But still, it is very interesting that the theoretically well founded approach based on fast-roll inflation works **better** than the purely phenomenological cutoff.

In Table V we report the most likely values (ML) of k_{tran} , n_s and r as well as the 95% CL lower bound on r for the Λ CDM+BNI model with sharp cutoff denoted Λ CDM+BNI+sharp cutoff. In Table VI we do the same when fast-roll is used instead of sharp cutoff. In this case we report also the best fit for the quartic coupling y for future use. In

Λ CDM+BNI+fastroll	k_{tran} (best fit)	n_s (best fit)	r (best fit)	r (95% CL)	y (best fit)
WMAP3	0.249 Gpc $^{-1}$	0.961	0.146	> 0.025	0.03
WMAP5	0.298 Gpc $^{-1}$	0.965	0.056	> 0.024	1.11
WMAP5+SDSS+SN	0.290 Gpc $^{-1}$	0.964	0.051	> 0.023	1.26
WMAP5+SDSS+ACBAR08	0.284 Gpc $^{-1}$	0.963	0.047	> 0.029	1.38

TABLE VI: The most likely values of k_{tran} , n_s , r and the quartic coupling y and the lower bound on r in the Λ CDM+BNI+fast roll model. We set $N = 50$ in the run with the WMAP3 dataset, while we set $N = 60$ in the other three runs.

fig. 35 we plot the probability and mean likelihood distributions of y , r and k_{tran} , with flat prior on the coupling y , in the case of the Λ CDM+BNI+fast-roll model (the plot when a sharp cut is used is almost identical). It is worth noticing that the introduction of the new MCMC parameter k_{tran} typically restores the peak in z (or equivalently in $y = 1 - z - \log z$) that was lost upon setting the asymmetry h to zero in the restriction of the Λ CDM+TNI model to the Λ CDM+BNI model (see the upper row in fig. 35). (The only exception to this rule is when the WMAP3 data alone are used, most likely because WMAP3 does not provide a tight enough upper bound for r , as can be appreciated also from Tables V and

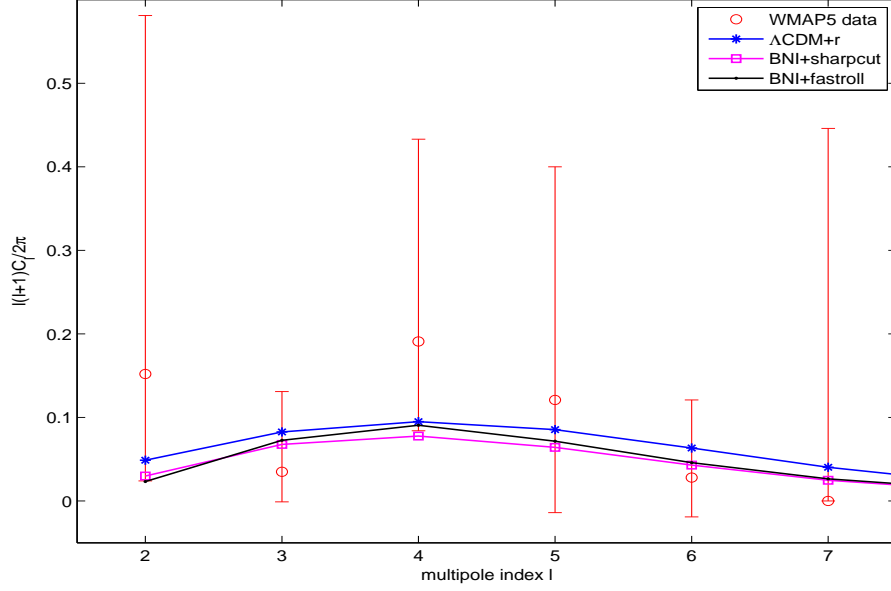


FIG. 38: Comparison, with the experimental WMAP-5 data, of the theoretical C_ℓ^{EE} multipoles computed in the best fit point of the Λ CDM+ r model, fast-roll and sharpcut models as functions of the natural logarithm of ℓ . Error bars of the WMAP-5 data are one-sigma (68% c.l.). Notice that both fast-roll and sharpcut models produce a suppression of the low EE multipoles including the EE quadrupole. The C_ℓ^{EE} units are $[\mu K^2]$.

It must be noticed that in all cases (except for the obsolete WMAP3 alone case), we have $w''(\chi) < 0$ at horizon exit for the best fit values in tables V and VI as follows from eq.(2.15). That is, the best fit corresponds to an inflaton field exiting the horizon in the **negative concavity region** $w''(\chi) < 0$ intrinsic to *new inflation*. The inflaton field at horizon exit takes the value $\varphi_{\text{exit}} \sim 7 M_{Pl}$ as stated in eq. (1.111). Notice that the energy density then is $\sim N M^4 \ll M_{Pl}^4$ well below the Planck energy scale guaranteeing the validity of the effective theory of inflation as discussed in sec. III A.

The slightly better fitting power of fast-roll over sharp-cutoff may be appreciated also from fig. 36 where the best fit for the C_ℓ^{TT} multipoles is compared to the experimental data at low ℓ . We see that the oscillatory form of the fast-roll transfer function $D_{\mathcal{R}}(k)$, by **depressing as well as enhancing** the primordial power spectrum at long wavelengths, leads also to new superimposed **oscillatory corrections** on the multipoles. As far as fitting to current data is concerned, such corrections are more effective than the pure reduction caused by a sharp cutoff.

We plot in fig. 37 the best fit for the C_ℓ^{TE} multipoles compared to the experimental data at low ℓ . We plot in fig. 38 the best fit for the C_ℓ^{EE} multipoles compared to the experimental WMAP-5 data at low ℓ . We see that both fast-roll and sharpcut models produce a suppression of the low EE multipoles including the EE quadrupole.

We did not display in figs. 36 and 37 the Λ CDM+sharp cutoff results since they are indistinguishable from the Λ CDM+BNI+sharp cutoff values.

Our MCMC analysis with the Λ CDM+BNI model predict **non-zero** lower bounds on r : see Tables V and VI. The best fit values of the other cosmological parameters remain practically unchanged as compared to the Λ CDM model. Similarly, their marginalized probability distributions are almost unchanged, with the natural exception of n_s , which in BNI has a theoretical upper limit [see eq. (2.69)].

In the case of the Λ CDM+BNI+fast-roll model with the CMB+LSS datasets, the most likely value of the quartic coupling y is slightly larger than unity. Then from fig. 29 we read a value ~ 14 for the ratio k_{tran}/m at the beginning of inflation.

It is important to notice that the value of $k_Q = 0.238 \text{ (Gpc)}^{-1}$ is **slightly smaller** than the characteristic scale k_{tran} as displayed in Table VI.

A k -mode crosses the horizon when $k = H(t) a(t) = a(\tau) m \sqrt{N} \mathcal{H}(\tau)$. We compute $\ln a$ and ϵ_v at horizon crossing for relevant wavenumbers k using the numerical solution of eqs.(1.89) and (1.92) for $\chi(\tau)$, $\dot{\chi}(\tau)$, $\mathcal{H}(\tau)$ and $\ln a(\tau)$ plus eq.(1.133). We display in Table VII the relevant wavenumbers: k_Q , k_{tran} , k_0 and the number of e-folds since the beginning of inflation when they exit the horizon. We see that the quadrupole modes **exit** the horizon during the fast-roll stage, approximately 2/10 of an e-fold before the end of fast-roll. The mode k_{tran} exit the horizon by

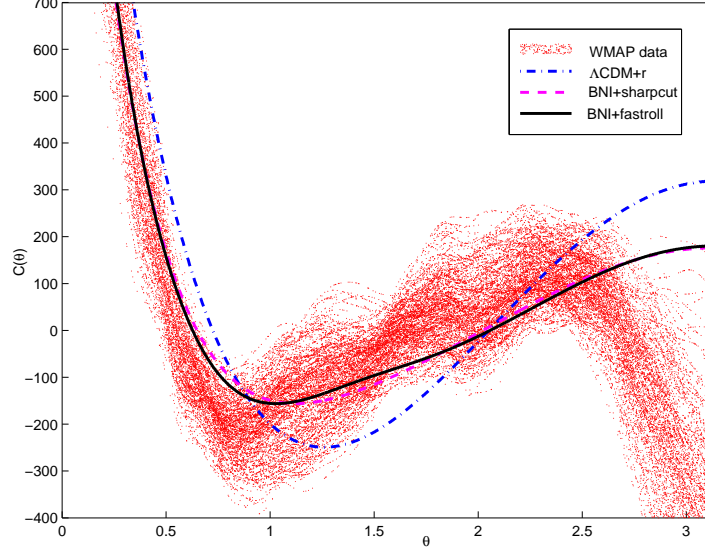


FIG. 39: The real space two point TT correlation function $C^{TT}(\theta)$ for Λ CDM, sharp cutoff and fast-roll models vs. the angle θ . The Λ CDM correlator differs from the two others only for large angles $\theta \gtrsim 1$. Since all l -modes except the lowest ones are practically identical in the three cases, this shows how important are the low multipoles in the large angle correlations. Also shown are the WMAP data. The truly observed correlator runs approximately in the middle of the red band. The width of the data band is mostly due to the cosmic variance. The WMAP $C^{TT}(\theta)$ plotted here may not coincide, especially for the largest values $\theta \sim \pi$, with the correlator directly measured from sky maps due to the pixel weighting in the WMAP data analysis. The $C^{TT}(\theta)$ units are $[\mu K^2]$.

k (today)	$\ln a$ at horizon exit	ϵ_v at horizon exit	k^{init}	ℓ
$k_Q = 0.238 \text{ Gpc}^{-1}$	0.822	$0.038 \gtrsim 1/N$	$1.39 \cdot 10^{14} \text{ GeV}$	2
$k_{tran} = 0.290 \text{ Gpc}^{-1}$	1.024	$0.017 \simeq 1/N$	$1.69 \cdot 10^{14} \text{ GeV}$	~ 2
$k_0 = 2 \text{ Gpc}^{-1}$ (WMAP)	2.97	$0.0031 \lesssim 1/N$	$1.17 \cdot 10^{15} \text{ GeV}$	25
$k = 16.1 \text{ Gpc}^{-1}$	5.06	$0.0033 \lesssim 1/N$	$9.41 \cdot 10^{15} \text{ GeV}$	220
$k_0 = 50 \text{ Gpc}^{-1}$ (CosmoMC)	6.19	$0.0034 \lesssim 1/N$	$2.91 \cdot 10^{16} \text{ GeV}$	510
$k = 0.71 \text{ Mpc}^{-1}$	8.86	$0.0037 \lesssim 1/N$	$4.2 \cdot 10^{17} \text{ GeV}$	10^4

TABLE VII: The number of efolds $\ln a$ since the beginning of inflation till relevant wavevectors exit the horizon and the parameter ϵ_v at horizon exit. k^{init} stands for the value at the beginning of inflation. k_0 's are pivot wavenumbers. ℓ stands for the C_ℓ to which the corresponding k -mode contributes most reentering the horizon. The quadrupole mode k_Q **exits** the horizon during the fast-roll stage, about 0.2 efolds before fast-roll ends. k_{tran} exits the horizon precisely at the **transition** from the fast-roll to the slow-roll stage. We used here eqs.(1.54), (1.64), (1.67), $N_{tot} = 64$ and $\beta \sim 2.5$. Recall that $1/N = 1/60 = 0.0166 \dots$

$\ln a = 1.024$, very close to the point $\ln a = 1.035$ where $\epsilon_v = 1/N$ (see fig. 26). That is, k_{tran} exits the horizon precisely when **fast-roll ends and becomes slow-roll**.

In Table VII we denote by k_0 the pivot scale in the WMAP [9, 10] and CosmoMC codes [43], where the indices n_s , r and the running of n_s are computed. Both k_0 's exit the horizon well inside the slow-roll regime.

5. Real Space Two Point TT-Correlator

We display in fig. 39 the real space two point TT-correlation function $C^{TT}(\theta)$ for Λ CDM, sharp cutoff and fast-roll models [23],

$$C^{TT}(\theta) = \frac{1}{4\pi} \sum_{l=2}^{\infty} (2l+1) C_l^{TT} P_l(\cos \theta) .$$

We see that the Λ CDM correlator becomes really different from the two others only for large angles $\theta \gtrsim 1$. Since all l -modes except the lowest ones are practically identical in the three cases, this shows how dominant are the low multipoles in the large angle correlations. We also show the WMAP data, the width of the data is mostly due to the cosmic variance.

As is clear from fig. 39, both fast-roll and sharp cutoff models reproduce the two point correlator $C^{TT}(\theta)$ better than the pure slow-roll Λ CDM+ r model.

6. Conclusions

The best values for the ratio and spectral index including the early fast-roll stage are given by the WMAP5+SN+SDSS line of Table VI: $r = 0.051$, $n_s = 0.964$ and $y = 1.26$.

Fast-roll provides a slightly better fit than a sharp cutoff both for the C_ℓ^{TT} and the C_ℓ^{TE} coefficients. Besides reproducing the quadrupole suppression, the fast-roll fit accounts for the oscillations of the lower multipole data.

We get the following picture of the inflationary universe explaining the quadrupole suppression from the effective (Ginsburg-Landau) theory of inflation combined with MCMC simulations of CMB+LSS data. A fast-roll stage lasting about one efold is followed by a slow-roll stage lasting ~ 63 efolds [see sec. ID 4]. After these $\sim 63 + 1 = 64$ inflation efolds, the radiation dominated era follows. The quadrupole modes exit the horizon **during** the fast-roll stage about 0.8 efold after the beginning of inflation and are therefore **suppressed** compared with the modes exiting the horizon later during the slow-roll stage.

The fast-roll stage explains the quadrupole suppression and **fixes the total number of efolds** of inflation to be $N_{tot} \simeq 64$ as shown in sec. ID 4.

III. QUANTUM LOOP CORRECTIONS

A. The domain of validity of the effective theory of inflation.

We discuss in the subsections below the validity domain of the effective theory of inflation focusing on three regimes where corrections could be expected: a) large (transplanckian) values of the inflaton field, b) large k fluctuation modes (transplanckian modes), c) parametric and spinodal resonant fluctuation modes.

We consider in this review the inflaton with the canonical kinetic term

$$X = \frac{\dot{\varphi}^2}{2} - \frac{(\nabla\varphi)^2}{2a^2(t)}.$$

Lagrangeans with general functions of X has been considered in the literature [57]. Since X has mass dimension fourth, these Lagrangeans introduce at least one new dimensionful parameter μ . The corrections to the canonical kinetic case will be in the Ginsburg-Landau context of the order

$$\mathcal{O}\left(\frac{M^4}{\mu^4}\right),$$

since $X \sim M^4$ during inflation (see sec. ID 2). Moreover, it must be $\mu \sim M_{Pl}$ in the Ginsburg-Landau context since M_{Pl} is the only available dimensionful parameter here. [$\mu \sim M$ is excluded since the dominant kinetic term is always canonical in Ginsburg-Landau effective theory.] Therefore, the observable effects of non-canonical kinetic terms in the Ginsburg-Landau effective theory are of the order

$$\mathcal{O}\left(\frac{M^4}{M_{Pl}^4}\right) \sim 10^{-11},$$

and can be safely neglected.

1. Large Inflaton Fields

It is sometimes stated that the validity of the effective field theory of inflation entails that

$$\frac{\varphi}{M_{Pl}} \ll 1. \quad (3.1)$$

From this stringent constraint on the validity of an effective field theory bounds on r have been proposed [46].

The validity of the constraint eq.(3.1) suggested that effective field theory predicts values of $r \ll 1$ probably too small to be observed in the next generation of CMB experiments [47]. Alternatively if larger values of r are measured then this would entail a breakdown of the effective field theory approach to inflation.

This line of reasoning is incorrect for three different but complementary reasons:

- The validity of an effective field theory expansion **does not** rely on $\varphi/M_{Pl} \ll 1$, instead it relies on a wide separation between the energy scale of inflation and the higher energy scale of the underlying microscopic theory. If the effective field theory emerges from integrating out degrees of freedom at the GUT scale, then $H/M_{GUT} \sim 10^{-2}$, if such scale is instead the Planck scale then $H/M_{Pl} \sim 10^{-5}$, and in either case an effective field theory description is valid. Indeed, detailed calculations discussed in secs. IIIB and IIIC reveal that the quantum corrections to slow-roll inflation are of the order $(H/M_{Pl})^2$ [19, 20, 42]. Any breakdown of an effective field theory is typically manifest in large quantum corrections but the results of [19, 20, 42] presented in secs. IIIB and IIIC unambiguously point out that quantum corrections are well under control for $H/M_{Pl} \ll 1$. This provides a reassuring confirmation of the validity of the effective field theory for a scale of inflation consistent with the WMAP data.
- Three simple examples highlight that the criterion $\varphi/M_{Pl} \ll 1$ *cannot* be the deciding factor for the reliability of the effective field theory: consider the following series

$$\sum_{p=0}^{\infty} (-1)^p \left(\frac{\varphi}{M_{Pl}} \right)^{2p} = \frac{1}{1 + \left(\frac{\varphi}{M_{Pl}} \right)^2} \quad (3.2)$$

$$\sum_{p=0}^{\infty} \frac{(-1)^p}{(2p)!} \left(\frac{\varphi}{M_{Pl}} \right)^{2p} = \cos \left(\frac{\varphi}{M_{Pl}} \right) \quad (3.3)$$

$$\sum_{p=0}^{\infty} \left(\frac{\varphi}{M_{Pl}} \right)^{2p} = \frac{1}{1 - \left(\frac{\varphi}{M_{Pl}} \right)^2} . \quad (3.4)$$

The sum of both series (3.2) and (3.3) is perfectly well defined for $\varphi > M_{Pl}$. In particular, the series (3.3) is a prototype for an axion-type potential [48], while certainly the series (3.4) breaks down for $\varphi \sim M_{Pl}$. The series (3.2)-(3.3) do not feature any real singularity in the variable φ/M_{Pl} whereas eq.(3.4) has a singularity at $\varphi = M_{Pl}$. These elementary examples highlight that what constrains the reliability of the effective field theory description of the inflationary potential is *not* the value of the ratio φ/M_{Pl} but the position of the *singularities* as a function of this variable. These singularities are determined by the large order behavior of the *coefficients* in the series. If the series has a non-zero radius of convergence or if it is just Borel summable, it defines the potential $V(\varphi)$ **uniquely**. Clearly, a thorough knowledge of the radius of convergence of the series in the effective field theory requires a detailed knowledge of the underlying microscopic theory. However, it should also be clear that the requirement $\varphi/M_{Pl} \ll 1$ is overly restrictive in general.

- One of the main results of ref.[11] (see sec. ID 2) is that the combination of WMAP data and slow-roll expansion suggest the universal form of the inflation potential eqs.(1.83)-(1.84). Even in the case when the coefficients in a χ -series expansion of $w(\chi)$ lead to a breakdown of the series at $\chi \sim 1$, namely at $\varphi \sim \sqrt{N} M_{Pl}$, there is still room for values of $M_{Pl} < \varphi < \sqrt{N} M_{Pl}$ for which the series would be reliable. However, no *a priori* physical reason for such a breakdown can be inferred without a reliable calculation of the effective field theory from a microscopic fundamental theory. Therefore, we expect that the effective field theory potential $V(\varphi) = N M^4 w(\chi)$ would be reliable *at least* up to $\varphi \sim \sqrt{N} M_{Pl}$ and most generally for values $\chi \gg 1$ and hence $\varphi \gg M_{Pl}$.

As mentioned above, the studies in ref.[19, 20, 42] reveal that quantum corrections in the effective field theory yields an expansion in $(H/M_{Pl})^2$ for *general inflaton potentials*. This indicates that the use of the inflaton potential $V(\varphi)$ from effective field theory is consistent for

$$\left(\frac{H}{M_{Pl}} \right)^2 \ll 1 \quad \text{and hence} \quad V(\varphi) \ll M_{Pl}^4 .$$

We find using eqs.(1.83)-(1.84):

$$w(\chi) \ll \frac{1}{N} \left(\frac{M_{Pl}}{M} \right)^4 \sim \frac{1}{N} 10^{12} . \quad (3.5)$$

This condition yields an **upper bound** in the inflaton field φ depending on the large field behaviour of $w(\chi)$. We find for relevant behaviours of the inflaton potential the following upper bounds on χ and φ :

$$\begin{aligned}
w(\chi) \stackrel{\chi \gg 1}{\simeq} \chi^2 & : \quad \chi \ll \frac{10^6}{\sqrt{N}} \quad , \quad \varphi \ll 10^6 M_{Pl} \\
w(\chi) \stackrel{\chi \gg 1}{\simeq} \chi^4 & : \quad \chi \ll \frac{10^3}{N^{\frac{1}{4}}} \quad , \quad \varphi \ll 2783 M_{Pl} \quad \text{for } N \simeq 60 \\
w(\chi) \stackrel{\chi \gg 1}{\simeq} \chi^n & : \quad \chi \ll \left(\frac{10^{12}}{N} \right)^{\frac{1}{n}} \quad , \quad \varphi \ll 10^{\frac{12}{n}} N^{\frac{1}{2} - \frac{1}{n}} M_{Pl} \\
w(\chi) \stackrel{\chi \gg 1}{\simeq} e^\chi & : \quad \chi \ll 12 \ln 10 - \ln N = 23.54 \quad , \quad \varphi \ll 182 M_{Pl} \quad \text{for } N \simeq 60 .
\end{aligned} \tag{3.6}$$

We see that the effective field theory is **consistent** for values of the inflaton field well **beyond** the Planck mass even for very steep potentials, such as the exponential function e^χ .

We remark that the arguments presented above suggest that the reluctance to use the inflaton potential $V(\varphi)$ for $\varphi \gtrsim M_{Pl}$ arises from a prejudice which is unwarranted under the most general circumstances, unless of course, the inflaton potential features singularities. The true upper bound for the validity of the effective field theory description of inflation is $V(\varphi) \ll M_{Pl}^4$ which in fairly general cases allows large values of $\frac{\varphi}{M_{Pl}}$ as emphasized by eqs.(3.6).

2. Transplanckian and Resonant Fluctuation Modes.

Fluctuation modes can have large wavenumbers going beyond the Planck mass. The question is whether such large k modes can have observable effects through the primordial power on CMB anisotropies.

The analysis presented in sec. ID gives for the cosmologically relevant modes the window eq.(1.55) where $\beta \sim 2$ according to the best fit eq.(2.24). Hence, the upper limit in eq.(1.55) becomes $\simeq 7 \times 10^{18} e^{N_{tot}-64}$ GeV just above the Planck mass for $N_{tot} \sim 64$.

Moreover, the CMB multipoles $\ell < 200$ where features have been observed [8, 9, 10], are definitely sub-Planckian for $N_{tot} \sim 64$ since they have $k < 4 \times 10^{16} e^{N_{tot}-64}$ GeV according to eqs.(1.64) and (1.67).

Inflaton modes with $k \sim m$ often exhibit resonant exponential growth just after the beginning of inflation [25, 26, 29]. This phenomena arises from spinodal or parametric instabilities in new and chaotic inflation, respectively. One can wonder whether such exponential mode growth can have observable consequences through the CMB spectrum. Since $m \simeq 10^{13}$ GeV [eq.(2.24)], these potentially growing modes are **below** the lower end $k^{init} \simeq 30 m$ of the observable window eq.(1.55) for $N_{tot} > 61$. It should be recalled that the nonlinear backreaction soon shuts off these instabilities [25, 29]. In addition, these instabilities are unimportant in the thermalization process in classical field theory [31].

B. Quantum Loop Corrections to the Inflaton Dynamics

The study of quantum corrections to the inflaton dynamics is necessary to establish the validity of slow-roll inflation as a reliable effective field theory description and in addition, it is important to understand novel phenomena associated with quantum loop corrections in an expanding cosmology.

We study several novel aspects of quantum fluctuations that **do not have counterpart** in Minkowski space-time. This study also leads to the conclusion that there is a small parameter $(H/M_{Pl})^2 \sim 10^{-9}$ (where H is the Hubble parameter during inflation), which emerges: this small ratio determines the magnitude of the quantum corrections. The reliability of the effective field theory approach is then a consequence of the smallness of this ratio during slow roll inflation.

1. Quantum Decay Rate

Particle production and decay are of fundamental importance in cosmology. Most of the treatments of particle decay in cosmology rely on the concept of the decay rate of a particle in Minkowski space time. The framework for obtaining the decay rate in Minkowski space time is the usual S-matrix approach or at a more fundamental level Fermi's golden rule which manifestly makes use of the energy-momentum conservation resulting in reaction thresholds [87]. In an expanding cosmology there is no global time-like Killing vector and energy is not conserved, although in

an isotropic and homogeneous cosmology momentum is conserved. The lack of energy conservation implies major modifications in the kinematics for decay since there are no longer reaction thresholds. Furthermore, the S-matrix theory based on the in-out formulation of quantum field theory is ill-suited to study time dependent phenomena in an expanding cosmology and a completely different approach is needed to understand particle production and decay. The non-equilibrium quantum field theory provides a systematic set of tools to study precisely such phenomena. Linear response is specially suited to study relaxation phenomena in general and is tailored to study particle decay in particular. The strategy is to study the effective equations of motion for the expectation value of the fields in presence of an external source as an initial value problem. An external source prepares the initial expectation value, which upon switching off the source relaxes towards equilibrium. According whether the field expectation value decays exponentially with time or not, the dynamics of relaxation is described by a decay rate or by some alternative concept.

In ref.[42] we study the quantum decay of a particle into other particles during inflation. The decaying particle could be the inflaton but our study is more general. In this section we provide an understanding of the concept of decay of a particle in a rapidly expanding cosmology. We introduce and implement a method that allows a systematic and unambiguous study of the relaxational dynamics of quantum fields and in particular allows to extract the decay law resulting from interactions.

In Minkowski space-time there are two alternative but equivalent manners to define the decay rate of a particle: (i) the total decay rate as the inclusive transition probability *per unit time* from an initial 'in' state to final 'out' states, (ii) the total decay rate as the imaginary part of the space-time Fourier transform of the self-energy of the particle evaluated on the particle's mass shell and divided by its mass-shell energy. Both definitions are equivalent by dint of the optical theorem, or alternatively, unitarity. The calculation of a total decay rate from definition (i) involves calculating the transition amplitude from some initial time $t_i \rightarrow -\infty$ to a final time $t_f \rightarrow +\infty$ and multiplying by its complex conjugate. In Minkowski space-time the transition amplitude from an asymptotic state in the past to an asymptotic state in the future is proportional to an energy conserving delta function. In squaring the amplitude, the square of this delta function is interpreted as the total time (T) elapsed in the reaction multiplying an energy conserving delta function. Dividing by the total time (T) of the reaction one extracts the decay rate.

The calculation of the decay rate from the total width via definition (ii) requires that the self-energy be a function of the time difference and invokes energy-momentum conservation at each interaction vertex. The space-time Fourier transform of the self-energy features branch cut singularities in the complex frequency plane and the imaginary part across these cuts at the position of the particle mass shell gives the decay width or decay rate [87].

The important point in this discussion is that in the two cases above referred the concept of a decay rate relies heavily on energy (and momentum) conservation. Therefore, the concept of a decay rate (an inclusive transition probability per unit time) may not have a translation to rapidly expanding cosmologies where there is no global timelike Killing vector associated with conservation of energy even when there may be space-like Killing vectors associated with spatial translational symmetries and momentum conservation. Such is the case for spatially flat FRW cosmologies. The manifest lack of energy conservation in an expanding cosmology makes possible processes that are forbidden in static space-times by energy conservation. In addition, contrary to Minkowski spacetime, cosmological modes in general do not decay exponentially with time, therefore the definition of the decay rate requires the kind of analysis we provide here.

The method:

Particle decay in de Sitter space-time was studied in reference [64] for some very special cases that allowed a solution of the equation of motion. In ref.[42] we introduced a method that allows to study the relaxation of quantum fields and particle decay in great generality. The main strategy is to study the effective equations of motion of the expectation values of fields as an initial value problem in linear response including the self-energy corrections. The solution of the equations of motion lead to an unambiguous identification of the decay law from the relaxation of the amplitude of the field as a consequence of the self-energy corrections (interactions). When self-energy corrections are included the equations of motion become non-local (non-Markovian) and cannot be solved in general in closed form.

When a perturbative solution of the equations of motion is attempted there emerge *secular terms*, namely terms that grow in time and invalidate the perturbative expansion. These secular terms indicate precisely the relaxation (or production) time scales. We implement the dynamical renormalization group introduced in [65] to provide a systematic resummation of these secular terms leading to the correct description of relaxation and decay. Such program has been successfully applied to a wide variety of non-equilibrium situations in Minkowski space time (see [65] and references therein).

In ref.[65] we study the relaxation of the expectation value of quantum fields as an initial value problem. In ref.[42], we illustrate its application and study the decay of a massive particle (it could be the inflaton) coupled to conformally coupled massless particles via a trilinear vertex in de Sitter space time.

This simple setting allows to present the main aspects of the program and reveal the important features associated with the expansion in a clear manner. The relaxation and decay law is studied to lowest order in the coupling both for

wavelengths that are inside and outside the Hubble radius during inflation. The decay constant for superhorizon modes have an interesting interpretation in terms of the Hawking temperature of de Sitter space-time. After extracting the decay law to lowest order in the loop expansion for the self-energy, we show that the limit of Minkowski space-time reproduces the known Minkowski space-time decay rates. In all cases we find that the decay is *enhanced* during inflation as compared to the Minkowski space-time result. The decay law for modes deep within the horizon feature a wavevector dependence that leads to a larger suppression of the amplitude for longer wavelengths [42].

We begin by studying in refs. [42] the general case of a cubic interaction of scalar particles minimally coupled to gravity, allowing the decay of one field into two others during de Sitter inflation. The masses of all particles are much smaller than the Hubble constant, which leads to a strong infrared behavior in the self-energy loops. We introduce an expansion in terms of the small parameter M^2/H^2 , where $M \ll H$ is the mass of the particle in the quantum loop, which naturally regulates the infrared behavior.

Long-time divergences associated with secular terms in the solutions of the equations of motion are systematically resummed by implementing the DRG introduced in ref.[65] and lead to the decay law. We then apply these general results to the case of quasi-de Sitter slow-roll inflation. We show that in this case a similar small parameter emerges which is a simple function of slow-roll parameters and regulates the infrared behavior *even* for massless particles. We study the decay of superhorizon fluctuations as well as of fluctuations with wavelengths deep inside the horizon. A rather striking aspect is that a particle **can decay** into *itself* precisely as a consequence of the lack of energy conservation in a rapidly expanding cosmology. We then focus on studying the decay of the inflaton quantum fluctuations into their *own quanta*, namely the *self-decay* of the inflaton fluctuations, discussing the potential implications on the power spectra of primordial perturbations and on non-gaussianity.

Our main results on quantum decay rate go as follows [42]:

- In the case of de Sitter inflation for particles with mass $M \ll H$ a small parameter $\sim M^2/H^2$ regulates the infrared regime. We introduce an expansion in this small parameter M^2/H^2 akin to the ε expansion in dimensionally regularized critical theories [83]. After implementing the DRG resummation, we obtain the decay laws in a M^2/H^2 expansion.
- Minimally coupled particles decay *faster* than those conformally coupled to gravity due to the strong infrared behavior both for superhorizon modes as well as for modes with wavelengths well inside the Hubble radius.
- The decay of short wavelength modes, those inside the horizon during inflation, is *enhanced* by soft collinear *bremsstrahlung radiation of superhorizon quanta* which becomes the dominant decay channel for the physical wave vectors which obey,

$$k_{ph}(\eta) \lesssim \frac{H}{\eta_v - \epsilon_v} = \frac{2 H}{n_s - 1 + \frac{1}{4} r} , \quad (3.7)$$

where η_v , ϵ_v are the slow-roll parameters eq.(1.131).

- Expanding cosmologies allow processes that are forbidden in Minkowski space-time by energy conservation [42, 66]: in particular, for particle masses $\ll H$, *kinematic thresholds* are absent allowing a particle to decay into *itself*. Namely, the *self-decay* of quantum fluctuations is a feature of an interacting theory in a rapidly expanding cosmology. A self-coupling of the inflaton leads to the self-decay of its quantum fluctuations both for modes inside as well as *outside* the Hubble radius.
- The results obtained in de Sitter space-time directly apply to the *self decay* of the quantum fluctuations of the inflaton during slow-roll (quasi de Sitter) expansion. In this case, a simple linear combination of slow-roll parameters regulates the infrared. For superhorizon modes we find that the amplitude of the inflaton quantum fluctuations relaxes as a power law η^Γ in conformal time η where Γ is the decay rate. To lowest order in slow-roll, we find Γ completely determined by the slow roll parameters and the amplitude of the power spectrum of curvature perturbations $\Delta_{\mathcal{R}}^2$ eq.(1.164):

$$\Gamma = \frac{8 \xi_v^2 \Delta_{\mathcal{R}}^2}{(\epsilon_v - \eta_v)^2} [1 + \mathcal{O}(\epsilon_v, \eta_v)] \quad (3.8)$$

where ξ_v , η_v , ϵ_v are the slow-roll parameters eqs.(1.131), (1.172) and (1.173). As a consequence, the growing mode which dominates at late time evolves as

$$\frac{\eta^{\eta_v - \epsilon_v + \Gamma}}{\eta} . \quad (3.9)$$

featuring an *anomalous dimension* Γ slowing down the growth of the dominant mode.

The decay of the inflaton quantum fluctuations with wavelengths deep within the Hubble radius during slow-roll inflation is **enhanced** by the infrared behavior associated with the collinear emission of ultrasoft quanta, namely *bremstrahlung radiation of superhorizon fluctuations*. The decay hastens as the physical wavelength approaches the horizon because the phase space for the emission of superhorizon quanta opens up as the wavelength nears horizon crossing.

- We discuss the implications of these results for scalar and tensor perturbations, and establish a connection with previous calculations of non-gaussian correlations.

2. Particle decay in inflationary cosmology

Let us first consider a simple model of two quantum scalar fields ϕ and φ with masses M and m , respectively, in an expanding FRW background minimally coupled to gravity with a cubic coupling $g \phi \varphi^2$. This is a paradigm to study the decay $\phi \rightarrow \varphi \varphi$ and the action for the model in cosmic time is

$$A = \int d^3x dt a^3(t) \left\{ \frac{1}{2} \dot{\phi}^2 - \frac{(\nabla\phi)^2}{2a^2} - \frac{1}{2} (M^2 + \xi_\chi \mathcal{R}) \phi^2 + \frac{1}{2} \dot{\varphi}^2 - \frac{(\nabla\varphi)^2}{2a^2} - \frac{1}{2} (m^2 + \xi_\delta \mathcal{R}) \varphi^2 - g \phi \varphi^2 + J(t) \phi \right\} \quad (3.10)$$

with

$$\mathcal{R} = 6 \left(\frac{\ddot{a}}{a} + \frac{\dot{a}^2}{a^2} \right) \quad (3.11)$$

being the Ricci scalar and ξ an arbitrary coupling to the Ricci scalar: $\xi = 0$ corresponds to minimal coupling and $\xi = 1/6$ corresponds to conformal coupling. The source $J(t)$ induces an expectation value of the field ϕ and allows to set up an initial value problem for its dynamics. In this case, neither ϕ nor φ are the inflaton.

It is convenient to pass to conformal time η [eq.(1.20)] and introduce a conformal rescaling of the fields,

$$a(t) \phi(\vec{x}, t) = \chi(\vec{x}, \eta) \quad , \quad a(t) \varphi(\vec{x}, t) = \delta(\vec{x}, \eta) \quad .$$

The action becomes (after discarding surface terms that will not change the equations of motion)

$$A[\chi, \delta] = \frac{1}{2} \int d^3x d\eta \left\{ \frac{1}{2} [\chi'^2 - (\nabla\chi)^2 - \mathcal{M}_\chi^2(\eta) \chi^2 + \delta'^2 - (\nabla\delta)^2 - \mathcal{M}_\delta^2(\eta) \delta^2] - ga(\eta) \chi \delta^2 - a^3(\eta) J(\eta) \chi \right\} , \quad (3.12)$$

with primes denoting derivatives with respect to conformal time η and

$$\mathcal{M}_\chi^2(\eta) = \left(M^2 + \xi_\chi \mathcal{R} \right) a^2(\eta) - \frac{a''(\eta)}{a(\eta)} \quad , \quad \mathcal{M}_\delta^2(\eta) = \left(m^2 + \xi_\delta \mathcal{R} \right) a^2(\eta) - \frac{a''(\eta)}{a(\eta)} \quad , \quad (3.13)$$

For inflationary cosmology the scale factor describes a de Sitter space-time, namely

$$a(t) = e^{Ht} \quad ; \quad a(\eta) = -\frac{1}{H\eta} \quad , \quad (3.14)$$

with H the Hubble constant. The Heisenberg equations of motion for the spatial Fourier modes of wavevector k of the fields in the non-interacting ($g = 0$) and source-free [$J(\eta) = 0$] theory are given by

$$\begin{aligned} \chi''_{\vec{k}}(\eta) + \left[k^2 - \frac{1}{\eta^2} \left(\nu_\chi^2 - \frac{1}{4} \right) \right] \chi_{\vec{k}}(\eta) &= 0 \quad ; \quad \delta''_{\vec{k}}(\eta) + \left[k^2 - \frac{1}{\eta^2} \left(\nu_\delta^2 - \frac{1}{4} \right) \right] \delta_{\vec{k}}(\eta) = 0 \quad , \\ \nu_\chi^2 &= \frac{9}{4} - \left(\frac{M^2}{H^2} + 12 \xi_\chi \right) \quad ; \quad \nu_\delta^2 = \frac{9}{4} - \left(\frac{m^2}{H^2} + 12 \xi_\delta \right) . \end{aligned} \quad (3.15)$$

The spatial Fourier transform of the free field Heisenberg operators $\chi_{\vec{k}}(\eta)$, $\delta_{\vec{k}}(\eta)$ are therefore written as

$$\chi_{\vec{k}}(\eta) = \alpha_{\vec{k}} g_{\nu_\chi}(k; \eta) + \alpha_{-\vec{k}}^\dagger g_{\nu_\chi}^*(k; \eta) \quad , \quad \delta_{\vec{k}}(\eta) = \beta_{\vec{k}} g_{\nu_\delta}(k; \eta) + \beta_{-\vec{k}}^\dagger g_{\nu_\delta}^*(k; \eta) \quad ,$$

where the Heisenberg operators $\alpha_{\vec{k}}$, $\alpha_{\vec{k}}^\dagger$ and $\beta_{\vec{k}}$, $\beta_{\vec{k}}^\dagger$ obey the usual canonical commutation relations eq.(1.122). The mode functions $g_\nu(k, \eta)$ with Bunch-Davis boundary conditions are given by eq.(1.137).

The equation of motion for the expectation value of the field χ is obtained by writing

$$\chi_{\vec{k}}(\eta) = X_{\vec{k}}(\eta) + \sigma_{\vec{k}}(\eta) \quad ; \quad \langle \chi_{\vec{k}}(\eta) \rangle = X_{\vec{k}}(\eta) \quad ; \quad \langle \sigma_{\vec{k}}(\eta) \rangle = 0. \quad (3.16)$$

in the above expressions $\langle \cdots \rangle$ stand for expectation values in the initial state which is prepared by switching on the external source term J to displace the field and switching the source off to let the field evolve. This is the usual method to prepare an initial value problem in linear response. Implementing the condition $\langle \sigma_{\vec{k}}(\eta) \rangle = 0$ order by order in an expansion in the coupling g yields the equation of motion including the self-energy to the given order. Up to one loop order we obtain

$$X_{\vec{k}}''(\eta) + [k^2 + \mathcal{M}_\chi^2(\eta)] X_{\vec{k}}(\eta) + 2g^2 a(\eta) \int_{\eta_0}^{\eta} d\eta' a(\eta') \mathcal{K}_k(\eta, \eta') X_{\vec{k}}(\eta') = 0. \quad (3.17)$$

The Feynman diagram for the self energy kernel \mathcal{K}_k is depicted in fig. 40. In the general case the self-energy kernel is a complicated non-local function of η, η' , but it simplifies in the case when the φ particles are massless and conformally coupled to gravity, in which case

$$g_{\nu_\delta}(k; \eta) = \frac{1}{\sqrt{2k}} e^{-i k \eta} \quad (3.18)$$

and the non-local kernel is given by

$$\mathcal{K}_k(\eta, \eta') = \int \frac{d^3 q}{(2\pi)^3} \frac{\sin[(q + |\vec{k} + \vec{q}|)(\eta - \eta')]}{2q|\vec{k} + \vec{q}|} = -\frac{1}{8\pi^2} \cos[k(\eta - \eta')] \mathcal{P}\left(\frac{1}{\eta - \eta'}\right) \quad (3.19)$$

where \mathcal{P} stands for the principal part. We *define* the principal part prescription as follows

$$\mathcal{P}\left(\frac{1}{\eta - \eta'}\right) \equiv \frac{\eta - \eta'}{(\eta - \eta')^2 + (\epsilon \eta')^2} = \frac{1}{2} \left[\frac{1}{\eta - \eta' + i\epsilon \eta'} + \frac{1}{\eta - \eta' - i\epsilon \eta'} \right] \quad ; \quad \epsilon \rightarrow 0^+ \quad (3.20)$$

This prescription for the principal part regulates the short distance divergence in the operator product expansion with a dimensionless infinitesimal quantity ϵ independent of time. Although the equation of motion (3.17) is linear, it is non-local and a general solution is unavailable. However for weak coupling g^2 a perturbative solution can be found by writing

$$X_{\vec{k}}(\eta) = \sum_{n=0}^{\infty} (g^2)^n X_{n, \vec{k}}(\eta), \quad (3.21)$$

leading to the hierarchy of coupled equations

$$X_{0, \vec{k}}''(\eta) + \left[k^2 - \frac{1}{\eta^2} \left(\nu_\chi^2 - \frac{1}{4} \right) \right] X_{0, \vec{k}}(\eta) = 0, \quad (3.22)$$

$$X_{n, \vec{k}}''(\eta) + \left[k^2 - \frac{1}{\eta^2} \left(\nu_\chi^2 - \frac{1}{4} \right) \right] X_{n, \vec{k}}(\eta) = \mathcal{R}_n(k; \eta) \quad ; \quad n = 1, 2, \dots \quad (3.23)$$

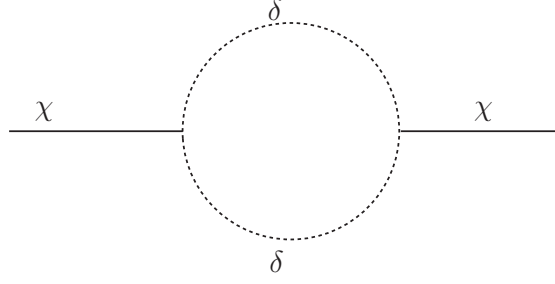
$$\mathcal{R}_n(k; \eta) = -2 a(\eta) \int_{\eta_0}^{\eta} d\eta' a(\eta') \mathcal{K}_k(\eta, \eta') X_{n-1, \vec{k}}(\eta'). \quad (3.24)$$

The hierarchy can be solved order by order by introducing the retarded Green's function

$$\mathcal{G}(k; \eta, \eta') = i \left[g_{\nu_\chi}(k; \eta) g_{\nu_\chi}^*(k; \eta') - g_{\nu_\chi}^*(k; \eta) g_{\nu_\chi}(k; \eta') \right] \Theta(\eta - \eta'). \quad (3.25)$$

Hence the solution of the hierarchy of equations for $n \geq 1$ is given by

$$X_{n, \vec{k}}(\eta) = \int_{\eta_0}^{\eta} d\eta' \mathcal{G}(k; \eta, \eta') \mathcal{R}_n(k; \eta'). \quad (3.26)$$

FIG. 40: Self energy loop of δ particles (dashed lines).

Superhorizon modes: $k = 0$ In this case the solution to the equation of motion at zeroth order as

$$X_{0,\bar{0}}(\eta) = a (-\eta)^{\beta_+} + b (-\eta)^{\beta_-}, \quad (3.27)$$

where a and b are constant coefficients and

$$\beta_{\pm} = \frac{1}{2} \pm \nu_{\chi}, \quad \nu_{\chi} = \sqrt{\frac{9}{4} - \frac{M^2}{H^2}}. \quad (3.28)$$

The retarded Green's function Eq.(3.25) necessary to solve the hierarchy of coupled equations, for $k = 0$ is given by

$$\mathcal{G}(\eta, \eta') = \frac{\sqrt{\eta \eta'}}{2 \nu_{\chi}} \left[\left(\frac{\eta'}{\eta} \right)^{\nu_{\chi}} - \left(\frac{\eta}{\eta'} \right)^{\nu_{\chi}} \right] \Theta(\eta - \eta'). \quad (3.29)$$

The first order correction $X_{1,\bar{0}}(\eta)$ is given by

$$\begin{aligned} X_{1,\bar{0}}(\eta) = & -\frac{1}{2 (2 \pi H)^2 \nu_{\chi}} \left(a (-\eta)^{\beta_+} \left\{ [\log \epsilon + \gamma + \psi(1 - \beta_+)] \log \frac{\eta}{\eta_0} + \text{non-secular} \right\} \right. \\ & \left. - b (-\eta)^{\beta_-} \left\{ [\log \epsilon + \gamma + \psi(1 - \beta_-)] \log \frac{\eta}{\eta_0} + \text{non-secular} \right\} \right), \end{aligned} \quad (3.30)$$

where the non-secular terms are terms **bounded** in the limit $\eta \rightarrow 0$. Therefore, to first order in the coupling we find the solution of the equation of motion for the $k = 0$ mode to be given by

$$\begin{aligned} X_0(\eta) = & a (-\eta)^{\beta_+} \left(1 - \frac{g^2}{2 (2 \pi H)^2 \nu_{\chi}} \left\{ [\log \epsilon + \gamma + \psi(\beta_-)] \log \frac{\eta}{\eta_0} + \text{non-secular} \right\} \right) + \\ & + b (-\eta)^{\beta_-} \left(1 + \frac{g^2}{2 (2 \pi H)^2 \nu_{\chi}} \left\{ [\log \epsilon + \gamma + \psi(\beta_+)] \log \frac{\eta}{\eta_0} + \text{non-secular} \right\} \right). \end{aligned} \quad (3.31)$$

where we used that $\beta_+ + \beta_- = 1$ [eq.(3.28)]. Obviously the **secular** terms, namely the terms $\propto \log \eta$ grow in the limit $\eta \rightarrow 0$ and would lead to a breakdown of the perturbative expansion. The *dynamical renormalization group* furnishes a systematic *resummation* of the perturbative expansion that yields an asymptotically convergent result. After a mass renormalization, the solution of the *dynamical renormalization group equation* yields

$$X_0(\eta) = \left[\frac{\eta}{\eta_0} \right]^{\Gamma_1} \left\{ a(\eta_0) (-\eta)^{\beta_+} [1 + \mathcal{O}(g^2)] + b(\eta_0) (-\eta)^{\beta_-} [1 + \mathcal{O}(g^2)] \right\}, \quad (3.32)$$

where η_0 is an arbitrary renormalization scale. We now clearly see that a decay rate Γ_1 can be unambiguously identified from the contribution that multiplies *both* solutions, it is given by

$$\Gamma_1 = \frac{g^2 \tanh \left[\pi \sqrt{\frac{M^2}{H^2} - \frac{9}{4}} \right]}{16 \pi H^2 \sqrt{\frac{M^2}{H^2} - \frac{9}{4}}}. \quad (3.33)$$

The decay rate in de Sitter space-time in cosmic time can be read off from the above expression since

$$\left[\frac{\eta}{\eta_0} \right]^{\Gamma_1} = e^{-\Gamma_1 H t} \equiv e^{-\Gamma_{dS} t} . \quad (3.34)$$

and $\Gamma_{dS} = H \Gamma_1$.

Minkowski space time limit:

Minkowski space time is recovered in the limit $H \rightarrow 0$. In such limit we find from eqs.(3.28) and (3.33)

$$\begin{aligned} \nu_\chi &\stackrel{H \rightarrow 0}{=} i \frac{M}{H} \\ \Gamma_1 &\stackrel{H \rightarrow 0}{=} \frac{g^2}{16\pi M H} \tanh \left[\frac{\pi M}{H} \right] \stackrel{H \rightarrow 0}{=} \frac{g^2}{16\pi M H} \\ \beta_\pm &\stackrel{H \rightarrow 0}{=} \pm i \frac{M}{H} . \end{aligned} \quad (3.35)$$

Therefore, we find in this limit

$$\left[\frac{\eta}{\eta_0} \right]^{\Gamma_1} = e^{-\frac{g^2}{16\pi M} t} = e^{-\Gamma_M t} , \quad (3.36)$$

which displays the exponential decay of the amplitude with the correct decay rate $\Gamma_M = g^2/(16\pi M)$ for long-wavelength excitations with mass M in Minkowski space-time. Since $-\eta = e^{-Ht}/H$, up to an overall normalization of the field, the dynamical renormalization group improved solution in this limit is given by

$$X_0(t) = e^{-\frac{g^2}{16\pi M} t} [A e^{iMt} + B e^{-iMt}] \quad (3.37)$$

which is the correct solution for a zero momentum excitation in Minkowski space-time [42].

Modes that cross the horizon during inflation $k \neq 0$, $\eta \rightarrow 0^-$.

For arbitrary k the integral equation (3.17) takes the form

$$X_k''(\eta) + \left[k^2 - \frac{1}{\eta^2} \left(\nu_\chi^2 - \frac{1}{4} \right) \right] X_k(\eta) - \left(\frac{g}{2\pi H} \right)^2 \frac{1}{\eta} \int_{\eta_0}^{\eta} \frac{d\eta'}{\eta'} \frac{(\eta - \eta') \cos k(\eta - \eta')}{(\eta - \eta')^2 + (\epsilon \eta')^2} X_k(\eta') = 0 \quad (3.38)$$

where we used eqs.(3.19)-(3.20).

To first order in g^2 the solution $X_{1,\vec{k}}(\eta)$ given by Eq.(3.26) becomes

$$X_{1,\vec{k}}(\eta) = \frac{1}{(2\pi H)^2} \int_{\eta_0}^{\eta} \frac{d\eta'}{\eta'} \mathcal{G}(k; \eta, \eta') \int_{\eta_0}^{\eta'} \frac{d\eta''}{\eta''} \frac{(\eta' - \eta'') \cos k(\eta' - \eta'')}{(\eta' - \eta'')^2 + (\epsilon \eta'')^2} X_{0,\vec{k}}(\eta'') , \quad (3.39)$$

where $\mathcal{G}(k; \eta, \eta')$ is given by eq.(3.25) and for simplicity we consider the solution

$$X_{0,\vec{k}}(\eta) = A_{\vec{k}} g_{\nu_\chi}(k; \eta) .$$

with $g_{\nu_\chi}(k; \eta)$ the mode function with Bunch-Davies initial condition eq.(1.137). Eq.(3.39) can be written in the following form

$$X_{1,\vec{k}}(\eta) = A_{\vec{k}} \int_{\eta_0}^{\eta} \frac{d\eta'}{\eta'} g_{\nu_\chi}(k; \eta') J(\eta, \eta') , \quad (3.40)$$

where

$$J(\eta, \eta') = \frac{\sqrt{\eta}}{8\pi^2 H^2} \int_{\eta'}^{\eta} \frac{d\eta''}{\sqrt{\eta''}} \frac{(\eta' - \eta'') \cos k(\eta' - \eta'')}{(\eta' - \eta'')^2 + (\epsilon \eta'')^2} \text{Im} \left[H_{\nu_\chi}^{(1)}(k \eta) H_{\nu_\chi}^{(2)}(k \eta'') \right] . \quad (3.41)$$

Our goal is to evaluate $X_{1,\vec{k}}(\eta)$ for $\eta \rightarrow 0^-$. In order to achieve this we need $g_{\nu_\chi}(k; \eta)$ and the integrand in Eq.(3.41) for small arguments:

$$g_\nu(k; \eta) \stackrel{\eta \rightarrow 0^-}{=} \frac{\sqrt{\pi \eta}}{2} i^{-\nu - \frac{1}{2}} \left\{ \frac{i \Gamma(\nu)}{\pi} \left(\frac{2}{k \eta} \right)^\nu [1 + \mathcal{O}(k^2 \eta^2)] + \frac{1 - i \cot \pi \nu}{\Gamma(\nu + 1)} \left(\frac{k \eta}{2} \right)^\nu [1 + \mathcal{O}(k^2 \eta^2)] \right\} ,$$

$$\text{Im} \left[H_{\nu_\chi}^{(1)}(k, \eta) H_{\nu_\chi}^{(2)}(k, \eta') \right] \stackrel{\eta, \eta' \rightarrow 0^-}{=} \frac{1}{\pi \nu} \left[\left(\frac{\eta}{\eta'} \right)^\nu - \left(\frac{\eta'}{\eta} \right)^\nu \right] \left[1 + \mathcal{O}(\eta^2, \eta'^2) \right]. \quad (3.42)$$

Inserting Eq.(3.42) in Eq.(3.40) and (3.41) yields,

$$X_{1, \vec{k}}(\eta) \stackrel{\eta \rightarrow 0^-}{=} A_{\vec{k}} \frac{2^{\nu-2} \Gamma(\nu)}{\sqrt{\pi} \nu i^{\nu+\frac{3}{2}} k^\nu} \eta^{\frac{1}{2}-\nu} S\left(\frac{\eta_0}{\eta}\right), \quad (3.43)$$

where

$$S\left(\frac{\eta_0}{\eta}\right) \stackrel{\eta \rightarrow 0^-}{=} -\frac{1}{2} \int_1^{\frac{\eta_0}{\eta}} \frac{dy}{y} (y^{-2\nu} - 1) \int_1^{\frac{\eta_0}{y\eta}} \frac{1}{(1+i\epsilon)t-1} \frac{dt}{t^{\nu+\frac{1}{2}}} + (\epsilon \rightarrow -\epsilon). \quad (3.44)$$

Carrying out the integrations leads to the following result

$$\eta^{\frac{1}{2}-\nu} S\left(\frac{\eta_0}{\eta}\right) \stackrel{\eta \rightarrow 0^-}{=} \eta^{\frac{1}{2}-\nu} \left\{ \left[\psi\left(\nu + \frac{1}{2}\right) + \gamma + \ln \epsilon \right] \log \frac{\eta}{\eta_0} + \mathcal{O}(\eta_0) \right\}. \quad (3.45)$$

Notice that this $\eta \rightarrow 0^-$ behavior turns out to be k -independent. This is due to the fact that the term k^2 in Eq.(3.38) becomes negligible compared to the $\frac{1}{\eta^2}$ term for $\eta \rightarrow 0^-$ after the modes cross the horizon.

Mass renormalization cancels the logarithmic short distance singularity $\ln \epsilon$ leading to the following result up to order g^2 ,

$$X_{0, \vec{k}}(\eta) + g^2 X_{1, \vec{k}}(\eta) \stackrel{\eta \rightarrow 0^-}{=} A_{\vec{k}} \frac{2^{\nu-1} \Gamma(\nu)}{\sqrt{\pi} i^{\nu-\frac{1}{2}} k^\nu} \eta^{\frac{1}{2}-\nu} \left[1 + \frac{g^2 \tan \pi \nu_\chi}{16 \pi \nu_\chi H^2} \log \frac{\eta}{\eta_0} + \mathcal{O}(\eta_0) \right]. \quad (3.46)$$

This result features the secular term $\log \eta$ which is resummed by implementing the DRG as in sec.IV-A with the result [42],

$$X_{\vec{k}}(\eta) \stackrel{\eta \rightarrow 0^-}{=} \frac{2^{\nu-1} \Gamma(\nu) \eta^{\frac{1}{2}-\nu}}{\sqrt{\pi} i^{\nu-\frac{1}{2}} k^\nu} A_{\vec{k}}(\tilde{\eta}_0) \left[\frac{\eta}{\tilde{\eta}_0} \right]^{\Gamma_1} [1 + \mathcal{O}(g^2)], \quad (3.47)$$

where Γ_1 was defined in eq.(3.108). It is clear from this result that the behaviour for $\eta \rightarrow 0^-$ and $k \neq 0$ and fixed, is the same as that for the case $k = 0$ [see eq.(3.32)]. This due to the fact that the physical wavenumbers $k \eta$ become so small for $\eta \rightarrow 0^-$ that they bear no relevance on the late time dynamics. While this result could be expected on physical grounds, it is important to see it emerge from the systematic implementation of the DRG method.

Wavelengths much smaller than the Hubble radius: $|k \eta| \gg 1$:

For $|k \eta| \gg 1$ corresponding to modes with wavelengths much smaller than the Hubble radius during inflation, the hierarchy of equations of motion up to $\mathcal{O}(g^2)$ is given by

$$X_{0, \vec{k}}''(\eta) + k^2 X_{0, \vec{k}}(\eta) = 0 \quad (3.48)$$

$$X_{1, \vec{k}}''(\eta) + k^2 X_{1, \vec{k}}(\eta) = \mathcal{R}_1(k; \eta), \quad (3.49)$$

with the inhomogeneity now given by

$$\mathcal{R}_1(k; \eta) = -\frac{\delta M_1^2}{H^2 \eta^2} X_{0, \vec{k}}(\eta) - 2 a(\eta) \int_{\eta_0}^{\eta} d\eta' a(\eta') \mathcal{K}_k(\eta, \eta') X_{0, \vec{k}}(\eta'). \quad (3.50)$$

where $\mathcal{K}_k(\eta, \eta')$ is given by Eq.(3.19) and we have explicitly introduced a mass renormalization counterterm δM_1^2 .

The solution of the zeroth order equation is

$$X_{0, \vec{k}}(\eta) = A_k e^{-i k \eta} + B_k e^{i k \eta}. \quad (3.51)$$

The counterterm δM_1^2 is chosen to cancel the short distance divergence proportional to $(\ln \epsilon)/\eta^2$. After straightforward but lengthy algebra we find the following expression for the inhomogeneity in the limit $|k \eta_0| \gg |k \eta| \gg 1$ [42]

$$\mathcal{R}_1(k; \eta) = \frac{1}{8\pi^2 \eta^2 H^2} \left\{ A_k e^{-i k \eta} \left[\ln \frac{\eta}{\eta_0} + i \frac{\pi}{2} \right] + B_k e^{i k \eta} \left[\ln \frac{\eta}{\eta_0} - i \frac{\pi}{2} \right] + \dots \right\}, \quad (3.52)$$

where the dots stand for terms that are subleading in the limit $|k \eta| \gg 1$. The inhomogeneous equation for the first order correction can now be solved in terms of the retarded Green's function

$$\mathcal{G}(\eta, \eta') = \frac{1}{k} \sin[k(\eta - \eta')] \theta(\eta - \eta'). \quad (3.53)$$

To leading order in the limit $|k \eta_0| \gg |k \eta| \gg 1$ we find

$$X_{1,\bar{k}}(\eta) = -\frac{A_k e^{-i k \eta}}{32 \pi H k} \left\{ a(\eta) - a(\eta_0) - \frac{2i}{\pi H \eta} \ln \frac{\eta}{\eta_0} + \dots \right\} - \frac{B_k e^{i k \eta}}{32 \pi H k} \left\{ a(\eta) - a(\eta_0) + \frac{2i}{\pi H \eta} \ln \frac{\eta}{\eta_0} + \dots \right\} \quad (3.54)$$

where again the dots stand for terms that are subleading in the $|k \eta_0| \gg |k \eta| \gg 1$ limit and $a(\eta) = -1/H\eta$ is the scale factor. The term $a(\eta) - a(\eta_0)$ in the above expression is truly a *secular* term, since it grows by a factor larger than e^{64} during inflation. The validity of the perturbative expansion for this term is determined by the requirement that $|k/Ha(\eta)| = |k \eta| \gg 1$, namely that the wavelengths are much smaller than the Hubble radius all throughout inflation.

Thus the solution up to this order is given by

$$\begin{aligned} X_{\bar{k}}(\eta) = & A_k e^{-i k \eta} \left\{ 1 - \frac{g^2}{32\pi H k} [a(\eta) - a(\eta_0)] + i \frac{g^2}{16\pi^2 H^2} \frac{\ln \frac{\eta}{\eta_0}}{k \eta} + \dots \right\} + \\ & + B_k e^{i k \eta} \left\{ 1 - \frac{g^2}{32\pi H k} [a(\eta) - a(\eta_0)] - i \frac{g^2}{16\pi^2 H^2} \frac{\ln \frac{\eta}{\eta_0}}{k \eta} + \dots \right\}, \end{aligned} \quad (3.55)$$

where the dots stand for terms that are of higher order in g^2 and subleading in the limit $|k \eta_0| \gg |k \eta| \gg 1$. The dynamical renormalization group resummation leads to the following improved solution

$$X_{\bar{k}}(\eta) = e^{-\frac{g^2}{32\pi H k} [a(\eta) - a(\eta_0)]} \left\{ A_k e^{-i[k \eta + \varphi_k(\eta)]} [1 + \mathcal{O}(g^4)] + B_k e^{i[k \eta + \varphi_k(\eta)]} [1 + \mathcal{O}(g^4)] \right\}, \quad (3.56)$$

where $\varphi_k(\eta)$ is a logarithmic phase that is not relevant for the decay of the amplitude, and the terms in the brackets are truly perturbative in the long time limit for wavelengths much smaller than the Hubble radius. In eq.(3.56) we have chosen the renormalization scale $\tilde{\eta}_0$ to coincide with η_0 . The DRG improved solution (3.56) reveals the decay of the amplitude with the scale factor. The result above has the correct limit in Minkowski space-time as can be seen from the following argument. In cosmic time, the difference $a(\eta) - a(\eta_0) = e^{Ht} - e^{Ht_0}$, therefore in the limit $H \rightarrow 0$

$$\frac{g^2}{32\pi H k} [a(\eta) - a(\eta_0)] \xrightarrow{H \rightarrow 0} \frac{g^2}{32\pi k} (t - t_0), \quad (3.57)$$

which gives the correct exponential relaxation of the amplitude of the field for large momentum in Minkowski space-time as shown in ref.[42].

The results for the decay laws reproduce the decay rates in Minkowski space time in the limit $H \rightarrow 0$ [see eqs. (3.36) and (3.57)] thus confirming the reliability of the DRG approach.

The asymptotic behavior of the power spectrum (here we do not include the k^3 normalization) of the unperturbed solution for modes deep inside the horizon $|k \eta| \gg 1$ and those well outside the horizon $|k \eta| \rightarrow 0$ is given by

$$|X_{0,\bar{k}}(\eta)|^2 \stackrel{|k \eta| \gg 1}{=} \frac{1}{2k}, \quad |X_{0,\bar{k}}(\eta)|^2 \stackrel{|k \eta| \rightarrow 0}{=} \frac{2^{2\nu-2} \Gamma^2(\nu) \eta}{\pi (k \eta)^{2\nu}}$$

Particle decay modifies the amplitude of the solution and consequently the power spectrum, which after the DRG resummation is given by

$$|X_{\bar{k}}(\eta)|^2 \stackrel{|k \eta| \gg 1}{=} \frac{1}{2k} e^{-\frac{g^2}{16\pi H k} [a(\eta) - a(\eta_0)]} \quad (3.58)$$

$$|X_{\bar{k}}(\eta)|^2 \stackrel{|k \eta| \rightarrow 0}{=} \frac{2^{2\nu-2} \Gamma^2(\nu) \eta}{\pi (k \eta)^{2\nu}} A_k^2(\tilde{\eta}_0) \left[\frac{\eta}{\tilde{\eta}_0} \right]^{2\Gamma_1} \quad (3.59)$$

where we have normalized the mode functions to Bunch-Davies initial conditions at the beginning of inflation $\eta = \eta_0$ in eq.(3.58). The solution for wavelengths larger than the Hubble radius is independent of the scale $\tilde{\eta}_0$ because the amplitude $A_{\bar{k}}(\tilde{\eta}_0)$ obeys the DRG equation. This amplitude at a given scale $\tilde{\eta}_0$ is obtained by matching the asymptotic

forms of the DRG improved solution at a scale $\tilde{\eta}_0$. Clearly this amplitude will depend on the decay law of modes deep inside the horizon, which reflects a larger suppression of the amplitude for long wavelength modes.

These results are general, hence they are also valid for the decay of the quantum fluctuations of the inflaton field. Since the quantum fluctuations of the inflaton field seed scalar density perturbations the result obtained above implies that the process of particle decay can lead to modifications of the power spectrum of superhorizon density perturbations which is obtained when the fluctuations freeze after horizon crossing as $\eta \rightarrow 0^-$. The new renormalization scale $\tilde{\eta}_0$ will lead to violations of scale invariance much in the same way as in the renormalization group approach to deep inelastic scattering.

Clearly in order to derive the corrections to the power spectrum of density perturbations from decay of quantum fluctuations, the full gauge invariant treatment of the density perturbations presented in sec. III C must be used.

3. Quantum corrections to the equations of motion for the inflaton

As mentioned above the rapid cosmological expansion and the lack of a global time-like Killing vector leads to new decay processes as a consequence of the lack of reaction thresholds. This new aspect of a rapidly expanding cosmology entails that in a non-linear field theory, the quanta of a field can decay into other quanta of the *same* field. This phenomenon is obviously not available in Minkowski space time by energy and momentum conservation. In the previous subsection we studied the decay of superhorizon fluctuations of one scalar field into the quanta of another field, but following the same method we can obtain the *self-decay* of modes that are inside the horizon during inflation.

Our approach relies on two distinct and fundamentally different expansions: (i) the effective field theory (EFT) expansion and (ii) the slow-roll expansion.

As mentioned above, the effective field theory approach relies on the separation between the energy scale of inflation and the cutoff scale, which here is the Planck scale. The scale of inflation is determined by the Hubble parameter during the relevant stage of inflation when wavelengths of cosmological relevance cross the horizon. Therefore, the dimensionless ratio that defines the EFT approximation is the ratio $[H(\Phi_0)/M_{Pl}]^2$, where $H(\Phi_0)$ is the Hubble parameter during the relevant inflationary stage. In scalar field driven inflation the reliability of this approximation *improves* upon dynamical evolution since the scale of inflation *diminishes* with time as shown in sec. I D 3. Phenomenologically, the EFT approximation is an excellent one since during inflation $(H/M_{Pl})^2 \sim 10^{-9}$ according to eq.(1.178).

We consider single field inflationary models described by a general self-interacting scalar field theory in a spatially flat FRW cosmological space time with scale factor $a(t)$. In comoving coordinates the action is given by

$$S = \int d^3x dt a^3(t) \left[\frac{1}{2} \dot{\phi}^2 - \frac{(\nabla\phi)^2}{2a^2} - V(\phi) \right]. \quad (3.60)$$

We consider a *generic* potential $V(\phi)$, the only requirement is that its *derivatives* be small in order to justify the slow-roll expansion as in the class of potentials eq.(1.83). In order to study the corrections from the quantum fluctuations we separate the classical homogeneous expectation value of the scalar field from the quantum fluctuations by writing

$$\phi(\vec{x}, t) = \Phi_0(t) + \varphi(\vec{x}, t), \quad (3.61)$$

with

$$\Phi_0(t) = \langle \phi(\vec{x}, t) \rangle \quad ; \quad \langle \varphi(\vec{x}, t) \rangle = 0, \quad (3.62)$$

where the expectation value is in the non-equilibrium quantum state. Expanding the Lagrangian density and integrating by parts, the action becomes

$$S = \int d^3x dt a^3(t) \mathcal{L}[\Phi_0(t), \varphi(\vec{x}, t)], \quad (3.63)$$

with

$$\begin{aligned} \mathcal{L}[\Phi_0(t), \varphi(\vec{x}, t)] = & \frac{1}{2} \dot{\Phi}_0^2 - V(\Phi_0) + \frac{1}{2} \dot{\varphi}^2 - \frac{(\nabla\varphi)^2}{2a^2} - \frac{1}{2} V''(\Phi_0) \varphi^2 \\ & - \varphi \left[\ddot{\Phi}_0 + 3H\dot{\Phi}_0 + V'(\Phi_0) \right] - \frac{1}{6} V'''(\Phi_0) \varphi^3 - \frac{1}{24} V^{(IV)}(\Phi_0) \varphi^4 + \text{higher orders in } \varphi. \end{aligned} \quad (3.64)$$

We will obtain the equation of motion for the homogeneous expectation value of the inflaton field by requiring the condition $\langle \varphi(\vec{x}, t) \rangle = 0$ consistently in a perturbative expansion by treating the *linear*, cubic, quartic (and higher order) terms in the Lagrangian density eq.(3.64) as perturbations.

The Friedmann equation and the classical equation of motion for Φ_0 are

$$H_0^2 = \frac{1}{3 M_{Pl}^2} \left[\frac{1}{2} (\dot{\Phi}_0)^2 + V(\Phi_0) \right] , \quad (3.65)$$

$$\ddot{\Phi}_0 + 3 H_0 \dot{\Phi}_0 + V'(\Phi_0) = 0 . \quad (3.66)$$

[H_0 stands in secs. IIIB and IIIC for the classical Hubble parameter during inflation. In the rest of the article H_0 stands for the Hubble constant today.]

We now introduce the effective mass of the fluctuations M^2 and the cubic and quartic self-couplings g , λ respectively as

$$M^2 \equiv M^2(\Phi_0) = V''(\Phi_0) = 3 H_0^2 \eta_v + \mathcal{O}(\epsilon_v \eta_v) , \quad (3.67)$$

$$g \equiv g(\Phi_0) = \frac{1}{2} V'''(\Phi_0) \quad , \quad \lambda \equiv \lambda(\Phi_0) = \frac{1}{6} V^{(IV)}(\Phi_0) . \quad (3.68)$$

In particular, the dimensionless ratio of the cubic coupling and the Hubble parameter is given to leading order in slow-roll by

$$\frac{g}{H_0} = \frac{3 \xi_v}{2 \sqrt{2} \epsilon_v} \frac{H_0}{M_{Pl}} = \frac{3}{2} \pi \Delta_{\mathcal{R}} \left[\frac{r}{2} \left(n_s - 1 + \frac{3r}{16} \right) - \frac{dn_s}{d \ln k} \right] = \mathcal{O} \left(\frac{M^2}{N M_{Pl}^2} \right) , \quad (3.69)$$

where the slow-roll parameters ϵ_v and ξ_v are given by eqs.(1.133) and (1.172), respectively and $\Delta_{\mathcal{R}}$ is given by eq.(1.164).

The quartic coupling λ can be conveniently written in terms of slow-roll and effective-field theory parameters as

$$\lambda = \frac{\sigma_v}{4 \epsilon_v} \left(\frac{H_0}{M_{Pl}} \right)^2 = 2 \pi^2 \Delta_{\mathcal{R}}^2 \sigma_v = \mathcal{O} \left(\frac{M^4}{N M_{Pl}^4} \right) , \quad (3.70)$$

where σ_v is given by eq.(1.173). Moreover, λ can be written solely in terms of CMB observables inserting the expression eq.(3.176) for σ_v into eq.(3.70).

During slow-roll the effective mass and couplings are not constants but *very slowly varying functions of time*. The time dependence of these couplings is implicit through their dependence on Φ_0 but is slow in the slow-roll stage.

Eqs.(3.69) and (3.70) show that $(g/H_0)^2$ and λ/N are of the *same order* in the EFT expansion, namely $\mathcal{O}(H_0^2/[N^3 M_{Pl}^2])$. That is, both the cubic and quartic self couplings are small, the quartic being of higher order in slow-roll than the cubic etc, namely

$$1 \gg \frac{g}{H_0} \gg \lambda \gg \dots \quad (3.71)$$

where the dots stand for self-couplings arising from higher derivative of the potential as displayed in eq.(3.64). This observation will be important in the calculation of the self-energy correction for the quantum fluctuations below. Eqs.(3.69) and (3.70) for g and λ must be compared with eqs.(1.87) and (1.97) for the couplings at zero inflaton field. We see that the hierarchy eq.(3.71) is fulfilled by eqs.(1.97).

The condition $\langle \varphi(\vec{x}, t) \rangle = 0$ up to leading order ($\mathcal{O}(g)$) leads to the equation of motion

$$\ddot{\Phi}_0(t) + 3 H \dot{\Phi}_0(t) + V'(\Phi_0) + g(\Phi_0) \langle [\varphi(\vec{x}, t)]^2 \rangle = 0 . \quad (3.72)$$

The first three terms here are the familiar ones for the classical equation of motion of the inflaton.

The last term in eq.(3.72) is the one-loop correction to the equations of motion of purely quantum mechanical origin. The one-loop quantum correction to the equations of motion is completely determined by the power spectrum of inflaton fluctuations,

$$\langle [\varphi(\vec{x}, t)]^2 \rangle = \int \frac{d^3 k}{(2\pi)^3} \langle |\varphi_{\vec{k}}(t)|^2 \rangle = \int_0^\infty \frac{dk}{k} \mathcal{P}_\varphi(k, t) . \quad (3.73)$$

In order to compute the one-loop contribution, it is convenient to work in conformal time and to conformally rescale the field

$$\varphi(\vec{x}, t) = \frac{\chi(\vec{x}, \eta)}{a(\eta)} , \quad (3.74)$$

$a(\eta)$ being the scale factor in conformal time. The spatial Fourier transform of the free field Heisenberg operators $\chi(\vec{x}, \eta)$, $\chi_{\vec{k}}(\eta)$ are written in terms of annihilation and creation operators that act on Fock states as

$$\chi_{\vec{k}}(\eta) = a_{\vec{k}} g_{\nu}(k, \eta) + a_{-\vec{k}}^{\dagger} g_{\nu}^*(k, \eta) \quad (3.75)$$

where the mode functions $g_{\nu}(k, \eta)$ with Bunch-Davis boundary conditions are given by eq.(1.137) and the index ν is given by

$$\nu = \frac{3}{2} + \epsilon_v - \eta_v + \mathcal{O}\left(\frac{1}{N^2}\right). \quad (3.76)$$

Notice that the index ν for inflaton fluctuations is similar but not identical to the index $\nu_{\mathcal{R}}$ for scalar curvature fluctuations eq.(1.135).

In the Bunch-Davis vacuum, defined so that $a_{\vec{k}}|0\rangle_{BD} = 0$ we find

$$\mathcal{P}_{\varphi}(k, t) = \frac{H_0^2}{8\pi} (-k\eta)^3 |H_{\nu}^{(1)}(-k\eta)|^2. \quad (3.77)$$

The momentum integral in eq.(3.73) features ultraviolet and infrared divergences. The ultraviolet divergences are absorbed into renormalization of the parameters in the tree level potential. The infrared divergences are a reflection of the *near* scale invariance of the inflaton fluctuations, and are regularized by a particular linear combination of slow-roll parameters

$$\Delta \equiv \eta_v - \epsilon_v = \frac{1}{2} \left(n_s - 1 + \frac{1}{4} r \right) = \mathcal{O}\left(\frac{1}{N}\right). \quad (3.78)$$

The infrared regularization by the slow-roll combination Δ is akin to the regularization of infrared divergences in critical phenomena through the expansion around four dimensions, namely the ϵ -expansion [83]. We find,

$$\ddot{\Phi}_0(t) + 3H_0\dot{\Phi}_0(t) + V_R'(\Phi_0) + \left(\frac{H_0}{4\pi}\right)^2 \frac{V_R'''(\Phi_0)}{\Delta} = 0. \quad (3.79)$$

An important aspect of this equation is the following: naively, the quantum correction is of order $V_R'''(\Phi_0)$, therefore of second order in slow roll, but the strong infrared enhancement arising from the quasi scale invariance of inflationary fluctuations brings about a denominator which is of first order in slow-roll $\mathcal{O}(1/N)$. Hence, the lowest order quantum correction in the slow-roll expansion, is actually of the same order as $V_R'(\Phi_0)$. To highlight this observation, it proves convenient to write eq.(3.79) in terms of the EFT and slow-roll parameters,

$$\ddot{\Phi}_0(t) + 3H_0\dot{\Phi}_0(t) + V_R'(\Phi_0) \left[1 + \left(\frac{H_0}{2\pi M_{Pl}}\right)^2 \frac{\xi_v}{2\epsilon_v \Delta} \right] = 0. \quad (3.80)$$

Since $\xi_v \sim \mathcal{O}(1/N^2)$ and $\Delta \sim \eta_v \sim \epsilon_v \sim \mathcal{O}(1/N)$ [see eqs.(1.131), (1.172) and (3.78)], the leading quantum corrections are of zeroth order in slow-roll ($\sim N^0$). This is a consequence of the infrared enhancement resulting from the nearly scale invariance of the power spectrum of scalar fluctuations. The quantum correction is suppressed by an EFT factor $H_0^2/M_{Pl}^2 \ll 1$.

4. Quantum corrections to the Friedmann equation: the one loop effective potential

The zero temperature effective potential in Minkowski space-time is often used to describe the scalar field dynamics during inflation, but this ignores the true nature of the quantum fluctuations in the nearly de-Sitter cosmology.

Since the fluctuations of the inflaton field are quantized, the interpretation of the ‘scalar condensate’ Φ_0 is that of the expectation value of the full quantum field ϕ in a homogeneous coherent quantum state. Consistently with this, the Friedmann equation must necessarily be understood in terms of the *expectation* value of the field energy momentum tensor, namely

$$H^2 = \frac{1}{3M_{Pl}^2} \left\langle \frac{1}{2} \dot{\phi}^2 + \frac{1}{2} \left(\frac{\nabla \phi}{a(t)} \right)^2 + V(\phi) \right\rangle. \quad (3.81)$$

Separating the homogeneous condensate from the fluctuations as in eq.(3.61) with the condition that the expectation value of the quantum fluctuation vanishes eq.(3.62), the Friedmann equation becomes

$$H^2 = \frac{1}{3 M_{Pl}^2} \left[\frac{1}{2} \dot{\Phi}_0^2 + V_R(\Phi_0) + \delta V_R(\Phi_0) \right] + \frac{1}{3 M_{Pl}^2} \left\langle \frac{1}{2} \dot{\varphi}^2 + \frac{1}{2} \left(\frac{\nabla \varphi}{a(t)} \right)^2 + \frac{1}{2} V''(\Phi_0) \varphi^2 + \dots \right\rangle \quad (3.82)$$

where V_R refers to the renormalized tree level potential and δV_R contains the counterterms that cancel the ultraviolet divergences. The dots inside the angular brackets correspond to terms with higher derivatives of the potential which are smaller in the slow-roll expansion. The quadratic term $\langle \varphi^2 \rangle$ has been calculated above to leading order in slow-roll and given by eq. (3.73). Calculating the expectation value in eq.(3.82) in free field theory corresponds to obtaining the corrections to the energy momentum tensor by integrating the fluctuations *up to one loop*.

The first two terms of the expectation value in eq.(3.82) feature ultraviolet divergences that are absorbed into the renormalization of the tree-level potential, but *do not* feature infrared divergences for $\nu = 3/2$ because the time and spatial derivatives introduce two extra powers of the loop momentum in the corresponding integrals. The last term does feature the infrared enhancement and leads to the following expression

$$H^2 = \frac{1}{3 M_{Pl}^2} \left[\frac{1}{2} \dot{\Phi}_0^2 + V_R(\Phi_0) + \left(\frac{H_0}{4\pi} \right)^2 \frac{V_R''(\Phi_0)}{\Delta} + \text{higher orders in slow-roll} \right] \equiv H_0^2 + \delta H^2, \quad (3.83)$$

where H_0 is the Hubble parameter in absence of quantum fluctuations:

$$H_0^2 = \frac{V_R(\Phi_0)}{3 M_{Pl}^2} \left[1 + \frac{\epsilon_v}{3} + \mathcal{O} \left(\frac{1}{N^2} \right) \right].$$

Using the lowest order slow-roll relation eq.(3.67), the last term in eq.(3.83) can be written as follows

$$\frac{\delta H^2}{H_0^2} = \left(\frac{H_0}{4\pi M_{Pl}} \right)^2 \frac{\eta_v}{\Delta}. \quad (3.84)$$

This equation defines the back-reaction correction to the scale factor arising from the quantum fluctuations of the inflaton.

Hence, while the ratio η_v/Δ is of order zero in slow roll, the one loop correction to the Friedmann equation is of the order $H_0^2/M_{Pl}^2 \ll 1$ consistently with the effective field theory expansion. The Friedmann equation suggests the identification of the effective potential

$$V_{eff}(\Phi_0) = V_R(\Phi_0) + \left(\frac{H_0}{4\pi} \right)^2 \frac{V_R''(\Phi_0)}{\Delta} + \text{higher orders in slow-roll} = \quad (3.85)$$

$$\begin{aligned} &= V_R(\Phi_0) \left[1 + \left(\frac{H_0}{4\pi M_{Pl}} \right)^2 \frac{\eta_v}{\Delta} + \text{higher orders in slow-roll} \right] = \\ &= V_R(\Phi_0) \left[1 + \frac{\Delta^2}{32} \frac{n_s - 1 + \frac{3}{8} r}{n_s - 1 + \frac{1}{4} r} + \text{higher orders in slow-roll} \right]. \end{aligned} \quad (3.86)$$

We see that the equation of motion for the inflaton eq.(3.79) takes the natural form

$$\ddot{\Phi}_0(t) + 3 H_0 \dot{\Phi}_0(t) + \frac{\partial V_{eff}}{\partial \Phi_0}(\Phi_0) = 0.$$

where the derivative of V_{eff} with respect to Φ_0 is taken at fixed Hubble and slow-roll parameters. The quantum corrections to the effective potential lead to loop corrections to the slow-roll parameters, for example defining the *effective* slow-roll parameters as

$$\epsilon_{eff} = \frac{M_{Pl}^2}{2} \left[\frac{V'_{eff}(\Phi_0)}{V_{eff}(\Phi_0)} \right]^2; \quad \eta_{eff} = M_{Pl}^2 \frac{V''_{eff}(\Phi_0)}{V_{eff}(\Phi_0)}, \quad (3.87)$$

eq.(3.85) yields to leading order in EFT and slow-roll expansions:

$$\begin{aligned} \epsilon_{eff} &= \epsilon_v \left[1 + \left(\frac{H_0}{4\pi M_{Pl}} \right)^2 \frac{4\eta_v \Delta - \xi_v}{\Delta^2} \right] \\ \eta_{eff} &= \eta_v \left\{ 1 + \left(\frac{H_0}{4\pi M_{Pl}} \right)^2 \frac{1}{\Delta^2} \left[\frac{\xi_v^2}{\eta_v \Delta} - \frac{\sigma_v}{2\eta_v} - \frac{\xi_v}{\eta_v} (\eta_v + 6\epsilon_v) + 4\eta_v (\eta_v + 4\epsilon_v) - 20\epsilon_v^2 \right] \right\}. \end{aligned} \quad (3.88)$$

A remarkable feature of the quantum corrections to the slow roll parameters is that they are of *zeroth* order in slow roll $\mathcal{O}(N^0)$. Again, this is a consequence of the infrared enhancement of the loop diagrams for a nearly scale invariant spectrum of fluctuations. Higher order slow-roll parameters can be obtained similarly. The smallness of the quantum corrections are determined by the EFT ratio H_0/M_{Pl} . Thus the validity of the EFT approach guarantees that the quantum corrections are small.

There is a striking difference between the effective potential in quasi de-Sitter space-time and the Minkowski case, in the latter it is given by

$$V_{eff}^{Minkowski}(\Phi_0) = V_R(\Phi_0) + \frac{[V_R''(\Phi_0)]^2}{64\pi^2} \ln \left[\frac{V_R''(\Phi_0)}{M^2} \right], \quad (3.89)$$

where M is a renormalization scale. Therefore the naive use of the Minkowski space-time effective potential in the dynamics of the inflaton field during slow-roll inflation is a gross and misleading approximation that cannot describe the infrared properties of inflationary dynamics.

Indeed, early papers (as refs. [32] and [59]) used effective potentials like eq.(3.89) during inflationary expansion. It will be interesting to revisit these early works at the light of our present knowledge on the effective potential during inflation.

5. Quantum corrections to superhorizon modes and their scaling dimensions

In order to study the equations of motion for the *quantum fluctuations* of the inflaton including self-energy corrections, it is convenient to first pass to conformal time and to implement the conformal rescaling of the field as in eq.(3.74). The action is now given by

$$S = \int d^3x d\eta \mathcal{L}_c[\chi, \Phi_0], \quad (3.90)$$

where the Lagrangian density $\mathcal{L}_c[\chi, \Phi_0]$ is given by

$$\begin{aligned} \mathcal{L}_c[\chi, \Phi_0] = & a^4(\eta) \left[\frac{1}{2} \dot{\Phi}_0^2 - V_R(\Phi_0) - \delta V_R(\Phi_0) \right] + \frac{\chi'^2}{2} - \frac{(\nabla\chi)^2}{2} - \frac{1}{2} \mathcal{M}^2(\eta) \chi^2 - \\ & - a^3(\eta) \chi \left[\ddot{\Phi}_0 + 3H\dot{\Phi}_0 + V_R'(\Phi_0) + \mathcal{C}_2[\Lambda, H] V_R'''(\Phi_0) + \dots \right] - \frac{1}{2} \delta \mathcal{M}^2(\eta) \chi^2 - \frac{g}{3} a(\eta) \chi^3 - \frac{\lambda}{4} \chi^4 + \dots \end{aligned} \quad (3.91)$$

where $a(\eta)$ is the scale factor in conformal time, the dots on Φ_0 stand for derivatives with respect to cosmic time, the primes on χ stand for derivatives with respect to conformal time, we have used the definitions given in eqs.(3.68) and the dots inside the angular brackets correspond to terms with higher derivatives of the potential which are smaller in the slow-roll expansion.

The effective (time dependent) mass term is given by

$$\mathcal{M}^2(\eta) = V_R''(\Phi_0) a^2(\eta) - \frac{a''(\eta)}{a(\eta)} = -\frac{1}{\eta^2} \left(\nu^2 - \frac{1}{4} \right), \quad (3.92)$$

where ν is given by eq.(3.76) and $\delta \mathcal{M}^2(\eta)$ and \mathcal{C}_2 are counterterms that will cancel the ultraviolet divergences in the one-loop self-energy. $-\mathcal{M}^2(\eta)$ is similar but not identical to the potential $W_{\mathcal{R}}(\eta)$ felt by the scalar curvature fluctuations eq.(1.135).

The effective equation of motion for the fluctuations is obtained in the linear response approach by introducing an external source that induces an expectation value for the field $\chi(\vec{x}, \eta)$, switching off the source this expectation value will evolve in time through the effective equation of motion of the fluctuations. The first step is to take the spatial Fourier transform of $\chi(\vec{x}, \eta)$ and write

$$\chi_{\vec{k}}(\eta) = X_{\vec{k}}(\eta) + \sigma_{\vec{k}}(\eta) \quad ; \quad \langle \chi_{\vec{k}}(\eta) \rangle = X_{\vec{k}}(\eta) \quad ; \quad \langle \sigma_{\vec{k}}(\eta) \rangle = 0, \quad (3.93)$$

where $X_{\vec{k}}(\eta)$ is the spatial Fourier transform of the expectation value of the fluctuation field χ induced by the external source term. Implementing the condition $\langle \sigma \rangle = 0$ up to one loop we obtain the effective equation of motion

$$X_{\vec{k}}''(\eta) + \left[k^2 - \frac{\nu^2 - \frac{1}{4}}{\eta^2} \right] X_{\vec{k}}(\eta) + \int_{\eta_0}^{\eta} \Sigma(k, \eta, \eta') X_{\vec{k}}(\eta') d\eta' = 0. \quad (3.94)$$

The counterterms cancel the UV divergent parts of the self-energy which yield a local term ($\propto \delta(\eta - \eta')$), after renormalization, the self-energy kernel is given by

$$\Sigma(k, \eta, \eta') = \frac{2g^2}{H_0^2 \eta \eta'} \mathcal{K}_\nu(k; \eta, \eta') . \quad (3.95)$$

The one-loop kernel $\mathcal{K}_\nu(k; \eta, \eta')$ is given by

$$\mathcal{K}_\nu(k; \eta, \eta') = 2 \int \frac{d^3 q}{(2\pi)^3} \text{Im} \left[g_\nu(q, \eta) g_\nu^*(q, \eta') g_\nu(|\vec{q} - \vec{k}|, \eta) g_\nu^*(|\vec{q} - \vec{k}|, \eta') \right] , \quad (3.96)$$

where the mode functions $g_\nu(k, \eta)$ are given by eq.(1.137). We are primarily interested in obtaining the superhorizon behavior of the fluctuations ($|k\eta| \ll 1$) to obtain the scaling behavior in this limit, therefore we set $k = 0$. To leading order in the slow-roll expansion and leading logarithmic order the kernel is given by

$$\begin{aligned} \mathcal{K}_\nu(0; \eta, \eta') = & -\frac{1}{8\pi^2} \frac{\eta - \eta'}{(\eta - \eta')^2 + (\epsilon \eta')^2} + \\ & + \frac{1}{6\pi^2} \left[\left(\frac{1}{2\Delta} + \frac{2}{3} \right) \left(\frac{\eta'}{\eta^2} - \frac{\eta}{\eta'^2} \right) - \frac{\eta'}{\eta^2} \ln \frac{\eta'}{\eta} + \left(\frac{\eta}{\eta'^2} - \frac{\eta'}{\eta^2} \right) \ln \left(1 - \frac{\eta}{\eta'} \right) + \frac{1}{\eta'} - \frac{1}{\eta} \right] , \end{aligned} \quad (3.97)$$

where $\epsilon \rightarrow 0$ furnishes a regularization.

The equation of motion (3.94) is solved in a perturbative loop expansion as follows

$$X_{\vec{k}}(\eta) = X_{0,\vec{k}}(\eta) + X_{1,\vec{k}}(\eta) + \text{higher loop corrections} , \quad (3.98)$$

where $X_{0,\vec{k}}(\eta)$ is the free field solution, $X_{1,\vec{k}}(\eta)$ is the one-loop correction, etc. This expansion to one loop order leads to the following hierarchy of coupled equations [see eqs.(3.22)-(3.24)],

$$X''_{0,\vec{k}}(\eta) + \left[k^2 - \frac{1}{\eta^2} \left(\nu^2 - \frac{1}{4} \right) \right] X_{0,\vec{k}}(\eta) = 0 , \quad (3.99)$$

$$X''_{1,\vec{k}}(\eta) + \left[k^2 - \frac{1}{\eta^2} \left(\nu^2 - \frac{1}{4} \right) \right] X_{1,\vec{k}}(\eta) = \mathcal{R}_1(k, \eta) . \quad (3.100)$$

The superhorizon solution of the zeroth order equation is

$$X_{0,0}(\eta) = A \eta^{\beta_+} + B \eta^{\beta_-} \quad ; \quad \beta_{\pm} \equiv \frac{1}{2} \pm \nu . \quad (3.101)$$

and after renormalization we find

$$\mathcal{R}_1(0, \eta) = A \frac{\eta^{\beta_+}}{\eta^2} (2\nu d^+) + B \frac{\eta^{\beta_-}}{\eta^2} (2\nu d^-) + F[\eta, \eta_0] , \quad (3.102)$$

where the coefficients d^{\pm} are entirely of quantum origin (one-loop) and given by

$$d^+ = -\frac{1}{2\nu} \left[\frac{3\lambda}{8\pi^2 \Delta} + \frac{1}{6\pi^2} \left(\frac{g}{H_0 \Delta} \right)^2 \right] \quad (3.103)$$

$$d^- = -\frac{1}{2\nu} \left[\frac{3\lambda}{8\pi^2 \Delta} + \frac{1}{2\pi^2} \left(\frac{g}{H_0 \Delta} \right)^2 \right] , \quad (3.104)$$

and $F[\eta, \eta_0]$ refers to the contribution of the lower integration limit and does not produce secular terms in the limit $\eta \rightarrow 0$.

The solution of the inhomogeneous eq.(3.100) is given by

$$X_{1,\vec{k}}(\eta) = \int_{\eta_0}^0 d\eta' \mathcal{G}_\nu(k; \eta, \eta') \mathcal{R}_1(k, \eta') . \quad (3.105)$$

$\mathcal{G}_\nu(k; \eta, \eta')$ is the retarded Green's function (3.25). Up to one loop order we find the superhorizon solution

$$X_0(\eta) = A \eta^{\beta_+} \left[1 + d^+ \ln \left(\frac{\eta}{\eta_0} \right) \right] + B \eta^{\beta_-} \left[1 - d^- \ln \left(\frac{\eta}{\eta_0} \right) \right] + \text{non-secular terms} . \quad (3.106)$$

The resummation of the logarithmic secular terms is performed by implementing the dynamical renormalization group resummation, leading to the following result

$$X_0(\eta) = A_{\bar{\eta}} \left(\frac{\eta}{\bar{\eta}} \right)^{\beta_+ + d^+} + B_{\bar{\eta}} \left(\frac{\eta}{\bar{\eta}} \right)^{\beta_- - d^-} = \left(\frac{\eta}{\bar{\eta}} \right)^{\Gamma} \left[A_{\bar{\eta}} \left(\frac{\eta}{\bar{\eta}} \right)^{\beta_+ + \gamma} + B_{\bar{\eta}} \left(\frac{\eta}{\bar{\eta}} \right)^{\beta_- - \gamma} \right], \quad (3.107)$$

where $\bar{\eta}$ is a renormalization scale; the amplitudes $A_{\bar{\eta}}$, $B_{\bar{\eta}}$ are given at this renormalization scale and obey a renormalization group equation, so that the full solution $X_0(\eta)$ is independent of the renormalization scale, as it must be. The exponents are given by

$$\gamma = \frac{1}{2} (d^+ + d^-) = -\frac{1}{2\nu} \left[\frac{3\lambda}{8\pi^2 \Delta} + \frac{1}{3\pi^2} \left(\frac{g}{H_0 \Delta} \right)^2 \right], \quad (3.108)$$

$$\Gamma = \frac{1}{2} (d^+ - d^-) = \frac{1}{12\pi^2 \nu} \left(\frac{g}{H_0 \Delta} \right)^2. \quad (3.109)$$

Since $\eta = -e^{-H_0 t}/H_0$, in cosmic time the amplitude of superhorizon fluctuations decays exponentially with the decay rate

$$\Gamma_{\varphi \rightarrow \varphi\varphi} = H_0 \Gamma = \frac{H_0}{12\pi^2 \nu} \left(\frac{g}{H_0 \Delta} \right)^2, \quad (3.110)$$

where the subscript $\varphi \rightarrow \varphi\varphi$ emphasizes that this is the rate of *self-decay* of inflaton fluctuations, a novel phenomenon which is a consequence of the inflationary expansion and the fact that in the expanding cosmology there is no global time-like Killing vector that would lead to reaction thresholds.

In addition in the limit $\eta \rightarrow 0^-$ the growing mode features a *novel* scaling dimension $-d^-$ namely

$$X_0(\eta) \stackrel{\eta \rightarrow 0}{\sim} B_{\bar{\eta}} \left(\frac{\eta}{\bar{\eta}} \right)^{\frac{1}{2} - \nu - d^-}. \quad (3.111)$$

This correction to scaling is related to the decay rate Γ of superhorizon fluctuations eq.(3.109). From eqs.(3.69), (3.70) and (3.104), to leading order in slow-roll and EFT expansions, d^- and the cosmic time decay rate $\Gamma_{\varphi \rightarrow \varphi\varphi}$ of superhorizon inflaton fluctuations are given by

$$-d^- = \left(\frac{H_0}{4\pi M_{Pl}} \right)^2 \frac{\sigma_v (\eta_v - \epsilon_v) + 6\xi_v^2}{2\epsilon_v (\eta_v - \epsilon_v)^2} = \Delta_{\mathcal{R}}^2 \frac{\sigma_v (\eta_v - \epsilon_v) + 6\xi_v^2}{4(\eta_v - \epsilon_v)^2}, \quad (3.112)$$

$$\Gamma_{\varphi \rightarrow \varphi\varphi} = \left(\frac{H_0}{4\pi M_{Pl}} \right)^2 \frac{H_0 \xi_v^2}{\epsilon_v (\eta_v - \epsilon_v)^2} = \frac{1}{2} \Delta_{\mathcal{R}}^2 \frac{H_0 \xi_v^2}{(\eta_v - \epsilon_v)^2} \quad (3.113)$$

where the slow-roll parameters are given by eqs. (1.131)-(1.172). Whereas the exponent $\nu = \frac{3}{2} - \Delta = \frac{3}{2} + \epsilon_v - \eta_v$ is determined by eq.(3.99) for the free mode functions, the novel scaling exponent $-d^-$ is determined by the quantum corrections arising from the interactions. Again eq.(3.112) highlights an important aspect of the effective field theory approach. These expressions are of *zero order* in slow roll N^0 . This is a consequence of the *infrared enhancement* of the self-energy for $\nu = 3/2 + \mathcal{O}(1/N)$ manifest as $\Delta^{-2} = (\eta_v - \epsilon_v)^{-2} = \mathcal{O}(N^2)$. However, the novel dimension is perturbatively small precisely because of the effective field theory factor $H_0^2/M_{Pl}^2 \ll 1$.

We get from eqs.(1.162), (1.164), (1.172) and (3.69) that

$$\frac{g}{H_0} = 3\pi \xi_v \Delta_{\mathcal{R}} = \frac{\sqrt{3}}{2N} \left(\frac{M}{M_{Pl}} \right)^2 \frac{|w'''(\chi)|}{\sqrt{w(\chi)}} \quad (3.114)$$

Using eq.(1.177) we get as estimate on the cubic coupling $g/H_0 \sim 10^{-6}$.

We can analogously estimate the rate $\Gamma_{\varphi \rightarrow \varphi\varphi}$ [Eq.(3.113)],

$$\frac{\Gamma_{\varphi \rightarrow \varphi\varphi}}{H_0} = \frac{1}{3\pi^2} \left(\frac{M}{M_{Pl}} \right)^4 \frac{w(\chi) [w'''(\chi)]^2}{2w(\chi) w''(\chi) - [w''(\chi)]^2} \sim \frac{1}{3\pi^2} \left(\frac{M}{M_{Pl}} \right)^4 \sim 10^{-11}. \quad (3.115)$$

This gives in cosmic time for a typical value $H \simeq 10^{14}$ GeV, $\Gamma_{\varphi \rightarrow \varphi\varphi} \sim 10^3$ GeV.

6. Connection with non-gaussianity

Non-gaussianity of the spectrum of fluctuations is associated with three (and higher) point correlation functions. An early assessment of non-gaussian features of temperature fluctuations in an interacting field theory was given in ref.[68]. In ref.[69] the simplest inflationary potential with a cubic self-interaction for the inflaton field was proposed as a prototype theory to study possible departures from gaussianity. The three point correlation function of a scalar field in a theory with cubic interaction as well as the four point correlation function in a theory with quartic interaction in de Sitter space-time were calculated in ref.[70].

The long time ($\eta \rightarrow 0$) behavior of the equal time three point correlation function in the scalar field theory defined by Eq.(3.64) for $M = 0$ (and hence $\nu = \frac{3}{2}$), is given by [69]

$$\langle \chi(\vec{k}, \eta) \chi(\vec{q}, \eta) \chi(-\vec{k} - \vec{q}, \eta) \rangle = \frac{2\pi^3}{3} a^3(\eta) g H^2 \frac{F(\vec{k}, \vec{q}; \eta)}{[k q |\vec{k} + \vec{q}|]^3} \quad (3.116)$$

where

$$F(\vec{k}, \vec{q}; \eta) = [k^3 + q^3 + |\vec{k} + \vec{q}|^3] [\ln(k_T \eta) + \gamma] - (k^2 + q^2 + |\vec{k} + \vec{q}|^2) k_T + k q |\vec{k} + \vec{q}| \quad ; \quad k_T = k + q + |\vec{k} + \vec{q}| \quad (3.117)$$

A diagrammatic interpretation of the equal time expectation value Eq.(3.116) is depicted in fig. 41, which illustrates the *similarity* with the *decay process* depicted in fig. 41.

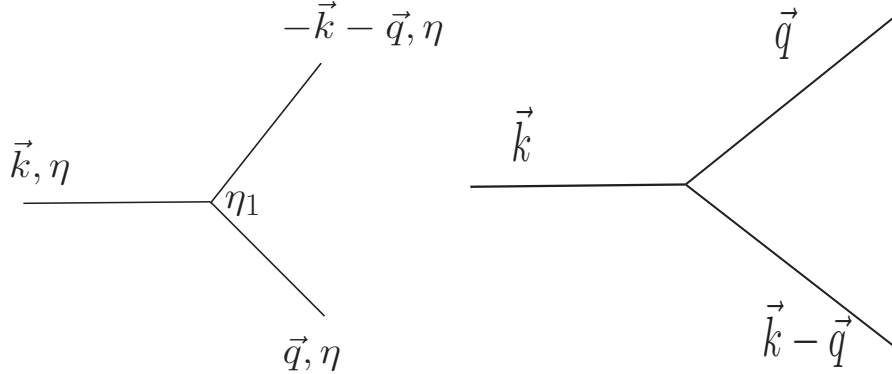


FIG. 41: Left panel: Equal-time three point function $\langle \chi(\vec{k}, \eta) \chi(\vec{q}, \eta) \chi(-\vec{k} - \vec{q}, \eta) \rangle$ in de Sitter space-time in the Born approximation. The conformal time coordinate η_1 of the vertex is integrated out. Right panel: Self-decay of quantum fluctuations of the inflaton. All lines correspond to the field ϕ , i.e, the quantum fluctuations of the inflaton.

Furthermore, the logarithmic secular term in Eq.(3.117) indicates that the three point function features secular divergences **even at the tree level**. It is argued in refs. [69, 70] that $-\ln[k_T \eta] \sim 60$ which is the number of e-folds from the time when fluctuations of wavenumber k_T first crossed the horizon till the end of inflation. However, such infrared logarithms are **secular terms** and have precisely the **same** origin as in the self-energy kernel and in the inflaton fluctuations discussed here (secs. IIIC and IIID). The same holds for the infrared logarithms in the three graviton scattering vertex [71, 72].

In particular, the self-energy computation corresponds to a further integration over the loop momentum q . In a fairly loose manner, the self-energy is basically the square of the three point correlation function integrated over the loop momentum. This is akin to the unitarity relation between the imaginary part of the forward scattering amplitude and the square of the transition amplitude in S-matrix theory.

In summary, the *interaction* between the quantum fluctuations gives rise to *non-gaussian* correlations which are determined by the three point function which is precisely related to the *self-energy* and the *decay* of the quantum fluctuations. Therefore, the decay of the quantum fluctuations of the scalar field will also lead to non-gaussian correlations and non-gaussianity in the power spectrum.

Then, there is a direct relationship between the self-energy, quantum decay and non-gaussian features of the power spectrum.

C. Quantum Loop Corrections to the inflaton potential and the power spectra from superhorizon modes and trace anomalies

Our goal is to obtain the *effective* potential that includes the one loop quantum corrections from fields that are *light* during the relevant inflationary stage.

Our program of study focuses on the understanding of quantum aspects of the basic inflationary paradigm. We previously addressed the decay of inflaton fluctuations in secs. III B 1-III B 2 [42]. In secs. III B 3-III B 4 [19] we focused on the quantum corrections to the equations of motion of the inflaton and the scalar fluctuations during slow-roll inflation. We integrated out not only the inflaton fluctuations but also the excitations associated with another scalar field. Since the power spectra of fields with masses $m \ll H$ are nearly scale invariant, strong infrared enhancements appear as revealed in these studies described in sec. III B [19, 42]. In addition, we find that a particular linear combination Δ of slow-roll parameters eq.(3.78) which measures the departure from scale invariance of the fluctuations provides a **natural** infrared regularization.

The small parameter that determines the validity of inflation as an effective *quantum field theory* below the Planck scale is $(H/M_{Pl})^2$ where H is the Hubble parameter during inflation and therefore the scale at which inflation occurs. The slow-roll expansion is in a very well defined sense an *adiabatic* approximation since the time evolution of the inflaton field is slow on the expansion scale. Thus the small dimensionless ratio $(H/M_{Pl})^2 \sim 10^{-9}$ [see eq.(1.178)], which is required for the validity of an effective field theory (EFT) is logically *independent* from the small dimensionless combinations of derivatives of the potential which ensure the validity of the slow-roll expansion.

Therefore, in this review article we invoke *two independent* approximations, the effective field theory (EFT) and the slow-roll approximation. The former is defined in terms of an expansion in the ratio $(H/M_{Pl})^2$, whereas the latter corresponds to an expansion in the (small) slow-roll parameters which is an expansion in $1/N$ (see sec. I D 2) [11]. Quantum loop corrections during inflation are considered also in ref.[55].

It is important to highlight the main differences between slow-roll inflation and the post-inflationary stage. During slow-roll inflation the dynamics of the scalar field is slow on the time scale of the expansion and consequently the change in the amplitude of the inflaton is small and quantified by the slow-roll parameters. The slow-roll approximation is indeed an *adiabatic approximation*. In striking contrast to this situation, during the post-inflationary stage of reheating the scalar field undergoes rapid and large amplitude oscillations that cannot be studied in a perturbative expansion [25, 27, 28, 29].

Brief summary of results in this section:

We obtain the quantum corrections to the inflaton potential up to one loop by including the contributions from scalar and tensor perturbations of the metric as well as one scalar and one fermion field coupled generically to the inflaton. Therefore, this study provides the most complete assessment of the general backreaction problem up to one loop that includes not only metric perturbations, but also the contributions from fluctuations of other light fields with a generic treatment of both bosonic and fermionic degrees of freedom. Motivated by an assessment of the quantum fluctuations that *could* be of observational interest, we focus on studying the effective inflaton potential during the cosmologically relevant stage of slow-roll inflation.

Both light bosonic fields as well as scalar density perturbations feature an infrared enhancement of their quantum corrections which is naturally regularized by the slow-roll parameters.

Fermionic contributions as expected do not feature any infrared enhancement and neither does the graviton contribution to the energy momentum tensor.

We find that in slow-roll and for light bosonic and fermionic fields there is a clean separation between the super and subhorizon contributions to the quantum corrections from scalar density metric and light bosonic field perturbations. For these fields the superhorizon contribution is of zero order in slow roll $\sim N^0$ as a consequence of the infrared enhancement regularized by slow-roll parameters. The subhorizon contribution to the energy momentum tensor from all the fields is completely determined by the trace anomaly of minimally coupled scalars, gravitons and fermionic fields.

We find the one loop effective potential to be

$$V_{eff}(\Phi_0) = V(\Phi_0) \left[1 + \frac{H_0^2}{3 (4\pi)^2 M_{Pl}^2} \left(\frac{\eta_v - 4\epsilon_v}{\eta_v - 3\epsilon_v} + \frac{3\eta_\sigma}{\eta_\sigma - \epsilon_v} + \mathcal{T} \right) \right] \quad (3.118)$$

where $V(\Phi_0)$ is the *classical* inflaton potential, $\eta_v, \epsilon_v, \eta_\sigma$ slow-roll parameters and $\mathcal{T} = \mathcal{T}_\Phi + \mathcal{T}_s + \mathcal{T}_t + \mathcal{T}_\Psi = -\frac{2903}{20} = -145.15$ is the total trace anomaly from the scalar metric, tensor, light scalar and fermion contributions.

The terms that feature ratios of slow-roll parameters arise from superhorizon contributions from curvature and scalar field perturbations. The last term in eq.(3.118) is independent of slow-roll parameters and is completely determined by the trace anomalies of the different fields. The term \mathcal{T} is the hallmark of the subhorizon contributions.

In the case when the mass of the light bosonic scalar field is much smaller than the mass of the inflaton fluctuations, we find the following result for the scalar curvature and tensor fluctuations including the one-loop quantum corrections,

$$\begin{aligned} |\Delta_{k,eff}^{\mathcal{R}}|^2 &= |\Delta_k^{\mathcal{R}}|^2 \left\{ 1 + \frac{2}{3} \left(\frac{H_0}{4\pi M_{Pl}} \right)^2 \left[1 + \frac{\frac{3}{8} r (n_s - 1) + 2 \frac{dn_s}{d \ln k}}{(n_s - 1)^2} + \frac{2903}{40} \right] \right\} \\ |\Delta_{k,eff}^{(T)}|^2 &= |\Delta_k^{(T)}|^2 \left\{ 1 - \frac{1}{3} \left(\frac{H_0}{4\pi M_{Pl}} \right)^2 \left[-1 + \frac{1}{8} \frac{r}{n_s - 1} + \frac{2903}{20} \right] \right\}, \\ r_{eff} &\equiv \frac{|\Delta_{k,eff}^{(T)}|^2}{|\Delta_{k,eff}^{\mathcal{R}}|^2} = r \left\{ 1 - \frac{1}{3} \left(\frac{H_0}{4\pi M_{Pl}} \right)^2 \left[1 + \frac{\frac{3}{8} r (n_s - 1) + \frac{dn_s}{d \ln k}}{(n_s - 1)^2} + \frac{8709}{20} \right] \right\}. \end{aligned} \quad (3.119)$$

The quantum corrections turn out to **enhance** the scalar curvature fluctuations $|\Delta_{k,eff}^{\mathcal{R}}|^2$ and to **reduce** the tensor fluctuations $|\Delta_{k,eff}^{(T)}|^2$ as well as their ratio r . The quantum corrections are always small, of the order $(H_0/M_{Pl})^2$, but it is interesting to see that these quantum effects are dominated by the trace anomalies and they correct both scalar and tensor fluctuations in a definite direction. Moreover, it is the tensor part of the trace anomaly which numerically yields the largest contribution.

Quantum trace (conformal) anomalies of the energy momentum tensor in gravitational fields constitute an important aspect of quantum field theory in curved backgrounds, (see for example [62] and references therein). In black hole backgrounds they are related to the Hawking radiation. It is interesting to see here that the trace anomalies appear in a relevant cosmological problem and dominate the quantum corrections to the primordial spectrum of curvature and tensor fluctuations.

1. Statement of the problem

Our goal is to obtain the one loop quantum corrections from fields with masses well below the energy scale of inflation M . Therefore, we consider the inflaton coupled to a scalar field σ and to Fermi fields with a generic Yukawa-type coupling. We take the fermions to be Dirac fields but it is straightforward to generalize to Weyl or Majorana fermions. We also include the contribution to the effective potential from scalar and tensor metric perturbations, thereby considering their *backreaction* up to one loop.

The Lagrangian density is taken to be

$$\mathcal{L} = \sqrt{-g} \left\{ \frac{1}{2} \dot{\varphi}^2 - \frac{1}{2} \left(\frac{\vec{\nabla} \varphi}{a} \right)^2 - V(\varphi) + \frac{1}{2} \dot{\sigma}^2 - \frac{1}{2} \left(\frac{\vec{\nabla} \sigma}{a} \right)^2 - \frac{1}{2} m_\sigma^2 \sigma^2 - G(\varphi) \sigma^2 + \bar{\Psi} \left[i \gamma^\mu \mathcal{D}_\mu \Psi - m_f - Y(\varphi) \right] \Psi \right\} \quad (3.120)$$

where $m_\sigma \ll M$, $m_f \ll M$, $G(\Phi)$ and $Y(\Phi)$ are generic interaction terms between the inflaton and the scalar and fermionic fields. Obviously this Lagrangian can be further generalized to include a multiplet of scalar and fermionic fields and such case can be analyzed as a straightforward generalization. For simplicity we consider one bosonic and one fermionic Dirac field.

The Dirac γ^μ are the curved space-time γ matrices and the fermionic covariant derivative is given by

$$\mathcal{D}_\mu = \partial_\mu + \frac{1}{8} [\gamma^c, \gamma^d] V_c^\nu (D_\mu V_{d\nu}) \quad , \quad D_\mu V_{d\nu} = \partial_\mu V_{d\nu} - \Gamma_{\mu\nu}^\lambda V_{d\lambda}$$

where the vierbein field is defined as

$$g^{\mu\nu} = V_a^\mu V_b^\nu \eta^{ab} \quad ,$$

η_{ab} is the Minkowski space-time metric and the curved space-time matrices γ^μ are given in terms of the Minkowski space-time ones γ^a by (greek indices refer to curved space time coordinates and latin indices to the local Minkowski space time coordinates)

$$\gamma^\mu = \gamma^a V_a^\mu \quad , \quad \{\gamma^\mu, \gamma^\nu\} = 2 g^{\mu\nu} \quad .$$

We will consider that the light scalar field σ has vanishing expectation value at all times, therefore inflationary dynamics is driven by one single scalar field, the inflaton ϕ . We now separate the homogeneous expectation value of the inflaton field from its quantum fluctuations as usual by writing

$$\varphi(\vec{x}, t) = \Phi_0(t) + \delta\varphi(\vec{x}, t) \quad .$$

We will consider the contributions from the quadratic fluctuations to the energy momentum tensor. There are *four* distinct contributions: i) scalar metric (density) perturbations, ii) tensor (gravitational waves) perturbations, iii) fluctuations of the light bosonic scalar field σ , iv) fluctuations of the light fermionic field Ψ .

Fluctuations in the metric are studied as usual, writing the metric as

$$g_{\mu\nu} = g_{\mu\nu}^0 + \delta^s g_{\mu\nu} + \delta^t g_{\mu\nu}$$

where $g_{\mu\nu}^0$ is the spatially flat FRW background metric which in conformal time is given by

$$g_{\mu\nu}^0 = a^2(\eta) \eta_{\mu\nu}$$

and $\eta_{\mu\nu} = \text{diag}(1, -1, -1, -1)$ is the flat Minkowski space-time metric. $\delta^{s,t} g_{\mu\nu}$ correspond to the scalar and tensor perturbations respectively. In longitudinal gauge

$$\delta^s g_{00} = a^2(\eta) 2\phi, \quad \delta^s g_{ij} = a^2(\eta) 2\psi \delta_{ij}, \quad \delta^t g_{ij} = -a^2(\eta) h_{ij}$$

where h_{ij} is transverse and traceless and we neglect vector modes since they are not generated in single field inflation.

Gauge invariant variables associated with the fluctuations of the scalar field and the potentials ϕ, ψ are constructed explicitly in ref.[5] where the reader can find their expressions. Expanding up to quadratic order in the scalar fields, fermionic fields and metric perturbations the part of the Lagrangian density that is quadratic in these fields is given by

$$\mathcal{L}_Q = \mathcal{L}_s[\delta\varphi^{gi}, \phi^{gi}, \psi^{gi}] + \mathcal{L}_t[h] + \mathcal{L}_\sigma[\sigma] + \mathcal{L}_\Psi[\bar{\Psi}, \Psi],$$

where

$$\begin{aligned} \mathcal{L}_t[h] &= \frac{M_{Pl}^2}{8} a^2(\eta) \partial_\alpha h_i^j \partial_\beta h_j^i \eta^{\alpha\beta}, \\ \mathcal{L}_\sigma[\sigma] &= a^4(\eta) \left\{ \frac{1}{2} \left(\frac{\sigma'}{a} \right)^2 - \frac{1}{2} \left(\frac{\nabla\sigma}{a} \right)^2 - \frac{1}{2} M_\sigma^2[\Phi_0] \sigma^2 \right\}, \\ \mathcal{L}_\Psi[\bar{\Psi}, \Psi] &= \bar{\Psi} \left[i \gamma^\mu \mathcal{D}_\mu \Psi - M_\Psi[\Phi_0] \right] \Psi, \end{aligned}$$

where the prime stands for derivatives with respect to conformal time and the labels (gi) stand for the gauge invariant quantities [5]. The explicit expression for $\mathcal{L}[\delta\varphi^{gi}, \phi^{gi}, \psi^{gi}]$ is given in ref.[5]. The effective masses for the bosonic and fermionic fields are given by

$$M_\sigma^2[\Phi_0] = m_\sigma^2 + G(\Phi_0), \quad M_\Psi[\Phi_0] = m_f + Y(\Phi_0). \quad (3.121)$$

We will focus on the study of the quantum corrections to the Friedmann equation, for the case in which both the scalar and fermionic fields are light in the sense that during slow-roll inflation,

$$M_\sigma[\Phi_0], M_\Psi[\Phi_0] \ll H_0, \quad (3.122)$$

at least during the cosmologically relevant stage corresponding to the 60 or so efolds before the end of inflation.

In conformal time the vierbeins V_a^μ are particularly simple

$$V_a^\mu = a(\eta) \delta_a^\mu \quad (3.123)$$

and the Dirac Lagrangian density simplifies to the following expression

$$\sqrt{-g} \bar{\Psi} \left(i \gamma^\mu \mathcal{D}_\mu \Psi - M_\Psi[\Phi_0] \right) \Psi = a^{\frac{3}{2}} \bar{\Psi} \left[i \not{\partial} - M_\Psi[\Phi_0] a(\eta) \right] \left(a^{\frac{3}{2}} \Psi \right) \quad (3.124)$$

where $i\not{\partial}$ is the usual Dirac differential operator in Minkowski space-time in terms of flat space time γ matrices.

From the quadratic Lagrangian given above the quadratic quantum fluctuations to the energy momentum tensor can be extracted.

The effective potential is identified with the expectation value of the 00 component of the energy momentum tensor in a state in which the expectation value of the inflaton field is Φ_0 . During slow roll inflation the expectation value Φ_0 evolves very slowly in time, the slow-roll approximation is indeed an adiabatic approximation, which justifies treating

Φ_0 as a constant in order to obtain the effective potential. The time variation of Φ_0 only contributes to higher order corrections in slow-roll. This is standard in *any* calculation of an effective potential. The energy momentum tensor is computed in the FRW inflationary background determined by the *classical* inflationary potential $V(\Phi_0)$, and the slow-roll parameters are also explicit functions of Φ_0 . Therefore the energy momentum tensor depends *implicitly* on Φ_0 through the background and *explicitly* on the masses for the light bosonic and fermionic fields given above.

Therefore the effective potential is given by

$$V_{eff}(\Phi_0) = V(\Phi_0) + \delta V(\Phi_0) \quad (3.125)$$

where

$$\delta V(\Phi_0) = \langle T_0^0[\Phi_0] \rangle_s + \langle T_0^0[\Phi_0] \rangle_t + \langle T_0^0[\Phi_0] \rangle_\sigma + \langle T_0^0[\Phi_0] \rangle_\Psi \quad (3.126)$$

(s, t, σ, Ψ) correspond to the energy momentum tensors of the quadratic fluctuations of the scalar metric, tensor fluctuations (gravitational waves), light boson field σ and light fermion field Ψ fluctuations respectively. Since these are the expectation values of a quadratic energy momentum tensor, $\delta V(\Phi_0)$ corresponds to the *one loop correction* to the effective potential.

2. Light scalar field coupled to the inflaton

We begin by analyzing the contribution to the effective potential from the light bosonic scalar field σ because this study highlights the main aspects which are relevant in the case of scalar metric (density) perturbations.

The bosonic Heisenberg field operators are expanded as follows

$$\sigma(\vec{x}, \eta) = \frac{1}{a(\eta)} \int \frac{d^3k}{(2\pi)^{\frac{3}{2}}} \left[e^{i\vec{k}\cdot\vec{x}} a_{\sigma, \vec{k}} S_\sigma(k, \eta) + e^{-i\vec{k}\cdot\vec{x}} a_{\sigma, \vec{k}}^\dagger S_\sigma^*(k, \eta) \right]. \quad (3.127)$$

During slow-roll inflation the effective mass of the σ field is given by eq.(3.121), just as for the inflaton, it is convenient to introduce a parameter η_σ defined to be

$$\eta_\sigma = \frac{M_\sigma^2[\Phi_0]}{3 H_0^2}. \quad (3.128)$$

Hence, the statement that the σ field is light corresponds to the condition

$$\eta_\sigma \ll 1. \quad (3.129)$$

This dimensionless parameter plays the same role for the σ field as the parameter η_v given by eq. (1.131) does for the inflaton fluctuation. It is indeed a slow roll parameter for the σ field.

The mode functions $S_\sigma(k, \eta)$ in eq.(3.127) obey the following equations up to quadratic order

$$S_\sigma''(k, \eta) + \left[k^2 + M_\sigma^2(\Phi_0) a^2(\eta) - \frac{a''(\eta)}{a(\eta)} \right] S_\sigma(k, \eta) = 0.$$

Using the slow-roll expressions eq.(1.134) and in terms of η_σ , these mode equations become

$$S_\sigma''(k, \eta) + \left[k^2 - \frac{\nu_\sigma^2 - \frac{1}{4}}{\eta^2} \right] S_\sigma(k, \eta) = 0 \quad ; \quad \nu_\sigma = \frac{3}{2} + \epsilon_v - \eta_\sigma + \mathcal{O}\left(\frac{1}{N^2}, \eta_\sigma^2, \frac{\eta_\sigma}{N}\right).$$

During slow-roll inflation Φ_0 is approximately constant, and the slow-roll expansion is an *adiabatic* expansion. As usual in the slow-roll approximation, the above equation for the mode functions is solved by assuming that Φ_0 , hence ν_σ are *constant*. This is also the same type of approximation entailed in *every* calculation of the effective potential. Therefore during slow-roll, the solution of the mode functions above are given by eq.(1.137),

$$S_\sigma(k, \eta) = \frac{1}{2} \sqrt{-\pi\eta} \, i^{\nu_\sigma + \frac{1}{2}} H_{\nu_\sigma}^{(1)}(-k\eta).$$

This choice of mode functions defines the Bunch-Davis vacuum, which obeys $a_{\vec{k}}|0\rangle_{BD} = 0$. It is important to highlight that there is no unique choice of vacuum or initial state, a recognition that has received considerable attention in the

literature, see for example [37, 85] and references therein. In this study we focus on Bunch-Davis initial conditions since this has been the standard choice to study the power spectra and metric perturbations, hence we can compare our results to the standard ones in the literature. The assessment for initial states others than Bunch-Davis is given in ref.[21].

The contribution to the effective potential from the light scalar field σ is given by

$$\langle T_{00} \rangle_\sigma = \frac{1}{2} \left\langle \dot{\sigma}^2 + \left(\frac{\nabla \sigma}{a(\eta)} \right)^2 + M_\sigma^2 [\Phi_0] \sigma^2 \right\rangle ,$$

where the dot stands for derivative with respect to cosmic time. The expectation values are in the Bunch-Davis vacuum state and yield the following contributions

$$\frac{1}{2} \langle (\dot{\sigma})^2 \rangle = \frac{H_0^4}{16\pi} \int_0^\infty \frac{dz}{z} z^2 \left| \frac{d}{dz} \left[z^{\frac{3}{2}} H_{\nu_\sigma}^{(1)}(z) \right] \right|^2 \quad (3.130)$$

$$\frac{1}{2} \left\langle \left(\frac{\nabla \sigma}{a^2(\eta)} \right)^2 \right\rangle = \frac{H_0^4}{16\pi} \int_0^\infty \frac{dz}{z} z^5 \left| H_{\nu_\sigma}^{(1)}(z) \right|^2 \quad (3.131)$$

$$\frac{M_\sigma^2 [\Phi_0]}{2} \langle \sigma^2(\vec{x}, t) \rangle = \frac{3 H_0^2 \eta_\sigma}{2} \int_0^\infty \frac{dk}{k} \mathcal{P}_\sigma(k, t) , \quad (3.132)$$

where $\mathcal{P}_\sigma(k, t)$ is the power spectrum of the σ field, which in terms of the spatial Fourier transform of the field $\sigma_{\vec{k}}(t)$ is given by

$$\mathcal{P}_\sigma(k, t) = \frac{k^3}{2\pi^2} \langle |\sigma_{\vec{k}}^2(t)| \rangle = \frac{H_0^2}{8\pi} (-k \eta)^3 \left| H_{\nu_\sigma}^{(1)}(-k \eta) \right|^2 .$$

For a light scalar field during slow-roll the power spectrum of the scalar field σ is nearly scale invariant and the index $\nu_\sigma \sim 3/2$. In the exact scale invariant case $\nu_\sigma = 3/2$,

$$z^3 \left| H_{\frac{3}{2}}^{(1)}(z) \right|^2 = \frac{2}{\pi} [1 + z^2]$$

and the integral of the power spectrum in eq. (3.132) not only features logarithmic and quadratic *ultraviolet* divergences but also a logarithmic *infrared* divergence. During slow-roll and for a light but massive scalar field the quantity

$$\Delta_\sigma = \frac{3}{2} - \nu_\sigma = \eta_\sigma - \epsilon_v + \mathcal{O} \left(\frac{1}{N^2}, \eta_\sigma^2, \frac{\eta_\sigma}{N} \right) \ll 1 ,$$

is a measure of the departure from scale invariance and provides a natural *infrared regulator*. We note that the contribution from eq.(3.132) to the effective potential, which can be written as

$$\frac{3 H_0^4 \eta_\sigma}{16 \pi} \int_0^\infty \frac{dz}{z} z^3 \left| H_{\nu_\sigma}^{(1)}(z) \right|^2 ,$$

is *formally* smaller than the contributions from eqs.(3.130)-(3.131) by a factor $\eta_\sigma \ll 1$. However, the logarithmic infrared divergence in the exact scale invariant case, leads to a single *pole* in the variable Δ_σ as described in refs. [19, 42]. To see this feature in detail, it proves convenient to separate the infrared contribution by writing the integral above in the following form

$$\int_0^\infty \frac{dz}{z} z^3 \left| H_{\nu_\sigma}^{(1)}(z) \right|^2 = \int_0^{\mu_p} \frac{dz}{z} z^3 \left| H_{\nu_\sigma}^{(1)}(z) \right|^2 + \int_{\mu_p}^\infty \frac{dz}{z} z^3 \left| H_{\nu_\sigma}^{(1)}(z) \right|^2 .$$

In the first integral we obtain the leading order contribution in the slow-roll expansion, namely the pole in Δ_σ , by using the small argument limit of the Hankel functions

$$z^3 \left| H_{\nu_\sigma}^{(1)}(z) \right|^2 \stackrel{z \rightarrow 0}{\simeq} \left[\frac{2^{\nu_\sigma} \Gamma(\nu_\sigma)}{\pi} \right]^2 z^{2\Delta_\sigma}$$

which yields

$$\int_0^{\mu_p} \frac{dz}{z} z^3 \left| H_{\nu_\sigma}^{(1)}(z) \right|^2 = \frac{2}{\pi} \left[\frac{1}{2\Delta_\sigma} + \frac{\mu_p^2}{2} + \gamma - 2 + \ln(2\mu_p) + \mathcal{O}(\Delta_\sigma) \right] ,$$

In the second integral for small but fixed μ_p , we can safely set $\Delta_\sigma = 0$ and by introducing an upper momentum (ultraviolet) cutoff Λ_p , we finally find

$$\int_0^{\Lambda_p} \frac{dz}{z} z^3 \left| H_{\nu_\sigma}^{(1)}(z) \right|^2 = \frac{1}{\pi} \left[\frac{1}{\Delta_\sigma} + \Lambda_p^2 + \ln \Lambda_p^2 + 2\gamma - 4 + \mathcal{O}(\Delta_\sigma) \right]$$

The simple pole in Δ_σ reflects the infrared enhancement arising from a nearly scale invariant power spectrum. While the terms that depend on Λ_p are of purely ultraviolet origin and correspond to the specific regularization scheme, the simple pole in Δ_σ originates in the *infrared* behavior and is therefore independent of the regularization scheme. A covariant regularization of the expectation value $\langle \sigma^2(\vec{x}, t) \rangle$ yields a result which feature the simple pole in Δ_σ plus terms which are ultraviolet finite and regular in the limit $\Delta_\sigma \rightarrow 0$. Such regular terms yield a contribution $\mathcal{O}(H^4 \eta_\sigma)$ to eq.(3.132) and are subleading in the limit of light scalar fields because they do not feature a denominator Δ_σ .

Therefore, to leading order in the slow-roll expansion and in $\eta_\sigma \ll 1$, the contribution from eq.(3.132) is given by,

$$\frac{M_\sigma^2[\Phi_0]}{2} \langle \sigma^2(\vec{x}, t) \rangle = \frac{3 H_0^4}{(4\pi)^2} \frac{\eta_\sigma}{\eta_\sigma - \epsilon_v} + \text{subleading in slow roll.}$$

In the first two contributions given by eqs.(3.130)-(3.131) extra powers of momentum arising either from the time or spatial derivatives, prevent the logarithmic infrared enhancements. These terms are infrared finite in the limit $\Delta_\sigma \rightarrow 0$ and their leading contribution during slow-roll can be obtained by simply setting $\nu_\sigma = 3/2$ in these integrals, which feature quartic, quadratic and logarithmic ultraviolet divergences. A covariant renormalization of these two terms leads to an ultraviolet and an infrared finite contribution to the energy momentum tensor of $\mathcal{O}(H_0^4)$, respectively. For the term given by eq.(3.132), the infrared contribution that yields the pole in Δ_σ compensates for the $\eta_\sigma \ll 1$ in the numerator, after renormalization of the ultraviolet divergence, the ultraviolet and infrared finite contributions to this term yields a contribution to the energy momentum tensor of order $\mathcal{O}(H_0^4 \eta_\sigma)$, without the small denominator, and therefore subleading. This analysis indicates that the leading order contributions to the energy momentum tensor for light scalar fields is determined by the infrared pole $\sim 1/\Delta_\sigma$ from eq.(3.132) and the fully renormalized contributions from (3.130)-(3.131), namely to leading order in slow-roll and η_σ

$$\langle T_{00} \rangle_\sigma = \frac{3 H_0^4}{(4\pi)^2} \frac{\eta_\sigma}{\frac{3}{2} - \nu_\sigma} + \frac{1}{2} \left\langle \dot{\sigma}^2 + \left(\frac{\nabla \sigma}{a(\eta)} \right)^2 \right\rangle_{ren} \quad (3.133)$$

In the expression above we have displayed explicitly the pole at $3/2 - \nu_\sigma = \eta_\sigma - \epsilon_v$.

In calculating the second term (renormalized expectation value) to leading order in eq.(3.133) we can set to zero the slow roll parameters ϵ_v , η_v as well as the mass of the light scalar, namely $\eta_\sigma = 0$. Hence, to leading order, the second term is identified with the 00 component of the renormalized energy momentum tensor for a free massless minimally coupled scalar field in exact de Sitter space time. Therefore we can extract this term from the known result for the renormalized energy momentum tensor for a minimally coupled free scalar boson of mass m_σ in de Sitter space time with a Hubble constant H_0 given by [62, 79, 80]

$$\begin{aligned} \langle T_{\mu\nu} \rangle_{ren} &= \frac{g_{\mu\nu}}{(4\pi)^2} \left\{ m_\sigma^2 H_0^2 \left(1 - \frac{m_\sigma^2}{2H_0^2} \right) \left[-\psi\left(\frac{3}{2} + \nu\right) - \psi\left(\frac{3}{2} - \nu\right) + \ln \frac{m_\sigma^2}{H_0^2} \right] + \frac{2}{3} m_\sigma^2 H_0^2 - \frac{29}{30} H_0^4 \right\}, \\ \nu &\equiv \sqrt{\frac{9}{4} - \frac{m_\sigma^2}{H_0^2}}. \end{aligned} \quad (3.134)$$

where $\psi(z)$ stands for the digamma function. This expression corrects a factor of two in ref.[62, 74]. In eq. (6.177) in [62] the D'Alembertian acting on $G^1(x, x')$ was neglected. However, in computing this term, the D'Alembertian must be calculated *before* taking the coincidence limit. Using the equation of motion yields the extra factor 2 and the expression eq.(3.134). This result eq.(3.134) for the renormalized energy momentum tensor was obtained by several different methods: covariant point splitting, zeta-function and Schwinger's proper time regularizations [62, 74].

The simple pole at $\nu = 3/2$ manifest in eq.(3.134)

$$\psi\left(\frac{3}{2} - \nu\right) \xrightarrow{\nu \rightarrow \frac{3}{2}} \frac{1}{\nu - \frac{3}{2}}.$$

coincides precisely with the similar simple pole in eq. (3.133) as can be gleaned by recognizing that $m_\sigma^2 = 3 H^2 \eta_\sigma$ as stated by eq.(3.128). This pole originates in the term $m_\sigma^2 \langle \sigma^2 \rangle$, which features an infrared divergence in the

scaling limit $\nu_\sigma = 3/2$. All the terms that contribute to the energy momentum tensor with space-time derivatives are infrared finite in this limit. Therefore, from the energy momentum tensor eq.(3.134) we can extract straightforwardly the leading contribution to the renormalized expectation value in eq.(3.133) in the limit $H_0 \gg m_\sigma$, and neglecting the slow-roll corrections to the scale factor. It is given by the last term in the bracket in eq.(3.134). Hence, we find the leading order contribution for $m_\sigma^2 \ll H_0^2$,

$$\langle T_{00} \rangle_\sigma = \frac{H_0^4}{(4\pi)^2} \left[\frac{3\eta_\sigma}{\eta_\sigma - \epsilon_v} - \frac{29}{30} + \mathcal{O}(\epsilon_v, \eta_\sigma, \eta_v) \right]. \quad (3.135)$$

The last term is completely determined by the trace anomaly [62, 73, 74, 75, 76, 79, 80] which is in turn determined by the short distance correlation function of the field and the background geometry.

3. Heavy scalar field coupled to the inflaton

We can study now the quantum corrections induced by **heavy** scalar particles with mass m_σ in the range

$$H_0^2 \ll m_\sigma^2 \ll M^2,$$

where the effective theory approach is valid. We obtain from eq.(3.134) for $m_\sigma^2 \gg H_0^2$,

$$\langle T_{00} \rangle_\sigma = -\frac{m_\sigma^2 H_0^2}{12 (4\pi)^2} \left[1 - \frac{32 H_0^2}{5 m_\sigma^2} + \mathcal{O}\left(\frac{H_0^4}{m_\sigma^4}\right) \right]. \quad (3.136)$$

This behavior can be compared with eq.(3.135) valid for $m_\sigma^2 \ll H_0^2$.

In any case the relative change of the effective potential induced by the quantum corrections is small:

$$\frac{\delta V_{eff}}{V_{eff}} = \frac{\langle T_{00} \rangle_\sigma}{3 M_{Pl}^2 H_0^2} = -\frac{1}{36 (4\pi)^2} \frac{m_\sigma^2}{M_{Pl}^2} \left[1 - \frac{32 H_0^2}{5 m_\sigma^2} + \mathcal{O}\left(\frac{H_0^4}{m_\sigma^4}\right) \right].$$

Therefore, we emphasize that in the slow-roll approximation there is a clean and unambiguous separation between the contribution from superhorizon modes, which give rise to simple poles in slow-roll parameters and that of subhorizon modes whose leading contribution is determined by the trace anomaly and the short distance behavior of the field.

4. Scalar curvature perturbations

The gauge invariant energy momentum tensor for quadratic scalar metric fluctuations has been obtained in ref.[20, 21, 77] where the reader is referred to for details.

We discussed in detail the zero-zero component of the gauge invariant energy momentum tensor in sec. II F 2. Just as in the case of the σ field, we expect an infrared enhancement arising from superhorizon modes, therefore, following ref.[20, 21, 77] we split the contributions to the energy momentum tensor as those from superhorizon modes, which yields the infrared enhancement, and the subhorizon modes for which we can set all slow-roll parameters to zero. Just as discussed above for the case of the σ field, since spatio-temporal derivatives bring higher powers of the momenta, we can neglect all derivative terms for the contribution from the superhorizon modes. Therefore, the contribution from superhorizon modes which reflects the infrared enhancement is extracted from [20, 21, 77]

$$\langle T_{00} \rangle_{IR} \approx \frac{1}{2} V''[\Phi_0] \langle (\delta\varphi(\vec{x}, t))^2 \rangle + 2 V'[\Phi_0] \langle \phi(\vec{x}, t) \delta\varphi(\vec{x}, t) \rangle. \quad (3.137)$$

The analysis of the solution of eq.(2.120) for superhorizon wavelengths in ref.[5] shows that in exact de Sitter space time $\phi_{\vec{k}} \sim \text{constant}$, hence it follows that during quasi-de Sitter slow-roll inflation for superhorizon modes

$$\dot{\phi}_{\vec{k}} \sim (\text{slow roll}) \times H_0 \phi_{\vec{k}} \quad (3.138)$$

Therefore, for superhorizon modes, the constraint equation (2.121) yields

$$\phi_{\vec{k}} = -\frac{V'(\Phi_0)}{2 V(\Phi_0)} \delta\varphi_{\vec{k}} + \text{higher orders in slow roll}. \quad (3.139)$$

Inserting this relation in eq.(2.120) and consistently neglecting the term $\dot{\phi}_{\vec{k}}$ according to eq.(3.138), we find the following equation of motion for the gauge invariant scalar field fluctuation in longitudinal gauge

$$\delta\ddot{\varphi}_{\vec{k}} + 3 H_0 \delta\dot{\varphi}_{\vec{k}} + \left[\frac{k^2}{a^2(\eta)} + 3 H_0^2 \eta_{\mathcal{R}} \right] \delta\varphi_{\vec{k}} = 0, \quad (3.140)$$

where we have used the definition of the slow-roll parameters ϵ_v ; η_v given in eq.(1.131), and introduced

$$\eta_{\mathcal{R}} \equiv \eta_v - 2 \epsilon_v \quad (3.141)$$

Eq.(3.140) is the equation of motion for a minimally coupled scalar field with mass squared $3 H_0^2 \eta_{\mathcal{R}}$ and we can use the results obtained in the case of the scalar field σ above. These superhorizon fluctuations $\delta\varphi_{\vec{k}}(t)$ coincide with the scalar curvature fluctuations $S_{\mathcal{R}}(k; \eta)$ for superhorizon modes studied in sec. IE 1, as it must be.

The quantum field $\delta\varphi(\vec{x}, t)$ is expanded as in eq.(1.121)

$$\delta\varphi(\vec{x}, \eta) \simeq \frac{u(\vec{x}, \eta)}{a(\eta)} = \frac{1}{a(\eta)} \int \frac{d^3 k}{(2\pi)^{\frac{3}{2}}} \left[\alpha_{\mathcal{R}}(\vec{k}) S_{\mathcal{R}}(k; \eta) e^{i\vec{k} \cdot \vec{x}} + \alpha_{\mathcal{R}}^\dagger(\vec{k}) S_{\mathcal{R}}^*(k; \eta) e^{-i\vec{k} \cdot \vec{x}} \right], \quad (3.142)$$

where the mode functions $S_{\mathcal{R}}(k; \eta)$ are given by eq.(1.137) with [see eq.(1.135)]

$$\nu = \nu_{\mathcal{R}} = \frac{3}{2} + \epsilon_v - \eta_{\mathcal{R}} = \frac{3}{2} + 3 \epsilon_v - \eta_v + \mathcal{O}\left(\frac{1}{N^2}\right) = \frac{3}{2} - \frac{1}{2}(n_s - 1) + \mathcal{O}\left(\frac{1}{N^2}\right). \quad (3.143)$$

In this case, the slow-roll quantity that regulates the infrared behavior is $\Delta_{\mathcal{R}} \equiv \eta_v - 3 \epsilon_v = \frac{1}{2}(n_s - 1)$.

Again we choose the Bunch-Davies vacuum state annihilated by the operators $a_{\delta, \vec{k}}$. Therefore, the contribution to $\langle T_{00} \rangle$ from superhorizon modes to lowest order in slow-roll is given by

$$\langle T_{00} \rangle_{IR} = 3 H_0^2 \left(\frac{\eta_v}{2} - 2 \epsilon_v \right) \left[\int_0^\infty \frac{dk}{k} \mathcal{P}_{\mathcal{R}}(k, \eta) \right]_{IR} \quad (3.144)$$

where the power spectrum of scalar fluctuations is given by

$$\mathcal{P}_{\mathcal{R}}(k, \eta) = \frac{k^3}{2\pi^2} \langle |\delta\varphi_{\vec{k}}(t)|^2 \rangle = \frac{H_0^2}{8\pi} (-k \eta)^3 \left| H_{\nu_{\mathcal{R}}}^{(1)}(-k \eta) \right|^2 \quad (3.145)$$

and the subscript IR in the integral refers only to the infrared pole contribution to $\Delta_{\mathcal{R}}$. Repeating the analysis presented in the case of the scalar field σ above, we finally find

$$\langle T_{00} \rangle_{IR} = \frac{3 H_0^4}{(4\pi)^2} \left[\frac{\eta_v - 4 \epsilon_v}{\eta_v - 3 \epsilon_v} + \mathcal{O}\left(\frac{1}{N}\right) \right] = \frac{3 H_0^4}{(4\pi)^2} \left[1 - \frac{r}{8(n_s - 1)} + \mathcal{O}\left(\frac{1}{N}\right) \right]. \quad (3.146)$$

Since both $n_s - 1$ and r are $\mathcal{O}(1/N)$, $\langle T_{00} \rangle_{IR}$ is generically infrared finite. The denominator $n_s - 1$ indicates that a near scale invariant primordial power produces infrared enhancement.

For subhorizon modes with wavevectors $k \gg a(t) H_0$, the solutions of the equation (2.120) are [5]

$$\phi_{\vec{k}}(t) \approx e^{\pm i k \eta} \Rightarrow \dot{\phi}_{\vec{k}}(t) \sim \frac{i k}{a(t)} \phi_{\vec{k}}(t) \quad (3.147)$$

For $k \gg a(t) H_0$ the constraint equation (2.121) entails that [20, 21, 77]

$$\phi_{\vec{k}}(t) \approx \frac{i a(t)}{2 M_{Pl} k} \dot{\Phi}_0 \delta\varphi_{\vec{k}}. \quad (3.148)$$

Replacing the expressions eqs.(2.122)-(2.123) in eq.(2.119) yields that all the terms featuring the gravitational potential ϕ are suppressed with respect to those featuring the scalar field fluctuation $\delta\varphi$ by powers of $H_0 a(t)/k \ll 1$ as observed in ref.[77]. Therefore, the contribution from subhorizon modes to $\langle T_{00} \rangle$ is given by

$$\langle T_{00} \rangle_{UV} \simeq \frac{1}{2} \langle (\dot{\delta\varphi})^2 \rangle + \frac{\langle (\nabla \delta\varphi)^2 \rangle}{2 a^2} \quad (3.149)$$

where we have also neglected the term with $V''[\Phi_0] = 3 H_0^2 \eta_v$ since $k^2/a^2 \gg H_0^2$ for subhorizon modes. Therefore, to leading order in slow-roll we find the renormalized expectation value of T_{00} given by

$$\langle T_{00} \rangle_{ren} \simeq \frac{3H_0^4}{(4\pi)^2} \frac{\eta_v - 4\epsilon_v}{\eta_v - 3\epsilon_v} + \frac{1}{2} \left\langle (\delta\dot{\varphi})^2 + \left(\frac{\nabla\delta\varphi}{a(\eta)} \right)^2 \right\rangle_{ren} \quad (3.150)$$

To obtain the renormalized expectation value in eq.(3.150) one can set all slow-roll parameters to zero to leading order and simply consider a massless scalar field minimally coupled in de Sitter space time. This is precisely what we have already calculated in the case of the scalar field σ above by using the known results in the literature for the covariantly renormalized energy momentum tensor of a massive minimally coupled field [62, 74, 79, 80], and we can just borrow the result from eq.(3.135). We find the following final result to leading order in slow-roll

$$\langle T_{00} \rangle_{ren} = \frac{H_0^4}{(4\pi)^2} \left[\frac{\eta_v - 4\epsilon_v}{\eta_v - 3\epsilon_v} - \frac{29}{30} + \mathcal{O}(\epsilon_v, \eta_\sigma, \eta_v) \right]. \quad (3.151)$$

The last term in eq.(3.151) is completely determined by the trace anomaly of a minimally coupled scalar field in de Sitter space time [62, 73, 74, 80].

5. Tensor perturbations

Tensor perturbations correspond to massless fields with two physical polarizations. They are treated in detail in sec. IE2.

The energy momentum tensor for gravitons only depends on derivatives of the field h_j^i therefore its expectation value in the Bunch Davies (BD) vacuum does not feature infrared singularities in the limit $\epsilon_v \rightarrow 0$. The absence of infrared singularities in the limit of exact de Sitter space time entails that we can extract the leading contribution to the effective potential from tensor perturbations by evaluating the expectation value of T_{00} in the BD vacuum in exact de Sitter space time, namely by setting all slow-roll parameters to zero. This yields the leading order in the slow-roll expansion.

Because de Sitter space time is maximally symmetric, the expectation value of the energy momentum tensor is given by [62, 82]

$$\langle T_{\mu\nu} \rangle_{BD} = \frac{g_{\mu\nu}}{4} \langle T_\alpha^\alpha \rangle_{BD} \quad (3.152)$$

and T_α^α is a space-time constant, therefore the energy momentum tensor is manifestly covariantly conserved. Of course, in a quantum field theory there emerge ultraviolet divergences and the regularization procedure must be compatible with the maximal symmetry. A large body of work has been devoted to study the trace anomaly in de Sitter space time implementing a variety of powerful covariant regularization methods that preserve the symmetry [62, 73, 74, 75, 76, 80] yielding a renormalized value of the expectation value of the $\langle T_{\mu\nu} \rangle_{BD}$ given by eq.(3.152). Therefore, the full energy momentum tensor is completely determined by the trace anomaly [62, 73, 80].

The contribution to the trace anomaly from gravitons has been given in refs. [62, 73, 80], it is

$$\langle T_\alpha^\alpha \rangle_t = -\frac{717}{80\pi^2} H_0^4 \quad (3.153)$$

From this result, we conclude that

$$\langle T_{00} \rangle_t = -\frac{717}{320\pi^2} H_0^4 \quad (3.154)$$

This result differs by a numerical factor from that obtained in ref. [78], presumably the difference is a result of a different regularization scheme.

6. Spinor fields

The Dirac equation in the FRW geometry is given by [see eq.(3.124)],

$$\left[i \not{\partial} - M_\Psi[\Phi_0] a(\eta) \right] \left(a^{\frac{3}{2}} \Psi(\vec{x}, \eta) \right) = 0. \quad (3.155)$$

The solution $\Psi(\vec{x}, \eta)$ can be expanded in spinor mode functions as

$$\Psi(\vec{x}, \eta) = \frac{1}{a^{\frac{3}{2}}(\eta)} \int \frac{d^3 k}{(2\pi)^{\frac{3}{2}}} \sum_{\lambda} e^{i\vec{k} \cdot \vec{x}} \left[b_{\vec{k}, \lambda} U_{\lambda}(\vec{k}, \eta) + d_{-\vec{k}, \lambda}^{\dagger} V_{\lambda}(-\vec{k}, \eta) \right], \quad (3.156)$$

where the spinor mode functions U, V obey the Dirac equations

$$\left[i \gamma^0 \partial_{\eta} - \vec{\gamma} \cdot \vec{k} - M(\eta) \right] U_{\lambda}(\vec{k}, \eta) = 0 \quad (3.157)$$

$$\left[i \gamma^0 \partial_{\eta} + \vec{\gamma} \cdot \vec{k} - M(\eta) \right] V_{\lambda}(\vec{k}, \eta) = 0 \quad (3.158)$$

and

$$M(\eta) \equiv M_{\Psi}[\Phi_0] a(\eta) \quad (3.159)$$

Following the method of refs.[27, 81], it proves convenient to write

$$U_{\lambda}(\vec{k}, \eta) = \left[i \gamma^0 \partial_{\eta} - \vec{\gamma} \cdot \vec{k} + M(\eta) \right] f_k(\eta) \mathcal{U}_{\lambda} \quad (3.160)$$

$$V_{\lambda}(\vec{k}, \eta) = \left[i \gamma^0 \partial_{\eta} + \vec{\gamma} \cdot \vec{k} + M(\eta) \right] g_k(\eta) \mathcal{V}_{\lambda} \quad (3.161)$$

with $\mathcal{U}_{\lambda}; \mathcal{V}_{\lambda}$ being constant spinors [27, 81] obeying

$$\gamma^0 \mathcal{U}_{\lambda} = \mathcal{U}_{\lambda} \quad , \quad \gamma^0 \mathcal{V}_{\lambda} = -\mathcal{V}_{\lambda} \quad (3.162)$$

The mode functions $f_k(\eta); g_k(\eta)$ obey the following equations of motion

$$\left[\frac{d^2}{d\eta^2} + k^2 + M^2(\eta) - i M'(\eta) \right] f_k(\eta) = 0 \quad (3.163)$$

$$\left[\frac{d^2}{d\eta^2} + k^2 + M^2(\eta) + i M'(\eta) \right] g_k(\eta) = 0 \quad (3.164)$$

Neglecting the derivative of Φ_0 with respect to time, namely terms of order $1/\sqrt{N}$ and higher, the equations of motion for the mode functions are given by

$$\left[\frac{d^2}{d\eta^2} + k^2 - \frac{\nu_+^2 - \frac{1}{4}}{\eta^2} \right] f_k(\eta) = 0 \quad (3.165)$$

$$\left[\frac{d^2}{d\eta^2} + k^2 - \frac{\nu_-^2 - \frac{1}{4}}{\eta^2} \right] g_k(\eta) = 0 \quad (3.166)$$

where

$$\nu_{\pm} = \frac{1}{2} \pm i \frac{M_{\Psi}[\Phi_0]}{H_0}$$

The scalar product of the spinors $U_{\lambda}(\vec{k}, \eta), V_{\lambda}(\vec{k}, \eta)$ yields

$$U_{\lambda}^{\dagger}(\vec{k}, \eta) U_{\lambda'}(\vec{k}, \eta) = \mathcal{C}^+(k) \delta_{\lambda, \lambda'} \quad , \quad V_{\lambda}^{\dagger}(\vec{k}, \eta) V_{\lambda'}(\vec{k}, \eta) = \mathcal{C}^-(k) \delta_{\lambda, \lambda'} \quad ,$$

where

$$\mathcal{C}^+(k) = f_k^{*\prime}(\eta) f_k'(\eta) + (k^2 + M^2(\eta)) f_k^*(\eta) f_k(\eta) + i M(\eta) \left(f_k'(\eta) f_k^*(\eta) - f_k(\eta) f_k^{*\prime}(\eta) \right) \quad ,$$

$$\mathcal{C}^-(k) = g_k^{*\prime}(\eta) g_k'(\eta) + (k^2 + M^2(\eta)) g_k^*(\eta) g_k(\eta) - i M(\eta) \left(g_k'(\eta) g_k^*(\eta) - g_k(\eta) g_k^{*\prime}(\eta) \right) \quad ,$$

are constants of motion by dint of the equations of motion for the mode functions $f_k(\eta)$, $g_k(\eta)$. The normalized spinor solutions of the Dirac equation are therefore given by

$$\begin{aligned} U_\lambda(\vec{k}, \eta) &= \frac{1}{\sqrt{\mathcal{C}^+(k)}} \left[i f'_k(\eta) - \vec{\gamma} \cdot \vec{k} f_k(\eta) + M(\eta) f_k(\eta) \right] \mathcal{U}_\lambda \\ V_\lambda(\vec{k}, \eta) &= \frac{1}{\sqrt{\mathcal{C}^-(k)}} \left[-i g'_k(\eta) + \vec{\gamma} \cdot \vec{k} g_k(\eta) + M(\eta) g_k(\eta) \right] \mathcal{U}_\lambda . \end{aligned}$$

We choose the solutions of the mode equations (3.165)-(3.166) to be

$$f_k(\eta) = \sqrt{\frac{-\pi k \eta}{2}} i^{\nu_+ + \frac{1}{2}} H_{\nu_+}^{(1)}(-k \eta) \quad , \quad g_k(\eta) = \sqrt{\frac{-\pi k \eta}{2}} i^{-\nu_- - \frac{1}{2}} H_{\nu_-}^{(2)}(-k \eta) . \quad (3.167)$$

We also choose the Bunch-Davies vacuum state such that

$$b_{\vec{k}, \lambda} |0\rangle_{BD} = 0 \quad , \quad d_{\vec{k}, \lambda} |0\rangle_{BD} = 0 \quad .$$

The choice of the mode functions eq.(3.167) yield the following normalization factors

$$\mathcal{C}^+(k) = \mathcal{C}^-(k) = 2 k^2 .$$

The energy momentum tensor for a spin 1/2 field is given by [62]

$$T_{\mu\nu} = \frac{i}{2} \left[\bar{\Psi} \gamma_{(\mu} \overleftrightarrow{\mathcal{D}}_{\nu)} \Psi \right]$$

and its expectation value in the Bunch-Davis vacuum is equal to

$$\langle T_{00} \rangle_{BD} = \frac{2}{a^4(\eta)} \int \frac{d^3 k}{(2\pi)^3} \left\{ M(\eta) - \text{Im} [g'_k(\eta) g_k^*(\eta)] \right\}$$

where $M(\eta)$ and $g_k(\eta)$ are given by eqs.(3.159) and (3.167), respectively. It is clear that this energy momentum tensor does not feature any infrared sensitivity because the real part of the Bessel functions index is $\text{Re} \nu_\pm = 1/2$. Of course this is expected since fermionic fields cannot feature large amplitudes due to the Pauli principle.

A lengthy computation using covariant point splitting regularization yields the following result

$$\langle T_{00} \rangle_\Psi = \frac{11 H_0^4}{960 \pi^2} \left\{ 1 + \frac{120}{11} \mathcal{M}^2 (\mathcal{M}^2 + 1) \left[-\text{Re} \psi(2 + i\mathcal{M}) - \frac{19}{12} - \gamma - 2 \ln 2 \right] \right\} \quad , \quad \mathcal{M} \equiv \frac{M_\Psi[\Phi_0]}{H_0} \quad (3.168)$$

The first term in the bracket in eq.(3.168) is recognized as the trace anomaly for fermions and is the only term that survives in the massless limit [62, 73, 74, 75, 76, 80]. For light fermion fields, $\mathcal{M} \ll 1$, and the leading contribution to the energy momentum tensor is completely determined by the trace anomaly, hence in this limit the contribution to the covariantly regularized effective potential from (Dirac) fermions is given by

$$\langle T_{00} \rangle_\Psi = \frac{11 H_0^4}{960 \pi^2} [1 + \mathcal{O}(\mathcal{M}^2)] .$$

This result is valid for Dirac fermions and it must be divided by a factor 2 for Weyl or Majorana fermions.

Gathering all the contributions we find that the effective potential at one-loop is given by,

$$\delta V(\Phi_0) = \frac{H_0^4}{(4\pi)^2} \left[\frac{\eta_v - 4 \epsilon_v}{\eta_v - 3 \epsilon_v} + \frac{3 \eta_\sigma}{\eta_\sigma - \epsilon_v} + \mathcal{T}_\Phi + \mathcal{T}_s + \mathcal{T}_t + \mathcal{T}_\Psi + \mathcal{O}(\epsilon_v, \eta_v, \eta_\sigma, \mathcal{M}^2) \right] ,$$

where (s, t, σ, Ψ) stand for the contributions of the scalar metric, tensor fluctuations, light boson field σ and light fermion field Ψ , respectively, where

$$\mathcal{T}_\Phi = \mathcal{T}_s = -\frac{29}{30} \quad ; \quad \mathcal{T}_t = -\frac{717}{5} \quad ; \quad \mathcal{T}_\Psi = \frac{11}{60} \quad (3.169)$$

The terms that feature the *ratios* of combinations of slow-roll parameters arise from the infrared or superhorizon contribution from the scalar density perturbations and scalar fields σ respectively. The terms $\mathcal{T}_{s,t,\Psi}$ are completely

determined by the trace anomalies of scalar, graviton and fermion fields respectively. Writing $H_0^4 = V(\Phi_0) H_0^2/[3 M_{Pl}^2]$ we can finally write the effective potential to leading order in slow-roll

$$V_{eff}(\Phi_0) = V(\Phi_0) \left[1 + \frac{H_0^2}{3 (4 \pi)^2 M_{Pl}^2} \left(\frac{\eta_v - 4 \epsilon_v}{\eta_v - 3 \epsilon_v} + \frac{3 \eta_\sigma}{\eta_\sigma - \epsilon_v} - \frac{2903}{20} \right) \right] \quad (3.170)$$

There are several remarkable aspects of this result:

(i) the infrared enhancement as a result of the near scale invariance of scalar field fluctuations, both from scalar density perturbations as well as from a light scalar field, yield corrections of *zeroth order in slow-roll*. This is a consequence of the fact that during slow-roll the particular combination $\Delta_\sigma = \eta_\sigma - \epsilon_v$ of slow-roll parameters yield a natural infrared cutoff.

(ii) the final one loop contribution to the effective potential displays the effective field theory dimensionless parameter H_0^2/M_{Pl}^2 confirming our previous study in sec. III B [19, 42],

(iii) the last term is completely determined by the trace anomaly, a purely geometric result of the short distance properties of the theory.

7. Quantum Corrections to the Scalar Curvature and Tensor power spectra

The quantum corrections to the effective potential lead to quantum corrections to the amplitude of scalar and tensor fluctuations. The scalar curvature and tensor fluctuations are given by eqs.(1.162) and (1.167), respectively.

We can include the leading quantum corrections in eqs.(1.162) and (1.167) replacing in it H and ϵ_v by the corrected parameters H_{eff} and ϵ_{eff} . That is,

$$H_{eff}^2 = H_0^2 + \delta H^2 \quad , \quad \epsilon_{eff} = \epsilon_v + \delta \epsilon_v \quad (3.171)$$

with

$$H_{eff}^2 = \frac{V_{eff}(\Phi_0)}{3 M_{Pl}^2} \quad , \quad \epsilon_{eff} = \frac{M_{Pl}^2}{2} \left[\frac{V'_{eff}(\Phi_0)}{V_{eff}(\Phi_0)} \right]^2 \quad , \quad (3.172)$$

and where $V_{eff}(\Phi_0)$ is given by eq.(3.170). We thus obtain,

$$\begin{aligned} \frac{\delta H^2}{H_0^2} &= \frac{1}{3} \left(\frac{H_0}{4 \pi M_{Pl}} \right)^2 \left[\frac{\eta_v - 4 \epsilon_v}{\eta_v - 3 \epsilon_v} + \frac{3 \eta_\sigma}{\eta_\sigma - \epsilon_v} - \frac{2903}{20} \right] \quad , \quad (3.173) \\ \frac{\delta \epsilon_v}{\epsilon_v} &= \frac{2}{3} \left(\frac{H_0}{4 \pi M_{Pl}} \right)^2 \left\{ \frac{\xi_v + 12 \epsilon_v (2 \epsilon_v - \eta_v)}{2 (\eta_v - 3 \epsilon_v)^2} + \frac{3 \eta_\sigma}{(\eta_\sigma - \epsilon_v)^2} \left[\eta_\sigma + \eta_v - 2 \epsilon_v - \sqrt{2 \epsilon_v} M_{Pl} \frac{d \log M_\sigma[\Phi_0]}{d \Phi_0} \right] - \frac{2903}{20} \right\} \end{aligned}$$

Inserting eq.(3.173) into eqs.(3.171) and (3.172) yields after calculation, for the scalar perturbations,

$$\begin{aligned} |\Delta_{k,eff}^{\mathcal{R}}|^2 &= |\Delta_k^{\mathcal{R}}|^2 \left[1 - \frac{\delta \epsilon_v}{\epsilon_v} + \frac{\delta H^2}{H^2} \right] = |\Delta_k^{\mathcal{R}}|^2 \left\{ 1 - \frac{1}{3} \left(\frac{H_0}{4 \pi M_{Pl}} \right)^2 \left[\frac{\xi_v + 12 \epsilon_v^2 - \eta_v^2 - 5 \epsilon_v \eta_v}{(\eta_v - 3 \epsilon_v)^2} + \right. \right. \\ &\quad \left. \left. + \frac{3 \eta_\sigma}{(\eta_\sigma - \epsilon_v)^2} \left[\eta_\sigma - 3 \epsilon_v + 2 \eta_v - 2 \sqrt{2 \epsilon_v} M_{Pl} \frac{d \log M_\sigma[\Phi_0]}{d \Phi_0} \right] - \frac{2903}{20} \right] \right\} \quad , \quad (3.174) \end{aligned}$$

and for the tensor perturbations,

$$|\Delta_{k,eff}^{(T)}|^2 = |\Delta_k^{(T)}|^2 \left[1 + \frac{\delta H^2}{H^2} \right] = |\Delta_k^{(T)}|^2 \left\{ 1 + \frac{1}{3} \left(\frac{H_0}{4 \pi M_{Pl}} \right)^2 \left[\frac{\eta_v - 4 \epsilon_v}{\eta_v - 3 \epsilon_v} + \frac{3 \eta_\sigma}{\eta_\sigma - \epsilon_v} - \frac{2903}{20} \right] \right\} \quad . \quad (3.175)$$

where $M_\sigma[\Phi_0]$ and η_σ are given by eqs.(3.121) and (3.128), respectively.

Since the field σ is assumed much lighter than the inflaton, and since

$$\eta_\sigma \sim \left(\frac{m_\sigma}{m_{inflaton}} \right)^2 \eta_v \quad ,$$

for $m_\sigma^2 \ll m_{inflaton}^2$, we can neglect terms proportional to η_σ . in the expressions for $|\Delta_k^{\mathcal{R}}|^2$ and $|\Delta_{k,eff}^{(T)}|^2$. Moreover, it is particularly illuminating to express the slow-roll parameters in eqs.(3.174)-(3.175) in terms of the observables n_s , r and the spectral running of the scalar index using

$$\begin{aligned} \epsilon_v &= \frac{r}{16} \quad , \quad \eta_v = \frac{1}{2} \left(n_s - 1 + \frac{3}{8} r \right) \quad , \\ \xi_v &= \frac{r}{4} \left(n_s - 1 + \frac{3}{16} r \right) - \frac{1}{2} \frac{dn_s}{d \ln k} \quad , \quad \eta_v - 3 \epsilon_v = \frac{1}{2} (n_s - 1) \quad , \\ \sigma_v &= -\frac{r}{8} \left[\left(n_s - 1 + \frac{r}{32} \right)^2 - \frac{9r^2}{1024} \right] + \frac{1}{4} \left(n_s - 1 - \frac{9r}{8} + \frac{r^2}{16} \right) \frac{dn_s}{d \ln k} \\ &\quad - \frac{1}{4} \left(1 - \frac{r}{6} \right) \left(n_s - 1 + \frac{3r}{8} \right) \frac{dr}{d \ln k} + \frac{1}{2} \left(1 - \frac{r}{6} \right) \frac{d^2 n_s}{d(\ln k)^2} . \end{aligned} \quad (3.176)$$

We find from eqs.(3.174)-(3.175),

$$\begin{aligned} |\Delta_{k,eff}^{\mathcal{R}}|^2 &= |\Delta_k^{\mathcal{R}}|^2 \left\{ 1 + \frac{2}{3} \left(\frac{H_0}{4 \pi M_{Pl}} \right)^2 \left[1 + \frac{\frac{3}{8} r (n_s - 1) + 2 \frac{dn_s}{d \ln k} + \frac{2903}{40}}{(n_s - 1)^2} \right] \right\} \\ |\Delta_{k,eff}^{(T)}|^2 &= |\Delta_k^{(T)}|^2 \left\{ 1 - \frac{1}{3} \left(\frac{H_0}{4 \pi M_{Pl}} \right)^2 \left[-1 + \frac{1}{8} \frac{r}{n_s - 1} + \frac{2903}{20} \right] \right\} . \end{aligned} \quad (3.177)$$

The denominators in $n_s - 1$ indicate that a near scale invariant primordial power produces infrared enhancement.

We see that the anomalies contribution $\frac{2903}{40} = 72.575$ and $\frac{2903}{20} = 145.15$ presumably dominate both quantum corrections. The other terms are expected to be of order one and anyway smaller than these large anomalies contribution. The anomalies contribution is dominated in turn by the tensor part \mathcal{T}_t [see eq.(3.169)]. Only fermions give contributions with the opposite sign. However, one needs at least 783 species of fermions to compensate the tensor part.

These quantum corrections also affect the ratio r of tensor/scalar fluctuations as follows,

$$r_{eff} \equiv \frac{|\Delta_{k,eff}^{(T)}|^2}{|\Delta_{k,eff}^{\mathcal{R}}|^2} = r \left\{ 1 - \frac{1}{3} \left(\frac{H_0}{4 \pi M_{Pl}} \right)^2 \left[1 + \frac{\frac{3}{8} r (n_s - 1) + \frac{dn_s}{d \ln k} + \frac{8709}{20}}{(n_s - 1)^2} \right] \right\} \quad (3.178)$$

We expect this quantum correction to the ratio to be negative as the anomaly contributions dominates: $\frac{8709}{20} = 435.45$.

The brackets in eqs.(3.177)-(3.178) are of order N^0 since the numerators are of the same order in $\mathcal{O}(1/N)$ than the denominators.

Therefore, the quantum corrections **enhance** the scalar curvature fluctuations while they **reduce** the tensor fluctuations as well as their ratio r . The quantum corrections are small, of the order $(H_0/M_{Pl})^2$, but it is interesting to see that the quantum effects are dominated by the trace anomalies and they correct both fluctuations in a definite direction.

8. Conclusions and further questions

The results of our study bring about several questions and implications:

- The effective theory of inflation indicates that the quantum inflaton decay rate into itself is of the order $\Gamma_{\varphi \rightarrow \varphi \varphi} / H_0 \sim 10^{-11}$ as shown in sec. IIIB 5. This corresponds to a decay rate in cosmic time $\Gamma_{\varphi \rightarrow \varphi \varphi} \sim 10^3$ GeV. Although these values may seem small, it must be noticed that the decay is a secular, namely cumulative effect.
- The generation of superhorizon fluctuations during inflation is usually referred to as ‘acausal’ since the superhorizon region is causally disconnected from the observer. We have found that fluctuation modes deep inside the horizon decay into superhorizon modes, and therefore there is a coupling between modes inside and outside the horizon in quantum theory. The phase space for this process opens up as the physical wavelength approaches the horizon. This process that couples modes inside and outside the horizon with a coupling that effectively depends on the wave vector leads to *distortions* in the power spectrum. These distortions are of the order $(M/M_{Pl})^2 \ll 1$ as shown in refs. [19, 20] (see sec.III C).

- In the non-interacting theory, the equation of motion for the gauge invariant Newtonian potential (equal to the curvature perturbation) features a constant of motion for superhorizon wavelengths [5, 34]. This is used to estimate the spectrum of density perturbations in inflationary universe models. It is conceivable that this conservation law will no longer hold in higher orders in slow-roll when interactions are included. We expect this to be the case for two reasons: the coupling between modes inside and outside the horizon as well as the decay of superhorizon modes. Clearly the violation of the conservation law, if present, will be small in slow-roll, but this non-conservation may also lead to small *distortions* in the power spectrum.
- While we have focused on the decay process during inflation, our results, in particular the decay of superhorizon fluctuations and the coupling between modes inside and outside the Hubble radius, raise the possibility of similar processes being available during the radiation dominated phase. If this would be the case, the decay of short wavelength modes into superhorizon modes can serve as an active process for seeding superhorizon fluctuations.

Forthcoming observations of CMB anisotropies as well as large scale surveys with ever greater precision will provide a substantial body of high precision observational data which may hint at corrections to the generic and robust predictions of slow-roll and fast-roll inflation. Such observations will pave the way for a better determination of inflaton potential. Studying the possible observational consequences of the quantum phenomena presented in this review article will therefore prove a worthwhile endeavor.

The quantum loop corrections turn to be of the order $(M/M_{Pl})^2 \sim 10^{-9}$ which validates the tree level results and the effective field theory approach to inflationary dynamics.

D. Outlook and future perspectives

This review presents the state of the art of the effective theory of inflation and its successful confrontation with the CMB and LSS data.

We can highlight as perspectives for a foreseeable future:

- Measurement of the tensor/scalar ratio r by the forthcoming CMB experiments. This would be the **first** detection of (linearized) gravitational waves as predicted by Einstein's General Relativity. In addition, since such primordial gravitational waves were born as quantum fluctuations, this would be the **first** detection of gravitons, namely, **quantized** gravitational waves at tree level. Such detection of the primordial gravitational waves will test our prediction $r \simeq 0.05$ based on the effective theory of slow-roll inflation (broken symmetric binomial and trinomial potentials) [14, 23].
- The running of the spectral index $dn_s/d\ln k$. Since the range of the cosmologically relevant modes is $\Delta \ln k < 9$, we have $\Delta n_s < 9/N^2 \sim 0.0025$, where we use the generic estimate eq.(1.171). Therefore, the effective theory of slow-roll inflation indicates that the detection of the running calls for measurements of n_s with a one per thousand precision on a wide range of wavenumbers.
- Non-gaussianity measurements. Although this subject is beyond the scope of this review, let us recall that primordial non-gaussianity is of the order $f_{NL} \sim 1/N$ in single-field slow-roll inflation [70]. Such small primordial non-gaussianity is hardly expected to be measured in a near future.
- More precise measurements of n_s together with better data on r and $dn_s/d\ln k$ will permit to better select the correct inflationary model. This will test our prediction that a broken symmetric inflaton potential with moderate nonlinearity (new inflation) best describes the data [14, 23].

Acknowledgments

We thank M. Giovannini, E. Komatsu, A. Lasenby, L. Page, R. Rebolo, D. Spergel for fruitful discussions. D. B. acknowledges support from the U.S. National Science Foundation through grant No: PHY-0553418.

-
- [1] Kazanas D, *ApJ* **241**, L59 (1980); Guth A, *Phys. Rev.* **D23**, 347 (1981); Sato K, *MNRAS*, **195**, 467 (1981).
 [2] Kolb EW and Turner MS, *The Early Universe*, Addison Wesley. Redwood City, C.A. 1990.

- [3] Dodelson S, *Modern Cosmology*, Academic Press, 2003.
Longair, MS, *Galaxy formation*, Springer-Verlag, Berlin, 1998.
Coles P and Lucchin F, *Cosmology*. J Wiley, Chichester, 1995.
- [4] M. Giovannini, Int. J. Mod. Phys. A22, 2697 (2007), astro-ph/0703730.
- [5] See for example: Hu W., Dodelson S., *Ann. Rev. Astron. Ap.* 40: 171 (2002); Lidsey J, Liddle A, Kolb E, Copeland E, Barreiro T, Abney M, *Rev. of Mod. Phys.* 69: 373, (1997). Hu W., astro-ph/0402060. Mukhanov VF, Feldman HA, Brandenberger RH, *Phys. Rep.* 215:203 (1992). A. Riotto, hep-ph/0210162. Liddle AR, Lyth DH, *Cosmological Inflation and Large Scale Structure*, Cambridge University Press, 1999.
- [6] M. S. Turner, Phys. Rev. D48, 3502 (1993). A. R. Liddle, P. Parsons, J. D. Barrow, Phys. Rev. **D50**, 7222 (1994). S. Dodelson, W. H. Kinney, E. W. Kolb, Phys. Rev. **D56**, 3207 (1997). S. M. Leach, A. R. Liddle, J. Martin, D. J. Schwarz, Phys. Rev. D66, 023515 (2002). N. Bartolo, S. Matarrese, A. Riotto, Phys. Rev. D64, 083514 (2001). N. Bartolo, E. Komatsu, S. Matarrese, A. Riotto, Phys. Rept. 402 (2004) 103. S. M. Leach, A. R. Liddle, Phys. Rev. D68, 123508 (2003). V. Barger, H. S. Lee, D. Marfatia, Phys. Lett. B565, 33 (2003). K. Kadota, S. Dodelson, W. Hu, E. D. Stewart, Phys. Rev. D72 (2005) 023510.
- [7] Cole et al. MNRAS, 362, 505 (2005). Eisenstein et al. ApJ, 633, 560 (2005). W. J. Percival et al. Ap. J. 657 (2007) 51 and MNRAS, 381 (2007) 1053.
- [8] C. L. Bennett *et.al.* (WMAP collaboration), Ap. J. Suppl. **148**, 1 (2003).
A. Kogut *et.al.* (WMAP collaboration), Ap. J. Suppl. **148**, 161 (2003).
D. N. Spergel *et. al.* (WMAP collaboration), Ap. J. Suppl. **148**, 175 (2003).
H. V. Peiris *et.al.* (WMAP collaboration), Ap. J. Suppl.**148**, 213 (2003).
- [9] D. N. Spergel *et. al.* (WMAP collaboration), ApJS, 170, 377 (2007).
L. Page, *et. al.* (WMAP collaboration), ApJS, 170, 335 (2007)
G. Hinshaw, *et. al.* (WMAP collaboration), ApJS, 170, 288 (2007).
N. Jarosik, *et. al.* (WMAP collaboration), ApJS, 170, 263 (2007).
- [10] E. Komatsu et al.(WMAP collaboration), arXiv:0803.0547.
G. Hinshaw et al.(WMAP collaboration), arXiv:0803.0732.
M. R. Nolta et al.(WMAP collaboration), arXiv:0803.0593.
- [11] D. Boyanovsky, H. J. de Vega, N. G. Sánchez, Phys. Rev. **D 73**, 023008 (2006).
- [12] D. Cirigliano, H. J. de Vega, N. G. Sánchez, Phys. Rev. **D 71**, 103518 (2005).
- [13] H. J. de Vega, N. G. Sánchez, Phys. Rev. **D 74**, 063519 (2006).
- [14] C. Destri, H. J. de Vega, N. G. Sánchez, astro-ph/0703417, Phys. Rev. **D77**, 043509 (2008).
- [15] G. F. Smoot *et. al.* (COBE collaboration), Astro. Phys. Jour. **396**, 1 (1992).
- [16] Statistical Physics, vol 9, E M Lifshitz, L P Pitaevsky, Pergamon Press, Oxford 1980, see secs. 142 part I and 45 part II.
L. D. Landau, Zh. Eksp. Teor. Fiz., **7**, 19 (1937) and **7**, 545 (1937) and in *Collected Papers of L. D. Landau*, Pergamon Press, Oxford, 1965. V. L. Ginsburg, Zh. Eksp. Teor. Fiz. **15**, 739 and **10**, 107 (1945). V. L. Ginsburg, L. D. Landau, Zh. Eksp. Teor. Fiz. **20**, 1064 (1950). V. L. Ginsburg, *About Science, Myself and Others*, Part I, Chapters 5-7, IoP, Bristol, 2005.
- [17] H. Leutwyler, Ann. Phys. 235, 165 (1994), hep-ph/9409423. S. Weinberg, hep-ph/9412326 and ‘The Quantum Theory of Fields’, vol. 2, Cambridge University Press, Cambridge, 2000.
- [18] D. Boyanovsky, H. J. de Vega, C. M. Ho, N. G. Sánchez, Phys. Rev. **D75**, 123504 (2007).
- [19] D. Boyanovsky, H. J. de Vega, N. G. Sánchez, Nucl. Phys. **B747**, 25 (2006).
- [20] D. Boyanovsky, H. J. de Vega, N. G. Sánchez, Phys. Rev. **D72**, 103006 (2005).
- [21] D. Boyanovsky, H. J. de Vega, N. G. Sánchez, Phys. Rev. **D 74**, 123006 (2006).
- [22] D. Boyanovsky, H. J. de Vega, N. G. Sánchez, Phys. Rev. **D 74**, 123007 (2006).
- [23] C. Destri, H. J. de Vega, N. G. Sánchez, Phys. Rev. **D 78**, 023013 (2008).
- [24] M. Kowalski *et al.*, arXiv:0804.4142.
- [25] D. Boyanovsky, H. J. de Vega, in *Astrofundamental Physics*, NATO ASI series vol. 562, 2000, Lectures at the Chalonge School, astro-ph/0006446. D. Boyanovsky, F. J. Cao, H. J. de Vega, Nucl. Phys. **B 632**, 121 (2002). D. Boyanovsky, D. Cormier, H. J. de Vega, R. Holman, *Phys. Rev.* D55: 3373 (1997); D. Boyanovsky, D. Cormier, H. J. de Vega, R. Holman, A. Singh, M. Srednicki, *Phys. Rev.* D56: 1939 (1997). D. Boyanovsky, H. J. de Vega, R. Holman, Phys. Rev. D49, 2769 (1994). D. Boyanovsky, H. J. de Vega, R. Holman, J. F. J. Salgado, Phys. Rev. **D54** 7570, (1996).
- [26] J. Traschen, R. Brandenberger, Phys. Rev. D42, 2491 (1990), Y. Shtanov, J. Traschen, R. Brandenberger, Phys. Rev. D51, 5438 (1995), L. Kofman, A. Linde, A. Starobinsky, Phys. Rev. Lett. 73, 3195 (1994); Phys. Rev. Lett. 76, 1011 (1996). A. Linde, in *Current Topics in Astrofundamental Physics*, ‘The Early Universe’, Proceedings of the Chalonge Erice School, N. Sánchez and A. Zichichi Editors, Nato ASI series C, vol. 467, 1995, Kluwer Acad. Publ.
D. I. Kaiser, Phys. Rev. D53 (1996) 1776.
- [27] J. Baacke, C. Patzold, Phys. Rev. **D62**, 084008 (2000).; *ibid* D61:024016,2000. J. Baacke, K. Heitmann, C. Patzold, Phys. Rev. D58:125013,1998; *ibid* D57:6406,1998 and D56:6556,1997.
- [28] S. A. Ramsey, B. L. Hu, Phys. Rev. **D56**. 661, (1997); *ibid* 678, (1997). S. A. Ramsey, B. L. Hu, A. M. Stylianopoulos, Phys. Rev. D57:6003,1998.
- [29] D. Boyanovsky, D. Cormier, H. J. de Vega, R. Holman, S. Prem Kumar, Phys. Rev. **D57**, 2166 (1998).
- [30] D. Boyanovsky, F. J. Cao, H. J. de Vega, *Nucl. Phys.* B 632: 121 (2002).
F. J. Cao, H. J. de Vega, N. Sanchez, *Phys. Rev.* D70: 083528 (2004).
- [31] D. Boyanovsky, C. Destri, H. J. de Vega, Phys. Rev. **D69**, 045003 (2004).

- C. Destri, H. J. de Vega, Phys. Rev. **D73**, 025014 (2006).
- [32] A. Albrecht, P. J. Steinhardt, Phys. Rev. Lett. **48**, 1220 (1982). A. D. Linde, Phys. Lett. **108B**, 389 (1982).
- [33] A. D. Linde, Phys. Lett. **129B**, 177 (1983).
- [34] A. A. Starobinsky, JETP Lett. **30**, 682 (1979). V. F. Mukhanov, G. V. Chibisov, Soviet Phys. JETP Lett. **33**, 532 (1981). S. W. Hawking, Phys. Lett. **B115**, 295 (1982). A. H. Guth, S. Y. Pi, Phys. Rev. Lett. **49**, 1110 (1982). A. A. Starobinsky, Phys. Lett. **B117**, 175 (1982). J. M. Bardeen, P. J. Steinhardt, M. S. Turner, Phys. Rev. **D28**, 679 (1983).
- [35] W.-M. Yao et al., Journal of Physics G **33**, 1 (2006).
- [36] D. Boyanovsky, hep-ph/0102120, in the Proceedings of the Nato ASI, Eds, H. J. de Vega, I. Khalatnikov, N. Sanchez, p. 3, Kluwer, Dordrecht, 2001.
D. Boyanovsky, H. J. de Vega, D. J. Schwarz, hep-ph/0602002, Ann. Rev. Nucl. Part. Sci. **56**, 441-500, (2006).
- [37] P. R. Anderson, C. Molina-Paris, E. Mottola, Phys. Rev. **D72**, 043515 (2005); S. Habib, C. Molina-Paris, E. Mottola, Phys. Rev. **D61**, 024010 (2000); P. R. Anderson, W. Eaker, S. Habib, C. Molina-Paris, E. Mottola, Phys. Rev. **D62**, 124019 (2000).
- [38] M. Giovannini, Int. J. Mod. Phys. **D14** 363 (2005).
- [39] M. Giovannini, Class. Quan. Grav. **20** 5455 (2003).
- [40] A. Lasenby, C. Doran, Phys. Rev. D **71**, 063502 (2005) and astro-ph/0411579.
- [41] V. A. Belinsky, L. P. Grishchuk, Ya. B. Zeldovich, I. M. Khalatnikov, Phys. Lett. **B 155**, 232, (1985), JETP **62**, 195 (1985).
- [42] D. Boyanovsky, H. J. de Vega, Phys. Rev. **D70**, 063508 (2004).
D. Boyanovsky, H. J. de Vega, N. G. Sánchez, Phys. Rev. **D 71**, 023509 (2005).
- [43] A. Lewis, S. Bridle, Phys. Rev. D **66**, 103511 (2002). <http://cosmologist.info/cosmomc/>
- [44] C. L. Reichardt *et al.*, arXiv:0801.1491.
- [45] A. Linde, Phys. Rev. D **49**, 748 (1994). J. García Bellido, A. Linde, Phys. Rev. D **57**, 6075 (1998). E. J. Copeland, A. R. Liddle, D. H. Lyth, E. D. Stewart, D. Wands, Phys. Rev. D **49**, 6410 (1994).
- [46] D. H. Lyth, Phys. Rev. Lett. **78**, 1861 (1997). G. Efstathiou, K. J. Mack, astro-ph/0503360.
- [47] L. Verde, H. V. Peiris, R. Jimenez, JCAP **0601** (2006) 019.
- [48] F. C. Adams, J. R. Bond, K. Freese, J. A. Frieman, A. V. Olinto, Phys. Rev. D **47**, 426 (1993).
- [49] H. M. Hodges, G. R. Blumenthal, L. A. Kofman, J. R. Primack, Nucl. Phys. B **335**, 197 (1990).
- [50] H. Peiris, R. Easther, JCAP **0607**, 002 and 0610, 017, (2006). F. Finelli, M. Rianna, N. Mandolesi, JCAP **0612** (2006) 006. A. R. Liddle et al., Phys. Rev. D **74**, 083512 (2006). K. M. Hufenberger, H. K. Eriksen, F. K. Hansen, Astrophys. J. **651**, L81 (2006). H. K. Eriksen et al., ApJ, **656**, 641 (2007). D. Parkinson, P. Mukherjee, A. R. Liddle, Phys. Rev. D **73** (2006) 123523. M. Viel, M. G. Haehnelt, A. Lewis, Mon. Not. Roy. Astron. Soc. Lett. **370** (2006) L51. B. Feng, J. Q. Xia, J. Yokoyama, astro-ph/0608365. M. Bridges, A.N. Lasenby, M.P. Hobson, MNRAS, **369**, 1123 (2006). Y. Wang, P. Mukherjee, Astrophys. J. **650** (2006) 1.
- [51] A. de Oliveira-Costa, M. Tegmark, M. Zaldarriaga, A. J. Hamilton, Phys. Rev. **D69**, 063516 (2004); E. Gaztanaga *et al.* Mon. Not. Roy. Astron. Soc. **346**, 47 (2003). A. Hajian, astro-ph/0702723. O. Doré et al. Ap J, **612**, 81 (2004). A. Shafieloo, T. Souradeep, Phys. Rev. D **70** (2004) 043523. A. de Oliveira-Costa, M. Tegmark, Phys. Rev. D **74** (2006) 023005.
- [52] D. Schwarz, G. Starkman, D. Huterer, C. Copi, Phys. Rev. Lett. **93**, 221301 (2004); C. Copi, D. Huterer, D. Schwarz, G. Starkman, Phys. Rev. **D75**, 023507 (2007); A. Rakic, D. Schwarz, Phys. Rev. **D75**, 103002 (2007).
- [53] N. J. Cornish, D. N. Spergel, G. D. Starkman, E. Komatsu, Phys. Rev. Lett. **92**, 201302 (2004); B. F. Roukema, B. Lew, M. Cechowska, A. Marecki, S. Bajtlik, Astronomy and Astrophysics **423**, 821 (2004); J. G. Cresswell, A. R. Liddle, P. Mukherjee, A. Riazuelo, Phys. Rev. **D 73**, 041302 (2006); M. Liguori, S. Matarrese, M. Musso, A. Riotto, JCAP **408**, 011 (2004); R. V. Buniy 2005; Int. J. Mod. Phys. **A20**, 1095 (2005); R. V. Buniy, A. Berera, T. W. Kephart, Phys. Rev. D **73** (2006) 063529; T. Multamaki, O. Elgaroy, Astronomy and Astrophysics **423**, 811 (2004); C. Gordon, W. Hu, Phys. Rev. **D70**, 083003 (2004); C. R. Contaldi et al., JCAP **0307** (2003) 002; T. R. Jaffe, A. J. Banday, H. K. Eriksen, K. M. Gorski, F. K. Hansen, ApJ **629**, L1 (2005); C. Gordon, W. Hu, D. Huterer, T. Crawford, Phys. Rev. **D72**, 103002 (2005); C-H. Wu, K.-W. Ng, W. Lee, D.-S. Lee, Y.-Y. Charng, JCAP **0702** (2007) 006; L. Campanelli, P. Cea, L. Tedesco, Phys. Rev. Lett. **97**, 131302 (2006), Phys. Rev. D **76**:063007, 2007; Y. S. Piao, Phys. Rev. D **71**, 087301 (2005); M. Kawasaki, F. Takahashi, Phys. Lett. **B570**, 151 (2003); L. R. Abramo, L. Sodre Jr, C. A. Wuensche, Phys. Rev. D **74** (2006) 083515; I-C. Wang, K-W. Ng, Phys. Rev. D **77** (2008) 083501; J. M. Cline, P. Crotty, J. Lesgourgues, JCAP **0309**:010, (2003).
- [54] M. B. Hoffman, M. S. Turner, Phys. Rev. D **64**, 023506 (2001), W. H. Kinney, Phys. Rev. D **66**, 083508 (2002), R. Easther, W. H. Kinney, Phys. Rev. D **67**, 043511 (2003). L. A. Boyle, P. J. Steinhardt, N. Turok, Phys. Rev. Lett. **96** (2006) 111301. W. H. Kinney, arXiv:0706.3699; B. A. Powel, W. H. Kinney, JCAP **0708**:006, (2007). W. H. Kinney, E. W. Kolb, A. Melchiorri, A. Riotto, Phys. Rev. D **74** (2006) 023502. C. Y. Chen et al., Class. Quant. Grav. **21**, 3223 (2004). E. Ramirez, A. R. Liddle, Phys. Rev. D **71**, 123510 (2005). R. Easther, J. T. Giblin, Phys. Rev. D **72**, 103505 (2005). S. Chongchitnan, G. Efstathiou, Phys. Rev. D **72**, 083520 (2005). M. Spalinski, arXiv:0706.2503.
- [55] S. Weinberg, Phys. Rev. D **72** (2005) 043514. N. Bartolo et al. JCAP **0801**:015, 2008. E. Dimastrogiovanni, N. Bartolo, arXiv:0807.2790. D. Seery, JCAP **11** (2007) 025, JCAP **02** (2008) 006.
- [56] C. Savage, K. Freese, W. H. Kinney, Phys. Rev. **D 74**, 123511 (2006); L. Alabidi, D. H. Lyth, JCAP **0605** (2006) 016 and 0608 (2006) 013; J. Martin, C. Ringeval, JCAP **0608** (2006) 009.
- [57] R. Bean, D. J. H. Chung, G. Geshnizjani, ArXiv **0801.0742**.
- [58] G. Dvali, Q. Shafi, R. Schaefer, Phys. Rev. Lett. **73**, 1886 (1994). V.N. Senoguz, Q. Shafi, Phys. Lett. **B567** (2003) 79, Phys. Rev. D **71** (2005) 043514. L. Randall, M. Soljatic, A. H. Guth, Nucl. Phys. B **472**, 377 (1996). K. Kadota, E. D. Stewart, JHEP **0307** (2003) 013 and JHEP **0312** (2003) 008.

- [59] A. Albrecht, P. J. Steinhardt, M. S. Turner, F. Wilczek, Phys. Rev. Lett. 48, 1437 (1982).
- [60] G. Mangano, G. Miele, C. Stornaio, Mod. Phys. Lett. A10, 1977 (1995).
- [61] See for example, R. D. Peccei, Nucl. Phys. Proc. Suppl. 137 (2004) 277.
G. Altarelli, F. Feruglio, New J. Phys. 6 (2004) 106.
- [62] T. S. Bunch, P. C. Davies, Proc. R. Soc. **A360**, 117 (1978); N. D. Birrell and P. C. W. Davies, *Quantum fields in curved space*, Cambridge University Press, Cambridge, 1982.
- [63] A. Vilenkin, L. H. Ford, Phys. Rev. **D26**, 1231 (1982); A. D. Linde, Phys. Lett. **116B**, 335 (1982); A. A. Starobinsky, Phys. Lett. **117B**, 175 (1982). E. Mottola, Phys. Rev. **D31**, 754 (1985). B. Allen, Phys. Rev. **D32**, 3136 (1985).
- [64] D. Boyanovsky, R. Holman, S. Prem Kumar, Phys. Rev. **D56**, 1958 (1997).
- [65] D. Boyanovsky, H. J. de Vega, Ann. of Phys. **307**, 335 (2003);
D. Boyanovsky, H. J. de Vega, R. Holman and M. Simionato, Phys. Rev. **D 60** 065003 (1999).
- [66] R. P. Woodard, astro-ph/0310757.
- [67] D. Polarski, A. A. Starobinsky, CQG **13**, 377 (1996).
- [68] T. J. Allen, B. Grinstein, M. B. Wise, Phys. Lett. **B197**, 66 (1987).
- [69] T. Falk, R. Rangarajan, M. Srednicki, Astrophys. J. **403**, L1 (1993); Phys. Rev. **D46**, 4232 (1992).
- [70] N. Bartolo, E. Komatsu, S. Matarrese, A. Riotto, Phys. Rept. 402, 103-266 (2004) and references therein.
V. Acquaviva, N. Bartolo, S. Matarrese, A. Riotto, Nucl. Phys. **B667**, 119 (2003).
- [71] A. D. Dolgov, M. B. Einhorn, V. I. Zakharov, Phys. Rev. **D52**, 717 (1995).
- [72] N. C. Tsamis, R. P. Woodard, Class. Quantum Grav. **11** 2969, (1994); Ann. of Phys. (N.Y.) **238**, 1 (1995).
- [73] M. J. Duff, Nucl. Phys. **B125**, 334 (1977);
S. M. Christensen, M. J. Duff, Nucl. Phys. **B170**, 480 (1980); Phys. Lett. **B76**, 571 (1978).
- [74] J. S. Dowker, R. Critchley, Phys. Rev. **D15**, 1484 (1977); *ibid* **D16**, 3390 (1977), **D13**, 224 (1976), **D13**, 3224 (1976).
- [75] M. V. Fischetti, J. B. Hartle, B. L. Hu, Phys. Rev. **D20**, 1757 (1979).
- [76] K. Fujikawa, Phys. Rev. **D23**, 2262 (1981).
- [77] L. R. Abramo, R. H. Brandenberger, V. F. Mukhanov, Phys. Rev. **D56**, 3248 (1997);
L. R. Abramo, Ph. D. Thesis, gr-qc/9709049.
- [78] F. Finelli, G. Marozzi, G. P. Vacca, G. Venturi, Phys. Rev. **D71**, 023522 (2005).
- [79] T. S. Bunch, P. C. W. Davies, Proc. R. Soc. London **A360**, 117 (1978);
A. Vilenkin, L. H. Ford, Phys. Rev. **D26**, 1231 (1982).
- [80] M. A. Castagnino, J. P. Paz, N. G. Sánchez, Phys. Lett. **B193**, 13 (1987).
- [81] D. Boyanovsky, M. D'Attanasio, H. J. de Vega, R. Holman, D.-S. Lee, Phys. Rev. **D52**, 6805 (1995).
- [82] S. Weinberg, *Gravitation and Cosmology: principles and applications of the general theory of relativity*. John Wiley and sons, N.Y. 1972.
- [83] K. G. Wilson, J. B. Kogut, Phys. Rept. 12: 75 (1974).
- [84] S. Furlanetto et al., Phys. Rept. 433: 181, (2006) and references therein.
R. Barkana, A. Loeb, Astrophys. J. 624:L65, (2005).
- [85] R. H. Brandenberger, J. Martin, Mod. Phys. Lett. **A16**, 999 (2001); C. P. Burgess, J. M. Cline, R. Holman, **JCAP 310**, 4 (2003); U. H. Danielsson, Phys. Rev. **D66**, 23511 (2002); L. Sriramkumar, T. Padmanabhan, Phys. Rev. **D 71**, 103512 (2005).
- [86] D. Boyanovsky, H. J. de Vega, N. Sanchez, Phys. Rev. **D 77**, 043518 (2008)
- [87] See, for example, M. Veltman, Diagrammatica, Cambridge Univ. Press, Cambridge, 1994.
- [88] E. Janke, F. Emde, F. Lösch, Tafeln Höherer Funktionen, Teubner, Stuttgart, 1960.
- [89] Handbook of Mathematical Functions, M. Abramowitz and I. A. Stegun, NBS, Washington, 1970.
- [90] A. P. Prudnikov, Yu. A. Brichkov, O. I. Marichev, Integrals and Series, vol I, Nauka, Moscow, 1981.